Understanding Amyotrophic Lateral Sclerosis Using the *Drosophila* Tripartite Synapse

A Thesis

Submitted in partial fulfillment of the requirements

of the degree of

Doctor of Philosophy

By

Shweta Tendulkar

20143317

IISER PUNE

Indian Institute of Science Education and Research Pune

2020

Certificate

Certified that the work incorporated in the thesis entitled "Understanding Amyotrophic Lateral Sclerosis Using the *Drosophila* Tripartite Synapse", submitted by Shweta Tendulkar was carried out by the candidate, under my supervision. The work presented here or any part of it has not been included in any other thesis submitted previously for the award of any degree or diploma from any other University or institution.

Dr. Girish Ratnaparkhi

Declaration

This thesis is a presentation of my original research work. Wherever contributions of others are involved, every effort is made to indicate this clearly, with due reference to the literature, and acknowledgment of collaborative research and discussions. The work was done under the guidance of Dr. Girish Ratnaparkhi, at the Indian Institute of Science Education and Research, Pune.

Shweta Tendulkar

20143317

In my capacity as supervisor of the candidate's thesis, I certify that the above statements are true to the best of my knowledge.

Dr. Girish Ratnaparkhi

Acknowledgements

My Journey at IISER has been a rollercoaster ride and I owe it to a lot of people for making it worthwhile!

Foremost, I express my gratitude to my supervisor Dr. Girish Ratnaparkhi for granting me the opportunity to work on a super exploratory project. He has always been fond of giving analogies in various situations and I vividly remember one of them. This was in the context of my PhD project when I was a naïve first-year graduate student and was 'shaken n baken' by my labmates after my first 'my plan' presentation. The analogy: "A PhD journey is like proposing to grow a field full of mango trees. You get all the requirements and tools for it. You sincerely follow every rule from the 'how to grow mango trees for dummies' book, but to your dismay, you aren't lucky. A little while later some good variety of grass grows on this field, so you divert your attention from 'the mango tree project' to 'the green grass project'. You take a lot of efforts and are successful in building a field full of exotic green grass, which ends up being your primary PhD question". Thanks to Girish, the grass is greener on my side today! He has been the perfect liberal advisor throughout this journey. I thank him for smoothly distracting me with all the side projects (even when I was being a rebellious kid) and at the same time giving me ample freedom to work on the tripartite synapse. A quality that sets him apart is that he is a wonderful human being and knows how to deal with every student in a different way. I admire and respect him for his style of mentorship. His indirect ways haven't just trained me for science but have also coached me for life. Not to forget, I have enjoyed every sarcastic exchange of comments in all these years.

A very special thank you to Dr. Anuradha Ratnaparkhi for her constant help with my work. She has been my go-to person for reagents, antibodies, any new techniques and honest scientific feedback. I have always found her unadulterated passion and love for science very inspiring. I cherish all our exciting chai-time discussions. I would like to thank Dr. Richa Rickhy for her inputs during the combined lab meetings and beyond. She has always been helpful with reagents and experimental advice. Her friendly chats from time to time have made me feel at home.

A big thank you to all the faculty members associated with my journey at IISER. Dr. Girish Deshpande for his timely feedback on my work. Dr. Suhita Nadkarni and Dr. Nixon Abraham, my Research Advisory Committee (RAC) members, for their valuable yearly inputs. Dr. Siddhesh

These people are solely responsible for the smooth functioning of our fly labs. Vijay and Santosh from IISER microscopy facility have been helpful with any and every microscopy related issues. Kalpesh, Piyush, Mrinalini, Mahesh, Tushar and Sayalee have been of constant help with running various errands. They make the IISER office a pleasant and approachable place. I thank all the security staff, housekeeping staff and gardeners at IISER for being prompt in their duties. Their contribution has made this campus a beautiful and secure place. Surender Anna deserves a special mention for being a delight in running the G1/LHC canteen and saving my share of idli-sambar for breakfast!

Funding agencies have played a crucial role in ensuring my scientific progress. I have been regularly supported by IISER Pune for my PhD. I am thankful to DMM (Disease Models and Mechanisms) and DST-SERB for granting me the funding to attend the CSHL-Neurobiology of *Drosophila* conference in October 2019.

I am grateful to my teachers and professors from college. Dr. Rajalakshmi Amudan has been a true inspiration to me for pursuing a PhD. I thank Dr. Laxmipriya Nampoothiri and Dr. Shashikant Acharya for believing in me and foreseeing my progress.

A big shout out to all the friends I made during my journey. Special thanks to Simran and Debayan for being the constant companions of joy and sorrow. Simran has been the joyful and spontaneous friend who made me see the brighter side of my life at IISER. Debayan has been the rational buffer to my aggressive reactions. Life at IISER would have been monochromatic if not for these two! The Drama Club at IISER has played a constructive role in keeping my spirits high in the past few years. This activity was indeed a character-building exercise for me. I met a bunch of wonderful people through this medium. Especially Sameer, Amogh, Sukanya, Rutwik, Dhriti, Anwesh and Harsha who have been my cheerleaders both on-stage and off-stage! I have thoroughly enjoyed our rehearsal sessions, random blabber, deep philosophies and endless deliberations. Hats off to Dr. Sudha Rajamani and Dr. Suhita Nadkarni for being the backbone of the drama club through all our projects. I acknowledge my school and college friends, Radhika, Chitra, Sukhbir, Nirali, Jayshree and Abhijeet, for staying in touch and constantly motivating me throughout this ride.

The most important part of this journey has been my amazing family. I have been blessed with the best set of parents who have supported me endlessly at my best and worst. My dad who has been my teacher for most of my school life has certainly bestowed upon me the curiosity and the zeal to do science. My mom has been a true inspiration to me for striking a healthy work-life balance. Special brownie points to my sister for all her attempts (both failed and successful) at cheering me up during my worst times and for the much needed impromptu meet-ups in Pune. It was a boon to have her around. My lovely grandmother has always believed in my progress and has wished the best for me. I dedicate my PhD thesis to her.

-Shweta.

Table of Contents

List of Figures

List of Tables

Abbreviations

- AAA+ ATPase: ATPases Associated with diverse cellular Activities
- ALS: Amyotrophic Lateral Sclerosis
- Arm: Armadillo
- ATF6: Activating Transcription Factor 6
- Babo: Baboon
- BDNF: Brain-Derived Neurotrophic Factor
- BDSC: Bloomington Drosophila Stock Center
- BiP: ER chaperone immunoglobulin binding Protein
- BMP: Bone Morphogenetic Proteins
- BRP: Bruch Pilot
- Caz: Cabeza
- CCD: Coiled Coiled Domain
- CERT: Ceramide Transfer protein
- CNS: Central Nervous System
- CSF: Cerebrospinal Fluid
- Daw: Dawdle
- DAPI: 4′,6-diamidino-2-phenylindole
- DLG: Disc Large
- DPiM: Drosophila Protein interaction Map
- Dpp: Decapentaplegic
- DPR: Dipeptide Repeats
- DREDD: Death-Related ced-3/Nedd2-like protein
- Dsh: Dishevelled
- ERAD: ER Associated Degradation
- ERQC: ER Quality Control
- FADD: Fas-Associated protein with Death Domain
- FAF1: Fas Associated Factor 1
- FALS: Familial-ALS
- FDA: Food and Drug Association
- FFAT: two Phenylalanines in an Acidic Tract
- FTD: Frontotemporal Dementia
- FUS: Fused in Sarcoma
- Fz: Frizzled,
- Gbb: Glass bottom boat
- GDNF: Glial-Derived Neurotrophic Factor
- GEF: Guanine nucleotide Exchange Factor
- GLT: Glutamate Transporter
- GRN: Gene Regulatory Network
- GTP: Guanosine Triphosphate
- HRP: Horseradish Peroxidase
- IBMPFD: Inclusion Body Myopathy with early-onset Paget disease and Frontotemporal Dementia
- IGF-1: Insulin Growth Factor-1
- IκK: TAK1-inhibitor of κB kinase
- IL-10: Interleukin-10

- IMD: Immune Deficiency
- iNOS: inducible Nitric Oxide Synthase
- IRE1: Inositol-Requiring protein-1
- LMN: Lower Motor Neurons
- LPS: Lipopolysaccharide
- MAD: Mothers against Dpp
- Mav: Maverick
- MBP: Myelin Basic Protein
- MCT: Monocarboxylate Transporter
- MSP: Major Sperm Protein
- mTOR: mammalian Target of Rapamycin
- NES: Nuclear Excision Sequence
- NF-κB: Nuclear Factor kappa-light-chain-enhancer of activated B cells
- NIG: National Institute of Genetics
- NLS: Nuclear Localization Sequence
- NMJ: Neuro Muscular Junction
- NO: Nitric Oxide
- OSBP: Oxysterol Binding Protein
- PERK: Protein kinase RNA like ER-Kinase
- PI4KIIα: Type II- Phosphtidylinositol 4-Kinase
- PNS: Peripheral Nervous System
- PTPIP51: Protein tyrosine phosphatase interacting protein 51
- Put: Punt
- ROS: Reactive Oxygen Species
- RRM: RNA Recognition Motifs
- Sax: Saxophone
- SALS: Sporadic-ALS
- SMA: Spinal Muscular Atrophy
- SOD1: Superoxide Dismutase-1
- TAB2-TAK1: TAK1-associated binding protein 2- TGF-β-activated kinase 1
- TBPH/TDP-43: Tar DNA Binding Protein
- TER94: Transitional Endoplasmic Reticulum ATPase
- TGFβ: Transforming Growth Factor-beta
- Tkv: Thickvein
- TMD: Transmembrance Domain
- TNFα: Tumour Necrosis Factor-alpha
- UMN: Upper Motor Neurons
- UPR: Unfolded Protein Response
- UPS: Ubiquitin Proteasomal System
- VAPB: Vesicle Associated membrane protein Associated Protein-B
- VCP: Valosin Containing Protein
- VDRC: Vienna Drosophila Research Center
- Wg: Wingless
- Wit: Wishful thinking
- Wnt: Wingless-related integration site
- Zw3: Zeste-white 3

Synopsis

Understanding Amyotrophic Lateral Sclerosis Using the *Drosophila* tripartite synapse

Shweta Tendulkar

20143317

Amyotrophic Lateral Sclerosis (ALS) is a progressive motor neurodegenerative disorder with a life expectancy of 3-5 years post-onset. The onset of the disease is usually in the fifth or sixth decade of the life of the patient. The initial symptoms of the disease are marked by limb weaknesses, followed by speech impairment, weakening of respiratory muscles and complete paralysis. Death in most cases is caused by choking as a consequence of respiratory failure. There is a rapid loss of motor neurons during the progression of the disease which leads to muscle atrophy. The atrophy is a consequence of the loss of connection between the motor neurons and the postsynaptic muscles in the NMJ (neuromuscular junction). In a typical case, the disease starts affecting the upper motor neurons followed by the lower motor neurons.

The disease is usually sporadic (SALS; Sporadic ALS), but a significant fraction (5-10%) of patients are familial (FALS; Familial ALS), where the disease is inherited. Intriguingly, there are more than 30 FALS independent genetic loci reported that cause disease and the list is still expanding. FALS patients show mutations in one or more of these genes. Generation of similar mutations in model organisms leads to disease phenotypes that resemble the disease in humans. These mutations have been reported to impair a diverse variety of cellular mechanisms that ultimately lead to motor neuron death. There are instances where a patient is observed to exhibit multiple ALS causing genes mutated, suggesting an oligogenic nature to ALS pathogenicity.

One of the recently discovered aspects of the disease is its non-cell autonomous nature. The non-neuronal cells of the PNS (peripheral nervous system) and well as CNS (central nervous

system) have been reported to contribute to ALS. A complete understanding of the relative contributions of these cells (muscle, glia) in the pathomechanisms of the disease is lacking.

For my thesis, I have worked on the two aspects of ALS i.e. its oligogenic behavior and its non-cell autonomous nature. My hypothesis concerning these aspects is as follows "*ALS loci interact with each other to form gene regulatory networks (GRNs) that are central to cellular homeostasis. In addition to their roles in motor neurons, mutations in ALS genes also contribute to the disease via their effects in muscle and glia. A perturbation in intracellular GRNs in either neurons, glia or muscle may also alter anterograde or retrograde signalling at the tripartite synapse, which in turn leads to death of motor neurons.*" The tripartite synapse is the junction which brings together the presynapse, the postsynapse and the glial cells. In the context of the tripartite synapse of the PNS, the glial cells surround the NMJ. To address my hypothesis, I have focused on *VAPB* (Vesicle associated membrane associated protein B) as a central locus to study the genetic interactions between ALS loci in a cell-specific manner in *Drosophila melanogaster*.

In Chapter I, I introduce ALS, followed by descriptions of the different ALS causing loci. This section covers an elaborate account of *SOD1, TDP43, FUS, c9orf72, VCP, VAPB, ubiquilin2, senataxin* and *alsin* from the list of 30 FALS causing loci. I highlight the pathogenic mechanisms associated with the ALS linked mutations in these loci and review the reported genetic interactions amongst these. Apart from the motor neurons, the non-neuronal cells i.e. the glial cells, muscles and cells of the immune system have been implicated in the disease. Although research in these aspects has been scarce in terms of patient-sample studies, there have been a few model organism-based studies which characterize the involvement of these cell types. Based on the evidence from various model studies, I present a combined overview of the contribution of the non-neuronal cells to ALS. The tripartite synapse has multiple signalling mechanisms which maintain its homeostasis, I summarize the perturbation of this homeostasis in the context of NF-κB pathway, TGF-β signalling and Wnt pathway in ALS. This chapter concludes with a survey of a list of open questions in the field.

In Chapter II, I describe and characterizes the model of ALS8 in *Drosophila melanogaster* that I have used in my work. ALS8 is the form of ALS caused by VAPB^{P56S} (VAP^{P58S} in flies). The ALS8 flies we characterized in this work exhibit survival defects, progressive motor defects, presence of VAP positive brain aggregates and defects in the NMJ morphology. In the end, we

draw parallels between the phenotypes associated with our model of ALS8, other overexpression models used in flies and human patients.

In Chapter III, I discuss and demonstrate cell autonomous and non-cell autonomous genetic interactions of *VAP^{P58S}* with other ALS loci. Using the ALS8 fly line described in the previous chapter, I screen for glial, muscle and motor neuronal interactions of VAP^{P58S} from a list of 7 ALS causing loci. The ALS loci I used to screen for cell-specific genetic interactions are *Drosophila* orthologues of *SOD1, TDP43 (TBPH), FUS (caz), VCP (TER94), VAP, senataxin* and *alsin.* The screening for these interactors was performed by overexpressing and downregulating them in a glial, muscle and motor neuron-specific manner in the ALS8 genetic background. I have further validated and characterized the interactions between *TER94* and *VAP^{P58S}*. One of our major findings in this chapter has been the suppression of ALS8 phenotype by *TER94^{R152H}* mutant and a non-ALS causing locus, *caspar.* Mammalian Caspar (FAF1) is a known physical interactor of VAP and VCP (mammalian TER94). Based on this information and their association with different cellular functions, I have attempted to explore the mechanisms behind the VAP^{P58S}-Caspar-TER94^{R152H} interaction in the latter part of this chapter.

Chapter IV draws attention to two major signalling pathways at the tripartite synapse, the Wnt pathway (Wingless in *Drosophila*) and the TGF-β/BMP pathway (Dpp in *Drosophila).* The tripartite synapse experiences a give and take of multiple signalling molecules due to the functioning of multiple pathways at this crucial junction. The pathways have diverse functions like the development of the synapse, controlling the neurotransmitter dynamics, regulation of energy metabolism, management of electrical inputs-outputs and a lot more. Most of these pathways have been extensively characterized in neurons, but their activity in the non-neuronal cells is far from understanding. Some of these are involved in retrograde, some in anterograde, while some others are involved in both kinds of signalling. The Wnt pathway and the TGF-β/BMP pathway are also involved in the development of the tripartite synapse. These pathways have been well characterized in the neurons and moderately characterized in the non-neuronal cells. I modulated these pathways in the glia of the ALS8 flies. I observed that their suppression caused the ALS8 flies' lifespan to improve. While this is a preliminary result and its needs further validation, this opens a lot of avenues for signalling based non-neuronal cell research in ALS8.

Chapter V describes cell-specific screens (Muscle, Glial and Pan-neuronal) for ALS loci variants. I consider bouton morphology as our readout to understand differential roles for the screened ALS genes in the context of neuronal architecture at the tripartite synapse. I have used the traditional *UAS-Gal4* system to observe perturbation in the bouton morphology on expressing various allelic variants of *SOD1, TDP43 (TBPH), FUS (caz), VCP (TER94),* and *VAP.* I have uncovered several loci variants, which on changing their activity at the NMJ, modulate bouton architecture. We now understand differential roles for the screened ALS genes in the context of neuronal architecture at the tripartite synapse.

Appendix I-V cover additional experiments connected to the theme of the thesis, while appendix VI draws attention to a Rab5-Rab7 convertor protein Monensin 1 (Mon1), and demonstrates its role in regulating dendritic arborization.

Publications

1. Monensin Sensitive 1 Regulates Dendritic Arborization in *Drosophila* by Modulating Endocytic Flux. Harish RK[1], Tendulkar S[1], Deivasigamani S, Ratnaparkhi A, Ratnaparkhi GS. *Front Cell Dev Biol.* 2019 Aug 2;7:145. doi: 10.3389/fcell.2019.00145. eCollection 2019.[1]Equal contribution

2. *Drosophila* Mon1 constitutes a novel node in the brain-gonad axis that is essential for female germline maturation. Dhiman N, Shweta K, Tendulkar S, Deshpande G, Ratnaparkhi GS, Ratnaparkhi A. *Development*. 2019 Jul 10;146(13):dev166504. doi: 10.1242/dev.166504.

3. A correlation of age dependent VAPB aggregation with motor function in a *Drosophila* model of Amyotrophic Lateral Sclerosis. Tendulkar S, Thulasidharan A, Garg L & Ratnaparkhi GS (Manuscript in Preparation).

4. A Caspar/VAPB/VCP complex in the glia regulates proteostasis and attenuates disease phenotypes in a *Drosophila* model of Amyotrophic Lateral Sclerosis. Tendulkar S & Ratnaparkhi GS (Manuscript in Preparation

Chapter I

Introduction

1. Summary

Research in the field of ALS is challenging, and with every discovery, our understanding of this disease increases. The multifactorial etiology and pathomechanisms of the specific motor neurodegeneration remain unsolved after years of research. The reasons for the complexity is the involvement of multiple ALS causing loci, perturbation of heterogeneous molecular pathways, non-cell autonomous nature of the disease, involvement of oligogenic interactions and the unknown sporadic causes.

In this chapter, we discuss the genetics of ALS and highlight the emerging themes which contribute to the complexities involved in its etiology. We also highlight the newly discovered potential for therapeutic interventions, which is a result of the advances in our understanding of this disease. We end this chapter with open questions in the field.

2. Introduction

Amyotrophic Lateral Sclerosis (ALS) is a progressive and fatal motor-neurodegenerative disorder with no known cure. It is commonly known as Lou Gehrig's disease after the famous baseball player who died from the disease in 1941, post which the disease gained more attention (www.alsa.org). ALS causes degeneration of the upper motor neurons (UMN) in the motor cortex and the lower motor neurons (LMN) in the brainstem and spinal cord. This degeneration leads to loss of contact between the motor neurons and muscles resulting in muscle atrophy (Wijesekera and Leigh, 2009; Zarei et al., 2015 and www.alsa.org).

2.1. Diagnostic criteria and tools

The diagnosis of ALS has been a challenge in the field due to the varied symptoms of patients, the difficulty to track heritability, its varied penetrance and presence of ALS-mimicking syndromes (Wijesekera and Leigh, 2009; Mejzini et al., 2019). The diagnosis is done using the revised El Escorial diagnostic criteria (Brooks et al., 2000; Zarei et al., 2015). This includes

evidence of UMN and/or LMN degeneration, followed by testing of a progressive spread of the disease. An important aspect of the diagnostic criteria is the absence of ALS-mimics, which are diseases which exhibit UMN or LMN degeneration (Cedarbaum et al., 1999; Brooks et al., 2000). The tools used for the diagnosis include electromyography, nerve conduction studies, MRI imaging, serological studies and genetic testing (Bali and Miller, 2013).

2.2. FDA approved drugs to treat ALS

The complexity of ALS makes it difficult to find a definite cure. The only FDA (Food and Drugs Administration) approved drugs, Riluzole and Edavarone, are known to delay the progression for some patients and are more effective during the early stages of the disease. Riluzole acts by reducing the glutamate excitotoxicity, by inhibiting glutamate release and inactivating voltage-dependent sodium channels, while Edavarone acts as a free radical scavenger, by reducing oxidative stress in the system. Precise mechanisms of both the drugs are still not clear (Jaiswal, 2019; Zarei et al., 2015).

2.3. Clinical symptoms at the onset and progression of ALS

The symptoms of ALS depend on the clinical onset of the disease, which in most cases is experienced around the late-fifties in the patient. The onset of ALS is of two kinds, the spinal onset, which affects the UMN and the bulbar onset, which affects the LMN. Spinal onset precedes the bulbar onset in around 2/3rd cases and results in weakness in the limbs. The features of bulbar onset include dysarthria and dysphagia (Wijesekera and Leigh, 2009; Zarei et al., 2015). As the disease progresses, most patients develop both, bulbar as well as spinal motor-neurodegenerative phenotypes. The progression takes around 5-10 years, during which the weakness of limbs occurs prior to their dysfunction, followed by paralysis. Towards the end, the patient also develops dyspnea along with dysarthria and dysphagia, eventually leading to compromised movement of all voluntary muscles due to paralysis. The death is caused by respiratory failure. (Wijesekera and Leigh, 2009; Zarei et al., 2015).

2.4. Sporadic and familial origins of ALS

Almost 10% of the ALS cases are of familial origin while the remaining 90% are sporadic, however, there could be discrepancies in these frequencies given the difficulty to trace heritability (Chen et al., 2013; Mejzini et al., 2019). Both the familial as well as sporadic cases are characterized by the occurrence of mutations in more than 30 different genes. A sporadic or

2

familial mutation in any of these genes can potentially cause ALS (Mejzini et al., 2019; www.alsod.ac.uk).

2.4.1. Environmental Factors

In about 90% of ALS cases, the cause of the disease is unknown. Typically, sporadic cases in diseases are termed non-genetic, but cases of sporadic ALS (SALS) have the presence of mutations. As the disease onset is late, tracing family history becomes impossible in many cases and because of lack of genetic evidence, these cases are termed as sporadic (Andersen and Al-Chalabi, 2011). However, there are a few environmental factors speculated to be contributing to these sporadic origins of ALS. Smoking or exposure to smoking from an early age could be a cause of ALS (Armon, 2003). Some case studies talk about athletes having a high risk of developing ALS, as cardiovascular fitness is a risk factor (Turner et al., 2012). In addition to these, exposure to formaldehyde, high concentrations of lead, extremely low-frequency electromagnetic radiations or having a diet with a high concentration of glutamate (Weisskopf et al., 2009; Zarei et al., 2015; Martin et al., 2017) also increases the risk of developing ALS. It is important to note that these are cohort-based statistical reports from various populations and are not necessarily applicable to all ethnicities.

2.4.2. Familial ALS (FALS)

Apart from the known clinical history of the FALS cases, there is no difference between FALS and SALS when it comes to their pathophysiology. Even the list of loci involved in causing FALS and SALS is not mutually exclusive, although the mutant variants in some cases are different (Andersen and Al- Chalabi, 2011). We have discussed a few FALS associated loci in this section.

2.4.2.1. ALS causing common gene variants

Out of all the known ALS causing loci, the frequency of occurrence of *SOD1, C9ORF72, TDP-43* and *FUS* mutant variants is very high (50% cases), while the patients with mutations in other loci are uncommon (Boylan et al., 2015; www.alsod.ac.uk).

Superoxide dismutase 1 (*SOD1*), a reactive oxygen species (ROS) scavenging Cu/Zn metalloenzyme, was the first identified ALS causative locus (Siddique et al., 1991; Rosen et al., 1993). SOD1 quenches oxidative stress in the cell by reducing superoxide to hydrogen peroxide. More than 180 *SOD1* mutant variants have been reported to cause ALS, most of them are autosomal dominant (Mathis et al., 2019). Various mechanisms are suspected to be involved in

SOD1 mediated ALS. Early studies proposed the possibility of the loss of enzymatic activity of SOD1 to be the cause, as reduced ROS levels could potentially increase the oxidative damage (Rosen et al., 1993). This loss-of-function theory was disproved when an animal model study on *SOD1^null^* mice did not exhibit ALS like phenotypes (Reaume et al., 1996). Furthermore, some studies proposed a toxic gain-of-function mechanism mediated via SOD1 aggregates which were present right from the early stages of the disease. These aggregates were speculated to accumulate or interact with essential cellular components and disrupt their functions (Bruijn et al., 1998). Apart from the aggregates, glutamate excitotoxicity and defects in axonal transport are a few other mechanisms via which mutant *SOD1* is reported to confer toxicity (Rothstein, 2009).

c9orf72 is a recently found, most common FALS locus. *c9orf72* has hexanucleotide (GGGGCC) repeat expansions in its first intron, normally repeating 6-10 times, but 100-1000s of times in an ALS patient. Almost 40% of FALS cases are associated with *c9orf72*. This locus causes comorbid FTD (frontotemporal dementia) along with ALS (Renton et al., 2014 and 2011). The function of the protein was unknown, until recently when it was found to be a GEF (guanine nucleotide exchange factor) which regulates GTPases involved in membrane trafficking pathways (Iyer et al., 2018). Its pathogenicity is mediated by gain-of-function as well as loss-of-function mechanisms. The hexanucleotide expansions undergo repeat-associated non-ATG dependent translations (RAN translations) resulting in the production of dipeptide repeats (DPRs) which form aggregates and are toxic to the cells (Ash et al., 2013; Mori et al., 2013). Another toxic gain-of-function mechanism is the accumulation of cytoplasmic RNA foci which sequester RNA binding proteins, leading to the dysfunction of a lot of regulatory pathways in the system (Donnelly et al., 2014; Mizielinska et al., 2014). Lastly, some studies support the theory of *c9orf72* expansions to be haploinsufficient as a result of its reduced transcript levels. This haploinsufficiency, in turn, leads to neurodegeneration mediated via increased neuroinflammation by the immune cells of the central nervous system (CNS), thus exhibiting a loss-of-function role (Shi et al., 2018; Burberry et al., 2020 and 2016). All in all, the effects of *c9orf72* are mediated via toxic gain-of-function effects in the neural cells and loss-of-function effects in the immune cells (O'Rourke et al., 2016 and Trageser et al., 2019).

TDP-43 (TAR DNA binding protein) and *FUS (fused in sarcoma)*, both encode proteins having redundant functions of RNA binding, alternative splicing, gene transcription, mRNA biosynthesis, mRNA stability and RNA translocation from the nucleus to the cytoplasm (Ling et

al., 2013). They are well-studied amongst all the ALS associated loci, typically localized predominantly in the nucleus and are known to interact physically with each other (Kim et al., 2010; and Ling et al., 2010). So far, more than 50 ALS causing mutant variants of *TDP-43* and *FUS* have been reported (Buratti et al., 2015; Lanson and Pandey, 2012) and patients of most mutant variants exhibit symptomatic overlap with FTD (Ling et al., 2013; Tan et al., 2017; Neumann et al., 2009). Both these proteins have RNA recognition motifs (RRM) involved in interacting with RNA molecules, a nuclear localization sequence (NLS) and a nuclear excision sequence (NES) responsible for translocating RNA from the nucleus to the cytoplasm and a glycine-rich region (Robberecht and Philips, 2013; Lanson and Pandey, 2012). The glycine-rich region has prion-like properties which increase the susceptibility of TDP-43/FUS to aggregate. Most reported cases of *TDP-43/FUS* mutations are in the NLS and glycine-rich regions (Rutherford et al., 2008 and Lanson and Pandey, 2012). ALS/FTD mutant variants of TDP-43 and FUS are therefore known to aggregate in the form of stress granules and mislocalize in the cytoplasm (Nishimura et al., 2009; Hostler et al., 2009; Neumann et al., 2006). These stress granules are known to exert toxicity on the system by accumulating crucial RNA binding proteins (Taylor et al., 2016). The mislocalization in the cytoplasm causes the loss of protein in the nucleus, which might impart a loss-of-function property (Rutherford et al, 2008; Guo et al., 2011; Acosta et al., 2014).

2.4.2.2. ALS causing rare gene variants

Gene variants of loci other than *c9orf72*, *SOD1*, *TDP-43* and *FUS* constitute the other 50% of FALS cases. Considering that these are more than around 25 loci, their frequency of occurrence in patients is very low. The wild type proteins of some of these loci are well characterized. Given the shortage of patient samples because of low occurrence, characterizing these ALS mutant variants has been a difficult task, although studying them in various model systems gives a lot of insight. We have discussed a few of these loci in this section.

The first-ever whole-exome sequencing used for screening mutation in ALS cases identified 5 ALS associated mutations in *VCP* (*Valosin containing protein*). About 1% of FALS cases are caused by mutations in *VCP* (Johnson et al., 2010). Before identification as an ALS locus, mutant *VCP* was known to cause inclusion body myopathy, Paget's disease of the bone and frontotemporal dementia (IBMPFD) (Watts et al., 2004). VCP is a type II AAA+ ATPase, involved in ubiquitin-dependent protein degradation pathway and hence maintains protein quality. It

functions in carrying polyubiquitinated substrates from ER, chromatin and mitochondria into the cytosol in order to carry them to the proteasome for degradation. It, therefore, regulates cellular homeostasis via the ERAD pathway (endoplasmic reticulum-associated degradation), chromatin-associated protein degradation and ribosome-associated degradation of proteins (Vaz et al., 2013). In addition to this, it also helps the proteasome with the degradation by unfolding of proteins. A few studies have also characterized involvement of VCP in lysosomal degradation of proteins (Meyer et al., 2012). Defects in the ubiquitin-dependent protein degradation pathway have been studied in the case of ALS mutants of *VCP*, where ubiquitinated inclusions of wild type TDP-43 were found in the system (Gitcho et al., 2009). Studies report these mutations to cause an imbalance in protein homeostasis leading to ER stress (Weihl et al., 2006). Apart from disruption of ubiquitin proteasomal system (UPS), defects in autophagy due to the possible accumulation of autophagosomes and defects in energy metabolism due to mitochondrial uncoupling are also speculated to be involved in *VCP* associated ALS/IBMPFD pathogenesis (Ju et al., 2009 and Bartolome F. et al., 2013). A loss in the protein quality control is thus implicated to be a cause of mutant *VCP* mediated motor neurodegeneration.

ubiquilin2 is another ALS associated locus which is involved in proteasomal degradation (Deng et al., 2012). It encodes a protein which is a member of the ubiquitin-like protein family and delivers ubiquitinated proteins to the proteasome for degradation, thus regulating the UPS. About 5 mutants in *ubiquilin2* have been identified to cause ALS (Chen et al., 2013). Cases of ALS with *ubiquilin2* mutations have shown comorbid FTD phenotypes (Renton et al., 2014; Daoud H. et al., 2012). The pathogenicity of *ubiquilin2* is mediated by the accumulation of protein inclusions as a result of the failure of UPS in case of ALS/FTD mutants. (Deng et al., 2012).

ALS associated mutants of *VAPB (vesicle-associated membrane protein (VAMP) associated protein B)* have been reported in familial cases only (Chen et al., 2013). So far only 2 mutant variants of *VAPB* have been discovered, $VAPB^{P56S}$ and $VAPB^{T46I}$, the former being more studied than the latter (Nishimura et al., 2004 and Chen et al., 2010). $VAPB^{P56S}$ is also known to be associated with SMA (spinal muscular atrophy) (Marques et al., 2006). VAPB is majorly an ER membrane protein also found on membranes of pre-Golgi intermediates, recycling endosomes, neuromuscular junctions and on plasma membranes. It is involved in vesicle trafficking, microtubule organization, regulation of ER-Golgi trafficking and lipid transport (Lev et al., 2008). The protein has 3 domains, the N-terminal MSP (Major sperm protein) domain, the α-CCD (coiled

coiled domain) and the C-terminal TMD (Transmembrane domain). The MSP domain plays an important role in executing most of the crucial functions of VAPB, these functions are disrupted in case of ALS *VAPB* mutants (Chai et al., 2008; Kanekura et al., 2006; Pennetta et al., 2002; Tsuda et al., 2008). VAPB^{P56S} not only aggregates on its own but also forms and mislocalizes inclusions of other ALS associated proteins like TDP-43 (Tudor et al., 2010) thus imparting toxicity to the system.

alsin encodes a protein which is homologous to Rho and Ran GEF and functions as a GTPase regulator (Hadano et al., 2001). While most other ALS mutant variants are autosomal dominant, mutations in *alsin* cause an autosomal recessive form of ALS (Hentati et al., 1994 and Hadano et al., 2001). Another striking feature of *alsin* associated ALS is its juvenile-onset, the median age of onset is around 6.5 years (Hadano et al., 2001 and Chen et al., 2013). The pathomechanism of mutant *alsin* seems to be due to the loss-of-function of the protein as loss of Alsin disrupts membrane organization and vesicle trafficking leading to aggregation of immature vesicles (Hadano et al., 2001; Otomo et al., 2008)

Another locus involved in causing the juvenile onset of ALS is *senataxin* (Chen et al., 2004). It is an RNA/DNA helicase homologue. Cases of ALS with mutant *senataxin* are rare but are found in both FALS and SALS scenarios. The proposed mechanism for mutant *senataxin* resulting in ALS is the loss-of-function of helicase activity or aberrant RNA processing which could cause motor neurodegeneration (Chen et al., 2004; Chen et al., 2013).

Table 1.1. List of ALS loci and their putative functions

Gene	Genetic subtype and Location	Protein	Common mode of inheritance	Putative protein function
SOD1	ALS1/21q22.1	Cu/Zn Super oxide dismutase 1	Dominant	Antioxidants in cytosol
alsin	ALS2/2q33.2	Alsin	Recessive	GTPase regulation and Endosomal trafficking
Unknown	ALS3/18q21	Unknown	Dominant	Disulfide redox protein
senataxin	ALS4/9q34	Senataxin	Dominant	DNA/RNA metabolism and helicase activity

SPG11	ALS5/15q21.1	Spatascin	Recessive	Support to the cytoskeleton and regulation of synaptic vesicle transport
FUS	ALS6/16q11.2	Fused in Sarcoma	Dominant	RNA transport, splicing, maintenance of genomic integrity, miRNA processing
Unknown	ALS7/20p13	Unknown	Dominant	Unknown
VAPB	ALS8/20q13.3	Vesicle associated membrane protein - associated protein B	Dominant	UPR, cytoskeletal organization, Lipid biosynthesis
ANG	ALS9/14q11.2	Angiogenin	Dominant	RNA processing and neurite outgrowth
TDP-43/TARDBP	ALS10/1p36.2	TAR DNA binding protein	Dominant	RNA transport, splicing, maintenance of genomic integrity, miRNA processing
FIG4	ALS11/6q21	Factor induced gene 4 homolog	Dominant	Polyphospho inositide phosphatase
OPTN	ALS12/10p15–p14	Optineurin	Dominant	Vesicular trafficking from Golgi to the plasma membrane, and endocytic trafficking
Unknown	ALS13/12q24	Unknown	Dominant	Unknown
VCP/p97	ALS14/9p13-p12	Valosin containing protein	Dominant	UPS, UPR, ERAD
UBQLN2	ALS15/ Xp11.23-p11.1	Ubiquilin2	Dominant (X linked)	UPS
SIGMAR1	ALS16/9p13.3	Sigma non-opioid intracellular receptor1	Recessive	ER chaperone, ion channels regulation, associates with neuron-specific molecules
CHMP2B	ALS17/ 3p11.2	Charged multivesicular body protein 2B	Dominant	Multivesicular body formation, Autophagy, protein sorting

PFN1	ALS18/17p13.2	Profilin1	Dominant	Growth regulator of actin filaments
ERBB4	ALS19/2q34	Erb-B2 Receptor Tyrosine Kinase 4	Dominant	Cell surface receptor for neuregulins and EGF family member and regulates development of various organs
HNRNPA1	ALS20/ 12q13.13	Heterogeneous Nuclear Ribonucleoprotein A1	Dominant	mRNA processing and transport
MATR3	ALS21/ 5q31.2	Matrin3	Dominant	DNA/RNA binding, chromatic reorganization
TUBA4A	ALS22/ 2q35	Tubulin Alpha 4A	Dominant	Cytoskeletal organization and axonal transport
ANXA11	ALS23/ 10q22.3	Annexin A11	Dominant	Calcium-dependent binding and cytokinesis
NEK1	ALS24/4q33	NIMA related kinase 1	Dominant	Serine/Threonine Kinase involved in cell cycle control
KIF5A	ALS25/12q13.3	kinesin family member 5A	Dominant	Microtubule-based motor proteins involved in the transport of organelles
c9orf72	9p21.2	Guanine nucleotide exchange factor C9orf72	Dominant	Regulation of membrane trafficking, transcription, splicing regulation
TBK1	12q14.2	Tank Binding Kinase 1	Dominant	Interferon production, autophagy
NEFH	22q12.2	Neurofilament protein, heavy polypeptide	Dominant	Neuron-specific intermediate filament functions in cytoskeletal remodelling
UNC13A	19p13.3	Unc-13 Homolog A	Not available	Neurotransmitter release at the synapses

DCTN1	2p13	Dynactin1	Dominant	Axon transport, cytoskeleton
SQSTM1	5q35	Sequestosome 1	Dominant	Protein degradation, Autophagy

Chen et al 2013; Mejzini et al., 2019; https://www.uniprot.org/

2.5. Evidence of oligogenicity in ALS

Initial years of research was focused on monogenic causes of FALS and SALS. A few cases of FALS had the presence of autosomal dominant mutations with incomplete penetrance; this is what led to the origin of the 'oligogenic inheritance' hypothesis (Van den Berg et al., 2012). When a disease is developed due to mutations in two or more than two genes in a single patient, it is defined as an oligogenic disease. Proofs from the literature have strong grounds for the monogenic basis of ALS, while the evidence for its oligogenic nature is recent. Oligogenicity in ALS could function in various ways:

1. One of the mutations could be the primary mutation with low penetrance. In such cases, the secondary mutation is necessary for the development of ALS as it acts synergistically with the primary mutation.

2. Two mutations could be equally potent and could cause aggravated defects as compared to their monogenic versions.

3. One of the mutations could be familial in origin while the other develops sporadically. This sporadic mutation could be developed due to independent causes or due to the presence of the initial familial mutation.

All the above mechanisms are hypotheses in the field and an immense amount of research is needed to test them.

Oligogenic basis of ALS came into the picture after the discovery of *c9orf72* locus, which is found in the most number of ALS patients but is less penetrant. According to the oligogenic inheritance hypothesis, a presence of the second mutation along with *c9orf72* will allow the development of ALS, thus making up for low penetrance of *c9orf72*. The *c9orf72* locus is reported to be coexisting with *TDP-43*, *optineurin (OPTN)* and *VAPB* in separate patient studies (Chio et al., 2012; Bury et al., 2016; Blitterswijk et al., 2012a). This angle of the disease increases the complexities in a patient, especially because of the possibility of each locus acting via distinct

pathologies and both together, aggravating the disorder (Renton et al., 2014). Alternatively, oligogenic mutations could follow overlapping mechanisms leading to an additive effect on the disease phenotype. There have been studies about genetic interaction between two different loci leading to a combined effect on neurodegeneration, like a study in *Drosophila* which talks about the interaction of *TDP-43* and *FUS* where neurodegeneration in the eye is exaggerated in the presence of mutants of *TDP-43* and *FUS* (Lanson et al., 2011). ALS associated mutant *TDP-43* is also known to disrupt *VAPB's* function of regulating the association between endoplasmic reticulum and mitochondria (Stoica et al., 2014).

Some studies have demonstrated the presence of one mutant locus affecting the expression levels of another wild type ALS locus. Aggregates of one kind of mutation have been known to accumulate proteins of other unaffected loci in them. Deng et al., 2010 have shown that patients of *TDP43^{G298S}* have the presence of wild type FUS inclusions in the mutant TDP-43 aggregates. Study in mice with ALS associated *SOD1* mutations have revealed that free VAPB levels were reduced in the end-stages of the disease, suggesting the association of wild type protein of an ALS locus with another mutated ALS locus (Teuling et al., 2007). In a study performed in mice, *VCP* and *TDP-43* were found to be genetically interacting with each other, and expression of a mutant version of *VCP* led to mislocalization of TDP-43 from the nucleus to the cytoplasm, which is a common feature of impaired proteostasis in ALS (Ritson et al., 2010).

There are a few reports which discuss the expression of one ALS locus rescuing the defect caused by another ALS locus. In two different studies in *Drosophila* by the Yamaguchi group, overexpression of *VCP* suppressed the defects caused by separate knockdowns of *TDP-43* and *FUS,* whereas the loss-of-function of *VCP* enhanced the defects (Azuma et al., 2014 and Kushimura et al., 2018). While this doesn't follow our theme of two or more mutations aggravating the disorder, it certainly is a proof for genetic interactions amongst these genes.

More animal model studies along with substantial patient data will help us find more genetic modifiers enabling us to understand the details of the concept of oligogeny and hence the pathomechanisms of ALS. The above studies leave us with ideas of complex interactions between multiple ALS loci. The evidence suggests the possibility of these loci being a part of a Gene Regulatory Network (GRN) which is probably altered during the disease progression (Deivasigamani et al., 2014).

2.6. Converging pathologies of ALS loci

Considering the evidence from the studies discussed so far, it is clear that different ALS loci follow a complex pathogenic cascade with a few common features, which eventually leads to motor neurodegeneration. The molecular pathways disrupted by the mutant variants are of crucial importance to the smooth functioning of the system and therefore their malfunctioning converges ultimately to cause cellular stress, leading to motor neuronal death. However, the question of why there is 'selective death of motor neurons in a ubiquitously expressed mutant background' is yet to be answered. Some theories suggest that motor neurons are the most sensitive and hence susceptible cells of them all, but an argument to this school of thought would be an example of other neurodegenerative disorders which manifest similar cellular stresses but do not exhibit selective motor neuron death. This section highlights a few of the different cellular mechanisms involved in ALS and also brings out the overlap and the interplay between the pathologies of different ALS loci (Fig. 1.2).

2.6.1. Dysfunction of RNA metabolism

Many aspects of RNA metabolism like RNA splicing, transcription, RNA transport and translation are affected due to mutations in RNA binding proteins (FUS, TDP-43 and HNRNPA1) or mutations in RNA processing proteins (senataxin and Angiogenin) (Damme et al., 2017; Mejzini et al., 2019). In addition to this, transcripts of hexanucleotide repeat expansions of *c9orf72* sequester RNA binding proteins resulting in their unavailability (Ash et al., 2013; Mori et al., 2013; Ling et al., 2013), this indirectly contributes to dysfunction of RNA metabolism.

2.6.2. Impaired proteostasis

Mutant proteins of *VAPB, VCP, ubiquilin2, c9orf72, FUS, TDP-43, SQSTM1, OPTN and TBK1* are reported to aggregate and exert toxicity on the system by accumulating other important proteins in their inclusions; at the same time the mislocalization of these proteins from their site of action also causes loss-of-function defects. Typically, in the case of misfolded proteins, the unfolded protein response (UPR) and autophagy pathways are activated, resulting in either refolding of the proteins or their degradation. However, in case of the above list, most of the proteins themselves are involved in UPS or autophagy pathways, and therefore mutations in these lead to disruption of the rescue via UPR/autophagy. This results in accumulations of their ubiquitinated aggregates along with other interacting proteins, causing ER stress and abnormalities

in autophagy, leading to disrupted protein quality control (Atkin et al., 2008; Ling et al., 2013; Ron and Walter 2007; Mejzini et al., 2019; Ramesh and Pandey, 2017).

2.6.3. Mitochondrial dysfunction and oxidative stress

Mitochondrial dysfunction and oxidative damage have been common contributors to motor neuron death due to mutations in *SOD1*. The ER membrane protein VAPB has a role in mitochondrial localization at the neuromuscular junction (NMJ) and this function is lost in case of its ALS mutant. Apart from *SOD1* and *VAPB*, ALS loci involved in RNA metabolism regulation (*TDP-43, FUS, C9orf72*) have been proposed to contribute to oxidative stress and mitochondrial dysfunction, but their exact mechanism is still unknown. (Carri et al., 2015; Damme et al., 2017)

2.6.4. Disruption of the cytoskeleton and axonal transport

Various ALS associated loci (*alsin, PFN1, TUBA4A, NEFH, DCTN1, VAPB)* are involved in the maintenance of cytoskeletal architecture and consequently also participate in the transport of various cargoes to and from the axons. Mutations in these lead to their loss-of-function effects (Andersen and Al-Chalabi, 2011; Damme et al., 2017).

2.6.5. Abnormal vesicular transport

Wild type proteins encoded by *VAPB, CHMP2, UNC13A, OPTN* are involved in different aspects of vesicular transport in the cell. ALS mutants of these proteins, therefore, contribute to the disruption of these functions (Andersen and Al-Chalabi, 2011; Damme et al., 2017).

2.6.6. Glutamate excitotoxicity

Glutamate is a neurotransmitter involved in signalling at the synapse, and its concentration is kept in check by glial cells. In a normal case scenario, the glutamate levels are lower in the synaptic cleft than inside the cells. In case of ALS and most other neurodegenerative disorders, the expression of glutamate transporters on the glial cells is lowered, causing excess glutamate accumulation at the synapse, leading to overstimulation of the ionotropic NMDA receptors on the post synapse. This leads to excess calcium, potassium and sodium ions traveling across the membranes and disrupting the membrane potential, the outcome of which is cell degeneration (Gusev et al., 2003; Perez-Nievas and Serrano-Pozo, 2018). Glutamate excitotoxicity is observed in most mutant variants of ALS, although, the exact mechanism that causes the reduction in glutamate transporter expression is not known. It is still unclear if altered glutamate signalling is a cause of the neurodegeneration or is its effect (Yamanaka and Komine, 2018 and Barbeito, 2018).

2.7. Non-cell autonomous nature of ALS

Much of the early work in ALS was focused on motor neurodegeneration, as it was thought to be a disease concerned only with motor neurons. It was only about 10 years ago that the neuron-centric research shifted attention to cells around the neurons. The first study that highlighted the importance of glial cells in ALS demonstrated the presence of SOD1 positive inclusions in the astrocytes of the spinal cords of $SOD1^{G85R}$ mice. These inclusions developed in the astrocytes at the age of 6 months, which was the pre-onset stage, as the motor neurodegeneration began after 7.5 months of age. These astrocytic inclusions were reported to increase with the progression of the disease and were proposed to be excellent markers for disease onset as well as progression. The disease progression also marked loss of Glutamate transporters (GLT-1) in the astrocytes, proposing glutamate excitotoxicity to be one of the pathogenic mechanisms of $SOD1^{G85R}$ associated ALS (Bruijn et al., 1997). This study opened a lot of new avenues in the research field of ALS, especially concerning targeted therapies. ALS has now been established as a non-cell autonomous disorder, although the details of the mechanisms involved in the non-cell autonomy are still blurry.

Non-cell autonomy and ALS: ALS is a disease which causes progressive degeneration of motor neurons. Cells other than motor neurons contribute to this degeneration. Involvement of 'non-neuronal' cells in a disease which exhibits specific degeneration of motor 'neuronal' cells makes it a non-cell autonomous disease.

Amongst the 30 ALS causing loci, very few have been studied concerning the non-cell autonomous perspective. The non-neuronal cells reported to be involved in ALS are glial cells, muscles and cells of the immune system. In this section, we have discussed the roles of these cells in the contribution to the non-cell autonomy associated with ALS.

2.7.1. Glial Cells

Glial cells have come a long way from being thought of as not so important cells present around neurons only to glue them together, to the most essential companions of the neurons. Mammals are known to have different types of functionally distinct glial cells in the CNS and PNS (Peripheral Nervous System), most of these have a role to play in ALS pathogenesis (Kunst et al., 2004). We have discussed a few of these cells in this section (Fig. 1.2).

2.7.1.1. Astrocytes: Role in progression and onset

Glial cells have provided a new scope to explore the causes of ALS. Astrocytes are the glial cells which are involved in maintaining the blood-brain barrier, provide structural support, nutrient support and regulate ionic as well as neurotransmitter levels at the synapse (Allan and Barres, 2009; Kunst et al., 2004). Various studies, mostly concerning the most prevalent and initially discovered ALS loci have described the contribution of astrocytes to the disease mechanisms.

After the first report about the presence of pre-onset inclusions of $SOD1^{G85R}$ in the astrocytes, different studies concerning astrocytes in various $SOD1$ mutants were carried out. Amongst all the studies, loss of astrocytic glutamate transporters leading to loss of astrocytic ability to uptake glutamate and hence cause glutamate excitotoxicity has been a common mechanism involved (Lin CL et al., 1998; Meyer et al., 2014; Yamanaka et al., 2008; Guo et al., 2003; Howland et al., 2002). Yamanaka et al., 2008 demonstrated the delay of disease progression by using the cre-lox excision system to excise the mutant $SOD1$ gene ($SOD1^{G37R}$). This study also brought into attention that, a steady increase of astrocyte number (astrogliosis) surrounding the dying motor neurons takes place from the onset as well as during the disease progression. In yet another study of $SOD1^{G93A}$, cultured astrocytes produce neuroinflammatory factors like tumour necrosis factor-alpha (TNFα), proinflammatory eicosanoids prostaglandin E2, inducible nitric oxide synthase (iNOS) and nitric oxide (NO) thus feeding into the inflammatory reactions concerned with ALS. These astrocytes which produced neuroinflammatory factors were called activated astrocytes (Hensley et al., 2006). Using chimeric mice, which use mixtures of wild type and mutated cells, neuronal degeneration was observed only when there was damage to non-neuronal cells possessing $SOD1$ mutations (Clement et al., 2003). This study highlighted the fact that damage to non-neuronal cells is essential for motor neurodegeneration.

Astrocytes have been studied to play a significant role in the *TDP-43* ALS mutant models as well. On selectively expressing mutant *TDP-43* in the astrocytes of rats and not in their motor neurons, astrocytes were observed to be contributing to the onset as well as the progression of ALS by causing motor neuron death (Tong et al., 2013). Co-culture studies with mutant motor neurons and non-mutated astrocytes for *TDP-43* proposed astrocytes to be protective, as the presence of healthy astrocytes caused a lowering of mutant TDP-43 aggregates in the corresponding motor neurons (Smethurst et al., 2020).

Very few studies concerning the role of astrocytes have been carried out on the mutants of ALS causing loci like *FUS* (Kobayashi et al., 2010)*, alsin* (Jacquier et al., 2009), *VCP* (Hall et al. 2017) and *c9orf72* (Zhao et al., 2020). Some of these are clues from the patient autopsy samples, as a result of which the possibility of investigating the contributions of the glial cells in the onset/progression stages is ruled out; while some others are astrocyte-motor neuron co-culture studies which characterize astrocytes as contributors to both onset as well as the progression of ALS. Considering the contribution of astrocytes in the progression and pathogenesis of ALS, they have tremendous potential of being promising therapeutic targets for ALS. To this end, Izrael et al., in 2018 came up with embryonic stem cell-derived astrocytes as an effective therapeutic option for ALS. These cells will behave as young astrocytes and hence delay the progression of the disorder. This therapeutic approach is under clinical trials currently and its application will help in extending the survival of the patients significantly (Izrael et al., 2018; Yamanaka and Komine, 2018).

2.7.1.2. Microglia: Immune cell action in ALS

Microglia are the macrophages of the CNS and are involved in its immune defense. Microglia have been reported to be activated along with astrocytes in *SOD1* mediated ALS (Yamanaka et al., 2008). Clusters of microglia and inflammatory mediators have been found in post mortem brain samples and cerebrospinal fluids (CSF) of ALS patients, implicating the activation of an inflammatory response. The reason behind this activation is still unclear (Wilms et al., 2003; Troost et al., 1990; Kawamata et al., 1992). Like astrocytes, these cells also are activated before the onset where they perform a neuroprotective role (called M2 microglia) by expressing anti-inflammatory cytokines and neurotrophic factors like IGF-1(Insulin growth factor-1), GDNF (glial-derived neurotrophic factor), BDNF (brain-derived neurotrophic factor), IL-10 (Interleukin-10) and TGFβ (transforming growth factor-beta). In the later stages, the microglia are proposed to play a neurotoxic role (M1 microglia) by expressing pro-inflammatory cytokines like IL-6, TNFα and NO (Appel et al., 2011). More evidence comes from co-culture studies, where the first stage and late-stage microglia were observed for markers of inflammation and the M2 to M1 transformation was tracked (Liao et al., 2012). In a $SOD1^{G37R}$ mice model of ALS, feeding Lipopolysaccharide (LPS) to the mice resulted in stimulation of the immune system which aggravated the disease condition, suggesting a neurotoxic role of microglia in the progression stages of the disorder (Nyugen et al., 2004). In another LPS treated mice study of mutant SOD1

model, microglia had the presence of inflammatory cytokine TNFα and IL-6 release (Weydt et al., 2004). $SOD1^{G93A}$ microglia are known to produce superoxides and other toxic substances thus causing motor neuron death in the late stages of the disease (Beers et al., 2008). Studies concerning other ALS loci like *TDP-43* and *c9orf72* also, describe the presence of M2-M1 microglial transition during the disease course (Spiller et al., 2018 and Rostalski et al., 2019).

It is speculated in the field that the transition between M2 to M1 microglia happens when the effect of M2 is dampened. The system probably tries to deal with the initial damage using anti-inflammatory cytokines, but when the situation goes out of hand it chooses self-destruction by expression of pro-inflammatory cytokines, probably to save the surroundings. These studies not only testify the importance of microglia in the onset and progression of ALS but also bring out the complex cross-talk between neurons and glial cells which is required for the smooth functioning of the system. There are a few therapeutic options used to delay the M1 phase of inflammation. Minocycline is a drug known to delay microglial activation, this tetracycline derivative delays motor neuron loss as well (Bosch et al., 2002). Delay in M2 phase onset leads to extending the survival of the patient (Fig. 1.1).
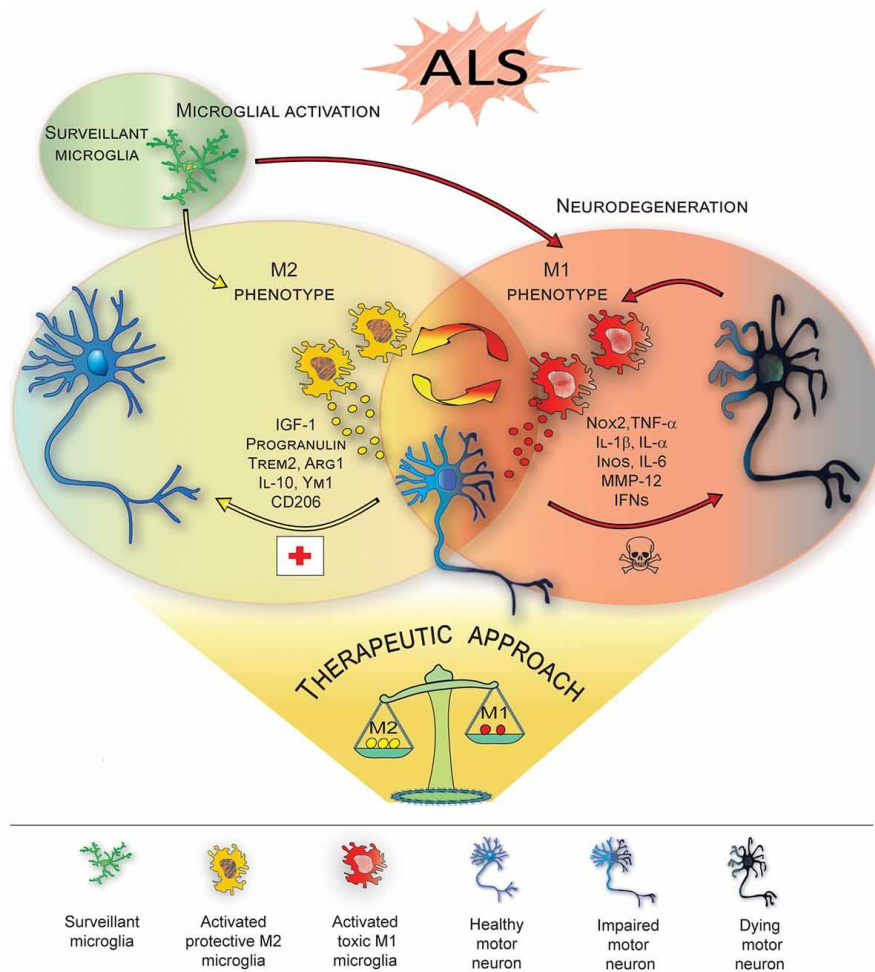
Figure 1.1. M2-M1 transition of microglia.
In the initial stages of inflammation, microglial cells are involved in the release of anti-inflammatory factors and act as neuroprotective to the motor neurons, this stage is called the M2 stage. In the late stages of the disease, when the situation becomes uncontrollable, these cells transform into M1 cells where they release pro-inflammatory factors and aid in cell death. The initial M2 phenotype can be made use of therapeutic purposes and extend the life span of the patient. Image courtesy: Geloso et al., 2017.

2.7.1.3. Oligodendrocytes

Oligodendrocytes are the glial cell types responsible for myelinating axons in CNS. Like in the case of astrocytes, oligodendrocytes isolated from *TDP-43* associated ALS patient samples were found to have ubiquitinated aggregates of TDP-43 (Neumann et al., 2007). A *SOD1^{G93A}* mouse model of ALS also displayed aggregates of the protein in oligodendrocytes. Furthermore, this study estimated that there was rapid death of the oligodendrocytes with the progression of the disease, but this was compensated by high turnover rate and therefore the number of these cells remained constant (Philips et al., 2013). However, the new cells were found to be dysfunctional as

the expression of important markers for functional oligodendrocytes, monocarboxylate transporter1 (MCT1) and myelin basic proteins (MBP) was reduced (Philips et al., 2013; Kang et al 2013 and Lee et al., 2012). MCT1 is responsible for the transport of lactate to motor neurons to support their metabolic requirements; while MBP is important for myelination of axons. As the expression of MCT1 as well as MBP was reduced in oligodendrocytes of ALS patients/animals, this might be one of the contributing factors for the motor neurodegeneration. Therapeutic introduction of non-mutated and functional oligodendrocytes by using embryonic stem cells could perhaps extend the progression stage and lengthen the lifespan of the patients.

2.7.1.4. Schwann cells: Glial cells of the PNS

Schwann cells are myelinating glial cells of the PNS. These cells mediate the degeneration of the LMNs. There have been only a couple of studies carried out concerning the contribution of Schwann cells. One of them talks about the inducible form of Nitric Oxide Synthase (iNOS) being upregulated in the Schwann cells of *SOD1^{G93A}* mice, suggesting the activation of inflammation which could lead to motor neurodegeneration (Chen et al., 2010). The second study contradicts the contribution of Schwann cells in the progression of the disease, by witnessing that the decrease in expression of mutant *SOD1^{G37R}* specifically in Schwann cells, resulted in accelerated progression of the disease (Lobsiger et al., 2009). It is, therefore, necessary to further investigate Schwann cells and obtain a clearer picture of their involvement. Schwann cells are important players at the NMJ, as they participate in crosstalk with the motor neurons and hence maintain the synaptic activity by regulating the release of neurotransmitters and other signalling molecules. These cells also participate in re-innervation of the synapse, and in a way maintain excitability of the neurons at the NMJ. Considering the contribution of Schwann cells, a lot of hypothetical theories have been proposed for their roles in the ALS pathophysiology, addressing these hypotheses could provide new perspectives to ALS research (Arbour et al., 2017).
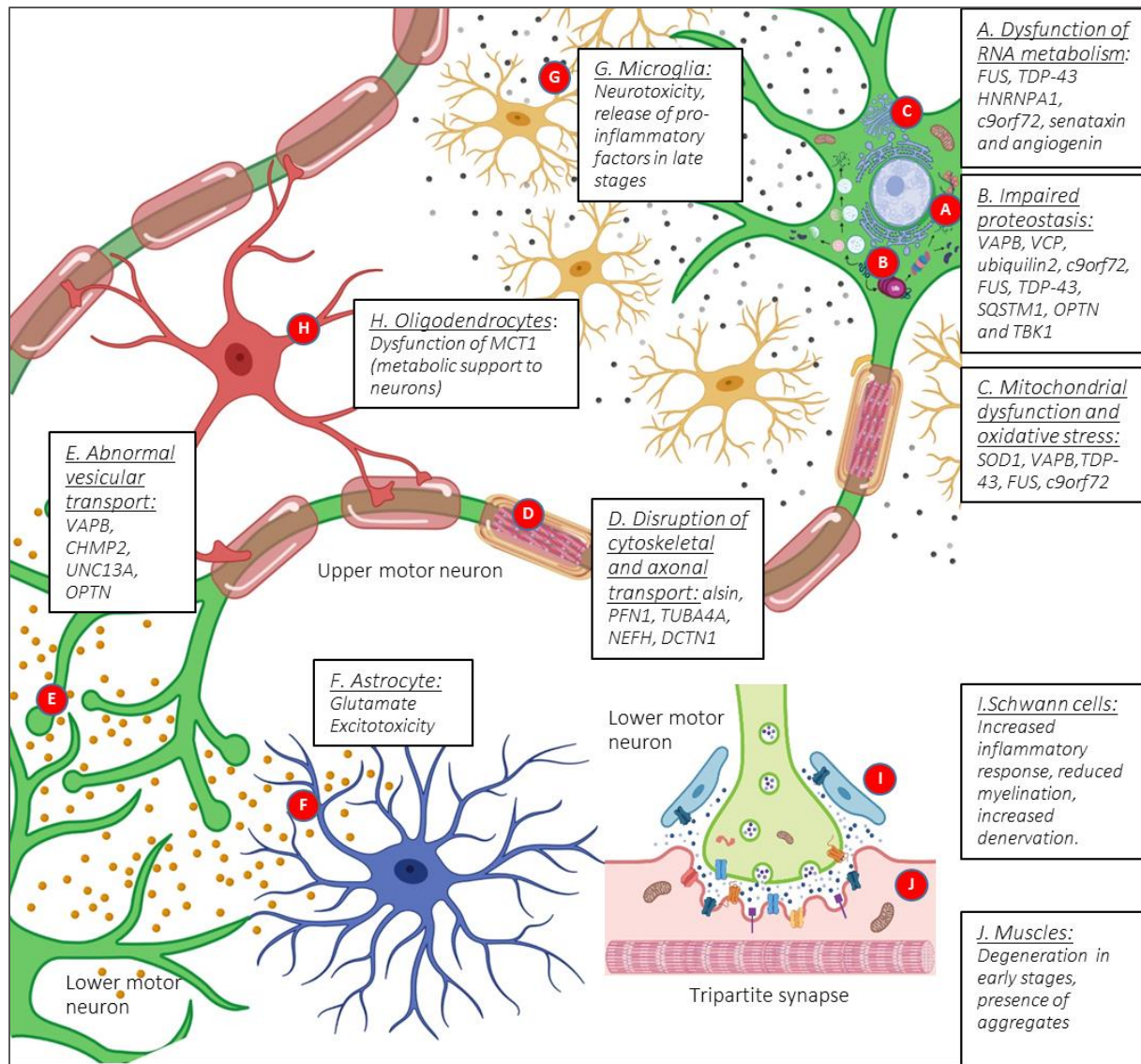
Figure 1.2. Pathomechanisms involved in ALS.

Over 30 genes are known to carry ALS causing mutations. Each mutant variant causes impairment of a molecular pathway that is crucial for the functioning of the cell. Glial cells also contribute to this impairment by exhibiting abnormalities in their cross-talk with neurons. Various disease mechanisms proposed to be causing ALS are **A)** Dysfunction of RNA metabolism: *FUS, TDP-43 HNRNPA1, c9orf72, senataxin and angiogenin;* **B)** Impaired proteostasis: *VAPB, VCP, ubiquilin2, c9orf72, FUS, TDP-43, SQSTM1, OPTN and TBK1;* **C)** Mitochondrial dysfunction and oxidative stress*: SOD1, VAPB, TDP-43, FUS, c9orf72;* **D)** Disruption of cytoskeletal and axonal transport: *alsin, PFN1, TUBA4A, NEFH, DCTN1;* **E)** Abnormal vesicular transport: *VAPB, CHMP2, UNC13A, OPTN;* **F)** Glutamate Excitotoxicity caused by astrocytes*;* **G)**. Release of pro-inflammatory factors in late stages by microglia causes neurotoxicity*;* **H)** Dysfunction of MCT1 (metabolic support to neurons) in oligodendrocytes; **I)** Increased inflammatory response, reduced myelination, increased denervation due to dysfunction in Schwann cells and **J)** Involvement of muscles degeneration in the early stages, the presence of aggregates. Image inspiration: Damme et al., 2017. Figure designed in: BioRender App.

2.7.2. Muscles: The unexplored targets of ALS

As described before, ALS causes progressive weakening of skeletal muscles, leading to muscular atrophy followed by paralysis. Expression of $SOD1^{G93A}$ specifically in the muscles of mice caused retraction of motor axons leading to muscle atrophy, thus proposing muscles to have a potential to be the primary affected cell type in the disease (Dobrowolny et al., 2008). The retraction effect on motor neurons was ameliorated on expressing Insulin Growth Factor1 (IGF-1) specifically in the muscles, suggesting that IGF-1 expressed from the muscles has therapeutic properties for motor neuron loss (Dobrowolny et al., 2005). In the case of some ALS patients, muscle exercise has been known to provide some relief from the disabilities associated with the disease (Drory et al., 2001). Various markers like Nogo (an inhibitor of axonal regeneration) are expressed from the muscles during the late stages of ALS and are proposed to be used as markers for the severity of ALS (Jokic et al., 2005). Studies using ALS mutant variants of *FUS, VCP* and *TDP-43* in different model organisms have identified muscles as potential targets for therapeutic purposes, considering their involvement in the early disease mechanisms (Diaper et al., 2013 and Nalbandian et al., 2013). Paying more attention to muscles as candidates of research would probably answer a few more questions about ALS considering our knowledge for their involvement in onset or progression is unclear.

2.7.3. Cells of the immune system

The third kind of non-neuronal cells implicated in the non-autonomous behaviour of ALS are the cells of the immune system. Like the microglial cells which are immune cells of the CNS, and have neuroprotective and neurotoxic roles based on the stages of the disease, the other cells of the immune system, namely T-cells, are also implicated in the inflammatory reactions manifesting in the disease. The neuroprotective behavior is conducted by activation of regulatory T (Tregs) lymphocytes which infiltrate the spinal cord of the patients and activate neuroprotective mechanisms in microglia. Presence of Tregs is also proposed to extend the life of the patients. In the later stages, the Tregs-M2 cell numbers reduce, while the Th1-M1 cell numbers increase leading to neurotoxicity (Chiu et al., 2008; Beers et al., 2008 and 2011).

2.7.4 The tripartite synapse: an apt site for studying ALS

The tripartite synapse is composed of three cells, the presynaptic cell, the postsynaptic cell and the glial cell which enwraps the synapse. In the context of ALS, the presynapse is the motor

neuron, the postsynapse is the muscle and this constitutes an NMJ (Fig. 1.3). Considering the contribution of non-neuronal cells to ALS pathology, and knowing that this is just the tip of the iceberg, the tripartite synapse has emerged as the perfect site for exploring the molecular mechanisms involved in ALS. The glial cells which envelop the NMJ in the PNS are Peripheral Schwann Cells and as described in section 2.7.1.4, play a crucial role in the functioning of the NMJ. Mammalian NMJ is majorly cholinergic, but recent studies have evidenced the presence and activity of glutamate at the NMJ (Liu et al., 2017; Colombo and Francolini, 2019; Nishimaru et al., 2005).

Considering the dense literature discussed in the glial cell's sections of this chapter (2.7.1), we have a fair understanding of the glial contribution to the ALS disease scenario. This contribution of glia occurs due to impairment of the cross-talk which takes place at the tripartite synapse. This cross-talk is mediated via various signalling pathways and neurotransmitters, which have specific ligands and receptors expressing in the three cells of the tripartite synapse. The release and binding of these signalling molecules from one cell type to the other amongst this trio maintains the homeostasis of this three-cell junction. To sum it all, the signalling between the glial cells and the NMJ leads to:

1. Synapse formation and synapse elimination.

2. Regulation of neurotransmission by maintaining various neurotransmitter levels as well as their specific synapses (Glutamatergic, GABAergic, Cholinergic and Glycinergic).

3. Providing metabolic support to the neurons via the glial-neuron lactate shuttle.

4. The glutamate-calcium cascade which keeps neuronal action potential under control.

5. Release of small molecules like ATP and D-serine by the glia, which act like gliotransmitters to maintain the synaptic activity.

6. The functioning of many signalling pathways (TGFβ, Wnt, TNFα) in a retrograde as well as anterograde manner at the tripartite synapse.

As discussed in the non-neuronal cell's section (2.7), some of these or a combination of these functions go haywire in case of ALS, as a result of impairment of the cross-talk at the tripartite synapse. The impairment depends on the locus which is affected and sometimes has a direct or indirect association with the function of the locus as discussed in 2.4.2. A lot of studies are currently focused at the tripartite junction of these cells to find answers concerning mechanisms

and also are trying to come up with effective therapeutic interventions to solve the complex puzzle of ALS.
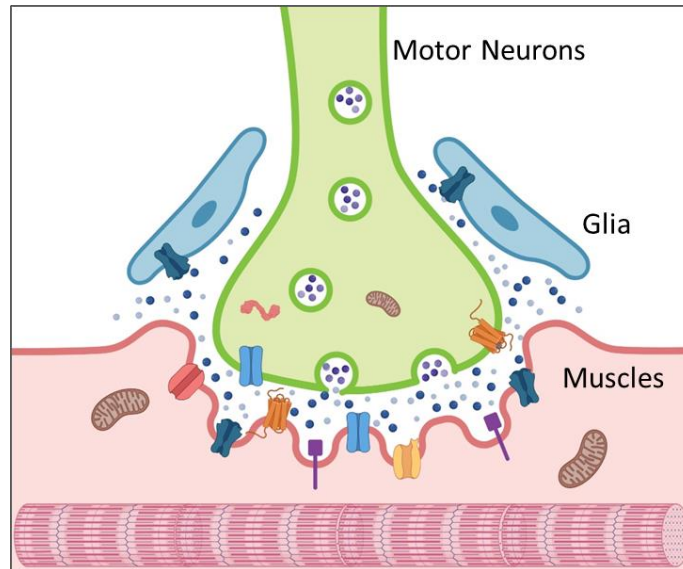
Figure 1.3. The Tripartite Synapse.
The tripartite synapse refers to functional and physical integration of glial cells with the synapse. The glial cells enwrap the synapse and are involved in crosstalk with the pre and post synapse. The coordinated activity at the tripartite synapse between the three cells results in the smooth functioning of the nervous system. There are various kinds of glial cells in the system, the astrocytes, oligodendrocytes, microglial cells and Schwann cells. While all of the glial function to coordinate the actions of the neurons, the astrocytes (in CNS) and Schwann cells (in PNS) are found at the synaptic junctions. In the case of PNS, the synapse can be a neuromuscular junction and the presynaptic cell is a motor neuron. The NMJ is predominantly cholinergic, but glutamate receptors and its release have been recently found at this cell junction. Figure designed in: BioRender App.

2.8. *Drosophila* models of ALS

Drosophila melanogaster has been used as a model organism in most neurodegenerative disorders including ALS. Due to the lack of sufficient patient samples, it is easier to model ALS in model organisms and study the fundamental mechanisms involved in the disease. These studies help us not only with understanding the disease mechanisms but also, provide clues about the therapeutic targets of ALS. Although modelling a mammalian disease in an invertebrate model system is not the best idea, but its short life span, easy handling, extensive and advanced genetic tools and about 60% homology with humans, helps researchers to gain great insights about the disease pathology (Damme et al., 2017)

Using the fruit fly has benefited the modelling of ALS as it is a genetic disease, and *Drosophila* is an excellent model for genetic studies. Transgenic flies for most of the ALS causing loci and their mutant variants have been generated in the fruit fly. The *UAS-Gal4* overexpression system adapted from yeast has worked wonders in terms of exploring cell-specific roles of the mutant variants and performing various genetic screens for uncovering genetic interactors amongst the ALS loci. Some of these studies have used human variants cloned in *Drosophila*, while some others have used *Drosophila* orthologues of these loci for the overexpression work. Apart from the *UAS-Gal4* system, making genomic constructs of the allelic variants, generating deletion or deficiencies using p-element excisions of these loci or the use of the newly discovered *Crispr-Cas9* system has helped us overcome a lot of challenges in the field of ALS research.

Various phenotypes commonly used in the fruit fly to study motor neurodegenerative disorders are motor defects in the larvae as well as adults, survival assays, lethality/eclosion rate, detection of protein aggregates, neuronal cell death, bouton size/number/various synaptic markers, differences in brain size, patterns in dendritic arborization, use of immunohistochemistry to observe different cellular defects. Another advantage of using *Drosophila* as a model system for studying a motor-neurodegenerative disorder is its functionally analogous cell types/organ system, similar cellular mechanisms and the similarity in neural signalling (Lin et al., 2017; Ugur et al., 2016).

Lastly, recent works in ALS have made use of the tripartite synapse of *Drosophila,* which is well characterized and acts as an excellent site to carry out motor neurodegenerative disorder studies. Even for non-neuronal work, *Drosophila* has analogues for all kinds of glial cells, which makes it easy for drawing parallels with this human disorder (Ou et al., 2014). We have described the *Drosophila* tripartite synapse using confocal microscopy images in the third larval NMJ (Fig. 1.4).
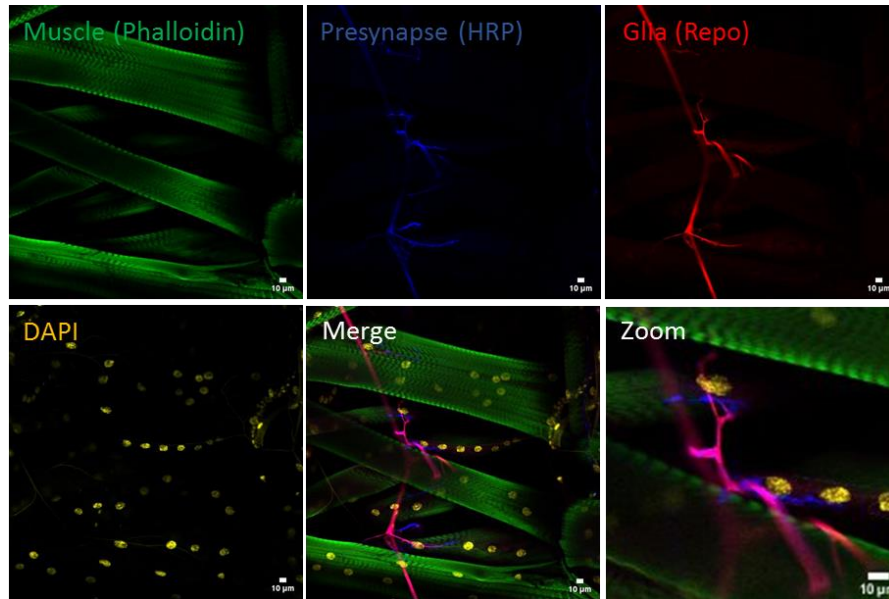
Figure 1.4. *Drosophila* **larval tripartite synapse.**
Confocal images for *Drosophila* third larval tripartite synapse. The larval NMJ is stained against phalloidin, a marker for muscles in green; presynaptic marker HRP (horseradish peroxidase) in blue; Glial marker (Repo) in red and DAPI as a marker for nucleus in yellow. The merged image shows co-localization (magenta) of glial marker on the axonal stalk. These are intensity projection images captured confocal microscopy. Refer to Materials and Methods, Chapter V, section 5.2.1 for the details on the dissections and staining protocol.

Examples of a few ALS loci studies characterized in *Drosophila* are as follows:

1. *SOD1:* Expression of human orthologues of wild type and mutant *SOD1 (A4V* and *G85R)* causes progressive climbing defects along with SOD1 aggregate accumulation in motor neurons and glial cells. This study also characterized defects in the neural circuit's electrophysiology (Watson et al., 2008).

2. *alsin: Drosophila* mutants of *alsin* show age-dependent climbing defects (Takayama et al., 2014).

3. *TDP-43/TBPH:* There are quite a lot of studies carried out on *TDP-43* in flies (the *Drosophila* orthologue is called *TBPH*). Perturbing of *TBPH* levels in the neurons caused a loss of presynaptic efficacy at the NMJ, followed by loss of neuronal connections and age-related neurodegeneration (Diaper et al., 2013). Muscle and Glia specific perturbation of *TBPH* levels are linked to sarcoplasmic aggregates, defects in localization of TBPH and premature lethality (Diaper et al., 2013a). In a study using overexpression of wild type and human mutant variants (*D169G, A315T, N345K, G298S*) of *TDP-43* in the motor neurons and glia, age-related neurodegeneration in the

adult fly retina, defects in the sleep patterns of adult flies and bouton defects in the third larval NMJs were observed (Estes et al., 2013).

4. *FUS/caz:* Overexpression of *caz (Drosophila* orthologue of *FUS)* and *FUS* mutant *(R521G)* disrupts the NMJ and causes motor neuron death (Xia et al., 2012). Overexpression of either wild type or human mutant variants (R521C and P525L) of *FUS* causes decreased presynaptic active zones and perturbed postsynaptic glutamate receptors (Machamer et al., 2014). In yet another study, overexpression of human mutants (*R521C, R518K, and R521H*) caused accumulation of ubiquitinated proteins, larval crawling defects and early lethality. This study also talks about the presence of genetic interaction between *FUS* and *TDP-43* and how it leads to their synergistic effects on neurodegeneration (Lanson Jr et al., 2011).

5. *VCP/TER94:* Overexpression of *Drosophila VCP* mutants, *TER94^{R152H} and TER94^{A229E}* (orthologues of human mutants) causes toxicity and degeneration by mis-localizing TDP-43 to the cytoplasm (Ritson et al., 2010). Another study with the same mutations proposes these be acting in a dominant-active manner when overexpressed along with wild type *TER94,* thus causing enhanced degeneration as compared to the mutants alone (Chang et al., 2011).

6. *VAPB: Drosophila* models of ALS8 have been generated by expressing the fly homolog of *VAP* carrying the corresponding ALS8 mutation, *VAP^{P58S}* (Ratnaparkhi et al., 2008; Chai et al., 2008; Tsuda et al., 2008). Overexpressing *VAP^{P58S}* in neurons and muscles affects the bouton size and number at the neuromuscular junction (NMJ) in *Drosophila* (Pennetta et al., 2002). A study in *Drosophila* suggests a dominant-negative mechanism of the mutant protein in the disease in which *VAP^{P58S}* behaves like a loss-of-function mutant and recruits the VAP^{WT} (VAP wild type) in its aggregates (Ratnaparkhi et al., 2008). However, this dominant-negative mechanism is contradicted by the genomic expression model of *VAP^{P58S}*, where the endogenous promoter of *VAP* is used to express the mutant in a *VAP^{null}* background and displays progressive survival as well as motor defects. These defects are completely rescued on the genomic expression of *VAP^{WT}* in combination with the genomic *VAP^{P58S}* in the *VAP^{null}* background, refuting the dominant-negative behavior. (Moustaquim-Barrette et al., 2013).

7. *c9orf72:* Orthologue for *c9orf72* is not yet found in *Drosophila*, however, studies concerning this locus use the expression of repeat expansions of GGGCCC to observe phenotypic changes. The expansions have been found to cause neurodegeneration by aggregation of DPRs,

accumulation of important RNA binding proteins in the RNA foci and cell-autonomous glutamate excitotoxicity (Mizielinska et al., 2014 and Xu and Xu, 2018).

2.9. Pathways perturbed in ALS

ALS is known to affect the functioning of different pathways, most of these provide molecular signals to regulate the communication at the synapse. Following are a few of these signalling pathways along with their defects in ALS:

2.9.1. TGFβ/BMP Pathway

The BMP (bone morphogenetic protein) pathway is involved in cell growth, cell differentiation and apoptosis. The levels of TGFβ1 in the CSF and serum have been reported to go up in case of terminal ALS patients (IłzJecka et al., 2002). TGFβ level is high in the astrocytes from spinal cord samples of patients as well (Endo et al., 2015). BMP pathway is involved in anterograde as well as retrograde signalling at the *Drosophila* NMJ in normal conditions, this pathway is speculated to be impaired in a model of mutant *VAP* (*VAP^{P58S}*) with a reduction in phosphorylated Smad, which is a transcription factor in the pathway (Ratnaparkhi et al., 2008). In the case of *SOD1* mutant mice models, excessive TGFβ is reported to inhibit the neuroprotective cytokines and accelerates disease progression; while administration of the TGFβ inhibitor is known to mitigate disease severity and extend survival (Endo et al., 2015). Amongst other phenotypes, deregulation of this pathway causes impaired synaptic growth, inhibition of neuroprotection and axonal degeneration (Kashima and Hata, 2018).

2.9.2. Wnt/βcatenin Pathway

Like the BMP pathway, this pathway is also involved in the development of the tripartite synapse. Wnt signalling is raised in the spinal cord of *SOD1^{G93A}* mice at the onset. Levels of Wnt inhibitors are also known to increase in these mice (Yu et al., 2013). Activation of Wnt signalling in the case of neurodegeneration leads to glial proliferation and could be involved in neuroprotection at the onset (Chen et al., 2012). Wnt and BMP pathways are known to interact and speculated to play vital roles in ALS progression (Pinto et al., 2013). Wnt pathway seems like a promising target to find an effective therapy for ALS.

2.9.3. NF-κB Pathway

NF-κB (Nuclear Factor kappa-light-chain-enhancer of activated B cells) has been involved in the interaction of several ALS genes (Dresselhaus and Meffert, 2019). This innate immune response pathway is known to be involved in the neuroinflammatory response in case of ALS. Astrocytic expression of NFκB promotes the proliferation of microglia and release of anti-inflammatory factors in the pre-symptomatic stages; whereas it regulates the release of pro-inflammatory factors in the late progressive stages of ALS (Alami et al., 2018). The activation of the NFκB pathway is proposed to be caused by Wnt released from the astrocytes in the early stages of the disease, and this helps with cell proliferation (Alami et al., 2018). NFκB is also activated by proteotoxic stress in the system, this causes accelerated neurodegeneration (Li et al., 2018). Inhibition of this pathway, therefore, causes lengthening of survival and delays motor neuron death in $SOD1^{G93A}$ mice (Frakes et al., 2014).

Apart from the three pathways described above, many other pathways are reported to be involved in ALS disease mechanisms, mTOR and Nrf2-ARE (Deivasigamani et al., 2014; Kraft et al., 2007) are some of them. Although every study describes one particular pathway and its impairment in case of the disease, it is important to understand that there is always a cross-talk between most of these pathways in the system and normal conditions there exists homeostasis between these. This homeostasis along with the smooth functioning of the gene regulatory network is lost in case of ALS and bringing it back to normal by targeting just one of the signalling moieties/pathomechanisms won't be enough. The field, therefore, requires a holistic approach to this scenario.

2.10. Open questions in the field

Considering all the discussed aspects of ALS, we realize that the more we know about the disease, the more we are puzzled about its mode of mechanisms. Although a lot of progress has been made with respect to understanding the disease, many questions remain unanswered.

Following are some of the open questions in the field:

1. Are ALS loci a part of a Gene Regulatory Network? Although we have clues for this to be true, more evidence needs to be collected to support this hypothesis. How does the alteration of the gene regulatory network of one locus affect the other?

2. Does the presence of multiple mutant variants in a single patient exacerbate the disease progression? Is there a way to find out if one of the mutations is a primary mutation and the creation/generation of the secondary mutation acts as an enhancer of the genetic penetrance? What are the pathogenic hallmarks of such combinations?

3. In the presence of a single mutation, why is there a change in the expression levels of another (wild type) disease-associated locus? Is this change responsible for the accumulation of the aggregates of its protein into the inclusions of the mutant genes' protein?

4. As glial cell contribution to the disease is crucial to both, the delaying of the disease severity at the onset as well as feeding into its rapid progression in the later stages will use of these cells as therapeutic targets provide an effective solution, if not cure, to the disease?

5. How exactly do muscles contribute to the pathogenesis of ALS? Do they participate in the onset or progression or both?

6. Considering the cross-talk between the neuronal and non-neuronal cells, will exploration of the perturbed pathways shed more light on our understanding of the non-cell autonomy, or is this perturbation only an outcome of the genetic aberrations?

7. Taking into account the oligogenicity and non-cell autonomy, ALS is a multifactorial disorder, but is there a central regulator involved which is a common thread amongst all the affected loci and the molecular pathways?

8. How important are glial-glial interactions (astrocyte-microglia, for instance) in the pathogenesis of ALS?

3. References

Abel, O. *et al*. ALSoD: A user-friendly online bioinformatics tool for amyotrophic lateral sclerosis genetics. *Hum. Mutat.* **33**, 1345–1351 (2012).Allen, N. J. & Barres, B. A. Neuroscience: Glia - more than just brain glue. *Nature* 457, 675–677 (2009).

Andersen, P. M. & Al-Chalabi, A. Clinical genetics of amyotrophic lateral sclerosis: What do we really know? *Nat. Rev. Neurol.* 7, 603–615 (2011).

Appel, S. H. *et al.* The Microglial-Motoneuron dialogue in ALS. 4–8 (2011).

Arbour, D., Vande Velde, C. & Robitaille, R. New perspectives on amyotrophic lateral sclerosis: the role of glial cells at the neuromuscular junction. *J. Physiol.* 595, 647–661 (2017).

Armon, C. An evidence-based medicine approach to the evaluation of the role of exogenous risk factors in sporadic amyotrophic lateral sclerosis. *Neuroepidemiology* 22, 217–228 (2003).

Ash, P. E. A. *et al.* NIH Public Access. 77, 639–646 (2014).

Atkin, J. D. *et al.* Endoplasmic reticulum stress and induction of the unfolded protein response in human sporadic amyotrophic lateral sclerosis. *Neurobiol. Dis.* 30, 400–407 (2008).

Azuma, Y. *et al.* Identification of ter94, drosophila VCP, as a strong modulator of motor neuron degeneration induced by knockdown of Caz, Drosophila FUS. *Hum. Mol. Genet.* 23, 3467–3480 (2014).

Bali, T. & Miller, T. M. Management of amyotrophic lateral sclerosis. *Mo. Med.* 110, 417–421 (2013).

Barbeito, L. Astrocyte-based cell therapy: new hope for amyotrophic lateral sclerosis patients? *Stem Cell Res. Ther.* 9, 241 (2018).

Bartolome, F. *et al.* Pathogenic VCP Mutations Induce Mitochondrial Uncoupling and Reduced ATP Levels. *Neuron* 78, 57–64 (2013).

Bear, Mark F., Barry W. Connors, M. A. P. Exploring the Brain.Pdf. (2007).

Beers, D. R., Henkel, J. S., Zhao, W., Wang, J. & Appel, S. H. CD4+ T cells support glial neuroprotection, slow disease progression, and modify glial morphology in an animal model of inherited ALS. *Proc. Natl. Acad. Sci. U. S. A.* 105, 15558–15563 (2008).

Beers, D. R. *et al.* Endogenous regulatory T lymphocytes ameliorate amyotrophic lateral sclerosis in mice and correlate with disease progression in patients with amyotrophic lateral sclerosis. *Brain* 134, 1293–1314 (2011).

Blitterswijk, M. Van *et al.* VAPB and C9orf72 mutations in 1 familial amyotrophic lateral sclerosis patient. *NBA* 33, 2950.e1-2950.e4 (2012).

Boylan, K. Familial ALS. *Neurol. Clin.* 33, 807–830 (2015).

Bruijn, L. I. *et al.* ALS-Linked SOD1 Mutant G85R Mediates Damage to Astrocytes and Promotes Rapidly Progressive Disease with SOD1-Containing Inclusions. 18, 327–338 (1997).

Bruijn, L. I. *et al.* Aggregation and motor neuron toxicity of an ALS-linked SOD1 mutant independent from wild-type SOD1. *Science (80-.).* 281, 1851–1854 (1998).

Buratti, E. Functional Significance of TDP-43 Mutations in Disease. *Adv. Genet.* 91, 1–53 (2015).

Burberry, A. *et al.* Loss-of-function mutations in the C9ORF72 mouse ortholog cause fatal autoimmune disease. *Sci. Transl. Med.* 8, (2016).

Burberry, A. *et al.* C9orf72 suppresses systemic and neural inflammation induced by gut bacteria. *Nature* 582, 89–94 (2020).

Bury, J. J. *et al.* Oligogenic inheritance of optineurin (OPTN) and C9ORF72 mutations in ALS highlights localisation of OPTN in the TDP-43-negative inclusions of C9ORF72-ALS. *Neuropathology* 36, 125–134 (2016).

Benjamin Rix Brooks, Robert G Miller, Michael Swash & Theodore L Munsat (2000) El Escorial revisited: Revised criteria for the diagnosis of amyotrophic lateral sclerosis, Amyotrophic Lateral Sclerosis and Other Motor Neuron Disorders

Carrì, M. T., Valle, C., Bozzo, F. & Cozzolino, M. Oxidative stress and mitochondrial damage: Importance in non-SOD1 ALS. *Front. Cell. Neurosci.* 9, 1–6 (2015).

Cedarbaum, J. M. *et al.* The ALSFRS-R: A revised ALS functional rating scale that incorporates assessments of respiratory function. *J. Neurol. Sci.* 169, 13–21 (1999).

Chai, A. *et al.* hVAPB, the causative gene of a heterogeneous group of motor neuron diseases in humans, is functionally interchangeable with its Drosophila homologue DVAP-33A at the neuromuscular junction. *Hum. Mol. Genet.* 17, 266–280 (2008).

Chen, S., *et al.* Genetics of amyotrophic lateral sclerosis: an update. *Mol Neurodegeneration* **8,** 28 (2013).

Chang, Y. C. *et al.* Pathogenic VCP/TER94 alleles are dominant actives and contribute to neurodegeneration by altering cellular ATP level in a drosophila IBMPFD model. *PLoS Genet.* 7, (2011).

Chen, H. *et al.* Characterization of the Properties of a Novel Mutation in VAPB in Familial Amyotrophic Lateral Sclerosis * □. 285, 40266–40281 (2010).

Chen, Y. *et al.* Activation of the Wnt/β-catenin signaling pathway is associated with glial proliferation in the adult spinal cord of ALS transgenic mice. *Biochem. Biophys. Res. Commun.* 420, 397–403 (2012).

Chen, Y. Z. *et al.* DNA/RNA helicase gene mutations in a form of juvenile amyotrophic lateral sclerosis (ALS4). *Am. J. Hum. Genet.* 74, 1128–1135 (2004).

Chiò, A. *et al.* HHS Public Access. 83, 730–733 (2015).

Chiu, I. M. *et al.* T lymphocytes potentiate endogenous neuroprotective inflammation in a mouse model of ALS. 105, 1–6 (2008).

Clement, A. M. *et al.* Wild-type nonneuronal cells extend survival of SOD1 mutant motor neurons in ALS mice. *Science (80-.).* 302, 113–117 (2003).

Cluskey, S. & Ramsden, D. B. Mechanisms of neurodegeneration in amyotrophic lateral sclerosis. *J. Clin. Pathol. - Mol. Pathol.* 54, 386–392 (2001).

Colombo, M. N. & Francolini, M. Glutamate at the Vertebrate Neuromuscular Junction: From Modulation to Neurotransmission. *Cells* 8, (2019).

Daoud, H. & Rouleau, G. A. Amyotrophic lateral sclerosis: A role for ubiquilin 2 mutations in neurodegeneration. *Nat. Rev. Neurol.* 7, 599–600 (2011).

Deivasigamani, S., Verma, H. K., Ueda, R., Ratnaparkhi, A. & Ratnaparkhi, G. S. A genetic screen identifies Tor as an interactor of VAPB in a Drosophila model of amyotrophic lateral sclerosis. *Biol. Open* 3, 1127–1138 (2014).

Deng, H. *et al.* HHS Public Access. 477, 211–215 (2012).

Deng, H. *et al.* FUS-Immunoreactive Inclusions Are a Common Feature in Sporadic and Non-SOD1 Familial Amyotrophic Lateral Sclerosis. (2010). doi:10.1002/ana.22051

Diaper, D. C. *et al.* Loss and gain of Drosophila TDP-43 impair synaptic efficacy and motor control leading to age-related neurodegeneration by loss-of-function phenotypes. *Hum. Mol. Genet.* 22, 1539–1557 (2013).

Diaper, D. C. *et al.* Drosophila TDP-43 dysfunction in glia and muscle cells cause cytological and behavioural phenotypes that characterize ALS and FTLD. 1–11 (2013). doi:10.1093/hmg/ddt243

Dobrowolny, G. *et al.* Skeletal Muscle Is a Primary Target of SOD1G93A-Mediated Toxicity. *Cell Metab.* 8, 425–436 (2008).

Dobrowolny, G. *et al.* Muscle expression of a local Igf-1 isoform protects motor neurons in an ALS mouse model. *J. Cell Biol.* 168, 193–199 (2005).

Donnelly, C. J. *et al.* NIH Public Access. 80, 415–428 (2014).

Dresselhaus, E. C. & Meffert, M. K. Cellular specificity of NF-κB function in the nervous system. *Front. Immunol.* 10, (2019).

Drory, V. E., Goltsman, E., Goldman Reznik, J., Mosek, A. & Korczyn, A. D. The value of muscle exercise in patients with amyotrophic lateral sclerosis. *J. Neurol. Sci.* 191, 133–137 (2001).

Endo, F. *et al.* Astrocyte-Derived TGF-β1 Accelerates Disease Progression in ALS Mice by Interfering with the Neuroprotective Functions of Microglia and T Cells. *Cell Rep.* 11, 592–604 (2015).

Estes, P. S. *et al.* Motor neurons and glia exhibit specific individualized responses to TDP-43 expression in a Drosophila model of amyotrophic lateral sclerosis. *DMM Dis. Model. Mech.* 6, 721–733 (2013).

Geloso, M. C. *et al.* The dual role of microglia in ALS: Mechanisms and therapeutic approaches. *Front. Aging Neurosci.* 9, (2017).

Gitcho, M. A. *et al.* VCP mutations causing frontotemporal lobar degeneration disrupt localization of TDP-43 and induce cell death. *J. Biol. Chem.* 284, 12384–12398 (2009).

Gitler, A. D. & Tsuiji, H. There has been an awakening: Emerging mechanisms of C9orf72 mutations in FTD/ALS. *Brain Res.* 1647, 19–29 (2016).

Guo, H. *et al.* Increased expression of the glial glutamate transporter EAAT2 modulates excitotoxicity and delays the onset but not the outcome of ALS in mice. *Hum. Mol. Genet.* 12, 2519–2532 (2003).

Guo, W. *et al.* An ALS-associated mutation affecting TDP-43 enhances protein aggregation, fibril formation and neurotoxicity. 18, (2011).

Gusev et al., Chapter 4. The Glutamate-Calcium Cascade The induction stage : energy-dependent ion pump failure and glutamate excitotoxicity. (2003).

Hadano, S. *et al.* A gene encoding a putative GTPase regulator is mutated in familial amyotrophic lateral sclerosis 2. *Nat. Genet.* 29, 166–173 (2001).

Hall, C. E. *et al.* Progressive Motor Neuron Pathology and the Role of Astrocytes in a Human Stem Cell Model of VCP-Related ALS. *Cell Rep.* 19, 1739–1749 (2017).

Hensley, K. *et al.* On the relation of oxidative stress to neuroinflammation: Lessons learned from the G93A-SOD1 mouse model of amyotrophic lateral sclerosis. *Antioxidants Redox Signal.* 8, 2075–2087 (2006).

Hentati, A. *et al.* Linkage of recessive familial amyotrophic lateral sclerosis to chromosome 2q33–q35. *Nat. Genet.* 7, 425–428 (1994).

Hosler, B. A., Cortelli, P., Jong, P. J. De, Yoshinaga, Y. & Haines, J. L. Mutations in the FUS/TLS Gene on Chromosome 16 Cause Familial Amyotrophic Lateral Sclerosis. 547, 1205–1209 (2009).

Howland, D. S. *et al.* Focal loss of the glutamate transporter EAAT2 in a transgenic rat model of SOD1 mutant-mediated amyotrophic lateral sclerosis (ALS). *Proc. Natl. Acad. Sci. U. S. A.* 99, 1604–1609 (2002).

Hung, S. *et al.* HHS Public Access. 24, 313–325 (2018).

Iyer, S., Subramanian, V. & Acharya, K. R. C9orf72, a protein associated with amyotrophic lateral sclerosis (ALS) is a guanine nucleotide exchange factor. *PeerJ* 2018, (2018).

Izrael, M. *et al.* Safety and efficacy of human embryonic stem cell-derived astrocytes following intrathecal transplantation in SOD1 G93A and NSG animal models. *Stem Cell Res. Ther.* 9, 1–17 (2018).

Jacquier, A., Bellouze, S., Blanchard, S., Bohl, D. & Haase, G. Astrocytic protection of spinal motor neurons but not cortical neurons against loss of Als2/alsin function. *Hum. Mol. Genet.* 18, 2127–2139 (2009).

Jaiswal, M. K. Riluzole and edaravone: A tale of two amyotrophic lateral sclerosis drugs. *Med. Res. Rev.* 39, 733–748 (2019).

Johnson, J. O. *et al.* Report Exome Sequencing Reveals VCP Mutations as a Cause of Familial ALS. 857–864 (2010). doi:10.1016/j.neuron.2010.11.036

Jokic, N. *et al.* Nogo expression in muscle correlates with amyotrophic lateral sclerosis severity. *Ann. Neurol.* 57, 553–556 (2005).

Jr, N. A. L. *et al.* A Drosophila model of FUS-related neurodegeneration reveals genetic interaction between FUS and TDP-43. 1–14 (2011). doi:10.1093/hmg/ddr150

Jr, N. A. L. & Pandey, U. B. FUS-related proteinopathies : Lessons from animal models. *Brain Res.* 1462, 44–60 (2012).

Ju, J. S. *et al.* Valosin-containing protein (VCP) is required for autophagy and is disrupted in VCP disease. *J. Cell Biol.* 187, 875–888 (2009).

Kanekura, K., Nishimoto, I., Aiso, S. & Matsuoka, M. Characterization of amyotrophic lateral sclerosis-linked P56S mutation of vesicle-associated membrane protein-associated protein B (VAPB/ALS8). *J. Biol. Chem.* 281, 30223–30233 (2006).

Kang, S. H. *et al.* Degeneration and impaired regeneration of gray matter oligodendrocytes in amyotrophic lateral sclerosis. *Nat. Neurosci.* 16, 571–579 (2013).

Kashima, R. & Hata, A. The role of TGF-β superfamily signaling in neurological disorders. *Acta Biochim. Biophys. Sin. (Shanghai).* 50, 106–120 (2018).

Kawamata, T., Akiyama, H., Yamada, T. & McGeer, P. L. Immunologic reactions in amyotrophic lateral sclerosis brain and spinal cord tissue. *Am. J. Pathol.* 140, 691–707 (1992).

Kraft AD, Resch JM, Johnson DA, Johnson JA. Activation of the Nrf2-ARE pathway in muscle and spinal cord during ALS-like pathology in mice expressing mutant SOD1. *Exp Neurol.* (2007).

Kim, S. H., Shanware, N. P., Bowler, M. J. & Tibbetts, R. S. Amyotrophic lateral sclerosis-associated proteins TDP-43 and FUS/TLS function in a common biochemical complex to co-regulate HDAC6 mRNA. *J. Biol. Chem.* 285, 34097–34105 (2010).

Kunst, C. B. Complex genetics of amyotrophic lateral sclerosis. *Am. J. Hum. Genet.* 75, 933–947 (2004).

Kushimura, Y. *et al.* Overexpression of ter94, Drosophila VCP, improves motor neuron degeneration induced by knockdown of TBPH, Drosophila TDP-43. *Am. J. Neurodegener. Dis.* 7, 11–31 (2018).

Lanson, N. A. *et al.* A Drosophila model of FUS-related neurodegeneration reveals genetic interaction between FUS and TDP-43. *Hum. Mol. Genet.* 20, 2510–2523 (2011).

Lee, Y. *et al.* Oligodendroglia metabolically support axons and contribute to neurodegeneration. *Nature* 487, 443–448 (2012).

Liao, B., Zhao, W., Beers, D. R., Henkel, J. S. & Appel, S. H. Transformation from a neuroprotective to a neurotoxic microglial phenotype in a mouse model of ALS. *Exp. Neurol.* 237, 147–152 (2012).

Lin, C. L. G. *et al.* Aberrant RNA processing in a neurodegenerative disease: The cause for absent EAAT2, a glutamate transporter, in amyotrophic lateral sclerosis. *Neuron* 20, 589–602 (1998).

Lin, G., Mao, D. & Bellen, H. J. Amyotrophic Lateral Sclerosis Pathogenesis Converges on Defects in Protein Homeostasis Associated with TDP-43 Mislocalization and Proteasome-Mediated Degradation Overload. *Curr. Top. Dev. Biol.* 121, 111–171 (2017).

Ling, S. C., Polymenidou, M. & Cleveland, D. W. Converging mechanisms in als and FTD: Disrupted RNA and protein homeostasis. *Neuron* 79, 416–438 (2013).

Ling, S., Albuquerque, C. P., Seok, J., Lagier-tourenne, C. & Tokunaga, S. ALS-associated mutations in TDP-43 increase its stability and promote TDP-43 complexes with FUS / TLS. (2010). doi:10.1073/pnas.1008227107/-/DCSupplemental.www.pnas.org/cgi/doi/10.1073/pnas.1008227107

Liu, L., MacKenzie, K. R., Putluri, N., Maletić-Savatić, M. & Bellen, H. J. The Glia-Neuron Lactate Shuttle and Elevated ROS Promote Lipid Synthesis in Neurons and Lipid Droplet Accumulation in Glia via APOE/D. *Cell Metab.* 26, 719-737.e6 (2017).

Lobsiger, C. S. *et al.* Schwann cells expressing dismutase active mutant SOD1 unexpectedly slow disease progression in ALS mice. *Proc. Natl. Acad. Sci. U. S. A.* 106, 4465–4470 (2009).

Machamer, J. B., Collins, S. E. & Lloyd, T. E. The ALS gene FUS regulates synaptic transmission at the Drosophila neuromuscular junction. 23, 3810–3822 (2014).

Martin, S., Al Khleifat, A. & Al-Chalabi, A. What causes amyotrophic lateral sclerosis? *F1000Research* 6, 1–10 (2017).

Mathis, S., Goizet, C., Soulages, A., Vallat, J. M. & Masson, G. Le. Genetics of amyotrophic lateral sclerosis: A review. *J. Neurol. Sci.* 399, 217–226 (2019).

Mejzini, R. *et al.* ALS Genetics, Mechanisms, and Therapeutics: Where Are We Now? *Front. Neurosci.* 13, 1–27 (2019).

Meyer, K. *et al.* Direct conversion of patient fibroblasts demonstrates non-cell autonomous toxicity of astrocytes to motor neurons in familial and sporadic ALS. *Proc. Natl. Acad. Sci. U. S. A.* 111, 829–832 (2014).

Meyer, H. & Weihl, C. C. The VCP/p97 system at a glance: Connecting cellular function to disease pathogenesis. *J. Cell Sci.* 127, 3877–3883 (2014).

Mizielinska, S. *et al.* F (8). 345, 1192–1195 (2014).

Moustaqim-barrette, A. *et al.* The amyotrophic lateral sclerosis 8 protein, VAP, is required for ER protein quality control. *Hum. Mol. Genet.* 23, 1975–1989 (2014).

Nalbandian, A. *et al.* A Progressive Translational Mouse Model of Human VCP Disease: The VCP R155H/+ Mouse. *Muscle Nerve* 47, 260–270 (2013).

Neumann, M. *et al.* TDP-43-positive white matter pathology in frontotemporal lobar degeneration with ubiquitin-positive inclusions. *J. Neuropathol. Exp. Neurol.* 66, 177–183 (2007).

Neumann, M. *et al.* A new subtype of frontotemporal lobar degeneration with FUS pathology. *Brain* 132, 2922–2931 (2009).

Neumann, M. *et al.* Ubiquitinated TDP-43 in Frontotemporal Lobar Degeneration and Amyotrophic Lateral Sclerosis.

Nguyen, M. D., D'Aigle, T., Gowing, G., Julien, J. P. & Rivest, S. Exacerbation of Motor Neuron Disease by Chronic Stimulation of Innate Immunity in a Mouse Model of Amyotrophic Lateral Sclerosis. *J. Neurosci.* 24, 1340–1349 (2004).

Nishimaru, H., Restrepo, C. E., Ryge, J., Yanagawa, Y. & Kiehn, O. Mammalian motor neurons corelease glutamate and acetylcholine at central synapses. *Proc. Natl. Acad. Sci. U. S. A.* 102, 5245–5249 (2005).

Nishimura, A. L. *et al.* A mutation in the vesicle-trafficking protein VAPB causes late-onset spinal muscular atrophy and amyotrophic lateral sclerosis. *Am. J. Hum. Genet.* 75, 822–831 (2004).

Nishimura, A. L. *et al.* References and Notes 1. 323, 1208–1211 (2009).

O'Rourke, J. G. *et al.* C9orf72 is required for proper macrophage and microglial function in mice. *Science (80-.).* 351, 1324–1329 (2016).

Otomo, A. *et al.* ALS2, a novel guanine nucleotide exchange factor for the small GTPase Rab5, is implicated in endosomal dynamics. *Hum. Mol. Genet.* 12, 1671–1687 (2003).

Ou, J. *et al.* Glial cells in neuronal development: Recent advances and insights from Drosophila melanogaster. *Neurosci. Bull.* 30, 584–594 (2014).

Ouali Alami, N. *et al.* NF-κB activation in astrocytes drives a stage-specific beneficial neuroimmunological response in ALS. *EMBO J.* 37, 1–23 (2018).

Pennetta, G., Hiesinger, P. R., Fabian-Fine, R., Meinertzhagen, I. A. & Bellen, H. J. Drosophila VAP-33A directs bouton formation at neuromuscular junctions in a dosage-dependent manner. *Neuron* 35, 291–306 (2002).

Perez-Nievas, B. G. & Serrano-Pozo, A. Deciphering the astrocyte reaction in Alzheimer's disease. *Front. Aging Neurosci.* 10, 1–23 (2018).

Philips, T. *et al.* Oligodendrocyte dysfunction in the pathogenesis of amyotrophic lateral sclerosis. *Brain* 136, 471–482 (2013).

Pinto, C., Cárdenas, P., Osses, N. & Henríquez, J. P. Characterization of Wnt/β-catenin and BMP/Smad signaling pathways in an in vitro model of amyotrophic lateral sclerosis. *Front. Cell. Neurosci.* 7, 1–15 (2013).

Ramesh, N. & Pandey, U. B. Autophagy dysregulation in ALS: When protein aggregates get out of hand. *Front. Mol. Neurosci.* 10, 1–18 (2017).

Ratnaparkhi, A., Lawless, G. M., Schweizer, F. E., Golshani, P. & Jackson, G. R. A Drosophila model of ALS: Human ALS-associated mutation in VAP33A suggests a dominant negative mechanism. *PLoS One* 3, (2008).

Reaume AG, Elliott JL, Hoffman EK, et al. Motor neurons in Cu/Zn superoxide dismutase-deficient mice develop normally but exhibit enhanced cell death after axonal injury. *Nat Genet*. (1996).

Renton, A. E., Chiò, A. & Traynor, B. J. State of play in amyotrophic lateral sclerosis genetics. *Nat. Neurosci.* 17, 17–23 (2014).

Renton, A. E. *et al.* NIH Public Access. 72, 257–268 (2012).

Ritson, G. P. *et al.* TDP-43 mediates degeneration in a novel Drosophila model of disease caused by mutations in VCP/p97. *J. Neurosci.* 30, 7729–7739 (2010).

Robberecht, W. & Philips, T. The changing scene of amyotrophic lateral sclerosis. *Nat. Rev. Neurosci.* 14, 248–264 (2013).

Ron, D. & Walter, P. Signal integration in the endoplasmic reticulum unfolded protein response. *Nat. Rev. Mol. Cell Biol.* 8, 519–529 (2007).

Rosen, D. R. *et al.* lateral sclerosis. 362, 59–62 (1993).

Rostalski, H. *et al.* Astrocytes and microglia as potential contributors to the pathogenesis of C9orf72 repeat expansion-associated FTLD and ALS. *Front. Neurosci.* 13, 1–11 (2019).

Rothstein, J. D. Current Hypotheses for the Underlying Biology of Amyotrophic Lateral Sclerosis. 3–9 (2009). doi:10.1002/ana.21543

Rutherford, N. J. *et al.* Novel Mutations in TARDBP (TDP-43) in Patients with Familial Amyotrophic Lateral Sclerosis. 4, 1–8 (2008).

Smethurst, P. *et al.* Distinct responses of neurons and astrocytes to TDP-43 proteinopathy in amyotrophic lateral sclerosis. *Brain* 143, 430–440 (2020).

Spiller, K. J. *et al. degeneration in a mouse model of TDP-43 proteinopathy*. 21, (2018).

Stevens, B. Glia: much more than the neuron's side-kick. *Curr. Biol.* 13, 469–472 (2003).

Stoica, R. *et al.* ER–mitochondria associations are regulated by the VAPB–PTPIP51 interaction and are disrupted by ALS/FTD-associated TDP-43. (2014). doi:10.1038/ncomms4996

Takayama, Y., Itoh, R. E., Tsuyama, T. & Uemura, T. Age-dependent deterioration of locomotion in Drosophila melanogaster deficient in the homologue of amyotrophic lateral sclerosis 2. *Genes to Cells* 19, 464–477 (2014).

Tan, R. H. *et al.* Distinct TDP-43 inclusion morphologies in frontotemporal lobar degeneration with and without amyotrophic lateral sclerosis. *Acta Neuropathol. Commun.* 5, 76 (2017).

Taylor, J. P., Brown, R. H. & Cleveland, D. W. Decoding ALS: From genes to mechanism. *Nature* 539, 197–206 (2016).

Teuling, E. *et al.* Motor Neuron Disease-Associated Mutant Vesicle- Associated Membrane Protein-Associated Protein (VAP) B Recruits Wild-Type VAPs into Endoplasmic Reticulum- Derived Tubular Aggregates. 27, 9801–9815 (2007).

Thun, M. J. The New England Journal of Medicine Downloaded from nejm.org on March 29, 2011. For personal use only. No other uses without permission. *N. Engl. J. Med.* 329, 977–986 (1991).

Tong, J. *et al.* Expression of ALS-linked TDP-43 mutant in astrocytes causes non-cell-autonomous motor neuron death in rats. 32, 1917–1926 (2013).

Trageser, K. J., Smith, C., Herman, F. J., Ono, K. & Pasinetti, G. M. Mechanisms of Immune Activation by c9orf72-Expansions in Amyotrophic Lateral Sclerosis and Frontotemporal Dementia. *Front. Neurosci.* 13, 1–15 (2019).

TROOST, D., van den OORD, J. J. & JONG, J. M. B. V. DE. Immunohistochemical characterization of the inflammatory infiltrate in amyotrophic lateral sclerosis. *Neuropathol. Appl. Neurobiol.* 16, 401–410 (1990).

Tsuda, H. *et al.* The Amyotrophic Lateral Sclerosis 8 Protein VAPB Is Cleaved, Secreted, and Acts as a Ligand for Eph Receptors. *Cell* 133, 963–977 (2008).

Tudor, E. L. *et al.* Amyotrophic lateral sclerosis mutant vesicle-associated membrane protein-associated protein-B transgenic mice develop TAR-DNA-binding protein-43 pathology. *Neuroscience* 167, 774–785 (2010).

Turner, M. R., Wotton, C., Talbot, K. & Goldacre, M. J. Cardiovascular fitness as a risk factor for amyotrophic lateral sclerosis: Indirect evidence from record linkage study. *J. Neurol. Neurosurg. Psychiatry* 83, 395–398 (2012).

Ugur, B., Chen, K. & Bellen, H. J. Drosophila tools and assays for the study of human diseases. *DMM Dis. Model. Mech.* 9, 235–244 (2016).

Van Blitterswijk, M. *et al.* Evidence for an oligogenic basis of amyotrophic lateral sclerosis. *Hum. Mol. Genet.* 21, 3776–3784 (2012).

Van Damme, P., Robberecht, W. & Van Den Bosch, L. Modelling amyotrophic lateral sclerosis: Progress and possibilities. *DMM Dis. Model. Mech.* 10, 537–549 (2017).

Van Den Bosch, L., Tilkin, P., Lemmens, G. & Robberecht, W. Minocycline delays disease onset and mortality in a transgenic model of ALS. *Neuroreport* 13, 1067–1070 (2002).

van der Zee, J. *et al.* A Pan-European Study of the C9orf72 Repeat Associated with FTLD: Geographic Prevalence, Genomic Instability, and Intermediate Repeats. *Hum. Mutat.* 34, 363–373 (2013).

Vaz, B., Halder, S. & Ramadan, K. Role of p97/VCP (Cdc48) in genome stability. *Front. Genet.* 4, 1–14 (2013).

Watson, M. R., Lagow, R. D., Xu, K., Zhang, B. & Bonini, N. M. A Drosophila model for amyotrophic lateral sclerosis reveals motor neuron damage by human SOD1. *J. Biol. Chem.* 283, 24972–24981 (2008).

Watts, G. D. J. *et al.* Inclusion body myopathy associated with Paget disease of bone and frontotemporal dementia is caused by mutant valosin-containing protein. *Nat. Genet.* 36, 377–381 (2004).

Weihl, C. C., Dalal, S., Pestronk, A. & Hanson, P. I. Inclusion body myopathy-associated mutations in p97/VCP impair endoplasmic reticulum-associated degradation. *Hum. Mol. Genet.* 15, 189–199 (2006).

Weisskopf, M. G. *et al.* Prospective study of chemical exposures and amyotrophic lateral sclerosis. *J. Neurol. Neurosurg. Psychiatry* 80, 558–561 (2009).

Weydt, P., Yuen, E. C., Ransom, B. R. & Möller, T. Increased cytotoxic potential of microglia from ALS-transgenic mice. *Glia* 48, 179–182 (2004).

Wijesekera, L. C. & Leigh, P. N. Amyotrophic lateral sclerosis. *Orphanet J. Rare Dis.* 4, 1–22 (2009).

Wilms, H. *et al.* Involvement of benzodiazepine receptors in neuroinflammatory and neurodegenerative diseases: Evidence from activated microglial cells in vitro. *Neurobiol. Dis.* 14, 417–424 (2003).

Xia, R. *et al.* Motor neuron apoptosis and neuromuscular junction perturbation are prominent features in a Drosophila model of Fus-mediated ALS. *Mol. Neurodegener.* 7, 10 (2012).

Xu, W. & Xu, J. C9orf72 dipeptide repeats cause selective neurodegeneration and cell-autonomous excitotoxicity in Drosophila glutamatergic neurons. *J. Neurosci.* 38, 7741–7752 (2018).

Yamanaka, K. *et al.* Mutant SOD1 in cell types other than motor neurons and oligodendrocytes accelerates onset of disease in ALS mice. 105, (2008).

Yamanaka, K. & Komine, O. The multi-dimensional roles of astrocytes in ALS. *Neurosci. Res.* 126, 31–38 (2018).

Yu L, Guan Y, Wu X, et al. Wnt Signaling is altered by spinal cord neuronal dysfunction in amyotrophic lateral sclerosis transgenic mice. *Neurochem Res*. (2013)

Zarei, S. *et al.* A comprehensive review of amyotrophic lateral sclerosis. *Surg. Neurol. Int.* 6, (2015).

Zhao, C. *et al.* Mutant C9orf72 human iPSC-derived astrocytes cause non-cell autonomous motor neuron pathophysiology. *Glia* 68, 1046–1064 (2020).

Chapter II

A *Drosophila* model for ALS8

1. Summary

In humans, ALS8 is caused by mutations in *VAPB*, a single pass ER resident membrane protein. For my research, I have used the *VAPB* locus to explore mechanisms of the disease. In this chapter, I use a variant of the null; *genomic*-rescue system developed by Hiroshi Tsuda's laboratory for my studies. The system employs rescues of lethality of *ΔVAP* with the expression of *VAP-33A^{P58S}*, driven by the *VAP* endogenous promoter and is referred to in this Thesis as the 'Tsuda model'.

The variation in our experiments is the use of the strong *Δ166* hypomorphic line rather than the *Δ31* line used in the Tsuda laboratory. As a first step, we have characterized the *ΔVAP; genomic VAP-33A^{P58S}* flies for their survival and motor defects and have found that our model is at par with the Tsuda model. Additionally, we have characterized VAP aggregates in the brain along with changes in lipid levels with age. The characterization sets up a platform for uncovering novel molecular mechanisms that may be an important facet of the disease (Chapter III, Chapter IV and Chapter V). The *ΔVAP*; *genomic*-rescue system offers distinct advantages over the overexpression systems that were used to model the disease previously (Deivasagamini et al, 2014; Chaplot et al., 2019).

2. Introduction

VAPB, an ALS8 causative locus, was found by Nishimura and group based on a linkage analysis study in a Caucasian Brazilian family in 2004 (Nishimura et al., 2004). As indicated in the introductory chapter, so far only two ALS causing mutations in this gene have been discovered, *VAPB^{P56S}* and *VAPB^{T46I}* (Chapter I, 2.4.2.2). In our work, we have focused on *VAPB^{P56S}*, a mutation in the N-terminal MSP domain of the protein as *VAPB^{P56S}* is a better studied mutation. My research utilizes the well-conserved *Drosophila* analogue of *VAPB^{P56S}* i.e. *VAP-33A^{P58S}* (hereafter referred to as *VAP^{P58S}*).

Various studies in *Drosophila* have used the *UAS-GAL4* system to characterize the ALS8 disease model. These studies have explored the effect of mutant *VAP* on its cellular functions like ER-Golgi trafficking, mitochondrial biogenesis, microtubule organization, vesicle trafficking,

autophagy and unfolded protein response (Pennetta et al., 2002, Tsuda et al., 2008; Han et al., 2013; Skehel et al., 1995; Soussan et al., 1999; Kawano et al., 2006; Sanheuza et al., 2014 and Ratnaparkhi et al., 2008). Most of these functions are mediated by the MSP domain (Fig. 2.1.) as a result of either its interaction with other proteins or its signalling at the NMJ. The VAP^{P58S} mutation disrupts the native state of the MSP domain, causing the misfolding of VAP and loss of its many functions (Nishimura et al., 2004; Kanekura et al., 2006 and Teuling et al., 2007).

In our lab, we used the overexpression system in the past to perform two separate screens, to identify genetic interactors of *VAP*. The first screen used overexpression of *VAP^{WT}* and a readout of adult thoracic macrochaetae numbers (Deivasigamani et al., 2014), while the second screen measured change in the kinetics of VAP^{P58S}:GFP aggregates (Chaplot et al., 2018) as a means to uncover genetic interactors.
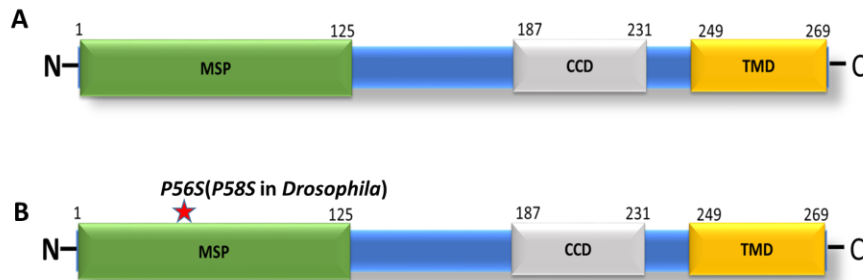
Figure 2.1. Structure of VAP.
A) VAP has three domains, the N-terminal Major sperm protein (MSP) domain, the central coiled coiled domain (CCD) and the C-Terminal Transmembrane domain. The MSP domain participates in the interactions and signalling functions of VAP. The TMD is involved in anchoring VAP on the membranes. **B)** The *P56S (P58S* in *Drosophila)* mutation occurs in the MSP domain and disrupts functions of VAP.

2.1. The Tsuda model for ALS8

Hiroshi Tsuda and colleagues developed a novel system to study the effect of replacing VAPB^{WT} with VAPB^{P58S} (Moustaqim-Barrette et al., 2013). Rather than using an expression system where the desired gene is overexpressed in presence of its endogenous copy, Tsuda and colleagues used an endogenous genomic promoter for expression of mutant and wild type *VAP* thus restoring the level of mRNA/protein to endogenous levels. This expression was carried out in

VAP^{null} genetic background. The *VAP^{null}* used in this work is the Δ*31* allele of *VAP*, which is the outcome of an imprecise excision of the P-element present in *yw, P{Mae-UAS.6.11}, Vap-33-1GG01069* site on the X chromosome of the fly. This imprecise excision led to complete loss of *VAP-33A*, resulting in no detection of protein in the western blot when probed with VAP antibody. The flies of *VAP^{Δ31}* show early lethality at the pupal stages with a few escaper flies. This study further characterized the flies of *VAP^{Δ31}* and demonstrated an increase in ER stress and the accumulation of ubiquitinated proteins. These flies also exhibited abnormalities in the transport of OSBP (Oxysterol binding protein), a protein known to interact with the MSP domain of VAP via its FFAT (two phenylalanines in an acidic tract) motif (Moustaqim-Barrette et al., 2013). OSBP is a lipid-binding protein, necessary for lipid transport from the ER to Golgi, hence involved in the maintenance of sterol homeostasis and vesicle transport. OSBP, like many other lipid-binding FFAT motif-containing proteins (Loewen et al., 2003; Kawano et al., 2006 and Baron et al., 2014), uses VAP as an adaptor on the ER for its ER-Golgi translocation (Wyles et al., 2002).

The *VAP^{Δ31}* flies were further introduced with a genomic copy of *VAP^{P58S}* and *VAP^{WT}* as two separate sets using a p-element site-specific insertion, to study the effects of physiologically regulated *VAP* (mutant or wild type) in a null background. To elaborate, the expression of the genomic copies of *VAP^{P58S}* and *VAP^{WT}* was regulated by their native promoters with expression of mRNA/protein at physiological levels. This system is an improvement over the *UAS-Gal4* overexpression system in terms of controlling the dosage of a gene. The genomic introduction of *VAP^{P58S}* and *VAP^{WT}* caused rescue of pupal lethality associated with *VAP^{Δ31}*. The *VAP^{Δ31}; genomic VAP^{P58S}* flies, however, exhibited reduced lifespan, progressive flight defect, progressive climbing defect, CNS defects, defects in ERQC (ER quality control), and defects in the transport of OSBP, suggesting that *genomic VAP^{P58S}* is a partial loss-of-function allele. These defects were not observed in the case of *VAP^{Δ31}; genomic VAP^{WT}* flies, making it a suitable control for the ALS8 disease model (Moustaqim-Barrette et al., 2013).

Based on the data published by the Tsuda laboratory (Moustaqim-Barrette et al., 2013) *VAP^{Δ31}; genomic VAP^{P58S}* flies appear to be an excellent disease model for studying ALS8 and for that reason we generated an equivalent model in our laboratory. A comparison of the Tsuda model of ALS8 with the overexpression system used for ALS8 studies is depicted in Figure 2.2.

A. Tsuda's model

Introduction and expression of *genomic VAP^{P58S}* in a *VAP^{null}* Fly

Transcriptional activation of VAP^{P58S} gene under physiologically regulated conditions

Enhancer

Promoter for VAP **VAP^{P58S}**

Endogenous promoter driven expression of VAP^{P58S} in the whole fly
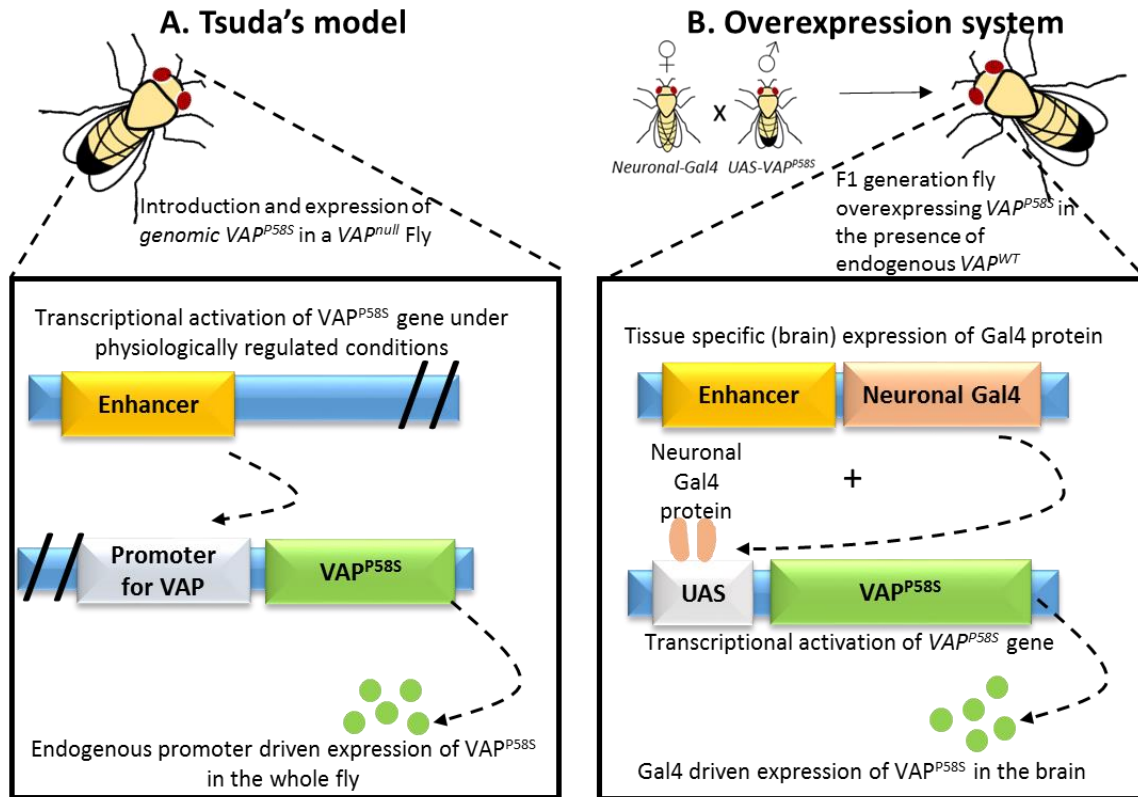
- Ubiquitous expression of VAP^{P58S}
- Absence of endogenous wild type VAP
- Regulated expression of *VAP^{P58S}*
- Short lifespan
- Progressive motor defects

B. Overexpression system

Neuronal-Gal4 *UAS-VAP^{P58S}*

F1 generation fly overexpressing *VAP^{P58S}* in the presence of endogenous *VAP^{WT}*

Tissue specific (brain) expression of Gal4 protein

Enhancer **Neuronal Gal4**

Neuronal Gal4 protein +

UAS **VAP^{P58S}**

Transcriptional activation of *VAP^{P58S}* gene

Gal4 driven expression of VAP^{P58S} in the brain

- Tissue (Brain) specific overexpression of VAP^{P58S}
- Presence of endogenous wild type VAP
- Excessive unregulated VAP^{P58S} expression
- No lifespan defects
- No motor defects
- Aggregates present in larval and adult brain

Figure 2.2. Comparison between the Tsuda's model for ALS8 and overexpression system used to study ALS8.

A) Tsuda's model: The *VAP^{P58S}* was introduced in the fly by means of p-element site specific insertion. The expression of *VAP^{P58S}* is controlled by the native promotor of VAP, cloned upstream of the gene. This expression is therefore termed as genomic expression as it is regulated by the inherent machinery of the fly. There is no endogenous expression of VAP, as the genomicVAPP58S is inserted in *VAP$^{\Delta31}$* flies (null for *VAP*). These flies exhibit progressive motor defects and lifespan defects. Tsuda and colleagues did not look for presence of VAP positive puncta in this study.

B) Overexpression system: Many studies have used the *UAS-Gal4* system to overexpress *VAP^{P58S}* in the neurons and study its effects in the flies. This site specific expression's dosage is not under the physiological regulation and therefore the excess levels of the resulting protein (VAP^{P58S}) can lead to artefacts. Also, the endogenous VAP^{WT} in these flies is not deleted and hence it can interfere with the results unlike the Tsuda's

system. These flies do not show any progressive motor defects. They have been used for VAP^{P58S} aggregate-related studies.

2.2. *VAP-33A$^{\Delta166}$; genomic VAP^{P58S}* fly line, is a ALS8 disease model in *Drosophila*

In this chapter, we have characterized another loss-of-function allele of *VAP* i.e. the *VAP-33A$^{\Delta166}$* (donated by Prof. Hugo Bellen). The original genetic background of this fly line is a genomic deletion in the X chromosome, created through imprecise excision of a P element *P{ry_t7.2_lArB}47,* around 600bp upstream of VAP-33A's AUG sequence. This caused the deletion of 1Kb in the *VAP-33A* gene, encoding a truncated protein of around 20KDa and leading to the creation of a strong hypomorphic allele of *VAP$^{\Delta166}$* (Pennetta et al., 2002). The difference between the *VAP$^{\Delta31}$* of Hiroshi Tsuda and *VAP$^{\Delta166}$* of Hugo Bellen is the complete absence of protein in *VAP$^{\Delta31}$* versus presence of truncated, non-functional protein in *VAP$^{\Delta166}$*. In the *VAP$^{\Delta166}$* fly, I introduced *genomic VAP^{P58S}* and *genomic VAP^{WT}* (donated by Prof. Hiroshi Tsuda), both genomic constructs being on the third chromosome, in two separate sets. The result of this modification was the generation of two critical lines that were used for all my research, namely *VAP-33A$^{\Delta166}$; +; genomic VAP^{P58S}* and *VAP-33A$^{\Delta166}$; +; genomic VAP^{WT}* (more information in Fig. 2.3). As detailed in this Chapter, our variation of the Tsuda model behaves at par with the original and we have used this system to explore ALS pathogenesis in the fly. All experiments were performed in males of the appropriate genotype. The details of crosses with full genotypes have been explained in Figure 2.3.

	Parents		F1	Referred to as
1	$\frac{\Delta VAP}{FM7a}$; $\frac{+}{+}$; $\frac{gVAP^{P58S}}{TM3Tb}$	$\frac{+}{Y}$; $\frac{+}{+}$; $\frac{+}{+}$	$\frac{\Delta VAP}{Y}$; $\frac{+}{+}$; $\frac{gVAP^{P58S}}{+}$	$\Delta VAP; gVAP^{P58S}$
2	$\frac{\Delta VAP}{FM7a}$; $\frac{+}{+}$; $\frac{gVAP^{WT}}{TM3Tb}$	$\frac{+}{Y}$; $\frac{+}{+}$; $\frac{+}{+}$	$\frac{\Delta VAP}{Y}$; $\frac{+}{+}$; $\frac{gVAP^{WT}}{+}$	$\Delta VAP; gVAP^{WT}$
3	$\frac{\Delta VAP}{FM7a}$; $\frac{+}{+}$; $\frac{gVAP^{P58S}}{TM3Tb}$	$\frac{\Delta VAP}{Y}$; $\frac{+}{+}$; $\frac{gVAP^{WT}}{TM3Tb}$	$\frac{\Delta VAP}{Y}$; $\frac{+}{+}$; $\frac{gVAP^{P58S}}{gVAP^{WT}}$	$\Delta VAP; gVAP^{P58S}/gVAP^{WT}$
4	$\frac{\Delta VAP}{FM7a}$; $\frac{+}{+}$; $\frac{gVAP^{P58S}}{TM3Tb}$	$\frac{\Delta VAP}{Y}$; $\frac{+}{+}$; $\frac{gVAP^{P58S}}{TM3Tb}$	$\frac{\Delta VAP}{Y}$; $\frac{+}{+}$; $\frac{gVAP^{P58S}}{gVAP^{P58S}}$	$\Delta VAP; gVAP^{P58S}/gVAP^{P58S}$

Figure 2.3. Schematic representation of the mating scheme used to obtain appropriate genotypes.
The original $VAP\text{-}33A^{\Delta166}$; +; genomic VAP^{P58S} fly line is balanced with FM7a on the first chromosome (X-Chromosome) and with TM3Tb on the third. This fly line is therefore heterozygous on the first and the third chromosome. The endogenous VAP gene is on the X-Chromosome and the heterozygous flies contain one copy of it, in case of females. In case of males, however, as there is only one X-chromosome, we maintain the non-FM7a males to ensure the presence of ΔVAP. The males are therefore complete nulls for VAP as they lack the FM7a. The $VAP\text{-}33A^{\Delta166}$; +; genomic VAP^{WT} fly line is balanced in a similar way as the $VAP\text{-}33A^{\Delta166}$; +; genomic VAP^{P58S}.

Presence of balancer chromosomes can have detrimental effects to the survival of the flies. To avoid these effects, we crossed these flies to wild-type flies and got rid of the balancer chromosomes. These crosses (Cross number 1 and 2) lead to flies with single copy of genomic VAP^{P58S} and genomic VAP^{WT} in $VAP^{\Delta166}$ backgrounds and are hereafter referred to as ΔVAP; $gVAP^{P58S}$ and ΔVAP; $gVAP^{WT}$ respectively.

The other genotypic combinations used in our experiments are ΔVAP; $gVAP^{P58S}/gVAP^{WT}$ (Cross number 3) with one copy of $gVAP^{P58S}$ and one of $gVAP^{WT}$ and ΔVAP; $gVAP^{P58S}/gVAP^{P58S}$ (Cross number 4) with two copies of $gVAP^{P58S}$.

The crosses depicted in the representation can have multiple outcomes, the F1 genotypes mentioned in the third column were the ones chosen for our experiments. For the ease of description, these F1 flies have been referred to as mentioned in the fourth the column respectively.

3. Results

3.1. The Δ*VAP; gVAP^{P58S}* flies have a reduced survival as compared to Δ*VAP; gVAP^{WT}* flies

The *VAP^{Δ31}; gVAP^{P58S}* flies survive for around 23 days (Median Lifespan) (Moustaqim-Barrette et al., 2013), which was far less as compared to the wild type flies (Median Lifespan is around 55 days); we were curious to find out if the Δ*VAP; gVAP^{P58S}* flies also showcase this defect. We performed survival assays on these flies along with the Δ*VAP; gVAP^{WT}*. Apart from this, we were interested in understanding if a change in the dosage and possibly the flux of *VAP^{WT}* or *VAP^{P58S}* has any effect on its dynamics in the system. For these reasons we also checked the lifespan of Δ*VAP; gVAP^{WT}/gVAP^{P58S}* and Δ*VAP; gVAP^{P58S}/gVAP^{P58S}*. The master control for all these experiments was the wild type flies (+/+).

The survival assay was performed as described in Material and Methods, Section 5.3. The Δ*VAP; gVAP^{P58S}* (*VAP^{P58S}* here is present as a single copy, Fig. 2.3) has a median lifespan of 27 days (Fig. 2.4A and B, Blue curve, number 3) which is significantly lesser than the wild type (Fig. 2.4A and B, Black curve, number 1) which has a median survival of 54 days. The Δ*VAP; gVAP^{WT}* flies (*VAP^{WT}* single copy, Fig. 2.3) show 61-day median survival value (Fig. 2.4A and B, Light Green curve, number 4), which is significantly higher (p<0.0001) than the Δ*VAP; gVAP^{P58S}*, but comparable to the wild type (p>0.05, not significant). Introduction of a second copy of *gVAP^{P58S}* in Δ*VAP; gVAP^{P58S}*, reduced the lifespan of the flies further (Fig. 2.3, Fig. 2.4A and B, Orange curve, number 2), suggesting that extra dosage of *gVAP^{P58S}* could be detrimental to the survival of the flies possibly because of increased toxicity of the mutant. Lastly, the introduction of a *gVAP^{WT}* copy in the Δ*VAP; gVAP^{P58S}* flies rescued their lifespan defects completely (Fig. 2.3, Fig. 2.4A and B, Red curve, number 5). This suggests that one copy of *gVAP^{WT}* is sufficient for the normal survival of the animal, but in the presence of one copy of *gVAP^{WT}*, an added copy of *gVAP^{P58S}* is harmless for the survival of the flies. So the *gVAP^{P58S}* here is indeed a partial loss-of-function allele which can be compensated by the presence of one copy of *gVAP^{WT}*.

A

	Genotypes	P-value, median lifespan
1	+/+ (wild type)	control,54
2	ΔVAP; gVAP^{P58S}/gVAP^{P58S}	***,21
3	ΔVAP; gVAP^{P58S}	***,27
4	ΔVAP; gVAP^{WT}	ns,61
5	ΔVAP; gVAP^{P58S} /gVAP^{WT}	ns,57
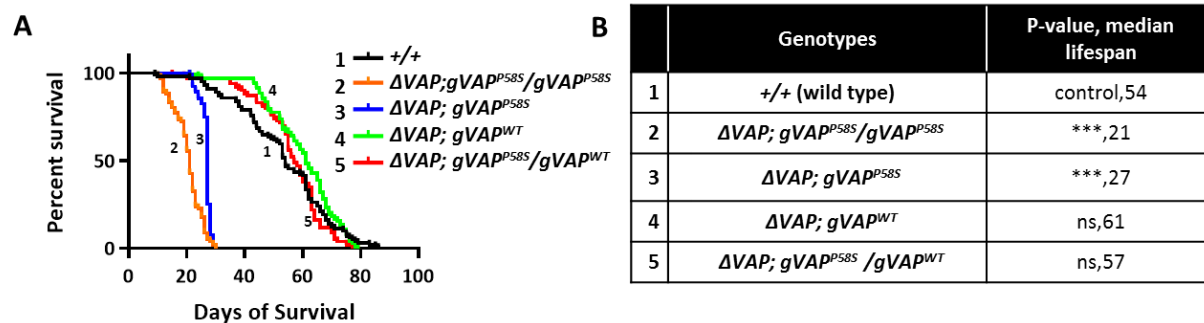
Figure 2.4. Δ*VAP; gVAP^{P58S}* flies exhibit lifespan defects.
A) Survival plots for +/+ (Wild Type, Master control, Black curve, number 1), Δ*VAP; gVAP^{P58S}/gVAP^{P58S}* (Orange curve, number 2), Δ*VAP; gVAP^{P58S}* (Blue curve, number 3)*, ΔVAP; gVAP^{WT}* (Light green curve, number 4) and Δ*VAP; gVAP^{WT}/gVAP^{P58S}* (Red curve, number 5).
B) Curve comparison was done using log-rank (Mantel-Cox test). P-values depict values of significance from log-rank test. Combined p-value for the whole set is <0.001. Median lifespan values for each set are also mentioned in the table. n=80-100 flies for each genotype.

3.2. The Δ*VAP; gVAP^{P58S}* flies exhibit progressive age-dependent motor defects

Having performed the survival analysis, we proceeded to explore the motor defects in the Δ*VAP; gVAP^{P58S}* flies. We performed an age dependent startle induced negative geotaxis assay for this purpose. This assay is typically performed to analyze the climbing abilities of flies (described in Materials and Methods, Section 5.4). We observed that these flies were perfectly mobile when then eclosed from their pupal cages. But in a few days, they lost their flying ability, which was followed by weakening in climbing and loss of grip. The climbing ability is completely lost as a fly approaches its day of death. We recorded the progressive stages of loss of climbing ability by utilizing this assay.

We analyzed the data by calculating the climbing index (described in Materials and Methods, Section 5.4). As we categorized the flies into Good Climbers (score =2), Bad Climbers (score = 1) and Non-Climbers (score =0) for the sake of calculating the climbing index, we also plotted the percentage of flies belonging to these three categories against the time intervals (Fig. 2.5A). This graph demonstrates the gradual loss of motor abilities as the Δ*VAP; gVAP^{P58S}* flies (E=Experiment) on the 10th day (Fig. 2.5A) has more percentage of good climbers than the bad climbers. Also, the number of non-climbers increases gradually from day 14 to day 30, when all the flies are converted to non-climbers. This conversion of good climbers to bad climbers to non-climbers is depicted in this result. The non-climbing stage is followed by death. The control flies (wild type, C=Control) on the other hand display mild deterioration of climbing abilities, as the

49

percentage of good climbers on the 30th day, was still close to 80% which was significantly better than the ΔVAP; $gVAP^{P58S}$ flies. The day-wise deterioration of motor abilities of the ΔVAP; $gVAP^{P58S}$ flies mimics the disease stages, the end stage of which is the death of the patient. An observation concerning this progression is that most flies go through all these stages and that death does not usually occur in case of a good climber or a bad climber. The climbing index of the ΔVAP; $gVAP^{P58S}$ flies falls to zero till day-30 but is more or less constant throughout the assay in case of the control flies (Fig. 2.5B).
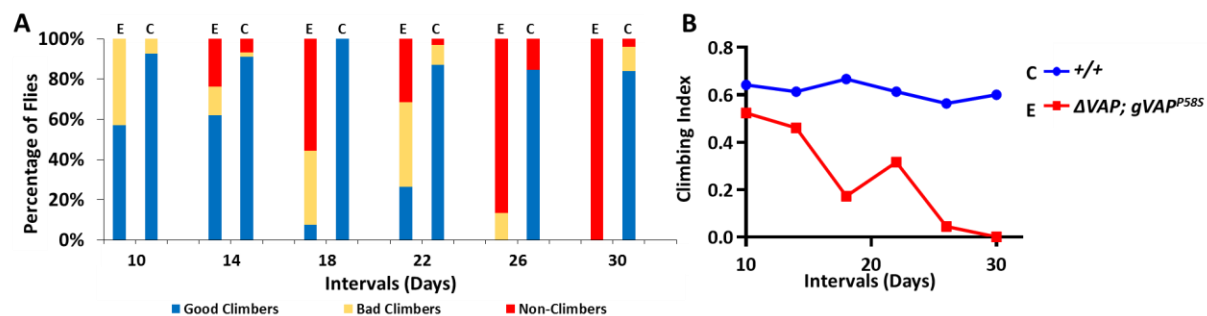
Figure 2.5. Adult climbing assays for ΔVAP; $gVAP^{P58S}$ flies.
A) Percentage of good climbers goes down with the age of ΔVAP; $gVAP^{P58S}$ flies (Marked as E), it remains constant for the wild type control (Marked as C).
B) Climbing index of ΔVAP; $gVAP^{P58S}$ flies (Red curve) is significantly reduced as compared to wild type control flies (Blue curve). n=15-20 flies, N=1. Statistical analysis was done using unpaired student's t-test Combined p-value for the whole set is <0.01

3.3. The ΔVAP; $gVAP^{P58S}$ flies show the presence of VAP positive cellular aggregates

On studies based on the overexpression system in our lab, we found that VAP positive puncta are observed in the brains of third instar larvae on the neuronal overexpression of VAP[P58S] (Chaplot et al., 2019). We probed for VAP puncta in the ΔVAP; $gVAP^{P58S}$ larval as well as adult stages. Both the larval as well as adult brains of the ΔVAP; $gVAP^{P58S}$ flies show the presence of VAP aggregates (Fig. 2.6). Details of the dissection and imaging is described in Materials and Methods, Section 5.6. Since this is a genomic expression system, unlike the overexpression system, there is a good possibility of VAP[P58S] aggregating throughout the animal. To confirm this, we also probed for VAP aggregates in third instar larval muscles of ΔVAP; $gVAP^{P58S}$. The muscles of the larvae also exhibit VAP positive puncta (Images not included).

In a few studies from the past, aggregates have proven to be a good readout for the onset and progression of ALS by either showing up in the pre-onset stages or increasing in quantity/size

during the disease progression (Bruijn et al., 1997; Stieber et al., 2000; Boillee et al., 2006 and Yamanaka et al., 2008). We haven't looked into this aspect in details, but a change in the dynamics of VAP aggregates over time will tell us more about their contribution to the disease. The quality and quantity of aggregates in the good climbers, bad climbers and non-climbers, if different, can shed light on the change in the scenario of aggregation patterns over time. These aspects could provide more information about the cause-effect relationship of aggregates with the ALS8 disease onset and progression. Aparna Thulasidharan, a graduate student in our lab is exploring these aspects of ALS8 using the $\Delta VAP; gVAP^{P58S}$ flies as a part of her work.
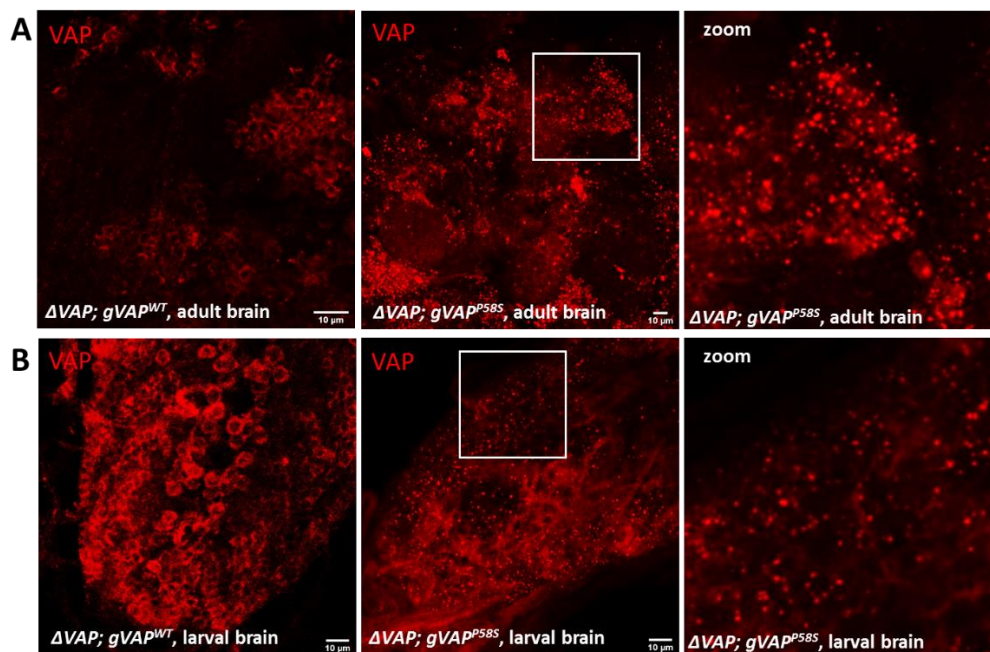
Figure 2.6. VAP^P58S aggregates in adult as well as third instar larval brains of $\Delta VAP; gVAP^{P58S}$.
A) and **B)** $\Delta VAP; gVAP^{P58S}$ adult brains as well as third instar larval brains show presence of VAP positive puncta, while the $\Delta VAP; gVAP^{WT}$ show VAP staining around membranes without any aggregates. Contributions: All images except for $\Delta VAP; gVAP^{P58S}$ larval brain, were contributed by Aparna Thulasidharan.

3.4. Lipid homeostasis is disrupted in $\Delta VAP; gVAP^{P58S}$ flies

Energy homeostasis and lipid metabolism are altered in ALS patients. Outcomes from a few studies have proposed using the change in lipid profiles as biomarkers for ALS (Aguilar, 2019). A lipid-rich diet is reported to prolong the life of ALS patients, whereas calorific restriction is reported to hamper the survival (Schmitt et al., 2014). Studies in mice have revealed the disease

to be manifesting excessive depletion of lipids via muscle metabolism and higher resting energy expenditure resulting in leaner animals (Dupuis et al., 2004; Fergani et al., 2007; Kim et al., 2011).

VAPB, as we know from earlier discussions, is involved in lipid metabolism as it acts as an adaptor for the FFAT motif-containing proteins which are involved in ER-Golgi lipid trafficking. Tsuda's model of ALS8 exhibits abnormalities in this lipid transfer as the FFAT motif fails to bind to the mutated MSP domain of VAP. This loss in transfer could cause dysregulation of lipids resulting in their imbalance in the system.

Evidence from the literature hints towards a possibility of $\Delta VAP; gVAP^{P58S}$ flies manifesting an imbalanced lipid profile. We performed LC-MS/MS lipidomics on the 15-day brains of $\Delta VAP; gVAP^{P58S}$ flies. This analysis was performed by Kriti Chaplot, a former graduate student in our lab, and has been reproduced in this chapter. Materials and Methods, Section 5.5 describes the detailed protocol used for this assay.

$\Delta VAP; gVAP^{P58S}$ flies indeed show an imbalanced lipid profile. The Cholesterol levels are highly reduced, while the Cholesteryl esters are high (Fig. 2.7A and B). As the VAP^{P58S} flies exhibit loss of OSBP-VAP interaction and as OSBPs are involved in the transport of Cholesterols, the reduced levels of Cholesterols are explained by this loss. Lowered Cholesterol levels are suspected to contribute to defective ERQC (Moustaqim-Barrette et al., 2013). Furthermore, the higher Cholesteryl esters suggest a loss in the regulation of Cholesterol to Cholesteryl ester conversion in the $\Delta VAP; gVAP^{P58S}$ flies. A study in $SOD1^{G93A}$ mice demonstrated an increase in Cholesteryl esters, which are a part of the neuroprotective lipid droplets in the astrocytes in the spinal cords of these animals (Chaves-Filho et al., 2019). In response to an increase in ROS in the system, lipids are formed in the neurons and are then transferred to the glial cells and stored in the form of lipid droplets. These lipid droplets are speculated to be neuroprotective (Liu et al., 2017). These lipid droplets are rich sources of Cholesteryl esters and Triacylglycerols. The $\Delta VAP; gVAP^{P58S}$ flies also show a rise of Triacylglycerols (Fig. 2.8P), suggesting a formation of high levels of lipid droplets in the system.

Other than the changes in Cholesterol, Cholesterol esters and Triacylglycerols, the levels of Ceramide, Ceramide-1-Phosphate and Sphingomyelin are increased in these flies (Fig. 2.7C, D and F). OSBPs are reported to be involved in CERT (Ceramide transfer proteins) and Sphingomyelin synthesis via activation of Cholesterol sensitive kinase, PI4KIIα (Banerji et al., 2010). In addition to this, VAP interacts with CERT, another FFAT motif-containing proteins,

involved in the transport of Ceramides (Perry and Ridgway, 2006). The loss of these connections as a result of VAP^{P58S} could be leading to the accumulation of Ceramides and Sphingomyelins. An investigation of CERT and OSBPs in the $\Delta VAP;\ gVAP^{P58S}$ flies would provide us with more information about the regulation of lipids in these flies.

The rescue genotypes ($\Delta VAP;\ gVAP^{WT}$ and $\Delta VAP;\ gVAP^{WT}/gVAP^{P58S}$) used in this experiment show lipid profiles similar to the master control, which is the +/+ (Wild Type flies) and corroborate with the trend of the lifespan rescue (Fig. 2.4, 2.7 and 2.8).

Most of the tested lipids are regulated by interconnected pathways and their flux is maintained via their interconversions. This interconversion seems to be lost as a result of the VAP^{P58S} mutation, causing a lot of downstream activities to be impaired. We are, however, not sure if this lipid profile is a gradually developed abnormality or exists in these flies from the beginning of their life. A time-based lipidomics analysis on the $\Delta VAP;\ gVAP^{P58S}$ flies, will enable us to understand the involvement of this impairment in the progression of ALS8.
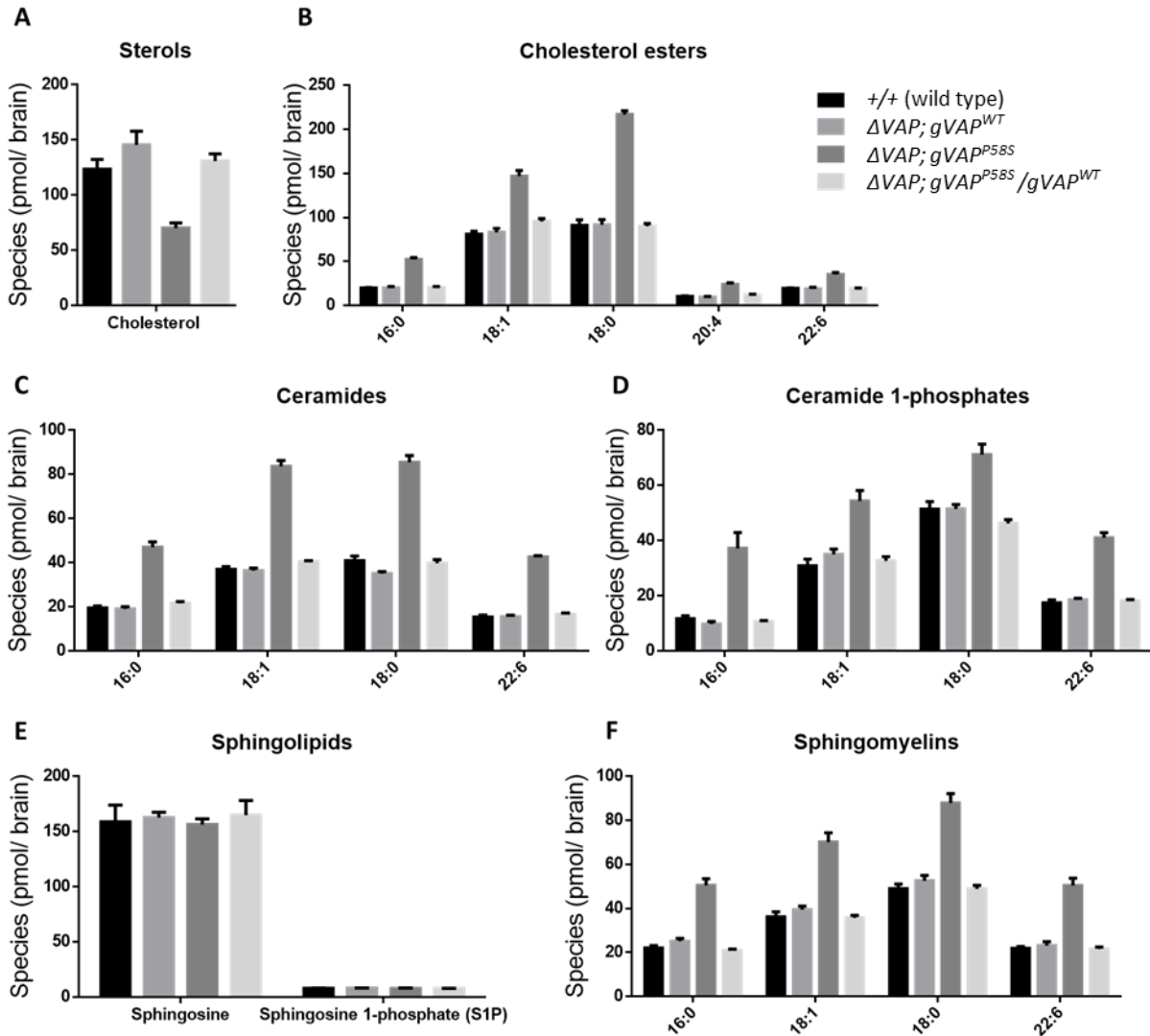
Figure 2.7. Lipid profiles for 15-day adult fly brains.
Levels of Cholesterol reduces in $\Delta VAP;\ gVAP^{P58S}$ (**A**) while levels of Cholesterol esters (**B**) Ceramides (**C**), Ceramide 1-phosphates (**D**) and Sphinogomyelins (**F**) increase in change in $\Delta VAP;\ gVAP^{P58S}$. but there is no change in Sphingosine and Sphingosine 1-phosphate as compared to control (**E**). Levels of all these lipids remains constant between +/+ (wild type control), $\Delta VAP;\ VAP^{WT}$, $\Delta VAP;\ gVAP^{P58S}$ and the $\Delta VAP;\ VAP^{P58S}/VAP^{WT}$ N=5, n=2 for each genotype. (Statistics in Table 2.1)

A Lyso-PC
B Lyso-PG
C Lyso-PA
D Lyso-PS
E Lyso-PE
F Lyso-PI
G Phosphatidylcholines
H Phosphatidylglycerol
I Phosphatidylethanolamines
J Phosphatidylserines
K Phosphatidic acid
L Phosphatidylinositol

Legend:
- +/+ (wild type)
- ΔVAP; gVAP^{WT}
- ΔVAP; gVAP^{P58S}
- ΔVAP; gVAP^{P58S} /gVAP^{WT}
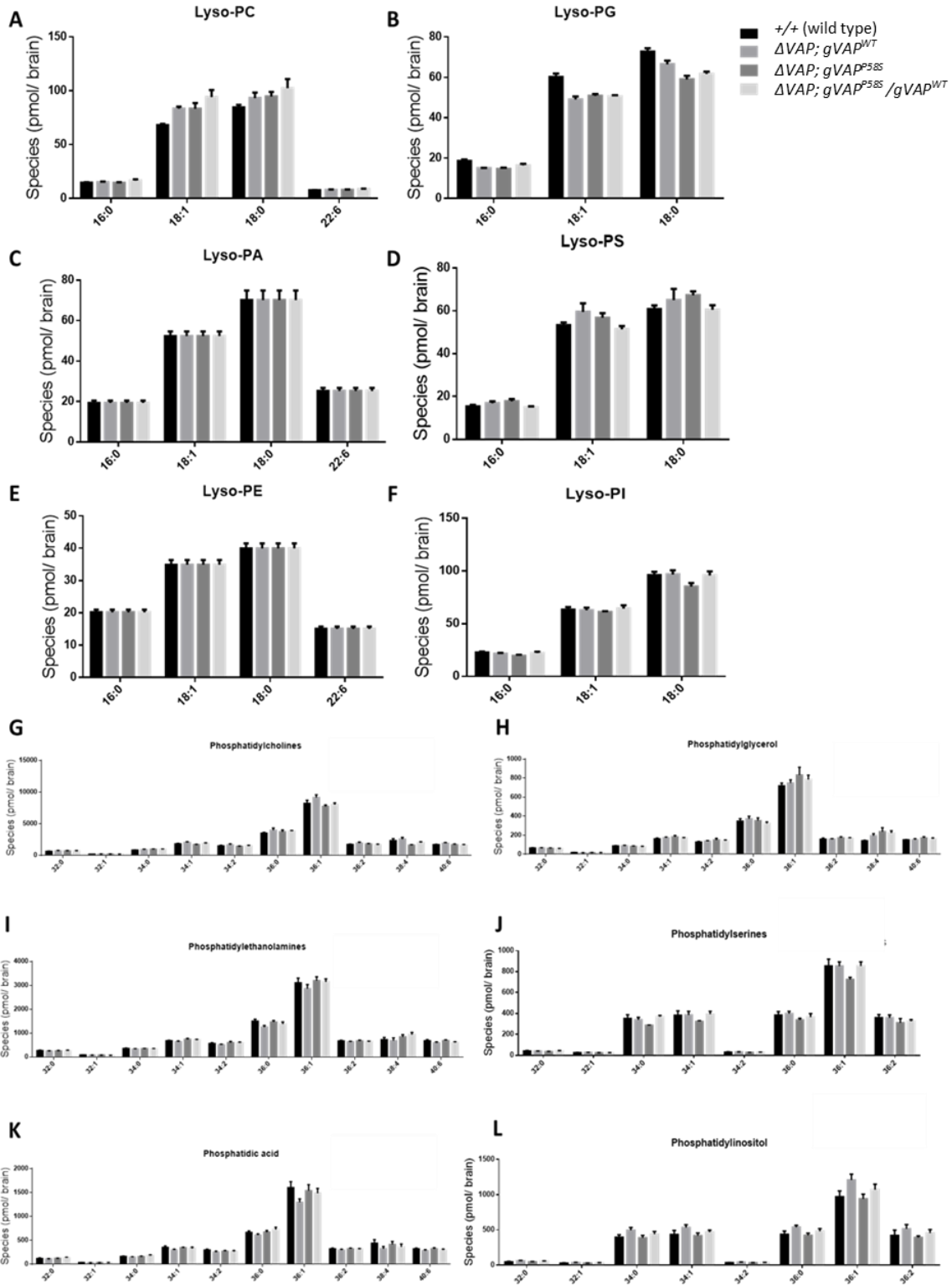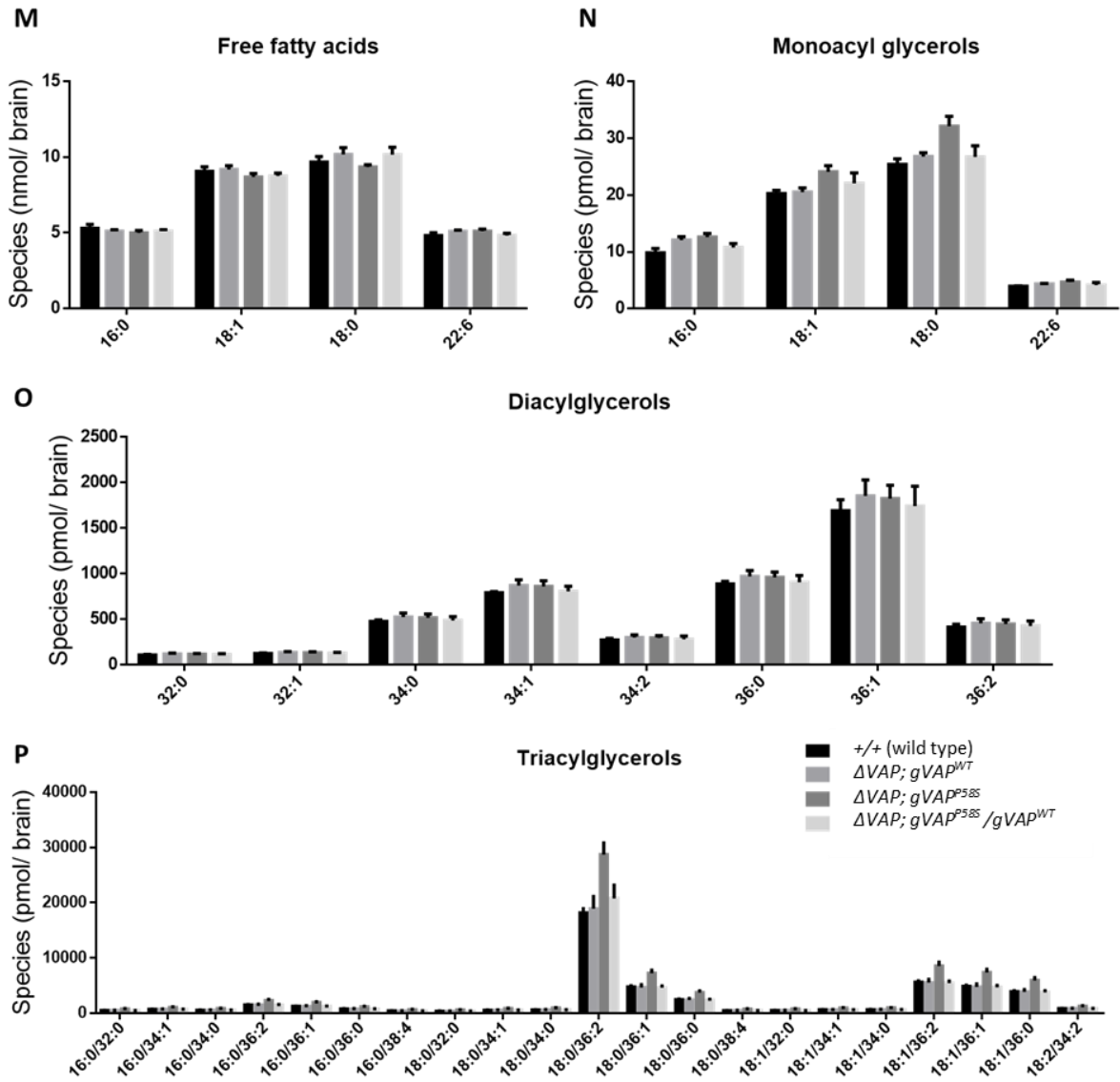
Figure 2.8. Lipid profiles for 15-day adult fly brains.

Phospholipids and its derivatives, Lyso-phospholipids, remain constant between genotypes. Free fatty acids and diacylglycerols, remain constant between $\Delta VAP;\ VAP^{WT}$, $\Delta VAP;\ gVAP^{P58S}$ and the $\Delta VAP;\ VAP^{P58S}/VAP^{WT}$, while Monoacylglycerols and Triacylglycerols are significantly upregulated in $\Delta VAP;\ gVAP^{P58S}$ as compared to +/+. N=5, n=2 for each genotype. (Statistics in Table 2.1)

Table 2.1. LC-MS quantitation of the different lipids in 15 day old male adult *Drosophila* brain of +/+ (Master Control) and *ΔVAP; VAP^P58S*

Unpaired t-test. * p < 0.05,** p < 0.01, *** p < 0.001, ****p < 0.0001. Internal Controls used are in red.

Lipid Class	Species targeted	+/+	*ΔVAP; VAP^{P58S}*	SEM	N	P value
Sterols	Cholesterol	123.602	70.066	9.97645	5	0.00067
	Cholesterol d7 (IS) (1000 pmol)					
Sphingolipids	Sphingosine	158.958	156.426	15.9503	5	0.87781
	17:1 Sphingosine (IS) (1000 pmol)					
	Sphingosine 1-phosphate (S1P)	7.95	7.808	0.39765	5	0.73025
	17:1 S1P (IS) (100 pmol)					
Ceramides	16:0	19.418	47.028	2.64931	5	< 0.0001
	18:1	36.972	83.654	2.95893	5	< 0.0001
	18:0	40.886	85.46	3.72467	5	< 0.0001
	22:6	15.41	42.666	1.02356	5	< 0.0001
	25:0 (IS) (100 pmol)					
Sphingomyelins	16:0	22.092	50.546	3.21331	5	< 0.0001
	18:1	36.2	70.098	4.85723	5	0.00012
	18:0	49	87.856	4.75395	5	< 0.0001
	22:6	21.952	50.438	3.41295	5	< 0.0001
	12:0 (IS) (100 pmol)					
Free fatty acids	16:0	5.312	4.996	0.30439	5	0.32955
	18:1	9.068	8.698	0.38152	5	0.36055
	18:0	9.682	9.362	0.38434	5	0.42923
	22:6	4.818	5.102	0.24318	4	0.27649
	17:1 (IS) (1 nmol)					
Monoacyl glycerols (MAG)	16:0	9.838	12.628	1.00069	5	0.02363
	18:1	20.272	24.11	1.22069	5	0.01372
	18:0	25.408	32.14	2.00656	5	0.01001
	22:6	3.94	4.688	0.3549	5	0.06812
	20:4 (d5-glycerol) IS (100 pmol)					
Cholesterol esters	16:0	19.886	52.328	2.20122	5	< 0.0001
	18:1	80.842	147.072	7.11331	5	< 0.0001
	18:0	91.174	216.99	7.4336	5	< 0.0001
	20:4	10.292	23.802	2.07339	5	0.00018

	22:6	19.51	35.346	2.25966	5	0.00011
	19:0 (IS) (100 pmol)					
Ceramide 1-phosphates	16:0	11.696	37.236	5.79717	5	0.00227
	18:1	30.812	54.378	4.50295	5	0.00079
	18:0	51.424	71.14	4.70065	5	0.00302
	22:6	17.434	41.006	2.19499	5	< 0.0001
	12:0 (IS) (100 pmol)					
Phosphatidylcholines (PC)	32:0	628.212	711.046	55.9976	5	0.17734
	32:1	180.852	199.776	23.6041	5	0.44587
	34:0	816.118	961.894	60.3242	5	0.04208
	34:1	1819.1	1710.57	94.4569	5	0.28377
	34:2	1482.29	1405.77	125.385	5	0.55861
	36:0	3511.78	3733.49	309.545	5	0.49421
	36:1	8225.52	7728.77	541.585	5	0.38584
	36:2	1714.37	1791.73	97.6716	5	0.4512
	38:4	2326.2	1621.72	331.106	5	0.06603
	40:6	1704.1	1680.71	121.697	5	0.85235
	37:4 (IS) (1000 pmol)					
Phosphatidylethanol amine (PE)	32:0	265.242	248.852	25.9196	5	0.54481
	32:1	79.646	71.918	6.06113	5	0.23809
	34:0	354.954	347.808	21.4105	5	0.74714
	34:1	679.088	734.454	46.1754	5	0.26482
	34:2	558.632	597.712	60.3513	5	0.53542
	36:0	1499.99	1461.53	105.541	5	0.72496
	36:1	3109.2	3195.31	252.917	5	0.74228
	36:2	670.47	669.014	43.1075	5	0.97388
	38:4	721.858	833.912	137.247	5	0.43788
	40:6	677.552	684.978	54.3529	5	0.8947
	37:4 (IS) (1000 pmol)					
Phosphatidic acid (PA)	32:0	118.768	121.55	12.5371	5	0.82995
	32:1	34.874	33.606	2.77189	5	0.65952
	34:0	162.676	160.438	12.6638	5	0.86412
	34:1	352.44	343.522	31.9209	5	0.78704
	34:2	297.018	269.316	26.481	5	0.32609

	36:0	664.362	671.34	44.2857	5	0.8787
	36:1	1601.65	1538.81	177.984	5	0.73313
	36:2	320.928	322.744	24.9255	5	0.94371
	38:4	438.834	412.598	97.1487	5	0.79395
	40:6	322.632	321.5	27.1055	5	0.96771
	37:4 (IS) (1000 pmol)					
Phosphatidylglycerol (PG)	32:0	66.186	62.748	5.10509	5	0.51964
	32:1	19.382	18.206	2.3381	5	0.62854
	34:0	87.86	82.572	7.59177	5	0.50582
	34:1	161.792	183.86	17.6426	5	0.24634
	34:2	129.454	150.482	18.117	5	0.27923
	36:0	349.86	354.964	36.8651	5	0.89331
	36:1	720.104	833.974	85.2196	5	0.21824
	36:2	159.176	172.816	17.1329	5	0.44893
	38:4	142.97	238.902	41.0155	5	0.0475
	40:6	152.3	172.316	13.3438	5	0.172
	37:4 (IS) (1000 pmol)					
Phosphatidylserine (PS)	32:0	42.408	34.758	5.26005	5	0.18393
	32:1	25.886	23.79	1.99113	5	0.32325
	34:0	352.874	286.754	34.4026	5	0.09084
	34:1	382.608	323.638	43.0836	5	0.20828
	34:2	30.846	27.042	2.46228	5	0.16095
	36:0	384.668	338.192	37.1862	5	0.24669
	36:1	854.914	724.418	66.871	5	0.0868
	36:2	359.662	311.132	50.175	5	0.36176
	37:4 (IS) (100 pmol)					
Phosphatidylinositol (PI)	32:0	48.394	46.718	7.33772	5	0.82506
	32:1	29.816	28.614	3.3468	5	0.72878
	34:0	397.564	387.87	49.8778	5	0.85074
	34:1	436.874	418.576	68.5851	5	0.79638
	34:2	35.4	33.86	4.25592	5	0.72684
	36:0	439.21	422.366	54.3965	5	0.76474
	36:1	970.734	940.922	104.638	5	0.78295
	36:2	422.786	393.146	76.7535	5	0.70944
	37:4 (IS) (100 pmol)					

Lyso-PC	16:0	14.672	14.536	0.6999	5	0.85077
	18:1	68.096	83.348	5.44837	5	0.02322
	18:0	84.596	94.718	4.79812	5	0.06792
	22:6	7.524	7.89	0.46267	5	0.45172
	17:1 (IS) (100 pmol)					
Lyso-PE	16:0	20.198	20.198	1.13977	5	> 0.9999
	18:1	34.912	34.912	2.0361	5	> 0.9999
	18:0	39.998	39.998	2.17457	5	> 0.9999
	22:6	15.056	15.056	0.99394	5	> 0.9999
	17:1 (IS) (100 pmol)					
Lyso-PA	16:0	19.316	19.316	1.63329	5	> 0.9999
	18:1	52.396	52.396	3.12222	5	> 0.9999
	18:0	70.198	70.198	6.61749	5	> 0.9999
	22:6	25.228	25.228	2.14932	5	> 0.9999
	17:1 (IS) (100 pmol)					
Lyso-PG	16:0	18.636	14.664	0.85701	5	0.00168
	18:1	60.14	50.85	2.02258	5	0.00177
	18:0	72.764	58.948	2.46404	5	0.00051
	17:1 (IS) (100 pmol)					
Lyso-PS	16:0	15.35	17.782	1.28968	5	0.09605
	18:1	53.242	56.752	2.49913	5	0.19779
	18:0	60.766	67.258	2.47682	5	0.0306
	17:1 (IS) (100 pmol)					
Lyso-PI	16:0	22.78	19.53	1.4634	5	0.05711
	18:1	63.42	61.12	2.51389	5	0.38698
	18:0	96.05	85.254	4.63121	5	0.04808
	17:1 (IS) (100 pmol)					
Triacylglycerols (TAG)	16:0/32:0	509.414	773.096	64.5083	5	0.0035
	16:0/34:1	722.98	1097.2	91.553	5	0.0035
	16:0/34:0	558.77	847.996	70.7568	5	0.0035
	16:0/36:2	1527.74	2318.52	193.461	5	0.0035
	16:0/36:1	1277.68	1939.02	161.796	5	0.0035
	16:0/36:0	777.404	1179.8	98.4443	5	0.0035
	16:0/38:4	437.344	663.72	55.3822	5	0.0035
	18:0/32:0	395.844	600.74	50.1263	5	0.0035

	18:0/34:1	558.126	847.022	70.6766	5	0.0035
	18:0/34:0	629.696	955.64	79.7393	5	0.0035
	18:0/36:2	18177.2	28702.1	2252.01	5	0.0016
	18:0/36:1	4772.29	7242.51	604.326	5	0.0035
	18:0/36:0	2468.29	3745.91	312.565	5	0.0035
	18:0/38:4	492.272	747.078	62.3368	5	0.0035
	18:1/32:0	508.844	772.226	64.4358	5	0.0035
	18:1/34:1	635.124	963.874	80.4283	5	0.0035
	18:1/34:0	643.982	977.318	81.5484	5	0.0035
	18:1/36:2	5642.12	8562.58	714.475	5	0.0035
	18:1/36:1	4873.5	7396.11	617.142	5	0.0035
	18:1/36:0	3930.1	5964.38	497.677	5	0.0035
	18:2/34:2	851.62	1292.43	107.843	5	0.0035
	17:0/34:1 (IS) (1000 pmol)					
Diacylglycerols (DAG)	32:0	108.008	116.6	9.95454	5	0.4132
	32:1	123.204	132.892	11.8082	5	0.43572
	34:0	475.398	516.43	44.9683	5	0.38819
	34:1	791.156	859.524	62.6835	5	0.30717
	34:2	272.826	295.304	30.2549	5	0.47876
	36:0	885.826	958.34	66.7929	5	0.30926
	36:1	1692.24	1826.68	190.4	5	0.5002
	36:2	412.706	447.318	54.9424	5	0.54628
	32:0 (d5-glycerol) (IS) (1000 pmol)					
	Unpaired t-test					
	* p < 0.05,** p < 0.01, *** p < 0.001, ****p < 0.0001					
	Internal Controls used are in RED					

4. Discussion

In human patients, a single copy of the mutation is found to lead to the diseased state. In the case of flies this is not true. In our fly model, shortening of life span and motor defects, which is our readout of the disease is found only in the case where the mutant allele is expressed in the absence of the wild type allele. In the fly model, the presence of the wild type allele, even in a single (or even smaller) dose rescues the phenotypes. In spite of this distinction, we still believe that the fly model is a useful reagent to explore mechanisms of initiation and progression of ALS8. In both cases (human, fly) the loss of cellular homeostasis and malfunction in the motor system of the organism is caused by a partial loss-of-function of the VAP protein – which is a direct result of the P56S/P58S mutation. The effects (disease/phenotypes) have strong parallels – presence of VAP positive aggregates, delayed adult onset, loss of motor function and shortened lifespans. For the fly model, all the characterization data shown in this Chapter is in the absence of the wild type protein. Addition of the wild type protein leads to a complete absence of phenotypes and leads to an organism that is equal in all aspects to the wild-type fly.

Characterization of the flies' survival, motor defects and VAP aggregates in these flies, helps us to draw parallels with the onset and progression of the disease (Table 2.2). It is interesting to note that the flies go through all the stages of motor deterioration before death. However, a lot of further work needs to be carried out to understand the detailed mechanisms causing these changes in these flies. Predicting the pre-onset or onset in patients is a difficult task, but this model can help us look into the details of the cellular mechanisms as the age progresses and shed some light on the timeline of onset. This can be done by conducting an age-dependent analysis of the VAP aggregates and the lipid profiles starting from the early stages of the life of these flies. Change in patterns in the aggregates or lipids would provide us with clues to the onset of ALS8. Some more parameters like ERQC should also be followed up in these flies to understand if the deterioration of the other phenotypes in these flies goes hand in hand with the failure of ERQC.

Table 2.2. Comparing different models for ALS8

√ represents presence of a characteristic, ✗ represents absence of a characteristic.

Characteristics	Overexpression system for VAP^{P58S}	Tsuda's model for ALS8	Our model for ALS8
VAP positive aggregates	√	Not checked	√
Progressive motor defects	✗	√	√
Shortened survival	✗	√	√
Defect in ERQC	Not checked	√	Not checked
Defects in lipid profile	Not checked	Not checked	√

Tsuda et al., 2008; Han et al., 2013; Ratnaparkhi et al., 2008; Chaplot et al., 2019 and Moustaqim-Barrette et al., 2013

Apart from understanding the onset point of the disease, it would be interesting to delve into the change of flux of VAP with age. Based on our observations, there could be optimal levels of VAP required to control its normal functions in the cell, these levels if impaired could lead to toxicity. In the case of the *VAP^{P58S}*, understanding the change in dynamics of VAP^{P58S} aggregates with time would be fascinating, especially as VAP is known to dimerize via its CCD domain. In addition to that, the presence or absence of aggregates in the rescue genotype Δ*VAP; gVAP^{WT}/gVAP^{P58S}*, and their changes with time would give us more ideas about the partial loss-of-function of *VAP^{P58S}* and its contribution in the maintenance of its cellular functions.

One aspect which has not been studied by us is the characteristics of larvae of Δ*VAP; gVAP^{P58S}*. Although the presence of aggregates has been confirmed in the third instar larvae of Δ*VAP; gVAP^{P58S}*, the motor abilities of these larvae and changes in the NMJ could characterize this genotype a little further.

Lastly, as evidenced above, this model has advantages over the overexpression models used in earlier studies. This model can in fact be combined with the *UAS-Gal4* for studying the spatial and temporal perturbation of other genes in the regulated background of Δ*VAP; gVAP^{P58S}*. This strategy can be used to understand the genetic interactions of various genes with *VAP* and its change in dynamics in the disease conditions.

5. Materials and Methods

5.1. *Drosophila* husbandry

All flies were raised at 25 ºC in standard corn meal agar. Crosses were set up at 25ºC.

5.2. Reagents

This Chapter incorporates numerous techniques and assays. We have mentioned fly lines and antibodies in this section while the rest of the reagents are mentioned along with the description of respective techniques.

Table 2.3. List of Fly lines used in the study
Description beside every fly line mentions the Bloomington number or the source from which the fly lines were obtained.

Fly line	Source	Full Genotype	Other Details (if any)
Canton-S (+/+)	BL 0001		Wild type control
ΔVAP; gVAP^{P58S}	Moustaqim-Barrette et al., 2013 and Pennetta et al., 2002	*Δ166/FM7A;+; genomic VAP^{P58S} (VK31)/TM3TB*	
ΔVAP; gVAP^{WT}	Moustaqim-Barrette et al., 2013 and Pennetta et al., 2002	*Δ166/FM7A;+; genomic VAP^{WT} (VK31)/TM3TB*	

Table 2.4. List of antibodies used in the study

Antibody Used	Name of antibody/ protein	Raised in	Source	Dilution for IHC
Anti-VAP	VAMP associated protein	Rabbit	In-House	1:500
DAPI (dye)	4,6 diamidino-2-phenylindole		Sigma	1:1000

5.3. Survival assay

Survival assays were carried out for the ALS8 model of disease, for testing the genetic interactions. 80-100 male flies of the required genotype were collected from the F1 generation and maintained in media containing vials. The crosses, as well as the eclosed flies, were maintained at 25 ºC. Each vial had 15 or less age-matched flies. All the flies were flipped every fourth day to avoid death by sticking to the media. The death toll of flies was recorded every day. The assay was

followed up till every fly in the control, as well as test vials, died. The data was plotted and analyzed using the log-rank test in prism7 survival assay which gives a value of significance on comparing the survival curves of the genotypes of interest. Along with the p-values generated from the log-rank test, we also took into account the median lifespan of each genotype as an additional criteria for comparison. (Estes et al., 2011; Moustaqim-Barrette et al., 2013 and Piper and Partridge, 2016)

5.4. Adult climbing assay

Motor performance of the respective genotype was analyzed using the standard climbing assay (Madabattula et al, 2015; Branco et al., 2008; Azuma et al., 2014, Shcherbata *et al.* 2007), with minor modifications. Three separate sets (biological replicates) of 30 age-matched adult males each were raised at 25 ºC. At the beginning of this startle induced negative geotaxis assay for climbing, each set of 30 flies was emptied in a 250 ml glass cylinder and tapped sufficiently to startle all the flies in the cylinder. Following this when flies started climbing to the top of the cylinder, they were scored in three groups which were based on their position at the end of 60 seconds starting from the startle. Flies which could not climb at all were scored 0 (Non-Climbers), flies which climbed till 80 mL mark were scored 1 (Bad Climbers) and flies which climbed further up from 80 mL to the top were scored 2 (Good Climbers) (Fig. 2.4). This was repeated thrice for each set of 30 flies.
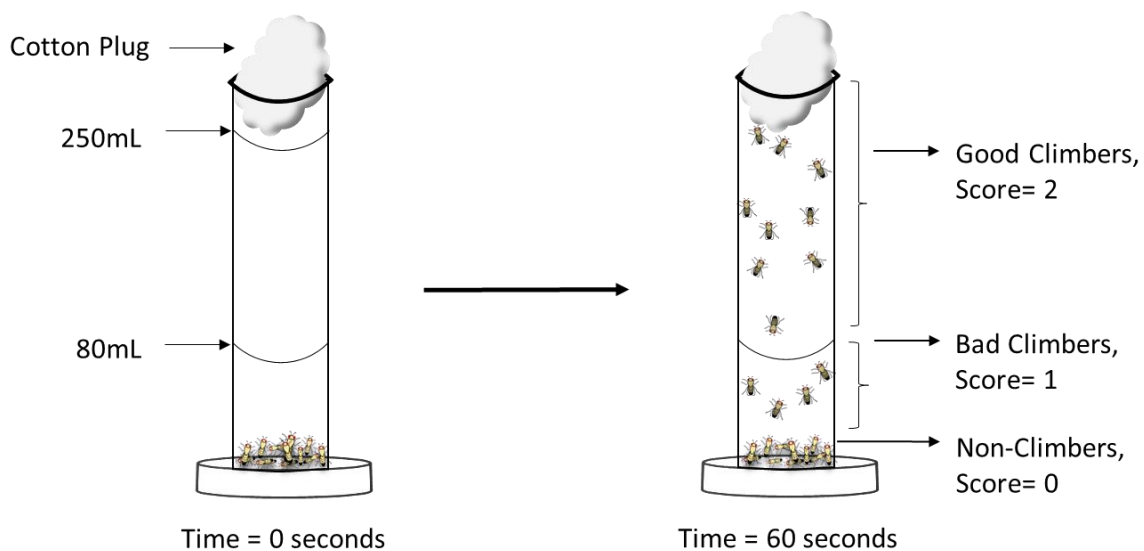
Figure 2.9. Representation of adult climbing assay.

The assay takes place in 60seconds right after the induction of startle. Flies are categorized and scored as good climbers, bad climbers and non-climbers. The 250mL cylinder is blocked with cotton plug during the assay to avoid flies from escaping.

We repeated climbing assays for every genotype at an interval of 5 Days till flies in at least one of the genotypes completely stopped climbing or were dead. This motor assay does not account for the death occurring as the assay proceeds. Each time a set was transferred from the vial to the cylinder for the assay, acclimatization was done for approximately 5 minutes. Also, the flies were exposed to CO2 only after a day's trial was complete, ensuring no effect of CO2 on the assay. Flies were transferred to a new vial every four days to avoid death due to sticky media. The conditions at which the assays were performed were constant for every set. Data was analyzed by calculating the climbing index for each technical repeat, which was then averaged. This average was averaged with other biological replicates to obtain a final value of the climbing index with error values. This data was plotted using Prism7 grouped representations and statistically analyzed using Two way ANOVA followed by multiple comparison testing by Tukey test.

The Climbing index is a proxy indicator for the fitness of a particular fly/genotype on a particular day. It helps in recognizing any progression of the motor defect in a set of flies. The formula for climbing index is (Azuma et al., 2014):

$$\text{Climbing Index} = \frac{\text{Sum of all three values (Each score * Number of flies having that score)}}{3 * \text{Total number of flies examined}}$$

We have also plotted the percentage of good performers, bad performers and non-climbers in some cases for more clarity.

5.5. Lipid extraction and targeted LC-MS lipidomics

15 day-old adult brains of the appropriate genotype were dissected in 1XPBS. 5 sets of 2 brains in each tube of a genotype were sonicated in 200ul of 1XPBS at 30 ºC till the tissues completely dissolved in the solution. These samples were then transferred to glass vials which were added with the master mix. The master mix is made of CHCl3: MeOH in 2:1 ratio (400:200ul for each reaction) along with 10ul internal control (10pmol/reaction). Each vial was rigorously vortexed till the lipids were taken by the lower CHCl3 layer. This was followed by centrifugation at 25 ºC for 5 minutes at 30,000rpm in the swinging bucket rotor. The bottom layer of lipid (organic layer) was then transferred to a fresh glass vial. The upper aqueous layer in the previous vial was

then added with 400ul of CHCl3, vortexed and centrifuged again like before and its lower organic layer was collected to be pooled with the organic layer from the previous batch. The vials were then exposed to N2 for drying. These samples of lipids were then added with CHCl3: MeOH for LC-MS analysis. The LC-MS analysis was done by Dr. Siddhesh Kamat. The values were further plotted using prism7. Statistical analysis was done using One way ANOVA for cholesterol, Two way ANOVA for all other lipids followed by multiple comparison testing by Tukey test (Chaplot et al., 2019).

5.6. Brain dissections and imaging

For third instar larval brains: Wandering third instar larvae were selected and the brains dissected in 1x PBS. Fixation was carried out in 4%PFA with 0.3% PBST for 20 minutes followed by three washes with 1x PBS. The brains were blocked in 2% BSA with 0.3%PBST for 1.5-hours and then incubated in primary antibodies overnight at 4 ℃. This was followed by 1.5- hour wash with blocking solution and incubation in Alexa Fluor secondary antibodies for 1.5 hours at room temperature, followed by four 20 minute washes with the blocking solution. DAPI (wherever used) is added to the blocking during the second wash (1:1000).

For the adult brain dissections: Brains of flies of a fixed age were dissected in ice cold 1XPBS. The brains were fixed in 1.2% PFA for 24 hours at 4 ℃, then washed in 5% PBST followed by washes in PAT buffer. The samples were then blocked in 5% BSA for two hours. The brains are incubated in primary for two overnights and then in secondary (anti- rabbit 1:1000, Invitrogen) for another two overnights. DAPI was added following secondary antibody wash and was allowed to sit for 30 minutes before proceeding with two more washes in PAT buffer.

Samples were then washed with 1XPBS, mounted in 70% glycerol with n-propyl gallate and the areas of the ventral nerve cord were imaged under Zeiss or Leica Confocal microscopes at 63X oil magnification and constant settings (Microscopes were fixed for each set of experiment).

5.6.1. Image analysis for VAP[P58S] aggregates

The image is projected at maximum intensity after which the mean intensity of the image is subtracted to remove low intensity background and the intensity of fixed (16bit) ROIs is measured. The mean intensity of ROIs without aggregates is subtracted from the mean intensity of ROIs with aggregates. This image is then converted into 8bit image and a threshold value is set.

Post this, the particles are analyzed (number, area, average size). This data is then represented graphically and analyzed statistically using student's t-test or one way ANOVA based on the number of genotypes. Quantitative analysis was not carried out for images in this chapter.

6. Contributions

The LC/MS work for $\Delta VAP; gVAP^{P58S}$ adult flies was carried out by Kriti Chaplot, a former PhD student in our lab. Aparna Thulasidharan imaged all the brain aggregate images, except for $\Delta VAP; gVAP^{P58S}$ larval brain.

7. Acknowledgements

8. References

Azuma, Y. *et al.* Identification of ter94, drosophila VCP, as a strong modulator of motor neuron degeneration induced by knockdown of Caz, Drosophila FUS. *Hum. Mol. Genet.* 23, 3467–3480 (2014).

Banerji, S., Ngo, M., Lane, C.F., Robinson, C.A., Minogue, S. and Ridgway, N.D. Oxysterol binding protein-dependent activation of sphingomyelin synthesis in the golgi apparatus requires phosphatidylinositol 4-kinase IIalpha. Mol. Biol. Cell. (2010).

Baron, Y. *et al.* VAPB/ALS8 interacts with FFAT-like proteins including the p97 cofactor FAF1 and the ASNA1 ATPase. *BMC Biol.* 12, 1–20 (2014).

Boillée, S. *et al.* Onset and progression in inherited ALS determined by motor neurons and microglia. *Science (80-).* 312, 1389–1392 (2006).

Branco, J. *et al.* Comparative analysis of genetic modifiers in drosophila points to common and distinct mechanisms of pathogenesis among polyglutamine diseases. *Hum. Mol. Genet.* 17, 376–390 (2008).

Bruijn, L. I. *et al.* ALS-Linked SOD1 Mutant G85R Mediates Damage to Astrocytes and Promotes Rapidly Progressive Disease with SOD1-Containing Inclusions. 18, 327–338 (1997).

Chaplot, K. Regulation of VAP (P58S) neuroaggregation in a Drosophila model of Amyotrophic Lateral Sclerosis. (2019).

Chaplot, K. *et al.* SOD1 activity threshold and TOR signalling modulate VAP(P58S) aggregation via reactive oxygen species-induced proteasomal degradation in a Drosophila model of amyotrophic lateral sclerosis. *DMM Dis. Model. Mech.* 12, (2019).

Chaves-Filho, A. B. *et al.* Alterations in lipid metabolism of spinal cord linked to amyotrophic lateral sclerosis. *Sci. Rep.* 9, 1–14 (2019).

De Aguilar, J. L. G. Lipid biomarkers for amyotrophic lateral sclerosis. *Front. Neurol.* 10, 1–6 (2019).

Deivasigamani, S., Verma, H. K., Ueda, R. & Ratnaparkhi, A. RESEARCH ARTICLE A genetic screen identifies Tor as an interactor of VAPB in a Drosophila model of amyotrophic lateral sclerosis. 4, 1–12 (2014).

Dupuis, L., Oudart, H., René, F., Gonzalez De Aguilar, J. L. & Loeffler, J. P. Evidence for defective energy homeostasis in amyotrophic lateral sclerosis: Benefit of a high-energy diet in a transgenic mouse model. *Proc. Natl. Acad. Sci. U. S. A.* 101, 11159–11164 (2004).

Emerman, A. B., Zhang, Z.-R., Chakrabarti, O. & Hegde, R. S. Trehalose Is a Key Determinant of the Quiescent Metabolic State That Fuels Cell Cycle Progression upon Return to Growth. *Mol. Biol. Cell* 21, 4325–4337 (2010).

Estes, P. S. *et al.* Wild-type and A315T mutant TDP-43 exert differential neurotoxicity in a Drosophila model of ALS. *Hum. Mol. Genet.* 20, 2308–2321 (2011).

Fergani, A. *et al.* Increased peripheral lipid clearance in an animal model of amyotrophic lateral sclerosis. *J. Lipid Res.* 48, 1571–1580 (2007).

Han, S. M. *et al.* Secreted VAPB/ALS8 Major Sperm Protein Domains Modulate Mitochondrial Localization and Morphology via Growth Cone Guidance Receptors. *Dev. Cell* 22, 348–362 (2012).

Jmg, L. T. O. LETTER TO JMG Key points. 315–320 (2004). doi:10.1136/jmg.2003.013029

Kanekura, K., Nishimoto, I., Aiso, S. & Matsuoka, M. Characterization of amyotrophic lateral sclerosis-linked P56S mutation of vesicle-associated membrane protein-associated protein B (VAPB/ALS8). *J. Biol. Chem.* 281, 30223–30233 (2006).

Kawano, M., Kumagai, K., Nishijima, M. & Hanada, K. Efficient trafficking of ceramide from the endoplasmic reticulum to the golgi apparatus requires a VAMP-associated protein-interacting FFAT motif of CERT. *J. Biol. Chem.* 281, 30279–30288 (2006).

Kim, S. M. *et al.* Amyotrophic lateral sclerosis is associated with hypolipidemia at the presymptomatic stage in mice. *PLoS One* 6, 1–5 (2011).

Lev, S., Halevy, D. Ben, Peretti, D. & Dahan, N. The VAP protein family : from cellular functions to motor neuron disease. (2008). doi:10.1016/j.tcb.2008.03.006

Liu, L., MacKenzie, K. R., Putluri, N., Maletić-Savatić, M. & Bellen, H. J. The Glia-Neuron Lactate Shuttle and Elevated ROS Promote Lipid Synthesis in Neurons and Lipid Droplet Accumulation in Glia via APOE/D. *Cell Metab.* 26, 719-737.e6 (2017).

Loewen, C. J. R., Roy, A. & Levine, T. P. A conserved ER targeting motif in three families of lipid binding proteins and in Opi1p binds VAP. *EMBO J.* 22, 2025–2035 (2003).

Madabattula, S. T. *et al.* Quantitative analysis of climbing defects in a drosophila model of neurodegenerative disorders. *J. Vis. Exp.* 2015, 1–9 (2015).

Moustaqim-barrette, A. *et al.* The amyotrophic lateral sclerosis 8 protein , VAP , is required for ER protein quality control. 23, 1975–1989 (2014).

Nishimura, A. L. *et al.* A Mutation in the Vesicle-Trafficking Protein VAPB Causes Late-Onset Spinal Muscular Atrophy and Amyotrophic Lateral Sclerosis. 2, 822–831 (2004).

Pennetta, G., Hiesinger, P. R., Fabian-fine, R., Meinertzhagen, I. A. & Bellen, H. J. Drosophila VAP-33A Directs Bouton Formation at Neuromuscular Junctions in a Dosage-Dependent Manner. 35, 291–306 (2002).

Perry, R. J., and Ridgway, N. D. Oxysterol-binding protein and vesicle associated membrane protein-associated protein are required for sterol-dependent activation of the ceramide transport protein. Mol. Biol. Cell. (2006).

Piper MD, Partridge L. Protocols to Study Aging in Drosophila. *Methods Mol Biol*. (2016).

Ratnaparkhi, A., Lawless, G. M., Schweizer, F. E., Golshani, P. & Jackson, G. R. A Drosophila model of ALS: Human ALS-associated mutation in VAP33A suggests a dominant negative mechanism. *PLoS One* 3, (2008).

Sanhueza, M. *et al.* Network Analyses Reveal Novel Aspects of ALS Pathogenesis. *PLoS Genet.* 11, 1–32 (2015).

Schmitt, F., Hussain, G., Dupuis, L., Loeffler, J. P. & Henriques, A. A plural role for lipids in motor neuron diseases: Energy, signaling and structure. *Front. Cell. Neurosci.* 8, 1–10 (2014).

Shcherbata, H. R. *et al.* Dissecting muscle and neuronal disorders in a Drosophila model of muscular dystrophy. *EMBO J.* **26**, 481–493 (2007).

Skehel, P. A., Martin, K. C., Kandel, E. R. & Bartsch, D. A VAMP-binding protein from Aplysia required for neurotransmitter release. *Science (80-).* 269, 1580–1583 (1995).

Sophie Mokas, J. R. M. *et al.* Uncoupling Stress Granule Assembly and Translation Initiation Inhibition. *Mol. Biol. Cell* 20, 2673–2683 (2009).

Soussan, L. *et al.* Mediated by COPI Vesicles. *J. Cell Biol.* 146, 301–311 (1999).

Stieber, A., Gonatas, J. O. & Gonatas, N. K. Aggregates of mutant protein appear progressively in dendrites, in periaxonal processes of oligodendrocytes, and in neuronal and astrocytic perikarya of mice expressing the SOD1(G93A) mutation of familial amyotrophic lateral sclerosis. *J. Neurol. Sci.* 177, 114–123 (2000).

Tsuda, H. *et al.* The Amyotrophic Lateral Sclerosis 8 Protein VAPB Is Cleaved , Secreted , and Acts as a Ligand for Eph Receptors. 963–977 (2008). doi:10.1016/j.cell.2008.04.039

Wyles, J. P., McMaster, C. R. & Ridgway, N. D. Vesicle-associated membrane protein-associated protein-A (VAP-A) interacts with the oxysterol-binding protein to modify export from the endoplasmic reticulum. *J. Biol. Chem.* 277, 29908–29918 (2002).

Yamanaka K, Chun SJ, Boillee S, et al. Astrocytes as determinants of disease progression in inherited amyotrophic lateral sclerosis. *Nat Neurosci*. (2008).

Chapter III

Elucidating cell autonomous and non-cell autonomous genetic interactions of *VAP^{P58S}* with other ALS loci

1. Summary

The genomic system described in Chapter II is an excellent model for studying genetic interactions of *VAP*. The strengths of the system includes an endogenously regulated promoter, a lack of wild type protein as a result of the null background, and shortened adult lifespan with progressive motor defects. Literature suggests presence of genetic interactions among ALS loci in the neuron (Hadano et al., 2010; Deng et al., 2010; Blitterswijk et al., 2012). Additionally, non-neuronal cells appear to be part of an extended genetic network of ALS (Bruijn et al., 1998; Hensley et al., 2006; Yamanaka et al., 2008; Tong et al., 2013). Our goal is to uncover and characterize these interactions using the $\Delta VAP; gVAP^{P58S}$ fly line.

We chose six *Drosophila* genes that are orthologous to ALS loci, namely *TBPH (Drosophila* orthologue of *TDP-43)*, *caz (Drosophila* orthologue of *FUS)*, *SOD1*, *TER94 (Drosophila* orthologue of *VCP)*, *alsin* and *senataxin*. Activity of these genes is either increased or decreased in the three cell types, muscle, glia and motor neurons in the background of the $\Delta VAP; gVAP^{P58S}$ fly line. Lifespan is the primary readout and enhancement/suppression of adult lifespan is used to identify autonomous or non-autonomous genetic interactions of *VAP* with other loci. Our results suggest differential interactions of the six loci with *VAP^{P58S}*, based on cell type. One interesting interaction is the *TER94- VAP ^{P58S}* in the glia, where overexpression of the *TER94^{R152H}* mutant increases the lifespan of $\Delta VAP; gVAP^{P58S}$. This result, when explored further leads to the gene *caspar*, which appears to be a physical interactor of both VAP and TER94. Increase in *caspar* activity suppresses the $\Delta VAP; gVAP^{P58S}$ lifespan and motor phenotypes – implicating the VAP-TER94-Caspar complex and a specific ERAD pathway in the disease model.

2. Introduction

Concepts of non-cell autonomy and oligogeny are relatively new to the field of ALS (Lattante et al., 2015, Haidet-Phillips., 2012). We have explored these ideas in the context of ALS8 in this Chapter.

2.1. Oligogenic nature of ALS: Contribution of *VAP^{P58S}* to the gene regulatory network

As discussed in Chapter I, (Section 2.5) sequencing studies in ALS patients have reported more than one ALS locus to be affected in a single subject, giving the disease an oligogenic nature (Lattante et al., 2015). So far, a few ALS causing genes have been known to be involved in its oligogenic etiology and *VAP* is one of them. A study reported the co-occurrence of mutant *VAPB* and *c9orf72* repeat expansion in a Dutch patient, feeding into our list of ALS loci being reported to contribute to the oligogenic nature of the disease (Blitterswijk et al., 2012).

Studies in various animal models or cell lines describe the involvement of *VAP* and its interactions with various other ALS loci. VAP, an ER membrane protein is known to associate with the mitochondrial protein PTPIP51 (Protein tyrosine phosphatase interacting protein 51) and hence participates in building up ER-mitochondrial connections. These connections are disrupted on the expression of *TDP-43* variants, suggesting interactions between VAP-PTPIP51 and TDP-43 (Stoica et al., 2014). Furthermore, in an independent transgenic mouse model, mutant VAP aggregates were observed to recruit and accumulate TDP-43 in the cytoplasm, leading to mislocalization of TDP-43 (Tudor et al., 2010). Stoica and colleagues further characterized the perturbation of VAP-PTPIP51 interactions by expressing variants of *FUS* (Stoica et al., 2016), reiterating the idea of interaction of *VAP* with other ALS loci. Delving more into studies related to VAP and other ALS loci, a study in mice with ALS associated *SOD1* mutations has revealed that free VAP levels were reduced in the end-stages of the disease, suggesting an association of wild type VAP protein with the mutated SOD1 (Teuling et al., 2007).

Our Lab (Deivasigamani et al., 2014) performed an enhancer-suppressor screen in *Drosophila* and identified *TDP-43*, *alsin* and *SOD1* as interactors of *VAP* thus strengthening the possibility of interaction between ALS loci. Besides the enhancer-suppressor screen, a targeted RNAi screen using the *UAS-GAL4* system by Chaplot et al., in 2019 also identified *TDP-43* and *SOD1* as interactors of *VAP^{P58S}* and characterized the *VAP^{P58S}*-*SOD1* interaction using aggregate changes as a readout in the *Drosophila* larval brain.

Consolidating all the above studies concerning interactions of *VAP* with numerous loci, we speculated that *VAP* can potentially affect the activity of other loci in an oligogenic manner. We have looked into these potential genetic interactions between VAP^{P58S} and other ALS loci in this Chapter.

2.2. Involvement of non- neuronal cells of the tripartite synapse in ALS pathogenesis

Chapter I discusses the significance of non-cell autonomy in ALS (Chapter I, Section 2.7). Although studies allude to the involvement of non-neuronal cells in the progression of ALS, substantial evidence to pinpoint specific roles for these cells is missing.

Tsuda and colleagues elucidated the non-cell autonomous contribution of *VAP* in ALS by demonstrating the signalling of VAP at the NMJ (Tsuda et al., 2008; Han et al., 2008 and 2013). The major sperm protein (MSP) domain of VAPB is cleaved and secreted from the neurons and binds to the receptors Ephrin, Robo and Clr-1 on the muscles (Han et al., 2012; Tsuda et al., 2008 and 2013), facilitating retrograde signalling at the neuromuscular junction (NMJ). This signalling is impaired in case of VAP^{P58S}, leading to disrupted mitochondrial localization (Tsuda et al., 2008). Apart from the involvement of neuron-muscle signalling, studies linking non-neuronal cells with *VAP* are otherwise lacking.

Along with exploring the oligogenic nature of *ALS8* (Section 2.1), we also aimed to uncover the significance of the non-neuronal cells of the tripartite synapse, namely the muscles and glia in ALS8 progression.

Our Hypothesis: *ALS loci interact with each other to form gene regulatory networks (GRNs) that are central to cellular homeostasis. In addition to their roles in motor neurons, mutations in ALS genes also contribute to the disease via their effects in muscle and glia. A perturbation in intracellular GRNs in either neurons, glia or muscle may also alter anterograde or retrograde signalling at the tripartite synapse, which in turn leads to death of motor neurons.*

We worked around our hypothesis in two steps:

1. Exploring cell-specific interactions between *VAP^{P58S}* and other loci: We screened for possible muscle/glial/motor neuron-specific genetic interactors of *VAP^{P58S}* from a list of selected ALS causing loci (Section 3.1).

Table 3.1. List of ALS causing loci, screened for cell-specific genetic interactions with *VAP^{P58S}*

Gene	*Drosophila* orthologue used in this study	Protein	Putative protein function
VAPB	*VAP33A*	Vesicle associated membrane protein - associated protein B	UPR, cytoskeletal organization, Lipid biosynthesis
SOD1	*SOD1*	Cu/Zn Super oxide dismutase 1	Antioxidants in cytosol
TDP-43/ TARDBP	*TBPH*	TAR DNA binding protein	RNA transport, splicing, maintenance of genomic integrity, miRNA processing
FUS	*Cabeza (caz)*	Fused in Sarcoma	RNA transport, splicing, maintenance of genomic integrity, miRNA processing
VCP/p97	*TER94*	Valosin containing protein	UPS, UPR, ERAD
alsin	*alsin*	Alsin	GTPase regulation and Endosomal trafficking
senataxin	*senataxin*	Senataxin	DNA/RNA metabolism and helicase activity

Chen et al 2013; Mejzini et al., 2019; https://www.uniprot.org/

2. Investigating signalling cascades/regulatory mechanisms concerning the genetic interactions at the tripartite synapse: We narrowed down on *TER94 (VCP)* as our target locus. In order to understand the mechanisms involved in the genetic interactions, we explored various

pathways/regulatory mechanisms running at the tripartite which were related to *VAP* and *TER94* (Section 3.2).

3. Results

3.1. Using Survival assays to test genetic interactions of ALS loci variants with VAP^{P58S}

The Δ*VAP; gVAP^{P58S}* fly exhibits defects in its motor abilities as well as lifespan (Chapter II, Section 3.1 and 3.2); we used these qualities to explore the genetic interactions of other ALS loci with *VAP^{P58S}* by overexpressing and downregulating them in the Δ*VAP; gVAP^{P58S}* background (hereafter referred as the *gVAP^{P58S}* background). We screened for a locus or loci that will either enhance or suppress the phenotypic defects. Our rationale being, a genetic interaction will bring out a change, either increase or decrease, in the lifespan and the motor activity of the fly (Fig. 3.2). In the context of our studies, an 'Enhancer' is defined as a result that modulates the activity of a gene that leads to *decrease* in value of the parameter being measured (Lifespan) while a 'Suppressor' leads to *increase* in the value.

As mentioned earlier, the concept of non-cell autonomy has been discussed and studied by a few groups of researchers in the field of ALS. Along with the intent of exploring the genetic interactions in this part of the Chapter (Section 3.1), we were curious to understand the dynamics of these interactions amongst different cell types. We used the Δ*VAP; gVAP^{P58S}* fly line as a tool for understanding the genetic interactions between *VAP^{P58S}* and variants of other ALS loci. We introduced a cell-specific Gal4 driver in chromosome II of the Δ*VAP; gVAP^{P58S}* fly line. Since the focus of our study is on the tripartite synapse system, Gal4 lines specific to the three cell types were introduced in the chromosome II. The three Gal4s were *MHC-Gal4* for muscles, *Repo-Gal4* for glial cells and *OK6-Gal4* for motor neurons as described (Fig. 3.1.)
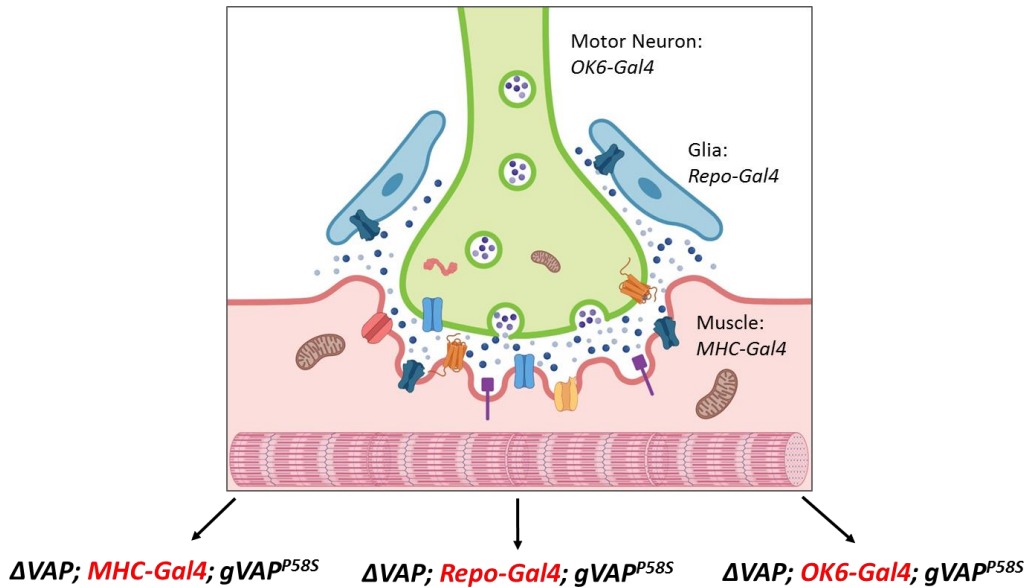
Figure 3.1. Muscle, Glia and Motor neurons specific Gal4 drivers in the Δ*VAP; gVAP^{P58S}* fly line.
Stable fly lines of Δ*VAP; MHC-Gal4; gVAP^{P58S}* for muscle expression, Δ*VAP; Repo-Gal4; gVAP^{P58S}* for glial expression and Δ*VAP; OK6-Gal4; gVAP^{P58S}* for motor neuronal expression were generated for cell-specific genetic interaction experiments by modifying the Δ*VAP; gVAP^{P58S}* fly line.

These three fly lines were further used to perturb the expression levels of *VAP, TBPH, caz, SOD1, TER94*, *alsin* and *senataxin* in muscle, glia and motor neurons separately in the *gVAP^{P58S}* background, followed by recording the suppression or enhancement of lifespan defects (Fig. 3.2).
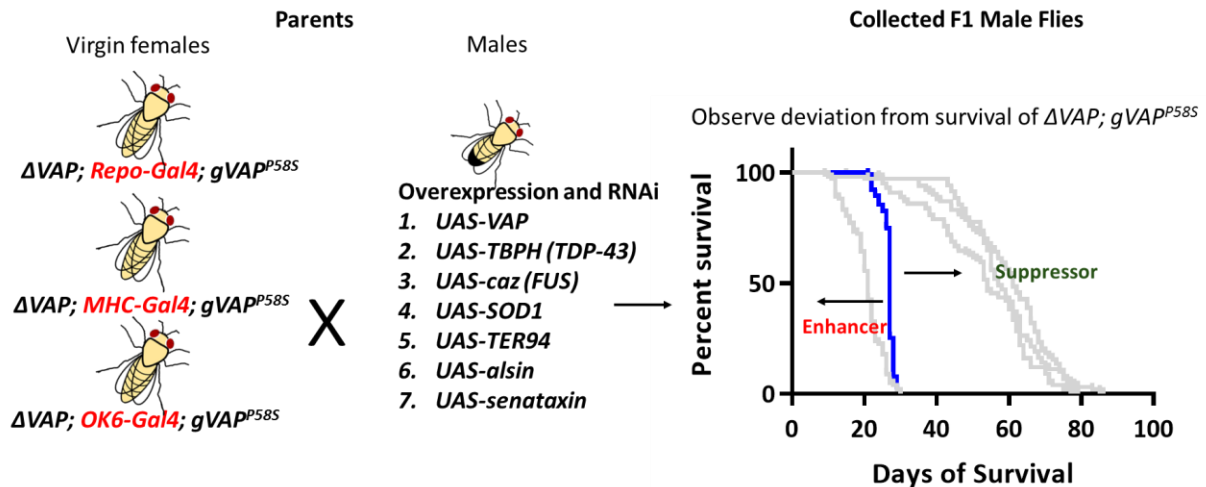
Figure 3.2. Scheme for the cell-specific genetic interaction screen.
The Δ*VAP; MHC-Gal4; gVAP^{P58S}* for muscle expression, Δ*VAP; Repo-Gal4; gVAP^{P58S}* for glial expression and Δ*VAP; OK6-Gal4; gVAP^{P58S}* for motor neuronal expression were used to overexpress and knockdown *VAP, TBPH, caz, SOD1, TER94*, *alsin* and *senataxin* in the three cell types in separate cell-specific screen. The survival of around 80-100 F1 male flies was observed for each locus variant. The blue curve in the

survival assay plot is a representative of Δ*VAP; X-Gal4; gVAP^{P58S}* /+ fly line which was the genotype of the control i.e. Δ*VAP; MHC-Gal4; gVAP^{P58S}* for the muscle-specific screen, Δ*VAP; Repo-Gal4; gVAP^{P58S}* for the glial-specific screen and Δ*VAP; OK6-Gal4; gVAP^{P58S}* for the motor neuron-specific screen. The ALS loci variants which caused a deviation from the lifespan of the control were considered as potential genetic interactors of *VAP^{P58S}.* A shift from the lifespan of the control to the right led to a suppression of the phenotype while towards the left led to enhancement. These ALS loci variants were therefore termed suppressors or enhancers.

The survival analysis was done using the log-rank test prism7 survival assay protocol where each curve was compared to the control and its value of significance was noted. It is important to note that, while the log-rank test considers the trend of change in lifespan as its measure for determination of significance, we also considered the median survival value in deciding our target genetic interactors. The results were depicted in the form of color tones representing different levels of statistical confidence based on the log-rank test for the 'Enhancers (E)' and 'Suppressors (S)'. Along with the values of statistical significance, we considered values of ΔML (Change in Median Lifespan) = Median Lifespan (Experiment) – Median Lifespan (Control) to narrow down on our targets.

Scheme for all crosses in the cell-specific screen and further experiments was fixed. We collected F1 males as the F1 females have one copy of wild type VAP as a result of the X chromosome from the parental UAS fly lines. UAS fly lines only on the 2nd or the 3rd chromosomes were used.

3.1.1. Screening ALS loci for alterations in the lifespan of Δ*VAP; gVAP^{P58S}* fly on their muscle expression

We carried out survival assays (Chapter II, Materials and Methods, Section 5.3) by overexpression and RNAi based knockdown of *VAP, TBPH, caz, SOD1, TER94, senataxin* and *alsin* in the muscles, using the Δ*VAP; MHC-Gal4; gVAP^{P58S}* fly line. It is important to note that this second chromosome *MHC-Gal4* expresses from the pupal stages of the fly. The Δ*VAP; MHC>+; gVAP^{P58S}* used as the control in this case is effectively the same as Δ*VAP; gVAP^{P58S}* /+ except for the presence of Gal4 and shows a median lifespan of 26 days. Considering the possibility that the introduction of a Gal4 could alter the lifespan of the original fly line, we used Δ*VAP; MHC>+; gVAP^{P58S}* as our master control for the muscle screen.

The results for the muscle-specific screen are as follows:

1. Most loci variants enhance the lifespan defect i.e. they reduce the lifespan even further. Figure 3.3 describes the survival plots for each locus we screened.

2. Overexpression of wild type *VAP* causes reduction of lifespan even further, with a median of 21 days, suggesting that an increase in the level of wild type *VAP* in a mutant (*VAP^{P58S}*) background makes the scenario even worse for survival of the fly. Moreover, using *VAP^{RNAi}*,

which knocks down the levels of VAP^{P58S} also reduces the lifespan further (median= 23) but this is not as detrimental as the toxic outcome of wild type overexpression (Fig. 3.3A, B and Table 3.2).

3. *TBPH, SOD1* and *TER94* overexpression as well as knockdown via the muscles in the $gVAP^{P58S}$ background reduces the survival of the flies, suggesting either the possibility of their interaction with *VAP* or toxic effect due to overexpression which is independent of genetic interactions or both. Overexpression and knockdown of these three genes in the muscles in a wild type background will clarify their roles further (Fig. 3.3C, D, F, G, H, I and and Table 3.2).

5. RNAi based muscle knockdown of *senataxin* also enhanced the lifespan defect significantly. Because of the unavailability of overexpression fly lines for *senataxin*, we could not study its effect in any of the screens (Fig. 3.3L and Table 3.2).

6. Three variants that did not show sufficient enhancement or suppression of the phenotype are $alsin^{RNAi}$, $alsin^{WT}$ and caz^{RNAi}. The weak effects could be because of weaker interactions with VAP^{P58S} or insufficient expression of the fly lines in muscles (Fig. 3.3E, J, K and Table 3.2).

Figure 3.3 consists of survival curves depicting the survival trends of muscle expression of each variant in $gVAP^{P58S}$ background.
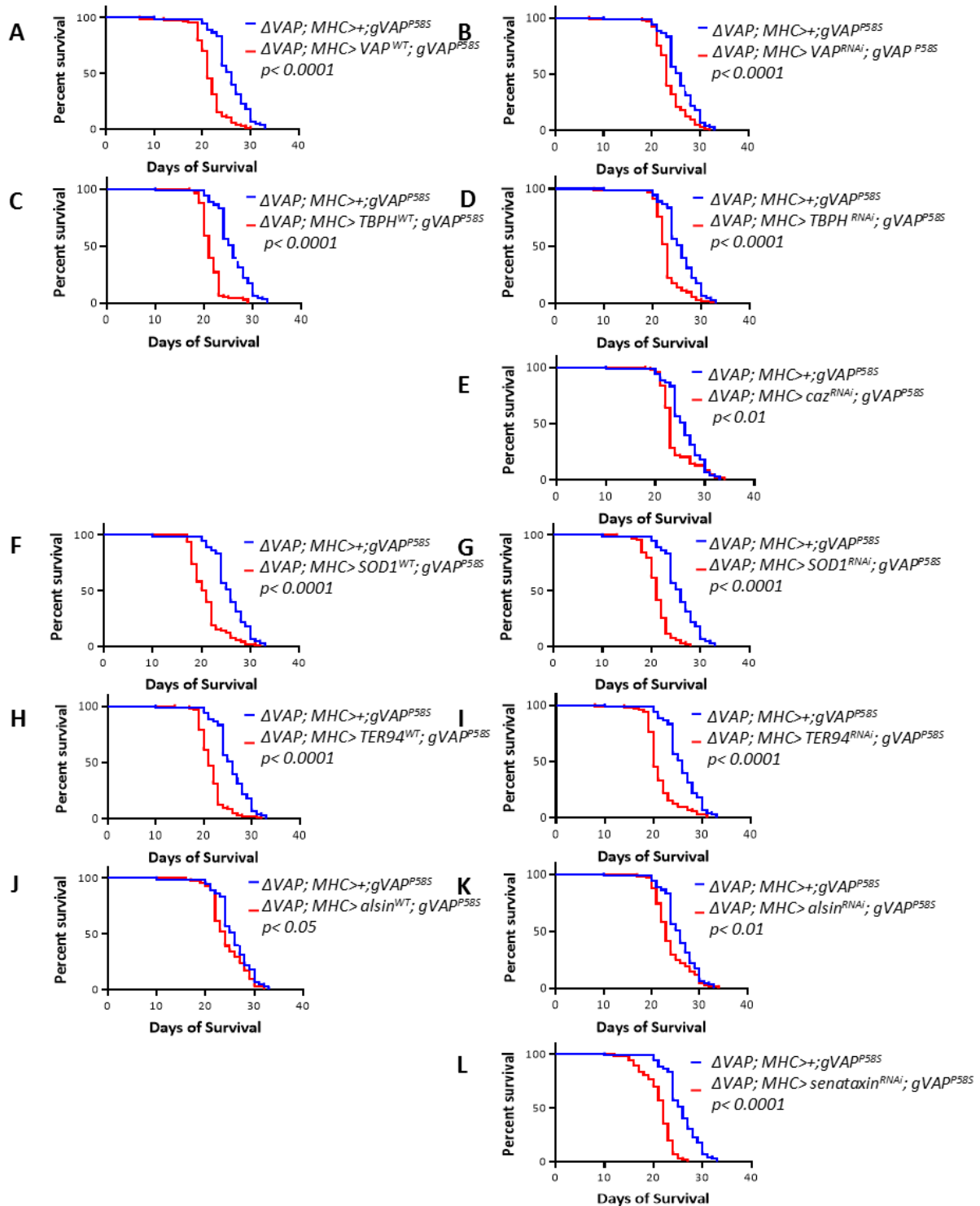
Figure 3.3. Survival assay results for possible interactors of *VAP^P58S* when expressed in muscles.**
Survival plots for muscle overexpression/RNAi based knockdown of *VAP, TBPH, caz, SOD1, TER94, alsin* and *senataxin*. The blue curve represents the Δ*VAP; MHC>+; gVAP^P58S* (median=26) which is the control and is constant in every graph. The red curve represents the locus studied and differs in every graph. The p-value from the log-rank test mentioned in each graph is the comparison of the red curve with the blue

curve in each graph. The median value for $VAP^{WT}= 21$, $VAP^{RNAi}= 23$, $TBPH^{WT}= 21$, $TBPH^{RNAi}= 23$, $caz^{RNAi}= 23$, $SOD1^{WT}= 21$, $SOD1^{RNAi}= 21$, $TER94^{WT}= 21$, $TER94^{RNAi}= 20$, $alsin^{WT}= 24$, $alsin^{RNAi}= 23$, $senataxin^{RNAi}= 22$.

Table 3.2. Representation of muscle-specific enhancers/suppressors of the $\Delta VAP; gVAP^{P58S}$ lifespan defect

The results are in the form of ∆ML (Change in Median Lifespan) = Median Lifespan (Experiment) – Median Lifespan (Control).

'OE' stands for overexpression and 'KD' stands for knockdown.

Color/Statistical Key: The 'red-yellow tones' indicate different levels of statistical confidence (log-rank test) for the 'Enhancers (E)' while the 'green tones' represent the same for 'Suppressors (S)'.

The *caz* overexpression construct is on the X chromosome of the fly line and hence could not be used for our assay.

ALS Loci	OE	KD
	∆ML	
VAP	-5	-3
TBPH (TDP43)	-5	-3
caz (FUS)	Not done	-3
SOD1	-5	-5
TER94 (VCP)	-5	-6
alsin	-2	-3
senataxin	Not done	-4

Key
E= Enhancers
S= Suppressors

E <0.001(***)	
E <0.01(**)	
E <0.05(*)	
>0.05	
S <0.05(*)	
S <0.01(**)	
S <0.001(***)	

3.1.2. Screening ALS loci for alterations in the lifespan of $\Delta VAP; gVAP^{P58S}$ flies on glial expression

We used a second chromosome *Repo-Gal4* driver by introducing it in the $gVAP^{P58S}$ background. Like the $\Delta VAP; MHC>+; gVAP^{P58S}$ in the previous part of our study, $\Delta VAP; Repo>+; gVAP^{P58S}$ was used as a control for glial specific survival assay screening. The median lifespan for the control is 30 days. We followed the same strategy of performing lifespan assays and picking up potential genetic interactors with VAP^{P58S} as in Section 3.1.1.

Observations from the glial screen are as follows:

1. None of the screened genes except *VAP* show strong (p<0.001) modification of the phenotype on their RNAi based glial knockdown (Fig. 3.4 and Table 3.3).

2. *VAP* overexpression and knockdown both show enhancement of lifespan defect. Similar to the muscle screen, *VAP* overexpression (median= 23 days) is more detrimental than the knockdown (median = 26 days) in comparison to the control which has a median lifespan of 30 days (Fig. 3.4A, B and Table 3.3).

3. Other than *VAP*, overexpression of *SOD1*, *TER94* and *alsin* show further reduction in survival. *TER94* overexpression is the most potent enhancer of them all as it shows a median value of 21 days (9-day median difference compared to control) while the median for both *SOD1* as well as *alsin* equals 25 days (Fig. 3.4F, H, J and Table 3.3).

4. No ALS locus variant except *caz^{RNAi}* suppresses the Δ*VAP; gVAP^{P58S}* lifespan defect when expressed in glial cells. The difference with *caz^{RNAi}* is very mild (1-day median difference compared to control, p<0.01) (Fig. 3.4E and Table 3.3).

5. Far lesser variants seem to be interacting via their glial expression as compared to the muscle expression (Fig. 3.4 and 3.3)

Figure 3.4 consists of survival curves depicting the survival trends of glial expression of each variant in *gVAP^{P58S}* background.
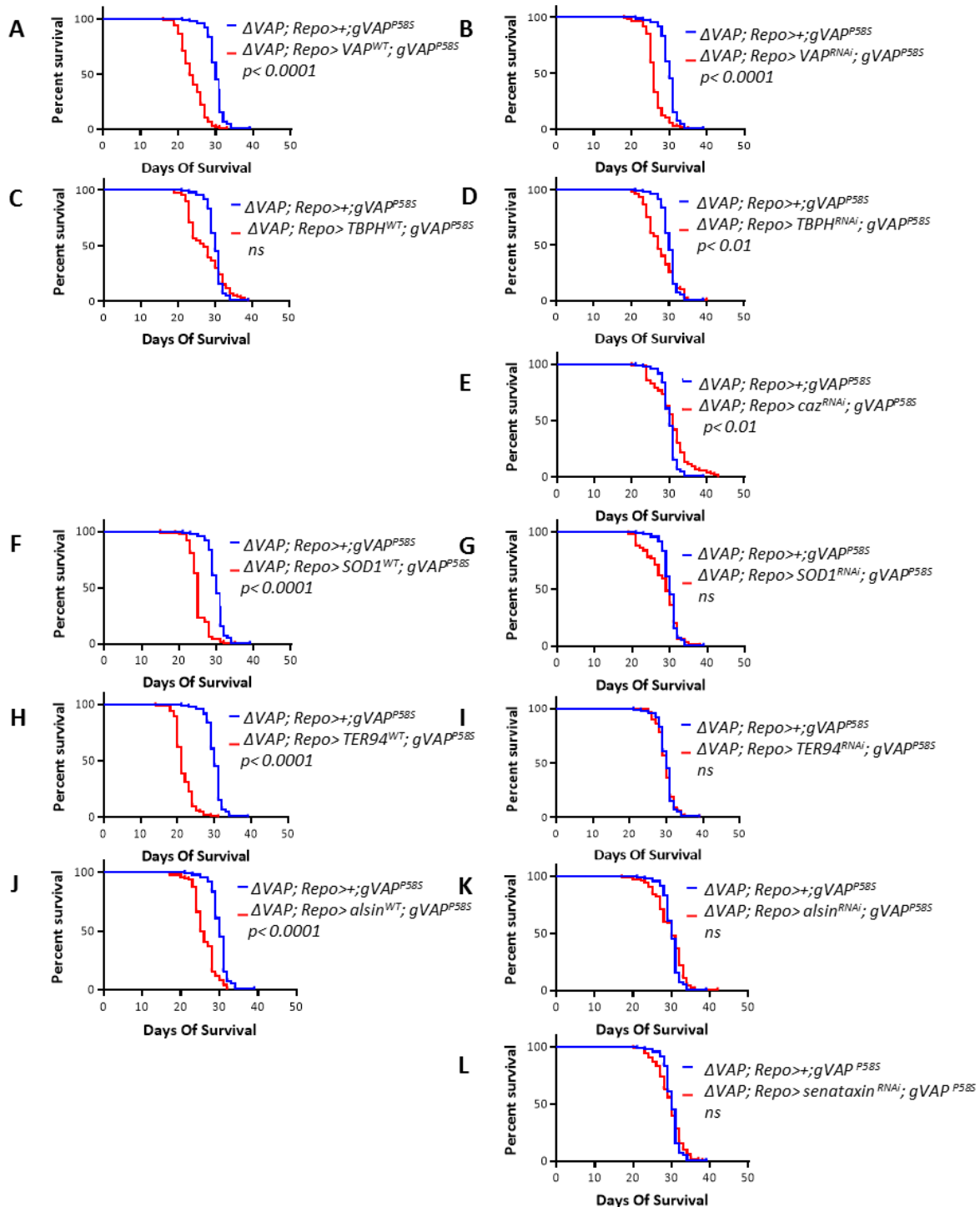
Figure 3.4. Survival assay results for possible interactors of *VAP^P58S* when expressed in glia.
Survival plots for muscle overexpression/RNAi based knockdown of *VAP, TBPH, caz, SOD1, TER94, alsin* and *senataxin*. The blue curve represents the Δ*VAP; Repo>+; gVAP^P58S* (median=30) which is the control and is constant in every graph. The red curve represents the locus studied and differs in every graph. The p-value from the log-rank test mentioned in each graph is the comparison of the red curve with the blue curve in each graph. The median value for *VAP^WT*= 23, *VAP^RNAi*= 26, *TBPH^WT*= 27, *TBPH^RNAi*= 27, *caz^RNAi*=

31, $SOD1^{WT}= 25$, $SOD1^{RNAi}= 29$, $TER94^{WT}= 21$, $TER94^{RNAi}= 30$, $alsin^{WT}= 25$, $alsin^{RNAi}= 30$, $senataxin^{RNAi}= 30$.

Table 3.3. Representation of glia specific enhancers/suppressors of the $\Delta VAP; gVAP^{P58S}$ lifespan defect

The results are in the form of ΔML (Change in Median Lifespan) = Median Lifespan (Experiment) – Median Lifespan (Control).

'OE' stands for overexpression and 'KD' stands for knockdown.

Color/Statistical Key: The 'red-yellow tones' indicate different levels of statistical confidence (log-rank test) for the 'Enhancers (E)' while the 'green tones' represent the same for 'Suppressors (S)'.

The *caz* overexpression construct is on the X chromosome of the fly line and hence could not be used for our assay.

ALS Loci	OE	KD
	ΔML	
VAP	-7	-4
TBPH (TDP43)	-3	-3
caz (FUS)	Not done	+1
SOD1	-5	-1
TER94 (VCP)	-9	0
alsin	-5	0
senataxin	Not done	0

Key
E= Enhancers
S= Suppressors

E <0.001(***)	
E <0.01(**)	
E <0.05(*)	
>0.05	
S <0.05(*)	
S <0.01(**)	
S <0.001(***)	

3.1.3. Screening ALS loci for alterations in the lifespan of $\Delta VAP; gVAP^{P58S}$ flies on their motor neuronal expression

Although our main aim of the study highlights the non-cell autonomous aspect of the disease, it is necessary to analyze and compare the results of the muscles and glia with the neurons. Therefore we performed a motor neuron-specific survival screen. We chose *OK6-Gal4*, a second chromosome driver expressed in motor neurons to be introduced in $\Delta VAP; gVAP^{P58S}$, instead of a pan-neuronal driver like *Elav-Gal4.*

Figure 3.5 consists of survival curves depicting the survival trends of motor neuronal expression of each variant in $gVAP^{P58S}$ background.

On performing the assay using the $\Delta VAP; OK6-Gal4; gVAP^{P58S}$ fly line with *VAP, SOD1, TBPH, caz, TER94, alsin* and *senataxin,* we made the following observations:

1. Downregulation of only 4 loci, *VAP, TBPH, alsin* and *caz* show a strong (p<0.001) perturbation of the lifespan phenotype, all three being suppressors. This suggests the presence of a contrasting gene regulatory network of these loci in the motor neurons as compared to muscles and glia (Fig. 3.5B, D, E, K and Table 3.4).

2. *VAP* overexpression does not show any difference, but RNAi shows suppression of phenotype. There is a possibility that the raised levels of *VAP* are not high enough to produce a difference since this is just motor neuronal and not pan-neuronal expression. Whereas, the downregulation is enough for suppressing the effect of VAP^{P58S} hinting towards its importance as well as differential role in the motor neurons (Fig. 3.5A, B and Table 3.4).

3. Neither the overexpression nor the downregulation of *TER94* causes any difference in lifespan as compared to control which is different from its muscle and glial expression (Fig. 3.5H, I and Table 3.4).

4. Amongst the overexpressed loci, only *SOD1* and *alsin* manifest changes in the lifespan defects. These nature of these changes is mild (p<0.01 and p<0.05) (Fig. 3.5F, J and Table 3.4).

5. A striking feature of the motor neuronal screen is the presence of suppressors as against enhancers in the muscle and glial screen (Table 3.2 Vs 3.3, 3.4).
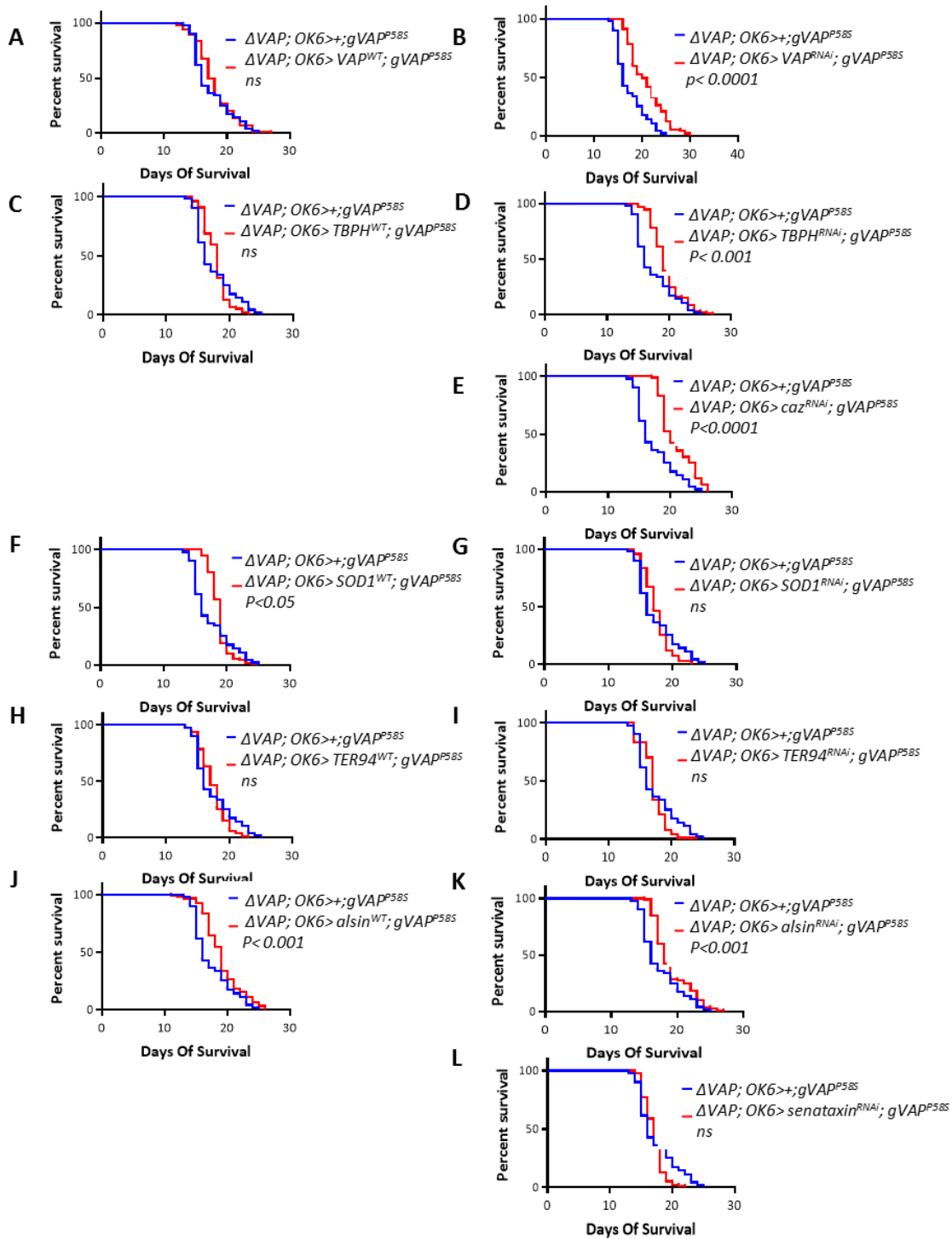
Figure 3.5. Survival assay results for possible interactors of *VAP^P58S* when expressed in motor neurons.

Survival plots for muscle overexpression/RNAi based knockdown of *VAP, TBPH, Caz, SOD1, TER94, Alsin* and *Senataxin*. The blue curve represents the Δ*VAP; OK6>+; gVAP^P58S* (median=16) which is the control and is constant in every graph. The red curve represents the locus studied and differs in every graph. The p-value from the log-rank test mentioned in each graph is the comparison of the red curve with the blue

curve in each graph. The median value for $VAP^{WT}= 17.5$, $VAP^{RNAi}= 20$ $TBPH^{WT}= 18$, $TBPH^{RNAi}= 19$, $caz^{RNAi}= 20$, $SOD1^{WT}= 19$, $SOD1^{RNAi}= 17$, $TER94^{WT}= 17$, $TER94^{RNAi}= 17$, $alsin^{WT}= 19$, $alsin^{RNAi}= 18$, $senataxin^{RNAi}= 17$.

Table 3.4. Representation of motor neuron-specific enhancers/suppressors of the ΔVAP; $gVAP^{P58S}$ lifespan defect

The results are in the form of ΔML (Change in Median Lifespan) = Median Lifespan (Experiment) – Median Lifespan (Control).

'OE' stands for overexpression and 'KD' stands for knockdown.

Color/Statistical Key: The 'red-yellow tones' indicate different levels of statistical confidence (log-rank test) for the 'Enhancers (E)' while the 'green tones' represent the same for 'Suppressors (S)'.

The *caz* overexpression construct is on the X chromosome of the fly line and hence could not be used for our assay.

ALS Loci	OE	KD
	ΔML	
VAP	+1.5	+4
TBPH (TDP43)	+2	+3
caz (FUS)	Not done	+4
SOD1	+3	+1
TER94 (VCP)	+1	+1
alsin	+3	+2
senataxin	Not done	+1

Key
E= Enhancers
S= Suppressors

E <0.001(***)	
E <0.01(**)	
E <0.05(*)	
>0.05	
S <0.05(*)	
S <0.01(**)	
S <0.001(***)	

3.1.4. ALS loci variants when expressed separately in muscle, glia and motor neurons, behave differentially in the $gVAP^{P58S}$ background

The enhancer-suppressor screen brought in various ideas of genetic interactions at the tripartite. Table 3.5 consolidates all the results from the three screens (Section 3.1.1, 3.1.2 and 3.1.3). Certain highlights from the combined results are as follows:

1. The trend of interaction of the screened loci with VAP^{P58S} is different from one another when expressed in muscles, glia and motor neurons separately. Some loci, like *senataxin* in muscles, seem to have more control over the phenotype via one of the cell types than others. A few loci behave in a contrasting manner via different cell types, like VAP^{RNAi} via muscles and motor neurons. Lastly, the strength of the outcome of a locus can be different in muscle, glia and motor neurons e.g. *TER94*

overexpression in glia exhibits stronger effects than its effects in muscle, whereas it shows no difference in the motor neurons.

2. The outcome of perturbing *VAP* levels is interesting, especially because it is in the *gVAP^{P58S}* background. Both overexpression and knockdown of *VAP* in muscles and glia act as enhancers, with the overexpression being worse than the knockdown, which could be an effect of the increased toxicity of the protein. Its overexpression in motor neurons, however, doesn't contribute to any changes to the lifespan, while its motor neuronal knockdown results in suppression of the phenotype. Based on the different outcomes of *VAP* overexpression and knockdown in muscles, glia and motor neurons, it is evident that degree of importance of *VAP* levels is different in the three cell types. This difference could be a function of its differential importance in the three cells or a function of its flux in the system (accumulation in aggregates or present in free form) or simply because of different levels of overexpression/knockdown considering three separate Gal4 strengths. It would be interesting to explore the effect of expressing the *VAP* mutant (*UAS-VAP^{P58S}*) in the three cells separately in the *gVAP^{P58S}* background and elaborate on our understanding of the regulation of VAP levels in the system (Related experiments in Appendix II).

3. *TBPH* overexpression as well as knockdown in the muscle results in enhancing the phenotype while its knockdown in motor neurons results in suppression.

4. *TER94* overexpression enhances the lifespan defect in the muscles as well as glia. Its effect in the glial overexpression is the strongest as the difference in trend is the best (Fig. 3.4) amongst all other loci variants, its median day survival is 21 days (control=30 days). However, it is interesting to note that its overexpression fails to cause any difference in the motor neurons.

5. *senataxin* knockdown only acts via muscles with a 4 days of lifespan defect enhancement.

6. *caz* knockdown has very mild effects in muscle and glia, but its effect is the strongest (suppressor, $p<0.001$) when expressed in motor neurons.

It is important to note that all the above observations (3.1.1 to 3.1.4) are in context of the *gVAP^{P58S}* genetic background.

Table 3.5. Consolidated representation of cell-specific enhancers/suppressors of the $\Delta VAP; gVAP^{P58S}$ lifespan defect

Muscle, Glia and Motor neuron-specific screens highlight differential importance of different loci with respect to their interaction with VAP^{P58S}.

The results are in the form of ΔML (Change in Median Lifespan) = Median Lifespan (Experiment) – Median Lifespan (Control).

'OE' stands for overexpression and 'KD' stands for knockdown.

Color/Statistical Key: The 'red-yellow tones' indicate different levels of statistical confidence (log-rank test) for the 'Enhancers (E)' while the 'green tones' represent the same for 'Suppressors (S)'.

The *caz* overexpression construct is on the X chromosome of the fly line and hence could not be used for our assay.

ALS Loci	Muscle		Glia		Motor Neurons	
	OE	KD	OE	KD	OE	KD
	ΔML					
VAP	-5	-3	-7	-4	+1.5	+4
TBPH (TDP43)	-5	-3	-3	-3	+2	+3
caz (FUS)	Not done	-3	Not done	+1	Not done	+4
SOD1	-5	-5	-5	-1	+3	+1
TER94 (VCP)	-5	-6	-9	0	+1	+1
alsin	-2	-3	-5	0	+3	+2
senataxin	Not done	-4	Not done	0	Not done	+1

Key
E= Enhancers
S= Suppressors

E <0.001(***)	
E <0.01(**)	
E <0.05(*)	
>0.05	
S <0.05(*)	
S <0.01(**)	
S <0.001(***)	

The log-rank test for survival is quite sensitive to changes, and therefore a slight change in the lifespan is reflected to be significant according to the test. It is important to note that while the test considers the trend of change in lifespan as its measure for determination of significance, we also considered the median survival value in deciding our target genetic interactors. Also, it is important to reiterate that all speculated genetic interactions can only be further confirmed by ruling out artefacts caused by overexpression/knockdown of a locus in the wild type background. To elaborate a little further, a locus expressed in the $gVAP^{P58S}$ background can lead to further change of lifespan, but this might be a result of its overexpression/knockdown alone and could have nothing to do with the interaction with VAP^{P58S}. To rule out any artefactual effects in our experiments from the above screen, we used controls which would only overexpress/knockdown these loci in wild type background i.e. the 'Gal4 controls' for our chosen targets.

3.2. Investigating signalling cascades/regulatory mechanisms concerning the genetic interactions with *VAP^{P58S}* at the tripartite synapse

Having explored the cell-specific genetic interactions, it was essential to study the mechanistic contribution of these interactions at the tripartite. Rationale behind this being, a genetic interaction that perturbs a phenotype could potentially be affecting the signalling at the interface of the cell types in action, which is the tripartite synapse in our context. As discussed in Chapter I, the tripartite synapse experiences functioning of a lot of signalling pathways which are regulated by many proteins, signalling molecules and neurotransmitters (Wu and Mei, 2010); some of the ALS loci directly or indirectly contribute to these pathways (Fuentes-Medel et al., 2009; Ratnaparkhi et al., 2008; Kerr et al., 2014). The idea of these pathways playing a role in the cell-specific interactions or vice versa is a step towards comprehending the significance of the non-cell autonomy in ALS.

Amongst the loci variants which caused a further change in the lifespan of the Δ*VAP; gVAP^{P58S}* fly line, *TER94* was an interesting target for further investigation. Highlighting the *TER94-VAP^{P58S}* interactions, *TER94^{WT}* glial overexpression leads to a significant enhancement of the lifespan phenotype of the Δ*VAP; gVAP^{P58S}* fly line which is about 9 days less than that of the control. This was the most pronounced difference as compared to any other enhancer or suppressor in our screen. Also, apart from its glial effects, *TER94* was also picked as an enhancer both on its overexpression and knockdown in muscles but did not show any difference via motor neurons, suggesting it controls lifespan by interacting with *VAP^{P58S}* via muscles and glia (Table 3.5; extended experiment in Appendix III).

In this part (3.2) of the Chapter, we further investigate the *TER94-VAP^{P58S}* interactions by delving deeper into the possible mechanisms underlying this interaction.

3.2.1. Glial expression of *TER94^{R152H}* and *caspar^{WT}* suppresses the survival defect of Δ*VAP; gVAP^{P58S}*

TER94 (mammalian VCP) is an ALS causing locus involved in protein quality control (Chapter I, Section 2.4.4.2 and 2.8). To validate the interaction of *TER94* with *VAP^{P58S}* via glia, we repeated the overexpression and downregulation of *TER94* in the glia in Δ*VAP; gVAP^{P58S}* using Δ*VAP; Repo-Gal4; gVAP^{P58S}*. This assay included the Gal4 controls (same variants expressed in wild type background and not in *gVAP^{P58S}* background) as well.

Along with the *TER94* wild type, we overexpressed two mutants of *TER94*, *A229E* and *R152H* (Ritson et al., 2010). These mutants are *Drosophila* orthologues of human VCP^{A232E} and VCP^{R155H} respectively, found in patients of ALS as well as IBMPFD. The *R155H* is the most frequently occurring allelic mutant, while *A232E* is the most potent allelic mutant in patients; their animal models manifest the occurrence of muscle as well as neurodegeneration (Ritson et al., 2010; Chang et al., 2011; Liang et al., 2014; Nalbandian et al., 2012). $TER94^{A229E}$ was lethal upon overexpression in the glia in wild type as well as $gVAP^{P58S}$ background, so we could not use it for further studies. Overexpressing the $TER94^{R152H}$ in the glia in the $gVAP^{P58S}$ background resulted in suppression of the lifespan phenotype by around 5 days (median value 35 Vs 30 Days, p<0.001). It is important to focus here on the fact that two ALS causing mutants $TER94^{R152H}$ and VAP^{P58S} interact with each other not to deteriorate but to ameliorate the condition. This could be an outcome of altered interaction between VAP and TER94, which is mediated via a protein called FAF1 in mammals (Baron et al., 2014).

FAF1, Fas-associated factor1 is a cofactor of p97/VCP and is involved in the ubiquitin proteasomal system (UPS) where it assists VCP in degradation of various ubiquitinated proteins. The C-Terminal UBX domain of FAF1 is known to interact with VCP (Song et al., 2005; Schuberth et al., 2008; Ewens et al., 2014; Baron et al., 2014). *caspar*, the *Drosophila* orthologue of *FAF1* has highly conserved domains in its encoded protein, hinting towards the possibility of its interactions with TER94 and VAP in *Drosophila* as well. Considering these potential interactions, we overexpressed and downregulated *caspar* in $gVAP^{P58S}$ background. The *caspar* glial overexpression led to suppression of lifespan phenotype which was stronger than the suppression by $TER94^{R152H}$ (median for *caspar* overexpression= 38). The RNAi based knockdown of *caspar* showed an enhancement in the initial stages but this enhancement was not consistent in the later stages leading to no significant difference as compared to the control (median= 26 Days, Fig. 3.6A curve 6). The 'Gal4 controls' (Fig. 3.6C and D) for all the above-tested loci follow a roughly similar trend of longevity as that of control flies (Control for this set= *+;Repo>+;+*). As discussed before, the log-rank test is a very sensitive test and therefore a small difference in trend can easily have a p value lesser than 0.05.The test claims the 'Gal4 control' curves as significantly different as compared to the control, but none of the variants show a drastic change in the lifespan, refuting the toxicity of these variants. The only exception is the *caspar* overexpression, which reduces the lifespan as compared to wild type flies (Fig. 3.6C, D). It is interesting how overexpression of

caspar in wild type background shows an opposite trend as compared to its overexpression in the *gVAP^{P58S}* background (Fig. 3.6A, curve 5 Vs Fig. 3.6C, curve5). We also tested for expression of Caspar at the NMJ by making use of antibody against Caspar. We used third instar larvae of Repo>UAS-GFP flies, to co-stain the NMJ with GFP for marking the glial cells. Anti-Caspar staining in the third instar larval NMJ (For NMJ dissections and staining protocol refer Chapter V, Materials and Methods, Section 5.2.1) demonstrates Caspar to be enriched at the pre-synaptic boutons as well as axons. The glial cells (marked with anti-GFP antibody) which surround the axonal stalk also express Caspar. Caspar is also expressed in the muscles, but the intensity seems low (Fig. 3.6E).
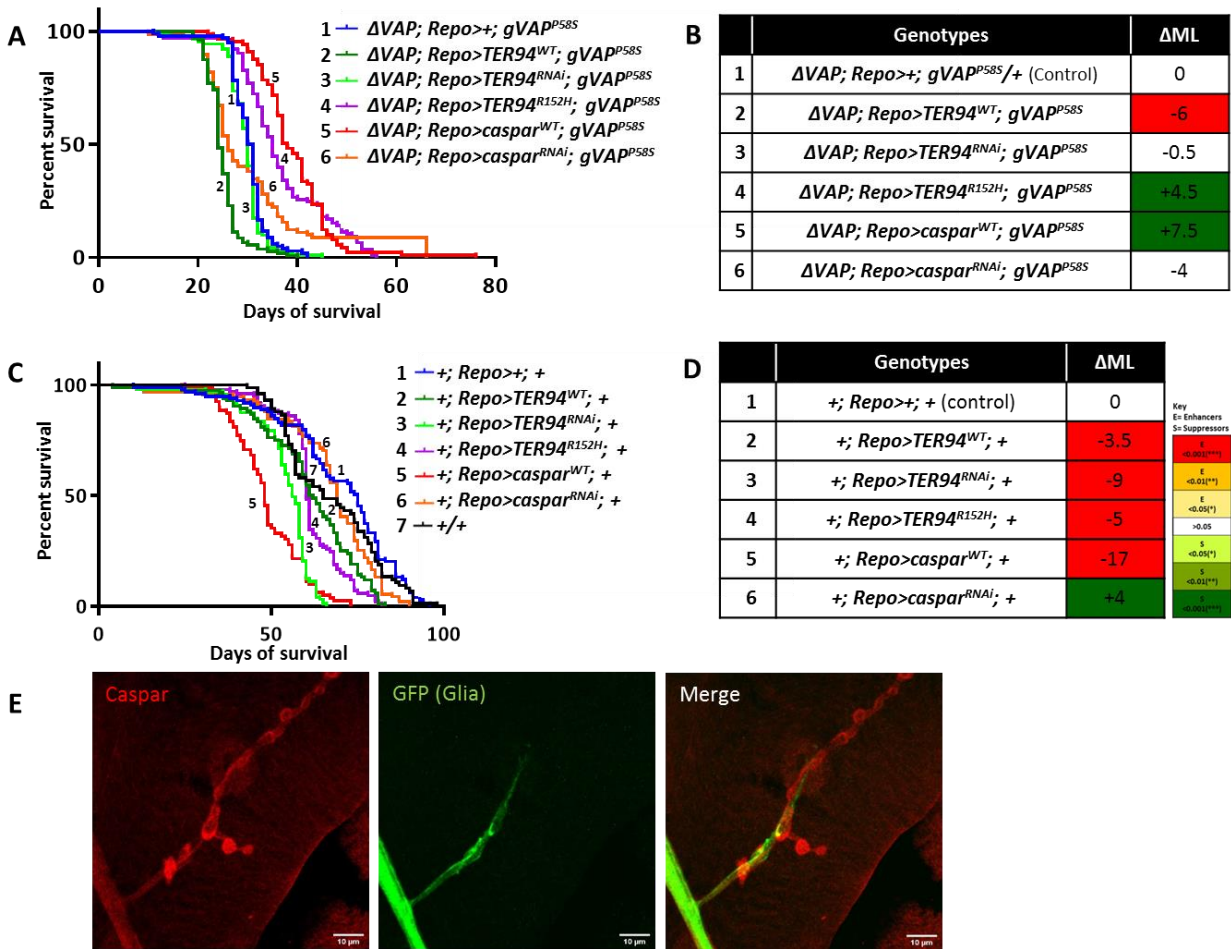
Figure 3.6. *TER94^{R152H}* and *caspar* overexpression in glia in Δ*VAP; gVAP^{P58S}* background leads to an increase in survival as compared to Δ*VAP; Repo>+; gVAP^{P58S}/+*.
A) Overexpression of *TER94^{WT}* (Dark green curve, number 2), *TER94^{RNAi}* (Light green curve, number 3), *TER94^{R152H}* (Purple curve, number 4), *caspar^{WT}* (Red curve, number 5) and *caspar^{RNAi}* (Orange curve, number 6) in the Δ*VAP; Repo-Gal4; gVAP^{P58S}* background. Δ*VAP; Repo>+; gVAP^{P58S}/+* (Curve 1 in blue

color) was used as the control. Curve comparison was done using log-rank (Mantel-Cox test). Combined p-value for the whole set is <0.001.

B) The tabulated results are in the form of ΔML (Change in Median Lifespan) = Median Lifespan (Experiment) – Median Lifespan (Control). Median Lifespan for control= 30.5 Days.

Color/Statistical Key: The 'red-yellow tones' indicate different levels of statistical confidence (log-rank test) for the 'Enhancers (E)' while the 'green tones' represent the same for 'Suppressors (S)'.

C) Overexpression of $TER94^{WT}$ (Dark green curve, number 2), $TER94^{RNAi}$ (Light green curve, number 3), $TER94^{R152H}$ (Purple curve, number 4), $caspar^{WT}$ (Red curve, number 5) and $caspar^{RNAi}$ (Orange curve, number 6) using *+; Repo-Gal4; +* background. *+; Repo>+;+* (Curve 1 in blue color, median lifespan= 75) was the control for curve 2-6, while *+/+* (wild type flies, black curve, number 7) was used as the master control (median lifespan= 65 Days) to compare with curve 1 only (p>0.05, not significant)

Figure C is the 'Gal4 control' for the respective loci expressions in Figure A. n=80-100 flies for every genotype. Curve comparison was done using the log-rank (Mantel-Cox test). Combined p-value for the whole set is <0.001.

D) The individual p-values and median are represented in the corresponding table. Depiction of values is the same as (B).

E) Anti-Caspar staining in the third instar larval NMJ, co-stained with GFP that marks the glial cells.

3.2.2. Glial expression of $TER94^{R152H}$ and $caspar^{WT}$ mitigates the climbing defect in Δ*VAP; gVAP^{P58S}* flies

As characterized in Chapter II, the Δ*VAP; gVAP^{P58S}* fly line develops progressive motor defects, which is reminiscent of the progressive stages of ALS (Chapter II, Section 3.2). In the context of our study, a plausible genetic interaction witnessed in the form of either enhancement or suppression in the longevity of the fly, should also ideally bring a change in the motor defects as well. Based on this premise, we performed climbing assays with all the variants used in Section 3.2.1. These assays were performed in a similar way to the ones in Chapter II and described in Materials and Methods 5.4, Chapter II. The results are represented in the form of enhancers and suppressors of the motor defects, with values of statistical significance in a similar form as the survival assays.

The climbing abilities were observed till day 35 of the life of the flies, post which some genotypes lost the ability to climb, while flies of some other genotypes like Δ*VAP; Repo>TER94^{WT}; gVAP^{P58S}* were dead. The *caspar* overexpression in the glia in *gVAP^{P58S}* background (Red curve, number 5) shows significantly better climbing ability with a consistent difference starting from day 5 to day 25 (Fig. 3.7A, C and E) as compared to other genotypes. A representation of the climbing index of *caspar* overexpression in the form of histograms portrays its better climbing ability in comparison to all other genotypes, with $TER94^{R152H}$ being the second-best (purple curve, number 4). Overexpression of $TER94^{WT}$ (Fig. 3.7A dark green curve, number

2) demonstrates the deterioration of the phenotype which goes hand in hand with the enhancement in its lifespan defect. Focusing further on the glial overexpression of $TER94^{WT}$ in $gVAP^{P58S}$ background, its climbing index is observed to go down to zero after the 20th day (Fig. 3.7A and C).

An important result which is not represented well by the longevity phenotype is the deterioration caused by $caspar^{RNAi}$. Although the median lifespan of $caspar^{RNAi}$ is way lesser than (26 days) the control (30.5 days), the statistical test deems it non-significant as the overall trend is nearly similar (Fig. 3.6A, curve 6 and Fig. 3.6E). This deterioration is reflected well in the progressive stages of climbing, especially on comparing the 20th and 25th day with that of the control (Fig. 3.7A, C and E), corroborating the idea of $caspar\text{-}VAP^{P58S}$ interaction. This result also proposes the importance of the levels of $caspar$ in regulating this genetic interaction.

The 'Gal4 controls' (Fig. 3.7B, D and F) are more or less constant with respect to climbing, except for the $TER94^{WT}$ showing deterioration towards the 35th day. Like the overexpression of $caspar^{WT}$ in the wild type background develops a survival defect as compared to the control (Fig. 3.6B), a similar shift is not reflected in its climbing abilities (Fig. 3.7B, D and F). The climbing assays nevertheless are only performed till the 35th day and such defects might develop later. Anyhow, this defect in the longevity of $+; Repo>caspar^{WT}; +$ is not of crucial importance to us given that the mitigation of the phenotype is only in the earlier stages (Day 10-25) and the longevity defect of $+; Repo>caspar^{WT}; +$ develops from day 40.
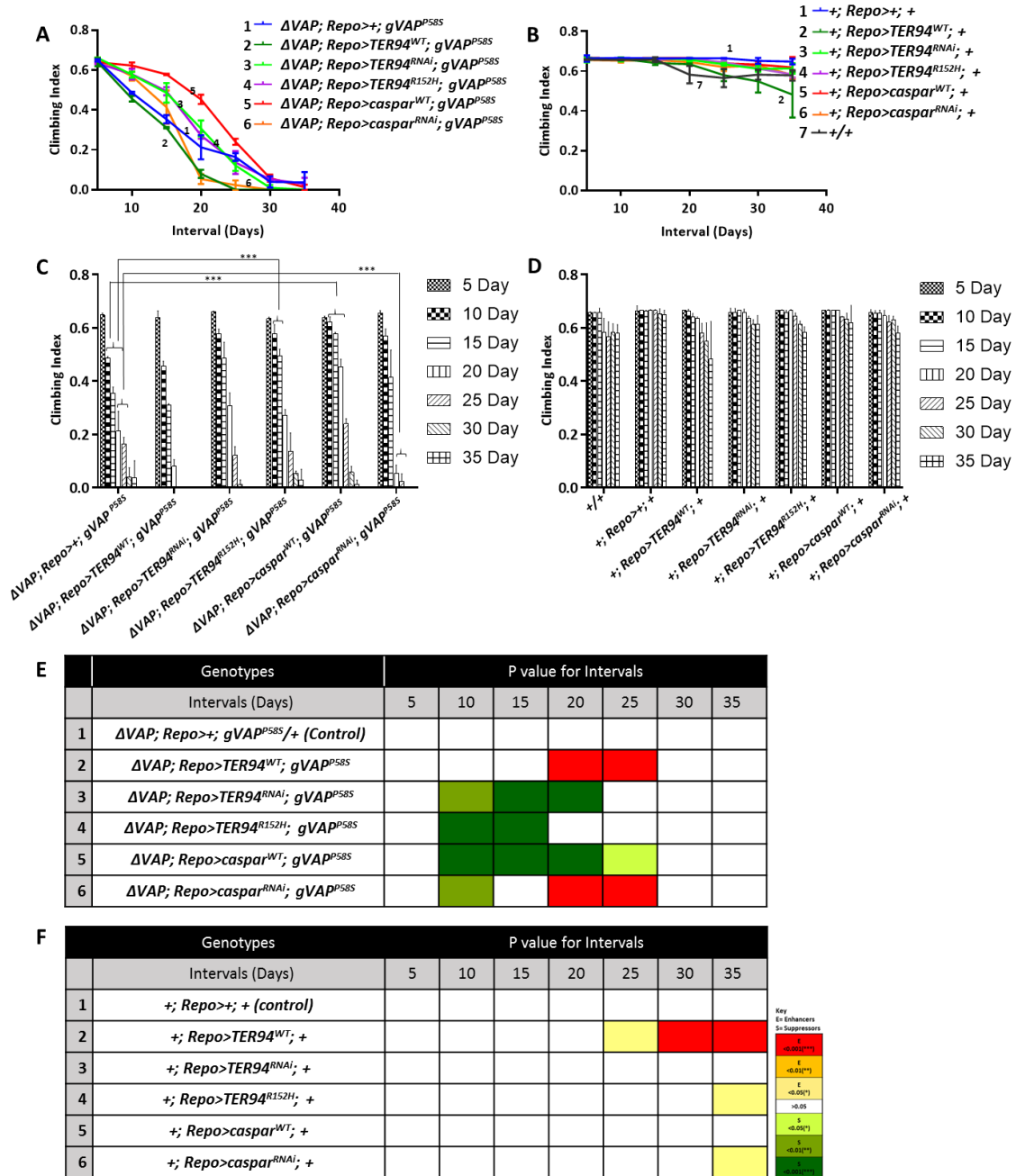
Figure 3.7. Glial overexpression of *caspar^WT* and *TER94^R152H* in *gVAP^P58S* background improves motor defects of the Δ*VAP; gVAP^P58S* flies.

A) Overexpression of *TER94^WT* (Dark green curve, number 2), *TER94^RNAi* (Light green curve, number 3), *TER94^R152H* (Purple curve, number 4), *caspar^WT* (Red curve, number 5) and *caspar^RNAi* (Orange curve, number 6) in the Δ*VAP; Repo-Gal4; gVAP^P58S* background. Δ*VAP; Repo>+; gVAP^P58S/+* (Curve 1 in blue color) was used as the control. The individual p-values are in the table (E).

B) Overexpression of *TER94^WT* (Dark green curve, number 2), *TER94^RNAi* (Light green curve, number 3), *TER94^R152H* (Purple curve, number 4), *caspar^WT* (Red curve, number 5) and *caspar^RNAi* (Orange curve, number 6) using *+; Repo-Gal4; +* background. *+; Repo>+;+* (Curve 1 in blue color) in was the control

95

for curve 2-6, The individual p-values are in the table (F). +/+ (wild type flies, black curve, number 7) was used as the master control to compare with curve 1 only, the p-values for this comparison were: Day 5>0.05 (not significant), Day 10> 0.05 (not significant), Day 15>0.05 (not significant), Day 20>0.01(**), Day 25>0.001(***), Day 30>0.05(*), Day 35>0.05(*).

C, D) Grouped representation of A and B respectively.

E, F) p-values for A and B respectively. Color/Statistical Key: The 'red-yellow tones' indicate different levels of statistical confidence for the 'Enhancers' while the 'green tones' represent the same for 'Suppressors'.

Figure B is the 'Gal4 control' for the respective locus expressions in Figure A. n=30, N= 3 for each genotype. Statistical analysis was done using Two way ANOVA followed by multiple comparison testing by Tukey test. Combined p-value for the whole set is <0.001 while individual level of significance is mentioned in E and F.

Contribution: Lovleen Garg contributed to this experiment by repeating the motor assays performed.

3.2.3. *caspar* doesn't change the larval crawling ability of the Δ*VAP; gVAP^{P58S}* larvae

The improvement in motor defects in the adult flies (Section 3.2.2) made us eager to know if Caspar levels brought changes to the larval crawling as well. Larval crawling is another motor function defect observed in various fly models of ALS and other neurodegenerative disorders (Lanson et al., 2011; Xia et al., 2012). These assays are beneficial simply because observing larval stages is quicker as compared to adults.

We did not explore the larval crawling of Δ*VAP; gVAP^{P58S}* in Chapter II, and were unaware if the Δ*VAP; gVAP^{P58S}* third instar larvae of the Δ*VAP; gVAP^{P58S}* had a crawling defect at all. The crawling assay was performed as described in Materials and Methods (Section 5.2). The genotypes compared were +/+ (master control, only used for comparison with the control), Δ*VAP; Repo>+; gVAP^{P58S}* (control)*, Δ*VAP; Repo>caspar^{WT}; gVAP^{P58S}*, and Δ*VAP; Repo>caspar^{RNAi} gVAP^{P58S}* (compared with control). In the interest of time, we have only chosen to follow up on the genotypes of prime importance in most of the work hereafter. There was no crawling defect found in the Δ*VAP; Repo>+; gVAP^{P58S}* larvae (Fig. 3.8, comparison outcome in red) evidencing that Δ*VAP; gVAP^{P58S}* doesn't manifest motor defects at the larval stages. The *caspar* overexpression/knockdown fly lines as compared to Δ*VAP; Repo>+; gVAP^{P58S}* intuitively did not show any significant change in the crawling abilities (Fig. 3.8, comparison outcome in blue).

It is important to note that the absence of larval crawling defect doesn't necessarily implicate absence of any other pathological aberration like the presence of aggregates or bouton

96

defects at the NMJ, especially as these defects are characterized to be present in $\Delta VAP;\ gVAP^{P58S}$ fly line (Chapter II).
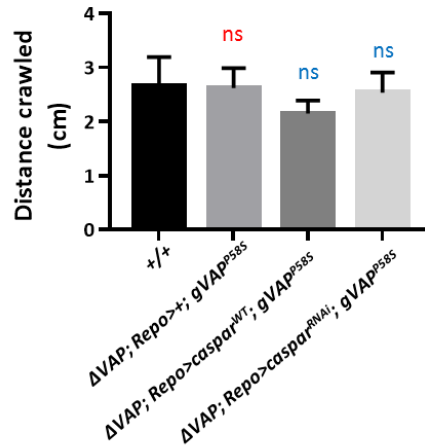
Figure 3.8. Third instar larvae of $\Delta VAP;\ gVAP^{P58S}$ flies do not exhibit crawling defects.
Graphical representation of distance travelled by third instar larvae in centimeters. The genotypes compared are +/+ (master control, Average distance travelled = 2.65±0.53 cm,; only used for comparison with the control, comparison in red), $\Delta VAP;\ Repo>+;\ gVAP^{P58S}$ /+ (control, Average distance travelled = 2.62 ±0.37 cm)*, $\Delta VAP;\ Repo>caspar^{WT};\ gVAP^{P58S}$*(Average distance travelled = 2.15 ±0.23cm)*, and* $\Delta VAP;\ Repo>caspar^{RNAi};\ gVAP^{P58S}$ (compared with control, Average distance travelled = 2.53 ±0.37cm*, in blue). Statistical analysis was done using One way ANOVA followed by multiple comparison testing by Tukey test. n= 10 larvae/genotype. ns= not significant

3.2.4. Caspar glial overexpression in the gVAP^{P58S} background does not lead to change in 'GLOBAL' VAP^{P58S} aggregation pattern in the third instar larval as well as adult brains

One of the crucial hallmarks of ALS is the formation of mutant protein aggregates, and their presence is a sign of impairment of UPR (unfolded protein response) (Cluskey and Ramsden, 2001). We have previously demonstrated aggregation of VAP^{P58S} in an overexpression model of the ALS in *Drosophila* larval brains as well as in SR2+ cell lines (Chaplot et al., 2018). The $\Delta VAP;\ gVAP^{P58S}$ flies also exhibit the presence of aggregates in the larval as well as adult stages (Unpublished). We were curious to know if glial perturbation of Caspar level leads to a change in the status of VAP^{P58S} aggregates. We compared $\Delta VAP;\ Repo>+;\ gVAP^{P58S}$ (control) with $\Delta VAP;\ Repo>caspar^{WT};\ gVAP^{P58S}$, and $\Delta VAP;\ Repo>caspar^{RNAi};\ gVAP^{P58S}$.

The $Repo>caspar^{WT};\ gVAP^{P58S}$ and $\Delta VAP;\ Repo>caspar^{RNAi};\ gVAP^{P58S}$, however, did not show any difference between the aggregates in terms of number/um^2 and size (in um^2) in larval (Fig. 3.9A to D) as well as in 5th, 10th and 15th-day adult brains (Fig. 3.9E to K) (Materials and

Methods, Section 5.6, Chapter II). This could either mean that Caspar doesn't change the aggregation pattern of VAP positive or our parameters (size and number of aggregates) are not suitable to resolve the differences. It is therefore also essential to check the aggregate density parameter to ensure no difference. We should also test for total ubiquitin levels to determine if Caspar affects other misfolded proteins in the system.

In order to know if the localization of the VAP^{P58S} aggregates changes on altering Caspar levels, we co-stained the larval third instar brains with antibodies against the glial nuclear marker, Repo and neuronal nuclear marker, Elav in two separate sets along with anti-VAP and DAPI. Before assessing the change in localization because of Caspar, we checked the localization of these aggregates in the control larvae. Fig. 3.9A describes multiple intensity projection images of the anti-Repo and anti-VAP staining of third instar brains along with the merged and zoomed-in images. The zoomed-in image (Fig. 3.9AI) for Δ*VAP; Repo>+; gVAP^{P58S}* has aggregates localized in the membranes around the nucleus of glia and this localization doesn't seem to change with Caspar's alteration (Fig. 3.9AII, III). Similarly in Fig. 3.9B, a set marked with antibodies against VAP and Elav, the aggregates localize to the membranes and this localization is not changed in the case of Caspar overexpression or knockdown (Fig. 3.9BII, III).

ΔVAP; Repo>+; gVAP^{P58S}

B I VAP Elav DAPI Merge Zoom 100%

ΔVAP; Repo>caspar^{WT}; gVAP^{P58S}

II VAP Elav DAPI Merge Zoom 100%

ΔVAP; Repo>caspar^{RNAi}; gVAP^{P58S}

III VAP Elav DAPI Merge Zoom 100%

Day 5 **Day 15** **Day 30**

E **I** *ΔVAP; Repo>+; gVAP^{P58S}*

II *ΔVAP; Repo>caspar^{WT}; gVAP^{P58S}*

III *ΔVAP; Repo>caspar^{RNAi}; gVAP^{P58S}*

Day 5 Adults **Day 15 Adults** **Day 30 Adults**

F **G** **H**
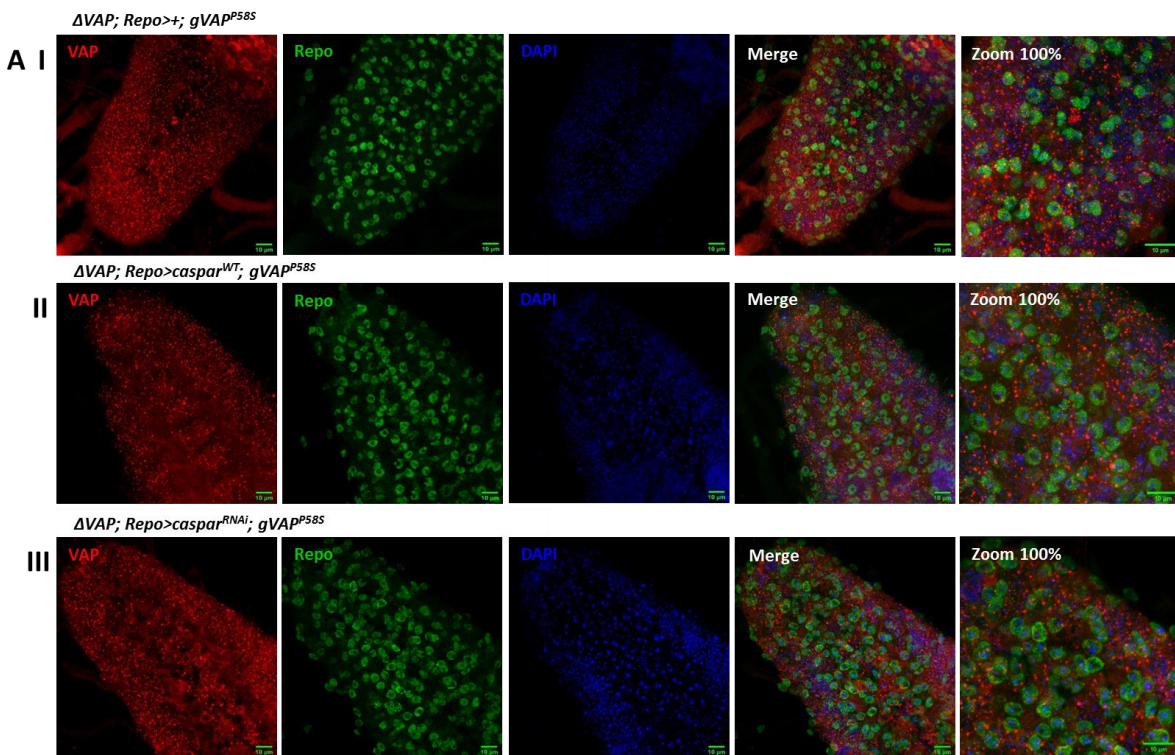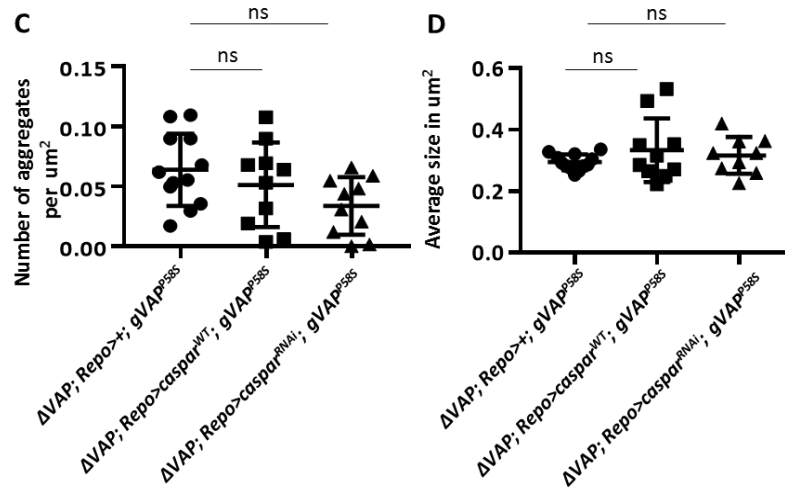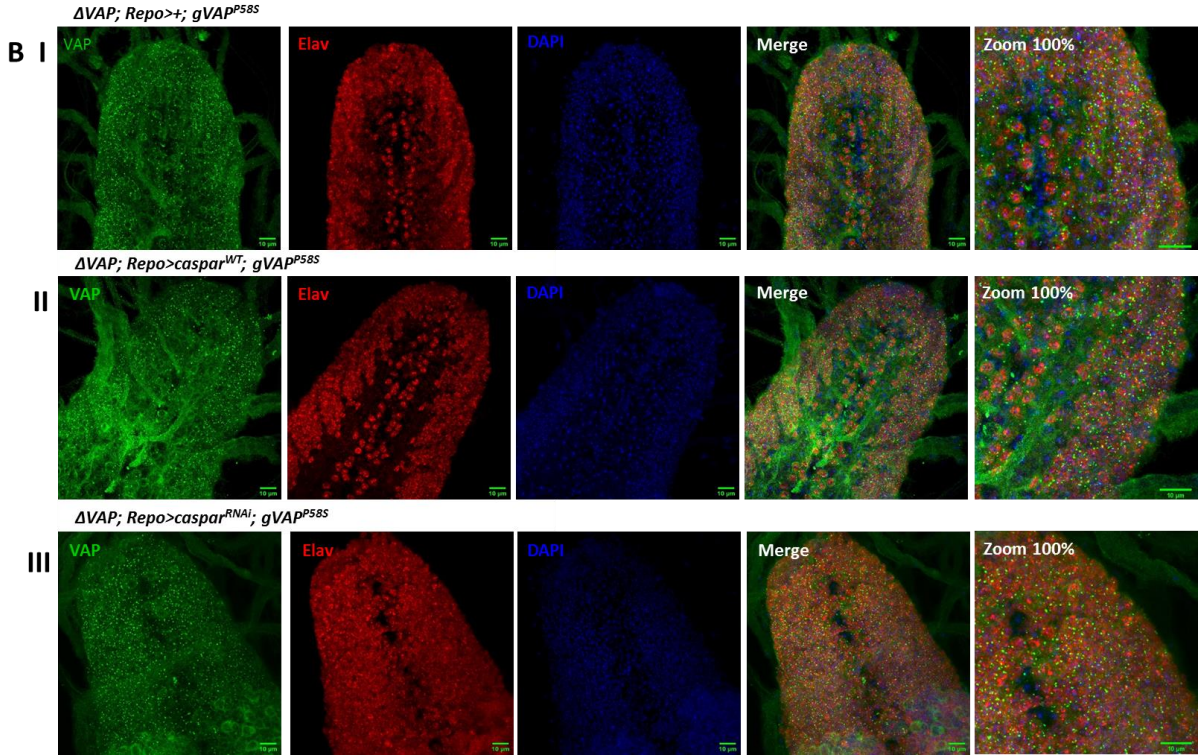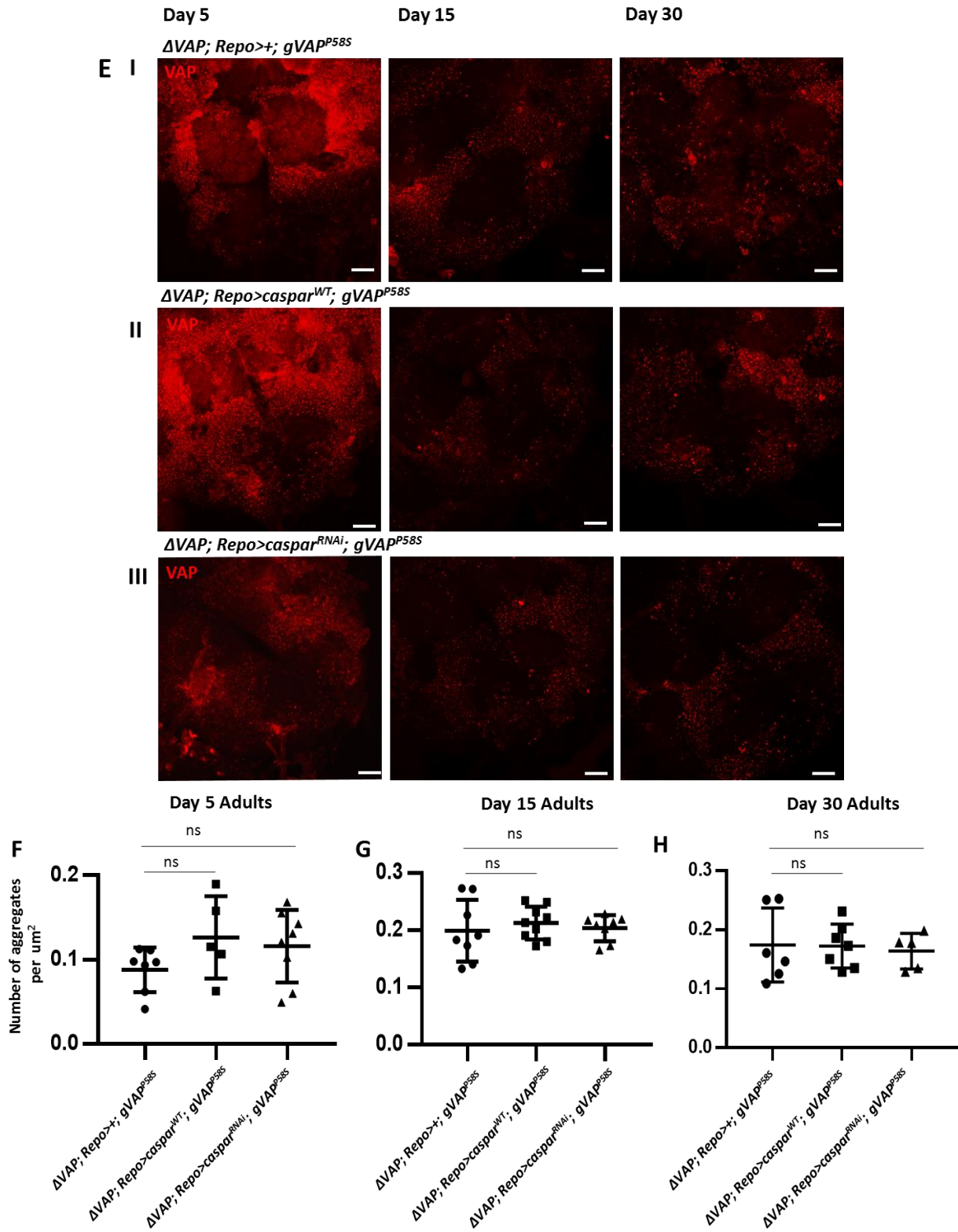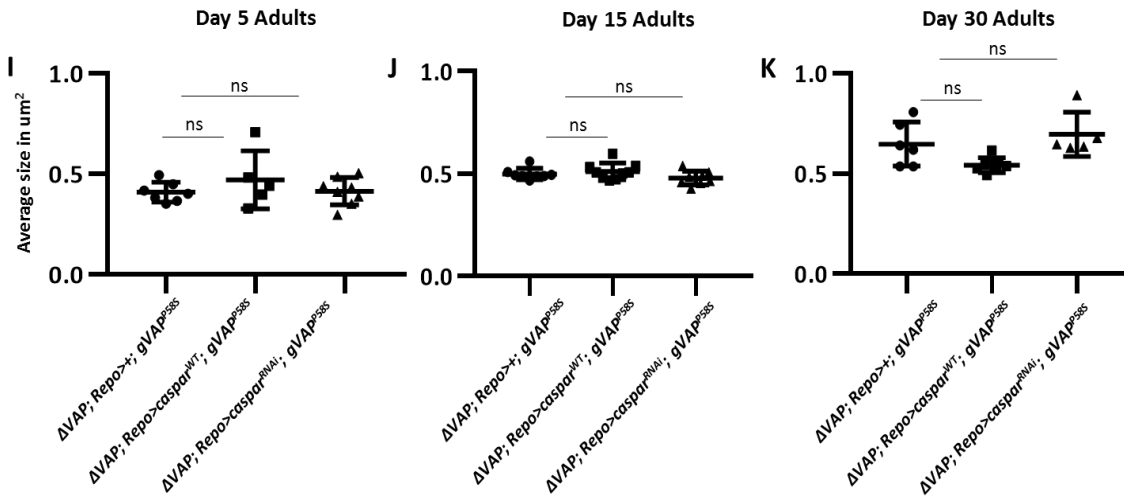
Figure 3.9. VAP^{P58S} aggregates are not altered in case of glial overexpression or knockdown of Caspar in the *gVAP^{P58S}* background.

A, B) Confocal images of third instar larval brains of Δ*VAP; Repo>+; gVAP^{P58S}* (I), Δ*VAP; Repo>caspar^{WT}; gVAP^{P58S}* (II) and Δ*VAP; Repo>caspar^{RNAi}; gVAP^{P58S}* (III). The markers used are VAP, Repo and DAPI in A and VAP, Elav and DAPI respectively in the separated channels. The fourth panel is the merged image followed by 100% zoom.

C, D) Graphical representation of number of aggregates/um^2 followed by size of aggregates in um^2. The genotypes compared are Δ*VAP; Repo>+; gVAP^{P58S} /+* (control)*, Δ*VAP; Repo>caspar^{WT}; gVAP^{P58S}*, and Δ*VAP; Repo>caspar^{RNAi}; gVAP$^{P58S.}$*

E) Confocal images of 5-day, 10-day and 15-day old adult brains of Δ*VAP; Repo>+; gVAP^{P58S}* (I), Δ*VAP; Repo>caspar^{WT}; gVAP^{P58S}* (II) and Δ*VAP; Repo>caspar^{RNAi}; gVAP^{P58S}* (III). The marker used for aggregates is VAP.

F, G, H, I, J, K) Graphical representation of number of aggregates/um^2 followed by size of aggregates in um^2 in 5-day, 10-day and 15-day old adult brains. The genotypes compared are Δ*VAP; Repo>+; gVAP^{P58S} /+* (control)*, Δ*VAP; Repo>caspar^{WT}; gVAP^{P58S}*, and Δ*VAP; Repo>caspar^{RNAi}; gVAP$^{P58S.}$* Statistical analysis was done using One way ANOVA followed by multiple comparison testing by Tukey test. n= ~10 flies/genotype. ns= not significant

Contributions: Aparna Thulasidharan contributed to this experiment by performing the dissections, staining and imaging of the adult brains. Lovleen Garg contributed to this experiment by performing image analysis for larval as well as adult brain aggregates.

3.2.5. Expression of Caspar in glia does not rescue lipid imbalance in Δ*VAP; gVAP^{P58S}*

Recent studies in ALS have revealed that patients suffer from dyslipidemia during the course of the disease and this might feed into the fast progression of the disease (Huisman et al., 2015; Dorst et al., 2013; Nagel et al., 2017; De Aguilar, 2019). Not just the level of lipids but also their carriers like APOE, which is produced by the glial cells and is the carrier for lipid droplets are perturbed in ALS (Benedetti et al., 2017). VAP has been implicated in the lipid transport from

the Golgi to ER. This transport is facilitated by the interaction of MSP domain of VAP with FFAT domain-containing proteins like CERT, OSBP and Nir2 (Wyles et al., 2002; Kawano et al., 2006; Loewen et al., 2003; Perry and Ridgway 2003). The disrupted MSP signalling of VAP because of the VAP^{P58S} also contributes to abnormal lipid metabolism (Han et al., 2012 and 2013).

As discussed in Chapter II, we analyzed $\Delta VAP; gVAP^{P58S}$ adult brains on the day 15 of their life for levels of lipids (Kriti Chaplot, Thesis and Chapter II, Section 3.4) and found several changes in its lipid profile. The lipids which are altered in $\Delta VAP; gVAP^{P58S}$ flies are Cholesterol, Cholesterol esters, Ceramides, Ceramide-1- phosphates, Sphingomyelin and Triacylglycerols. Out of these, Cholesterol levels are raised as compared to the control while all other lipids are lowered.

To check if the dosage of Caspar regulates these lipid levels, we performed a lipid Mass spectrometry analysis on 15-day adult fly brains of $\Delta VAP; Repo>+; gVAP^{P58S}$ (used as control), $\Delta VAP; Repo>caspar^{WT}; gVAP^{P58S}$, and $\Delta VAP; Repo>caspar^{RNAi}; gVAP^{P58S}$. The +/+ (wild type flies) were used as master controls for this experiment. We tested only the lipids which changed in the case of $\Delta VAP; gVAP^{P58S}$ adult flies tested earlier (Chapter II, Section 3.4).

The observations from the lipid data are as follows:

1. Cholesterol (Fig. 3.10A), Cholesterol esters (Fig. 3.10B), Ceramides, Ceramide- 1-phosphates (Fig. 3.10C), Sphingomyelin (Fig. 3.10D) and Triacylglycerols (Fig. 3.10D) levels are raised in $\Delta VAP; Repo>+; gVAP^{P58S}/+$ flies which is consistent with our previous results (Chapter II, Section 3.4, Fig. 2.7) for $\Delta VAP; gVAP^{P58S}$ thus confirming the change.

2. Cholesterol levels do not change on glial overexpression/knockdown of Caspar in $gVAP^{P58S}$ background. (Fig. 3.10A)

3. The levels of Cholesterol esters, Ceramides, Ceramide- 1-phosphates, Sphingomyelin and Triacylglycerols that are raised in $\Delta VAP; Repo>+; gVAP^{P58S}/+$ flies show a slight but not significant trend of reduction in almost all cases of Caspar overexpression as compared to $\Delta VAP; Repo>+; gVAP^{P58S}/+$. Although it is slightly ($p<0.05$) significant in some cases of Cholesterol esters (18:0, Fig. 3.10B), Sphingomyelin (18:0, Fig. 3.10E) and a bit more ($p<0.01$) for Triacylglycerols (18:0/36:2, Fig. 3.10F).

4. The levels of Cholesterol esters, Ceramides, Ceramide- 1-phosphates, Sphingomyelin and Triacylglycerols that are raised in $\Delta VAP; Repo>+; gVAP^{P58S}/+$ flies show a trend of further

increase when Caspar is downregulated. Although not stark, this increase is significant in some Triacylglycerols (18:1/36:1 and 36:2, p<0.001; 18:0/36:2 p<0.05), Ceramides (18:1, P<0.01), Ceramide 1-phosphates (18:0), Cholesterol esters (18:0 and 18:1, p<0.05).

5. While this could be just a coincidence but most lipids which show a slight change with perturbed Caspar levels are the ones which have 18 carbon chains.
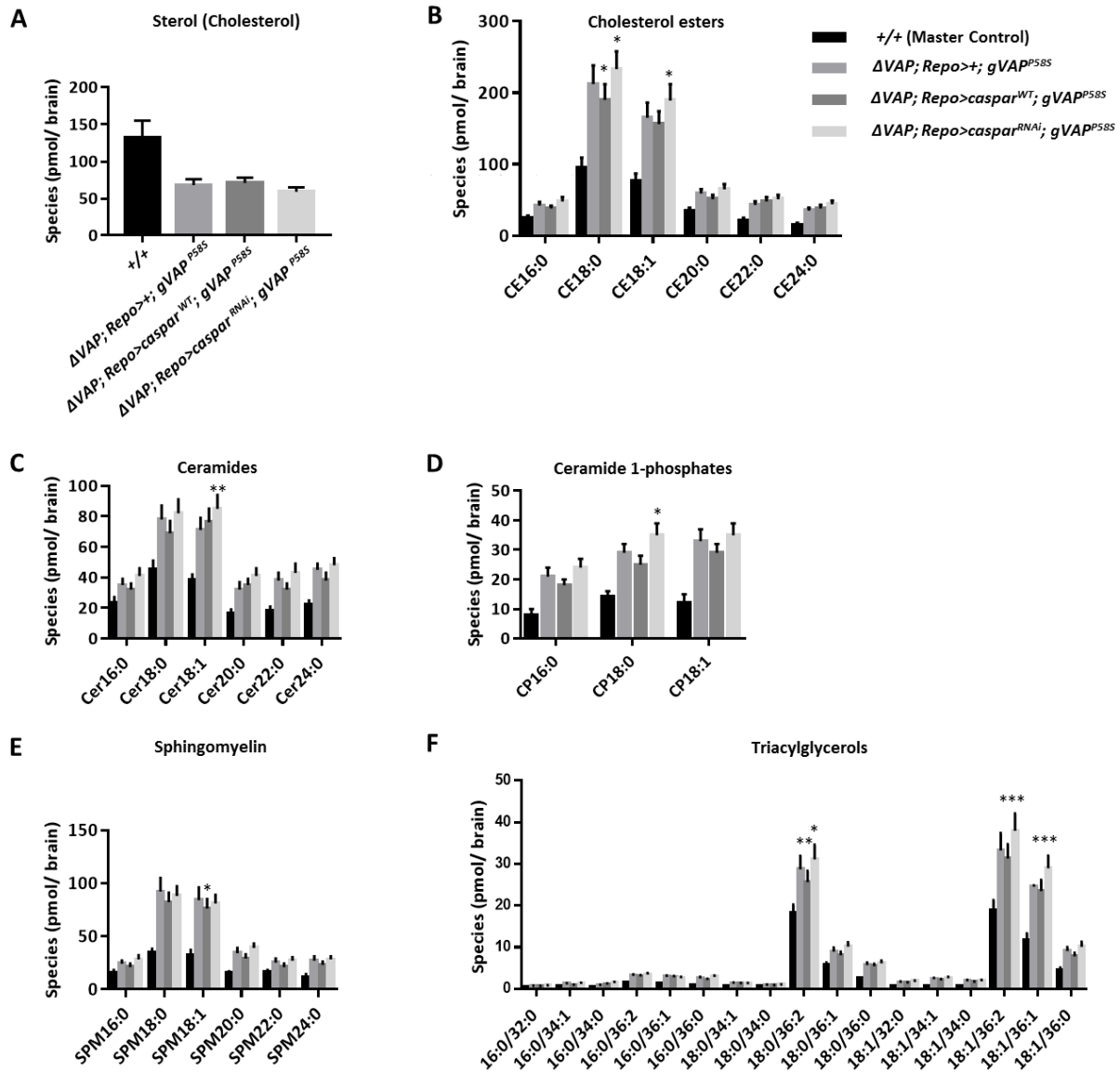
Figure 3.10. Lipids levels in case of perturbation of Caspar in the glia in *gVAP^{P58S}* background. Graphical representation of levels of Cholesterol (**A**), Cholesterol esters (**B**), Ceramides, Ceramide- 1-phosphates (**C**), Sphingomyelin (**D**) and Triacylglycerols (**D**) in 15 day adult brains quantified using LC-MS. Statistical analysis was done using One way ANOVA for cholesterol, Two way ANOVA for all others

followed by multiple comparison testing by Tukey test. ns indicates no significance.* Indicates $p < 0.05$.** Indicates $p < 0.01$. *** Indicates $p < 0.001$. The master control (+/+) was used only to compare values with $\Delta VAP; Repo>+; gVAP^{P58S} /+$ (p-values not represented*)*. $\Delta VAP; Repo>caspar^{WT}; gVAP^{P58S}$, and $\Delta VAP; Repo>caspar^{RNAi}; gVAP^{P58S}$ were compared with $\Delta VAP; Repo>+; gVAP^{P58S} /+$ and the p-values depicted in the graphs are recordings of this comparison.

Contribution: Dr. Siddhesh Kamat helped with design and performing the mass spectrometry experiment.

Table 3.6 mentions the detailed values of each lipid analyzed using the Mass spectrometry along with the comparisons. It compares master control (wild type flies) with $\Delta VAP; Repo>+; gVAP^{P58S} /+$ (red asterisk*)*, comparisons of $\Delta VAP; Repo>caspar^{WT}; gVAP^{P58S}$, and $\Delta VAP; Repo>caspar^{RNAi}; gVAP^{P58S}$ with $\Delta VAP; Repo>+; gVAP^{P58S} /+$ (blue asterisk); also $\Delta VAP; Repo>caspar^{WT}; gVAP^{P58S}$ with $\Delta VAP; Repo>caspar^{RNAi}; gVAP^{P58S}$ (black asterisk).

Table 3.6. LC-MS quantitation of Cholesterol, Cholesterol esters, Ceramides, Ceramide-1-phosphates, Sphingomyelin and Triacylglycerols in 15 day old adult *Drosophila* brain of +/+, Δ*VAP; Repo>+; gVAP^{P58S}*, Δ*VAP; Repo>caspar^{WT}; gVAP^{P58S}* and Δ*VAP; Repo>caspar^{RNAi}; gVAP^{P58S}*

ns = not significant, * p < 0.05,** p < 0.01, *** p < 0.001, ****p < 0.0001. * Comparison with CS (Master Control/Wild Type); * Comparison with VAP^{P58S}; * Comparison between Δ*VAP; Repo>caspar^{WT}; gVAP^{P58S}* and Δ*VAP; Repo>caspar^{RNAi}; gVAP^{P58S}*.Statistical analysis was done using One way ANOVA for cholesterol, Two way ANOVA for all others followed by multiple comparison testing by Tukey test.

Species Targeted	Summary	Adjusted P Value
Cholesterol		
+/+(Master Control) vs. ΔVAP; Repo>+; gVAP(P58S)	****	<0.0001
ΔVAP; Repo>+; gVAP(P58S) vs. ΔVAP; Repo>Caspwt; gVAP(P58S)	ns	0.9829
ΔVAP; Repo>+; gVAP(P58S) vs. ΔVAP; Repo>Caspi; gVAP(P58S)	ns	0.6987
ΔVAP; Repo>Caspwt; gVAP(P58S) vs. ΔVAP; Repo>Caspi; gVAP(P58S)	ns	0.4842
Cholesterol esters		
CE16:0		
+/+(Master Control) vs. ΔVAP; Repo>+; gVAP(P58S)	ns	0.1505
ΔVAP; Repo>+; gVAP(P58S) vs. ΔVAP; Repo>Caspwt; gVAP(P58S)	ns	0.9585
ΔVAP; Repo>+; gVAP(P58S) vs. ΔVAP; Repo>Caspi; gVAP(P58S)	ns	0.8754
ΔVAP; Repo>Caspwt; gVAP(P58S) vs. ΔVAP; Repo>Caspi; gVAP(P58S)	ns	0.5943
CE18:0		
+/+(Master Control) vs. ΔVAP; Repo>+; gVAP(P58S)	****	<0.0001
ΔVAP; Repo>+; gVAP(P58S) vs. ΔVAP; Repo>Caspwt; gVAP(P58S)	*	0.0345
ΔVAP; Repo>+; gVAP(P58S) vs. ΔVAP; Repo>Caspi; gVAP(P58S)	*	0.0477
ΔVAP; Repo>Caspwt; gVAP(P58S) vs. ΔVAP; Repo>Caspi; gVAP(P58S)	****	<0.0001
CE18:1		
+/+(Master Control) vs. ΔVAP; Repo>+; gVAP(P58S)	****	<0.0001
ΔVAP; Repo>+; gVAP(P58S) vs. ΔVAP; Repo>Caspwt; gVAP(P58S)	ns	0.6729
ΔVAP; Repo>+; gVAP(P58S) vs. ΔVAP; Repo>Caspi; gVAP(P58S)	*	0.0173
ΔVAP; Repo>Caspwt; gVAP(P58S) vs. ΔVAP; Repo>Caspi; gVAP(P58S)	***	0.0004
CE20:0		
+/+(Master Control) vs. ΔVAP; Repo>+; gVAP(P58S)	*	0.012
ΔVAP; Repo>+; gVAP(P58S) vs. ΔVAP; Repo>Caspwt; gVAP(P58S)	ns	0.7479
ΔVAP; Repo>+; gVAP(P58S) vs. ΔVAP; Repo>Caspi; gVAP(P58S)	ns	0.8754
ΔVAP; Repo>Caspwt; gVAP(P58S) vs. ΔVAP; Repo>Caspi; gVAP(P58S)	ns	0.3012
CE22:0		
+/+(Master Control) vs. ΔVAP; Repo>+; gVAP(P58S)	*	0.0345
ΔVAP; Repo>+; gVAP(P58S) vs. ΔVAP; Repo>Caspwt; gVAP(P58S)	ns	0.9232
ΔVAP; Repo>+; gVAP(P58S) vs. ΔVAP; Repo>Caspi; gVAP(P58S)	ns	0.7479
ΔVAP; Repo>Caspwt; gVAP(P58S) vs. ΔVAP; Repo>Caspi; gVAP(P58S)	ns	0.9818
CE24:0		
+/+(Master Control) vs. ΔVAP; Repo>+; gVAP(P58S)	ns	0.065
ΔVAP; Repo>+; gVAP(P58S) vs. ΔVAP; Repo>Caspwt; gVAP(P58S)	ns	0.9818
ΔVAP; Repo>+; gVAP(P58S) vs. ΔVAP; Repo>Caspi; gVAP(P58S)	ns	0.6729
ΔVAP; Repo>Caspwt; gVAP(P58S) vs. ΔVAP; Repo>Caspi; gVAP(P58S)	ns	0.8754

Ceramides		
Cer16:0		
+/+(Master Control) vs. ΔVAP; Repo>+; gVAP(P58S)	**	0.0088
ΔVAP; Repo>+; gVAP(P58S) vs. ΔVAP; Repo>Caspwt; gVAP(P58S)	ns	0.8498
ΔVAP; Repo>+; gVAP(P58S) vs. ΔVAP; Repo>Caspi; gVAP(P58S)	ns	0.3729
ΔVAP; Repo>Caspwt; gVAP(P58S) vs. ΔVAP; Repo>Caspi; gVAP(P58S)	ns	0.0785
Cer18:0		
+/+(Master Control) vs. ΔVAP; Repo>+; gVAP(P58S)	****	<0.0001
ΔVAP; Repo>+; gVAP(P58S) vs. ΔVAP; Repo>Caspwt; gVAP(P58S)	ns	0.0785
ΔVAP; Repo>+; gVAP(P58S) vs. ΔVAP; Repo>Caspi; gVAP(P58S)	ns	0.7029
ΔVAP; Repo>Caspwt; gVAP(P58S) vs. ΔVAP; Repo>Caspi; gVAP(P58S)	**	0.0038
Cer18:1		
+/+(Master Control) vs. ΔVAP; Repo>+; gVAP(P58S)	****	<0.0001
ΔVAP; Repo>+; gVAP(P58S) vs. ΔVAP; Repo>Caspwt; gVAP(P58S)	ns	0.5342
ΔVAP; Repo>+; gVAP(P58S) vs. ΔVAP; Repo>Caspi; gVAP(P58S)	**	0.0015
ΔVAP; Repo>Caspwt; gVAP(P58S) vs. ΔVAP; Repo>Caspi; gVAP(P58S)	ns	0.0785
Cer20:0		
+/+(Master Control) vs. ΔVAP; Repo>+; gVAP(P58S)	***	0.0002
ΔVAP; Repo>+; gVAP(P58S) vs. ΔVAP; Repo>Caspwt; gVAP(P58S)	ns	0.8498
ΔVAP; Repo>+; gVAP(P58S) vs. ΔVAP; Repo>Caspi; gVAP(P58S)	ns	0.0785
ΔVAP; Repo>Caspwt; gVAP(P58S) vs. ΔVAP; Repo>Caspi; gVAP(P58S)	ns	0.3729
Cer22:0		
+/+(Master Control) vs. ΔVAP; Repo>+; gVAP(P58S)	****	<0.0001
ΔVAP; Repo>+; gVAP(P58S) vs. ΔVAP; Repo>Caspwt; gVAP(P58S)	ns	0.3729
ΔVAP; Repo>+; gVAP(P58S) vs. ΔVAP; Repo>Caspi; gVAP(P58S)	ns	0.5342
ΔVAP; Repo>Caspwt; gVAP(P58S) vs. ΔVAP; Repo>Caspi; gVAP(P58S)	*	0.0195
Cer24:0		
+/+(Master Control) vs. ΔVAP; Repo>+; gVAP(P58S)	****	<0.0001
ΔVAP; Repo>+; gVAP(P58S) vs. ΔVAP; Repo>Caspwt; gVAP(P58S)	ns	0.2396
ΔVAP; Repo>+; gVAP(P58S) vs. ΔVAP; Repo>Caspi; gVAP(P58S)	ns	0.8498
ΔVAP; Repo>Caspwt; gVAP(P58S) vs. ΔVAP; Repo>Caspi; gVAP(P58S)	*	0.0404
Ceramide 1-phosphates		
CP16:0		
+/+(Master Control) vs. ΔVAP; Repo>+; gVAP(P58S)	****	<0.0001
ΔVAP; Repo>+; gVAP(P58S) vs. ΔVAP; Repo>Caspwt; gVAP(P58S)	ns	0.4228
ΔVAP; Repo>+; gVAP(P58S) vs. ΔVAP; Repo>Caspi; gVAP(P58S)	ns	0.4228
ΔVAP; Repo>Caspwt; gVAP(P58S) vs. ΔVAP; Repo>Caspi; gVAP(P58S)	*	0.0175
CP18:0		
+/+(Master Control) vs. ΔVAP; Repo>+; gVAP(P58S)	****	<0.0001
ΔVAP; Repo>+; gVAP(P58S) vs. ΔVAP; Repo>Caspwt; gVAP(P58S)	ns	0.1837
ΔVAP; Repo>+; gVAP(P58S) vs. ΔVAP; Repo>Caspi; gVAP(P58S)	*	0.0175
ΔVAP; Repo>Caspwt; gVAP(P58S) vs. ΔVAP; Repo>Caspi; gVAP(P58S)	****	<0.0001
CP18:1		
+/+(Master Control) vs. ΔVAP; Repo>+; gVAP(P58S)	****	<0.0001
ΔVAP; Repo>+; gVAP(P58S) vs. ΔVAP; Repo>Caspwt; gVAP(P58S)	ns	0.1837
ΔVAP; Repo>+; gVAP(P58S) vs. ΔVAP; Repo>Caspi; gVAP(P58S)	ns	0.7351
ΔVAP; Repo>Caspwt; gVAP(P58S) vs. ΔVAP; Repo>Caspi; gVAP(P58S)	*	0.0175

Sphingomyelins		
SPM16:0		
+/+(Master Control) vs. ΔVAP; Repo>+; gVAP(P58S)	ns	0.0845
ΔVAP; Repo>+; gVAP(P58S) vs. ΔVAP; Repo>Caspwt; gVAP(P58S)	ns	0.8547
ΔVAP; Repo>+; gVAP(P58S) vs. ΔVAP; Repo>Caspi; gVAP(P58S)	ns	0.7114
ΔVAP; Repo>Caspwt; gVAP(P58S) vs. ΔVAP; Repo>Caspi; gVAP(P58S)	ns	0.2504
SPM18:0		
+/+(Master Control) vs. ΔVAP; Repo>+; gVAP(P58S)	****	<0.0001
ΔVAP; Repo>+; gVAP(P58S) vs. ΔVAP; Repo>Caspwt; gVAP(P58S)	*	0.0442
ΔVAP; Repo>+; gVAP(P58S) vs. ΔVAP; Repo>Caspi; gVAP(P58S)	ns	0.7114
ΔVAP; Repo>Caspwt; gVAP(P58S) vs. ΔVAP; Repo>Caspi; gVAP(P58S)	ns	0.3847
SPM18:1		
+/+(Master Control) vs. ΔVAP; Repo>+; gVAP(P58S)	****	<0.0001
ΔVAP; Repo>+; gVAP(P58S) vs. ΔVAP; Repo>Caspwt; gVAP(P58S)	ns	0.1509
ΔVAP; Repo>+; gVAP(P58S) vs. ΔVAP; Repo>Caspi; gVAP(P58S)	ns	0.8547
ΔVAP; Repo>Caspwt; gVAP(P58S) vs. ΔVAP; Repo>Caspi; gVAP(P58S)	ns	0.5453
SPM20:0		
+/+(Master Control) vs. ΔVAP; Repo>+; gVAP(P58S)	****	<0.0001
ΔVAP; Repo>+; gVAP(P58S) vs. ΔVAP; Repo>Caspwt; gVAP(P58S)	ns	0.5453
ΔVAP; Repo>+; gVAP(P58S) vs. ΔVAP; Repo>Caspi; gVAP(P58S)	ns	0.5453
ΔVAP; Repo>Caspwt; gVAP(P58S) vs. ΔVAP; Repo>Caspi; gVAP(P58S)	*	0.0442
SPM22:0		
+/+(Master Control) vs. ΔVAP; Repo>+; gVAP(P58S)	ns	0.0845
ΔVAP; Repo>+; gVAP(P58S) vs. ΔVAP; Repo>Caspwt; gVAP(P58S)	ns	0.7114
ΔVAP; Repo>+; gVAP(P58S) vs. ΔVAP; Repo>Caspi; gVAP(P58S)	ns	0.9509
ΔVAP; Repo>Caspwt; gVAP(P58S) vs. ΔVAP; Repo>Caspi; gVAP(P58S)	ns	0.3847
SPM24:0		
+/+(Master Control) vs. ΔVAP; Repo>+; gVAP(P58S)	***	0.0003
ΔVAP; Repo>+; gVAP(P58S) vs. ΔVAP; Repo>Caspwt; gVAP(P58S)	ns	0.7114
ΔVAP; Repo>+; gVAP(P58S) vs. ΔVAP; Repo>Caspi; gVAP(P58S)	ns	0.9933
ΔVAP; Repo>Caspwt; gVAP(P58S) vs. ΔVAP; Repo>Caspi; gVAP(P58S)	ns	0.5453
Triacylglycerols		
16:0/32:0		
+/+(Master Control) vs. ΔVAP; Repo>+; gVAP(P58S)	ns	0.9925
ΔVAP; Repo>+; gVAP(P58S) vs. ΔVAP; Repo>Caspwt; gVAP(P58S)	ns	0.9998
ΔVAP; Repo>+; gVAP(P58S) vs. ΔVAP; Repo>Caspi; gVAP(P58S)	ns	0.9998
ΔVAP; Repo>Caspwt; gVAP(P58S) vs. ΔVAP; Repo>Caspi; gVAP(P58S)	ns	0.9983
16:0/34:1		
+/+(Master Control) vs. ΔVAP; Repo>+; gVAP(P58S)	ns	0.9266
ΔVAP; Repo>+; gVAP(P58S) vs. ΔVAP; Repo>Caspwt; gVAP(P58S)	ns	0.9803
ΔVAP; Repo>+; gVAP(P58S) vs. ΔVAP; Repo>Caspi; gVAP(P58S)	ns	0.9992
ΔVAP; Repo>Caspwt; gVAP(P58S) vs. ΔVAP; Repo>Caspi; gVAP(P58S)	ns	0.9542
16:0/34:0		
+/+(Master Control) vs. ΔVAP; Repo>+; gVAP(P58S)	ns	0.9447
ΔVAP; Repo>+; gVAP(P58S) vs. ΔVAP; Repo>Caspwt; gVAP(P58S)	ns	0.9925
ΔVAP; Repo>+; gVAP(P58S) vs. ΔVAP; Repo>Caspi; gVAP(P58S)	ns	0.8551
ΔVAP; Repo>Caspwt; gVAP(P58S) vs. ΔVAP; Repo>Caspi; gVAP(P58S)	ns	0.9542
16:0/36:2		
+/+(Master Control) vs. ΔVAP; Repo>+; gVAP(P58S)	ns	0.2107
ΔVAP; Repo>+; gVAP(P58S) vs. ΔVAP; Repo>Caspwt; gVAP(P58S)	ns	0.9974
ΔVAP; Repo>+; gVAP(P58S) vs. ΔVAP; Repo>Caspi; gVAP(P58S)	ns	0.9852
ΔVAP; Repo>Caspwt; gVAP(P58S) vs. ΔVAP; Repo>Caspi; gVAP(P58S)	ns	0.948
16:0/36:1		
+/+(Master Control) vs. ΔVAP; Repo>+; gVAP(P58S)	ns	0.1874
ΔVAP; Repo>+; gVAP(P58S) vs. ΔVAP; Repo>Caspwt; gVAP(P58S)	ns	0.9992
ΔVAP; Repo>+; gVAP(P58S) vs. ΔVAP; Repo>Caspi; gVAP(P58S)	ns	0.9784
ΔVAP; Repo>Caspwt; gVAP(P58S) vs. ΔVAP; Repo>Caspi; gVAP(P58S)	ns	0.9934

16:0/36:0		
+/+(Master Control) vs. ΔVAP; Repo>+; gVAP(P58S)	ns	0.1744
ΔVAP; Repo>+; gVAP(P58S) vs. ΔVAP; Repo>Caspwt; gVAP(P58S)	ns	0.9803
ΔVAP; Repo>+; gVAP(P58S) vs. ΔVAP; Repo>Caspi; gVAP(P58S)	ns	0.9511
ΔVAP; Repo>Caspwt; gVAP(P58S) vs. ΔVAP; Repo>Caspi; gVAP(P58S)	ns	0.7945
18:0/34:1		
+/+(Master Control) vs. ΔVAP; Repo>+; gVAP(P58S)	ns	0.7813
ΔVAP; Repo>+; gVAP(P58S) vs. ΔVAP; Repo>Caspwt; gVAP(P58S)	ns	0.9995
ΔVAP; Repo>+; gVAP(P58S) vs. ΔVAP; Repo>Caspi; gVAP(P58S)	ns	0.9989
ΔVAP; Repo>Caspwt; gVAP(P58S) vs. ΔVAP; Repo>Caspi; gVAP(P58S)	ns	>0.9999
18:0/34:0		
+/+(Master Control) vs. ΔVAP; Repo>+; gVAP(P58S)	ns	0.9892
ΔVAP; Repo>+; gVAP(P58S) vs. ΔVAP; Repo>Caspwt; gVAP(P58S)	ns	0.9999
ΔVAP; Repo>+; gVAP(P58S) vs. ΔVAP; Repo>Caspi; gVAP(P58S)	ns	>0.9999
ΔVAP; Repo>Caspwt; gVAP(P58S) vs. ΔVAP; Repo>Caspi; gVAP(P58S)	ns	0.9994
18:0/36:2		
+/+(Master Control) vs. ΔVAP; Repo>+; gVAP(P58S)	****	<0.0001
ΔVAP; Repo>+; gVAP(P58S) vs. ΔVAP; Repo>Caspwt; gVAP(P58S)	**	0.0014
ΔVAP; Repo>+; gVAP(P58S) vs. ΔVAP; Repo>Caspi; gVAP(P58S)	*	0.0255
ΔVAP; Repo>Caspwt; gVAP(P58S) vs. ΔVAP; Repo>Caspi; gVAP(P58S)	****	<0.0001
18:0/36:1		
+/+(Master Control) vs. ΔVAP; Repo>+; gVAP(P58S)	***	0.0005
ΔVAP; Repo>+; gVAP(P58S) vs. ΔVAP; Repo>Caspwt; gVAP(P58S)	ns	0.7541
ΔVAP; Repo>+; gVAP(P58S) vs. ΔVAP; Repo>Caspi; gVAP(P58S)	ns	0.4388
ΔVAP; Repo>Caspwt; gVAP(P58S) vs. ΔVAP; Repo>Caspi; gVAP(P58S)	ns	0.0634
18:0/36:0		
+/+(Master Control) vs. ΔVAP; Repo>+; gVAP(P58S)	***	0.0007
ΔVAP; Repo>+; gVAP(P58S) vs. ΔVAP; Repo>Caspwt; gVAP(P58S)	ns	0.9904
ΔVAP; Repo>+; gVAP(P58S) vs. ΔVAP; Repo>Caspi; gVAP(P58S)	ns	0.9342
ΔVAP; Repo>Caspwt; gVAP(P58S) vs. ΔVAP; Repo>Caspi; gVAP(P58S)	ns	0.8073
18:1/32:0		
+/+(Master Control) vs. ΔVAP; Repo>+; gVAP(P58S)	ns	0.6058
ΔVAP; Repo>+; gVAP(P58S) vs. ΔVAP; Repo>Caspwt; gVAP(P58S)	ns	0.9989
ΔVAP; Repo>+; gVAP(P58S) vs. ΔVAP; Repo>Caspi; gVAP(P58S)	ns	0.9925
ΔVAP; Repo>Caspwt; gVAP(P58S) vs. ΔVAP; Repo>Caspi; gVAP(P58S)	ns	0.9744
18:1/34:1		
+/+(Master Control) vs. ΔVAP; Repo>+; gVAP(P58S)	ns	0.1744
ΔVAP; Repo>+; gVAP(P58S) vs. ΔVAP; Repo>Caspwt; gVAP(P58S)	ns	0.995
ΔVAP; Repo>+; gVAP(P58S) vs. ΔVAP; Repo>Caspi; gVAP(P58S)	ns	0.9942
ΔVAP; Repo>Caspwt; gVAP(P58S) vs. ΔVAP; Repo>Caspi; gVAP(P58S)	ns	0.9599
18:1/34:0		
+/+(Master Control) vs. ΔVAP; Repo>+; gVAP(P58S)	ns	0.4461
ΔVAP; Repo>+; gVAP(P58S) vs. ΔVAP; Repo>Caspwt; gVAP(P58S)	ns	0.9784
ΔVAP; Repo>+; gVAP(P58S) vs. ΔVAP; Repo>Caspi; gVAP(P58S)	ns	>0.9999
ΔVAP; Repo>Caspwt; gVAP(P58S) vs. ΔVAP; Repo>Caspi; gVAP(P58S)	ns	0.9744
18:1/36:2		
+/+(Master Control) vs. ΔVAP; Repo>+; gVAP(P58S)	****	<0.0001
ΔVAP; Repo>+; gVAP(P58S) vs. ΔVAP; Repo>Caspwt; gVAP(P58S)	ns	0.0851
ΔVAP; Repo>+; gVAP(P58S) vs. ΔVAP; Repo>Caspi; gVAP(P58S)	****	<0.0001
ΔVAP; Repo>Caspwt; gVAP(P58S) vs. ΔVAP; Repo>Caspi; gVAP(P58S)	****	<0.0001
18:1/36:1		
+/+(Master Control) vs. ΔVAP; Repo>+; gVAP(P58S)	****	<0.0001
ΔVAP; Repo>+; gVAP(P58S) vs. ΔVAP; Repo>Caspwt; gVAP(P58S)	ns	0.5288
ΔVAP; Repo>+; gVAP(P58S) vs. ΔVAP; Repo>Caspi; gVAP(P58S)	****	<0.0001
ΔVAP; Repo>Caspwt; gVAP(P58S) vs. ΔVAP; Repo>Caspi; gVAP(P58S)	****	<0.0001
18:1/36:0		
+/+(Master Control) vs. ΔVAP; Repo>+; gVAP(P58S)	****	<0.0001
ΔVAP; Repo>+; gVAP(P58S) vs. ΔVAP; Repo>Caspwt; gVAP(P58S)	ns	0.389
ΔVAP; Repo>+; gVAP(P58S) vs. ΔVAP; Repo>Caspi; gVAP(P58S)	ns	0.6058
ΔVAP; Repo>Caspwt; gVAP(P58S) vs. ΔVAP; Repo>Caspi; gVAP(P58S)	*	0.0264

3.2.6. Glial overexpression of *caspar* rescues the bouton size of $\Delta VAP; Repo>+; gVAP^{P58S}$ third instar larvae

Bouton size and number is used as one of the common readouts for *Drosophila* models of ALS (Lin et al., 2017; Pennetta et al., 2002; Estes et al., 2011). As discussed in Chapter I and IV, *VAP* is involved in maintenance of the bouton size and number at the *Drosophila* third instar NMJ (Pennetta et al., 2002). An increase in bouton size and reduction in bouton number is reported in studies of VAP^{P58S} in *Drosophila* (Pennetta et al., 2002; Ratnaparkhi et al., 2008; Deivasigamani et al., 2014 and Chapter IV).

We were curious to know if *caspar* is involved in the maintenance of bouton morphology (Materials and Methods, Section 5.2, Chapter V). Before investigating the role of *caspar*, we confirmed if our control ($\Delta VAP; Repo>+; gVAP^{P58S}$) could indeed reproduce the previous results from various studies. The $\Delta VAP; Repo>+; gVAP^{P58S}$ fly line has an increased bouton size and a reduced bouton number (Fig. 3.11 legend) as compared to the wild type flies (master control) hence confirming similarity with bouton morphology defects observed by other research groups.

We observed that, this increased size of boutons is rescued by *caspar* overexpression in the glial cells in $gVAP^{P58S}$ background, suggesting *caspar's* potential role in bringing back the homeostasis at the NMJ. The resulting bouton size is therefore similar to wild type (Bouton size for Wild type = 3.77 um Vs $\Delta VAP; Repo>caspar^{WT}; gVAP^{P58S}$= 3.64 um, p>0.05, ns). *caspar* overexpression, however, doesn't change the number of boutons. Also, the knockdown of *caspar* doesn't seem to change the bouton architecture as compared to the control (Fig. 3.11). The rescue in boutons size suggests that overexpression of *caspar* could potentially bring back the structural homeostasis at the NMJ. A follow up on trans-synaptic signalling markers could shed more light on this aspect.
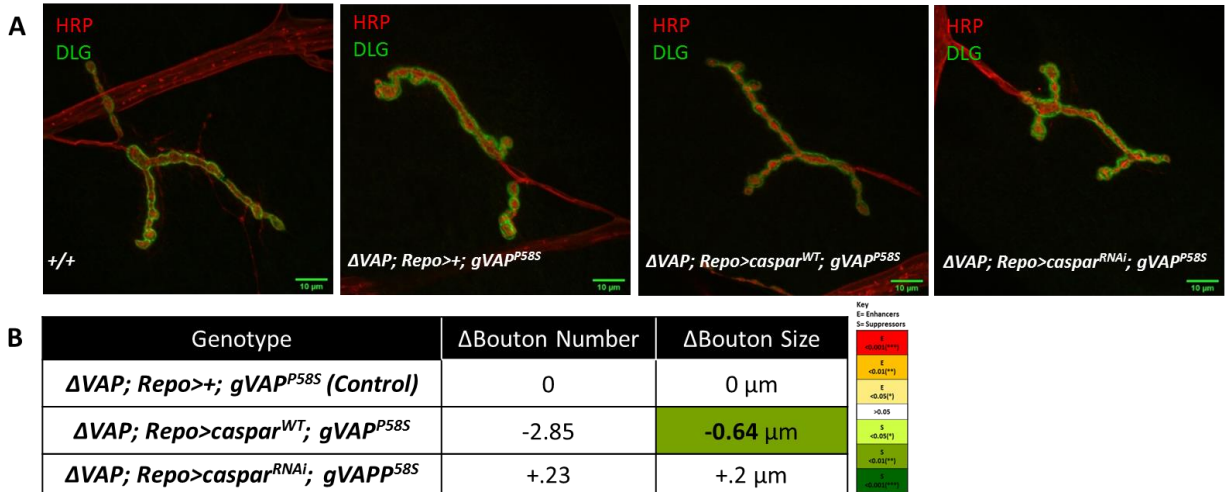
Figure 3.11. Effects of *caspar* overexpression/knockdown in the glia on the bouton morphology of gVAP^P58S^ larvae.

A) Confocal images of boutons at the NMJ of +/+ (master control), ΔVAP; Repo>+; gVAP ^P58S^ /+ (compared with master control), ΔVAP; Repo>caspar^WT^; gVAP^P58S^, and ΔVAP; Repo>caspar^RNAi^; gVAP^P58S^.The markers used were HRP and DLG.

B) Tabular representation of ± ΔBouton number and size for ΔVAP; Repo>+; gVAP^P58S^ /+ (Average bouton size= 4.31±0.64μm. Average bouton number= 22.35±4.48); ΔVAP; Repo>caspar^WT^; gVAP^P58S^ (Average bouton size= 3.64 ±0.43μm. Average bouton number= 19.5±3.72) and ΔVAP; Repo>caspar ^RNAi^; gVAP^P58S^ (Average bouton size= 4.51±0.72μm. Average bouton number= 22.58±4.1). Values are represented in the form of ΔBN (Change in bouton number) and ΔBS (Change in Bouton size) = Bouton Number/Size (Experimental)- Bouton Number/Size (Control). Color/Statistical Key: The 'red-yellow tones' indicate different levels of statistical confidence for the 'Enhancers' while the 'green tones' represent the same for 'Suppressors'.

ΔVAP; Repo>caspar^WT^; gVAP ^P58S^ and ΔVAP; Repo>caspar^RNAi^; gVAP^P58S^ were compared with ΔVAP; Repo>+; gVAP^P58S^ /+. Wild type = +/+ (Average bouton size= 3.77±0.39μm. Average bouton number=29±4.88) was used as the master control for comparison with ΔVAP; Repo>+; gVAP^P58S^ /+. The p-values for this comparisons were: boutons size <0.01 and bouton number <0.001. The number of larvae used for each experiment are 4-7 and the neuromuscular junctions observed are 10-15 (all the crosses were performed at 25^0 C). Unpaired Student's t-test was used for comparison.

3.2.7. Caspar and TER94^R152H^ do not seem to mitigate ER stress associated with VAP^P58S^

One other common hallmark of ALS is ER stress (Prell et al., 2012; Atkin et al., 2008). In fact UPR (Unfolded protein response) and ER (endoplasmic reticulum) stress is one of the facets of VAP^P56S^-associated ALS pathology and have been studied in various model systems, one of them being *Drosophila* (Moustaqim-Barrette et al., 2013). The VAP^P58S^ protein has been shown to interact with ATF6 (Activating transcription factor 6) leading to inhibition of the activity of UPR which results in an increase in ER stress and protein aggregation (Kanekura et al., 2006; Gkogkas

110

et al., 2006). There are also reports of VCP (TER94) and FAF1 (mammalian Caspar) interactions to be crucial in promoting ERAD (ER-associated degradation) as it feeds into VCP's function of protein degradation (Lee et al., 2013).

Considering the dense literature, we investigated whether *caspar* controls the lifespan/motor defects of $\Delta VAP; gVAP^{P58S}$ fly by bringing in changes via the ERAD pathway. We used anti-BiP antibody to stain third instar larval brains of +/+ (master control), $\Delta VAP; Repo>+; gVAP^{P58S}$ /+ (control; compared with master control)*, $\Delta VAP; Repo>caspar^{WT}; gVAP^{P58S}$, $\Delta VAP; Repo>caspar^{RNAi}; gVAP^{P58S}$ and $\Delta VAP; Repo>TER94^{R152H}; gVAP^{P58S}$(compared with control). Co-stains used along with BiP were Elav, the neuronal marker and DAPI for the nucleus to observe any change in localization of BiP (For Larval brain dissection and staining protocol refer Materials and Methods, Section 5.6, Chapter II). BiP (ER chaperone immunoglobulin binding Protein) is a commonly used ER stress marker, free molecules of which increase in the presence of ER stress (Ron and Walter, 2007). The larval brains of master control show a fuzzy BiP staining (Fig. 3.12A) indicating its lower levels, while the $\Delta VAP; Repo>+; gVAP^{P58S}$ /+ (Fig. 3.12B) larval brains show presence of bright puncta suggesting its upregulation and the presence of increased ER stress in the system. This upregulation of BiP is however not reduced or increased on overexpression/downregulation of Caspar or TER94^{R152H} (Fig. 3.12C-E) which seems to be refuting our hypothesis about Caspar's involvement in regulating ER stress. Based on the co-stains used, the localization of the BiP granules did not seem to change (Fig. 3.12B-E, zoom).

Although Caspar or TER94^{R152H} might bring no change to the ER stress in the larval brains, there is a chance that we observe a difference in the adult brains. This could be because Caspar and TER94^{R152H} suppress the defects in the adult stages and not in the larvae (Section 3.2.1, 3.2.2 and 3.2.3). It would also help to quantify the difference in cell death in these tissues, as increased ER stress eventually results in apoptosis (Hetz and Papa, 2018; Ron and Walter, 2007).
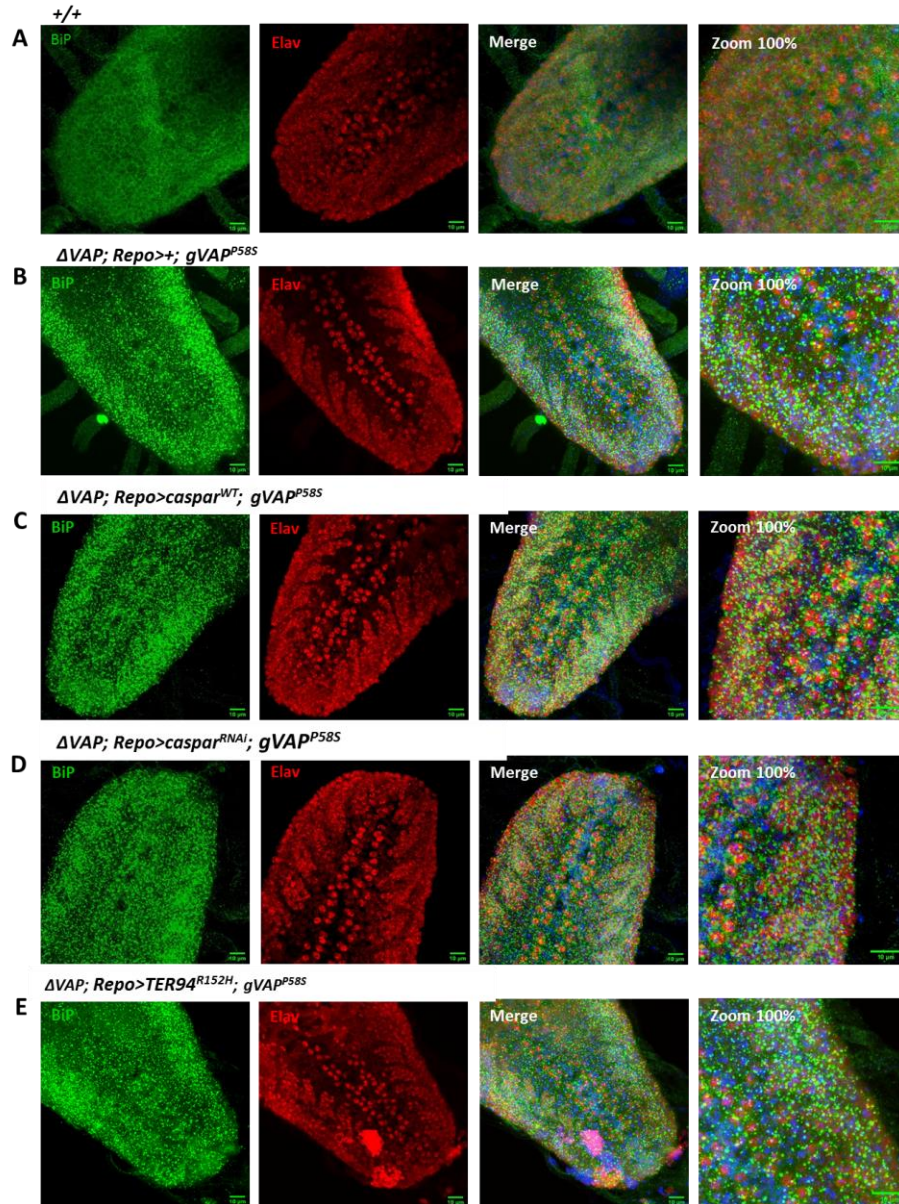
Figure 3.12. Overexpression/Downregulation of Caspar does not seem to change intensity or localization of BiP.
Confocal images of +/+ (master control), $\Delta VAP;\ Repo>+;\ gVAP^{P58S}\ /+$ (compared with master control), $\Delta VAP;\ Repo>caspar^{WT};\ gVAP^{P58S}$, $\Delta VAP;\ Repo>caspar^{RNAi};\ gVAP^{P58S}$ and $\Delta VAP;\ Repo>TER94^{R152H};\ gVAP^{P58S}$ third instar larval brains stained with BiP antibody. The co-stains used are Elav for neurons and DAPI for nucleus.

3.2.8. Caspar might be interacting with VAP^{P58S} via the NF-κB pathway

Caspar is a known negative regulator of the NF-κB (Nuclear Factor Kappa B) pathway and its role is conserved across mammalian systems as well (Kim et al., 2006; Park et al., 2004). The IMD (Immune Deficiency) pathway in *Drosophila* (Fig. 3.13A) and the orthologous TNFα in

mammals is an arm of the NF-κB innate immune pathway activated upon bacterial infections and causes release of pro-inflammatory cytokines (Myllymaki et al., 2014; Engstrom et al., 1993; Reichhart et al., 1992). Cytokines are also released by the microglial cells in case of neurodegenerative disorders, acting as either neuroprotective or neurotoxic agents, depending on the stage of the disease (Smith et al., 2012; Petersen et al., 2012; Liao et al., 2012, Chapter I). NF-κB levels have been reported to be high in case of ALS patients as well as in mouse model studies (Haidet-Phillips., 2012; Frakes 2014). Studies have also proved that downregulation of the components of NF-κB pathway in glia results in reduced neuronal death and increased longevity (Petersen et al., 2012; Li et al., 2018; Chinchore et al., 2012).
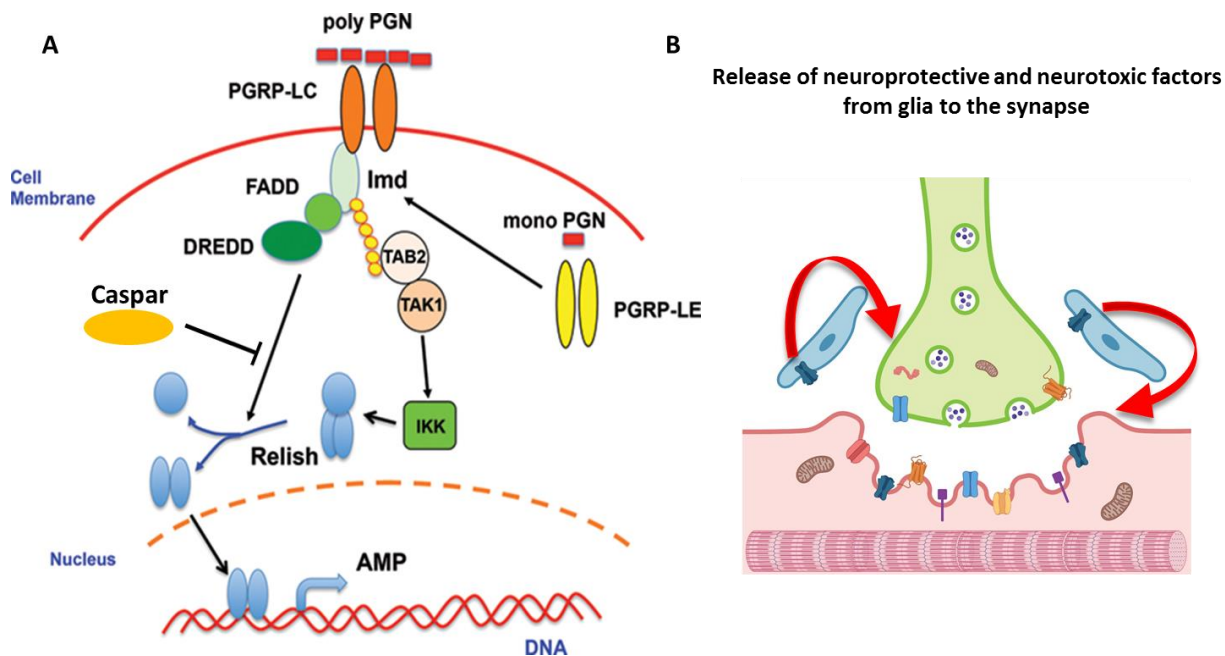
Figure 3.13. IMD Pathway in *Drosophila.*
A) IMD Pathway is activated by bacterial infection and also by stress associated with neurodegenerative disorders. After the ligand mediated activation, IMD forms a complex with FADD (Fas-associated protein with death domain) and the caspase DREDD (FADD-death-related ced-3/Nedd2- like protein). DREDD cleaves IMD and polyubiquitinates it. Post this the TAB2-TAK1 (TAK1-associated binding protein 2-TGF-β)-activated kinase 1)complex binds to IMD-FADD-DREDD complex via the polyubiquitin chain. This activates the IκK (TAK1)-inhibitor of κB kinase) kinase. Relish or NF-κB1 (p105), is bound by IκB. The IκK kinase phosphorylates IκB and makes the complex ready for DREDD mediated cleavage which releases relish precursor for p50 of the canonical pathway. P50-RelA translocate into the nucleus to produce AMPs (antimicrobial peptides) and increased inflammatory factors. Dredd mediated cleavage of relish is blocked by Caspar/FAF1. Adapted and modified from Rosales, 2017.
B) NF-κB signalling at the tripartite synapse has been reported to occur in the glial to neuronal cell direction via release of neuroprotective and neurotoxic factors by the glial cells.

Glial Caspar overexpression causing improvement in the lifespan/motor abilities of the ΔVAP; $gVAP^{P58S}$ flies hints towards a mechanism which could be working via the NF-κB pathway. We used *IMD knockdown, relish overexpression, relish knockdown* and *relish loss-of-function* variants to answer our questions. Relish is a transcription factor in the IMD pathway and is orthologous to mammalian NF-κB1 (p105) (Fig. 3.13A). It positively regulates the pathway by undergoing cleavage and translocating to the nucleus. This cleavage is inhibited by Caspar, thus inhibiting the pathway (Kim et al., 2006). In our survival analysis, $relish^{RNAi}$ and IMD^{RNAi} suppressed the phenotype, whereas $relish^{WT}$ overexpression enhanced the survival defect. We also used a loss-of-function allele of relish, rel^{E20}, in the background of ΔVAP; $gVAP^{P58S}$ and demonstrated it to be suppressing the lifespan phenotype (Fig. 3.14). We intend to redo this assay with the 'Gal4 controls' and more components of the pathway to validate this result.

In order to support this angle of reduced inflammation causing enhanced survival, we intend to check the ΔVAP; $gVAP^{P58S}$ flies for presence of antimicrobial peptides which will act as evidence for increase in inflammation.
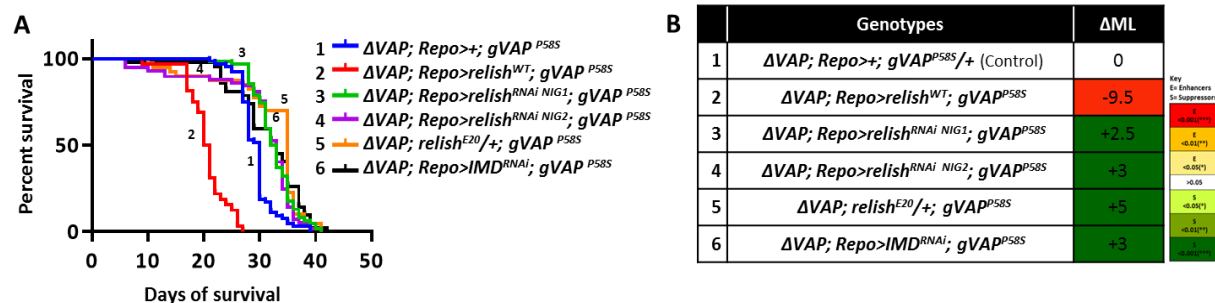
Figure 3.14. Downregulation of IMD pathway components suppress the lifespan defect of ΔVAP; $gVAP^{P58S}$ via glia.
A) Overexpression of $relish^{WT}$ (Red curve, number 2), $relish^{RNAi\ NIG1}$ (Light green curve, number 3), $relish^{RNAi\ NIG2}$ (Purple curve, number 4), $relish^{E20}$ (Orange curve, number 5) and IMD^{RNAi} (Black curve, number 6) in the ΔVAP; $Repo\text{-}Gal4$; $gVAP^{P58S}$ background. ΔVAP; $Repo>+$; $gVAP^{P58S}/+$ (Curve 1 in blue color) was used as the control. n=80-100 flies for each genotype. Curve comparison was done using log-rank (Mantel-Cox test). Combined p-value for the whole set is <0.001. $relish^{E20}$ was not driven by Repo-Gal4 as it is not a UAS fly line.
B) The results are in the form of ΔML (Change in Median Lifespan) = Median Lifespan (Experiment) – Median Lifespan (Control). Median Lifespan for control= 30 Days.
Color/Statistical Key: The 'red-yellow tones' indicate different levels of statistical confidence (log-rank test) for the 'Enhancers (E)' while the 'green tones' represent the same for 'Suppressors (S)'.

4. Discussion

In this study we have demonstrated the cell-specific interactions of ALS loci with VAP^{P58S}, supporting the idea of an existing gene regulatory network among the ALS loci, at the tripartite synapse. We have highlighted the differential interactions of the screened loci (*VAP, TDP-43, caz, SOD1*, *TER94, alsin* and *senataxin*), when expressed in muscles, glia and motor neurons (Sections 3.1.1- 3.1.3) and have listed the major findings (Sections 3.1.1- 3.1.4). This data supports our hypothesis of ALS loci variants contributing to the disease via muscle and glia, besides neurons. These results not only underpin the non-cell autonomous aspect of ALS but also corroborate the oligogenic nature of the disease, by displaying the aggravation of the disease phenotypes in certain cases where overexpression or knockdown of a particular locus is carried out in the VAP^{P58S} genetic background.

4.1. The proteostasis perspective

The interaction of VAP^{P58S} and *TER94* has been of particular interest to us. VAP has been implicated in various cellular functions and the ERAD pathway is one of them. VAP^{P58S} (or VAP^{P56S} in mammals) is reported to be involved in the impairment of the UPR and ERAD, hence causing an increase in the ER stress in mammalian as well as *Drosophila* model systems (Moustaqim-Barrette et al., 2013 and Gkogkas et al., 2008). One of the ways by which VAP regulates ER stress in the system is by inhibiting ATF6 (activating transcription factor 6) which is one of the ER stress sensors. In a study in HeLa cell lines, this inhibition was characterized to be stronger than the inhibition caused by wild type VAP, leading to suppression of UPR in ALS8 (Gkogkas et al., 2008). In our work, we have confirmed the increase in ER stress in the Δ*VAP; gVAP^{P58S}* flies (Fig. 3.12A and B). Furthermore, Baron et al., in 2014 demonstrated the presence of physical interaction between VAP and VCP (mammalian TER94) via the non-canonical FFAT-motif of FAF1 (mammalian Caspar) using HeLa cell lines. They also reported the interaction of VAP with ubiquitinated proteins and suspect that this interaction is potentially facilitated by FAF1.

TER94/VCP has been extensively studied AAA+ ATPase, involved in directing ubiquitinated proteins to the proteasome for degradation. It, therefore, contributes to ERAD and its downstream process of ubiquitin-mediated protein degradation (Boom and Meyer, 2017). While

VAP, according to the evidence from literature, acts at the initiation of UPR/ERAD (Gkogkas et al., 2008, Moustaqim-Barrette et al., 2013).

In case of increased misfolded proteins, when ER stress increases, we understand that a combination of the ERAD pathway sensors, namely ATF6, PERK and IRE1 (Activating transcription factor-6, Protein kinase RNA like ER-Kinase and Inositol-requiring protein-1 respectively) are activated. These proteins have binding sites for unfolded proteins which are initially blocked by BiP. Due to increased ER stress and more load of unfolded proteins, BiP is released from its position and is free in the ER lumen (Bertolotti et al., 2000; Ron and Walter, 2007). The unfolded proteins then bind to their sites on the lumenal side of ER stress sensors, thus activating downstream transcription factors (like Xbp1) responsible for the expression of UPR effector genes. Post the activation of UPR genes, the misfolded proteins are polyubiquitinated and degraded by the UPS. This stage is where the VAP-FAF1-VCP complex comes into the picture.

VCP uses FAF1 as its co-factor to pull ubiquitinated proteins out of the ER for degradation. FAF1, which has a UBA and UBX domain interacts with VCP via its UBX domain and with the ubiquitinated proteins via its UBA domain. This interaction assists in stable VCP-FAF1 complex formation. The VCP-FAF1 complex is then recruited on VAP, where the FFAT domain of FAF1 connects with the MSP domain of VAP. VAP, therefore, acts as its adapter on the ER membrane. Following the formation of the VAP-FAF1-VCP connection, VCP pulls these polyubiquitinated proteins into the cytoplasm and recruits it to the proteasome (Fig. 3.15) (Lee et al., 2013 and Baron et al., 2014).
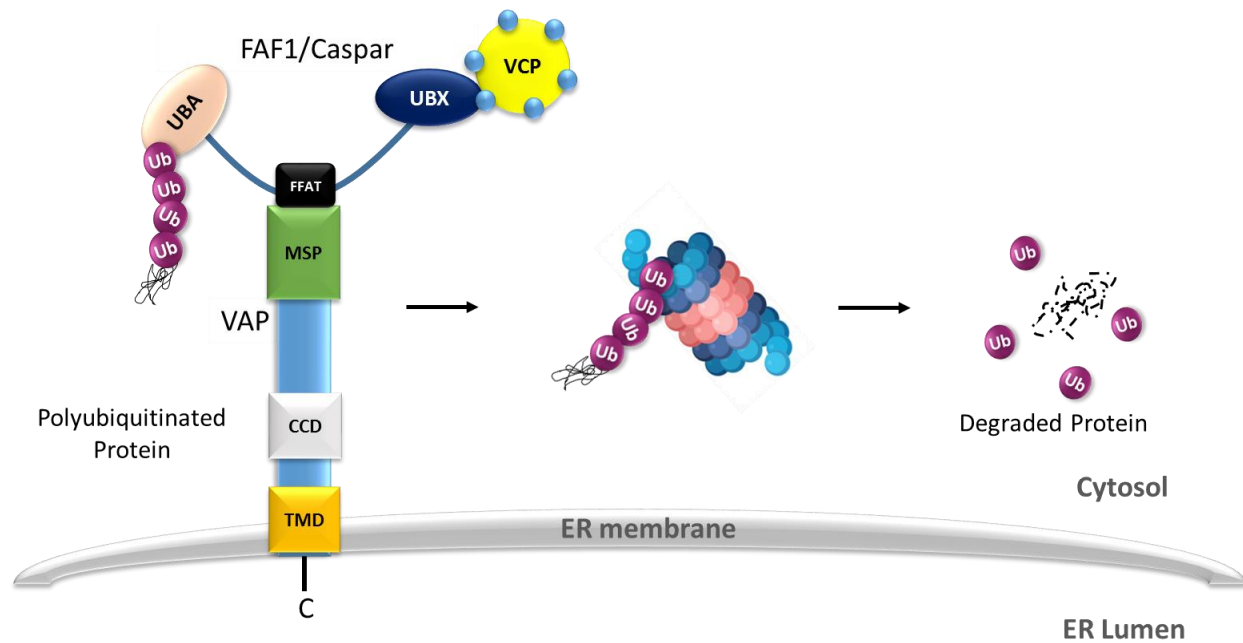
Figure 3.15. Role of VAP-FAF1-VCP complex in ERAD.
In case of increased misfolded proteins, there is an increase in ER stress and increased activation of UPR/ERAD genes. In order to reduce the misfolded protein load, the VCP-FAF1 complex binds to VAP. VAP acts an adapter to make this complex stable. VCP-FAF1 then pulls the misfolded protein in the cytoplasm by binding to its polyubiquitin tail and takes it to the proteasome for degradation. Presence of VAP^{P58S} contributes to the increased ER stress in the system. These conditions do not hamper the VAP^{P58S}-FAF1-VCP stable complex formation and the downstream protein degradation. Image inspiration: Baron et al, 2014 and BioRender App.

4.2. The Immune system perspective

Several studies have confirmed the activation of the NF-κB pathway in ALS patient samples as well as animal model-based studies (Haidet-Phillips et al., 2012; Frakes et al., 2014; Alami et al., 2018; Chapter I, Section 2.9.3). Microglia and astrocytes are reported to release anti and pro-inflammatory factors during the initial and late stages of the disease respectively. The pro-inflammatory factors are released as a result of activation of the inflammatory pathways in the system (Chapter I, Section 2.7.3, 2.7.1.2 and 2.9.3). There exists crosstalk between ER stress and NF-κB pathway, wherein increased ER stress caused by an activated UPR is reported to activate the NF-κB pathway (Schmitz et al., 2018). ER stress has been observed to co-occur with activation of the NF-κB pathway in various SOD1^{G93A} model studies (Prell et al., 2012, 2014; Nagata et al., 2007). However, the detailed mechanisms underlying these processes are poorly understood.

Increased inflammation hasn't been explored in ALS8 studies. Although we intend to check the levels of inflammation in the $\Delta VAP; gVAP^{P58S}$ flies, we presume an increase, considering

117

evidence from the literature and the fact that ER stress is high in these flies (Section 3.2.7). Furthermore, FAF1 is known to suppress activation of the NF-κB pathway, contributing to the regulation of inflammation in the system (Park et al., 2004). There are reports of VCP being involved in the regulation of NF-κB signalling by causing ubiquitination and degradation of the NF-κB inhibitor IKBα (Asai et al., 2002 and Li et al., 2014).

4.3. Working model

Considering our data along with the information available from literature, we have come up with a working model. Our model combines the proteostasis perspective and the immune system perspective. We hypothesize that convergence and crosstalk between these mechanisms in the glia leads to regulation of the lifespan and motor functions of the $\Delta VAP; gVAP^{P58S}$ flies.

In case of $\Delta VAP; gVAP^{P58S}$ flies, the constitutively high ER stress increases the load of polyubiquitinated proteins (Fig. 3.16AIa). As mentioned in Section 3.2.7, VAP^{P56S} is reported to block ATF6 which is one of the initial detectors/sensors of ER stress for the ERAD pathway. This blocking leads to inhibition of ATF6 dependent transcriptional activation of downstream UPR genes (Gkogkas et al., 2008). This causes an increase in misfolded proteins in the system and overloads the UPS. Assuming this to be true in the case of *Drosophila* as well, the load of misfolded proteins is going to be very high. These proteins include aggregated VAP^{P58S} and other misfolded proteins (Moustaqim-Barrette et al., 2013). In addition to the load from UPR, ER stress presumably activates NF-κB signalling (Prell et al., 2012; Nagata et al., 2007) and hence contributes to the deterioration of the system by increasing inflammation (Fig. 3.16AIIa) and the consequent cell death.

According to Baron et al., 2014 the presence of mutant VAP (VAP^{P56S}) doesn't disrupt the interaction between VAP and the VAP-FAF1 complex. Also, this complex does not ubiquitinate and degrade VAP itself. Presuming this to be true in *Drosophila*, glial overexpression of Caspar causes more Caspar-TER94 molecules to bind to VAP^{P58S}, leading to higher turnover of misfolded protein degradation (Fig. 3.16AIb). So even though the ER stress remains persistently high and VAP^{P58S} aggregates do not clear up (Section 3.2.7 and 3.2.4), the downstream protein degradation stays highly activate. This substantially clears the load of misfolded proteins on the ER and partially rescues the defects related to $\Delta VAP; gVAP^{P58S}$ flies (Fig. 3.16AIc). Simultaneously Caspar,

being the negative regulator of NF-κB pathway, blocks the NF-κB signalling which leads to lowered inflammation in the $\Delta VAP; gVAP^{P58S}$ flies (Fig. 3.16AIIc). The extra Caspar thus causes damage control and extends the survival of $\Delta VAP; gVAP^{P58S}$ flies. This arrangement fails when Caspar is knocked down.

In the case of TER94 glial overexpression, we seem to end up targeting/degrading a lot of other essential proteins, which are not upregulated during ER stress or are unrelated to TER94-Caspar specific interactions. This rampant throwing of proteins under the degradation bus causes harm to the system and therefore leads to further aggravation of the observed phenotypes. Moreover, as VCP (mammalian TER94) is reported to be involved in ubiquitination and degradation of the NF-κB inhibitor IκBα (Asai et al., 2002 and Li et al., 2014), excess TER94 probably causes more Relish molecules to translocate into the nucleus and leads to increased inflammation, which is detrimental to the flies. On the other hand, when we knockdown TER94, the UPS is downregulated, leading to lesser degradation of misfolded proteins, which again causes worsening of the phenotype.

The TER94^{R152H} (VCP^{R155H} in mammals), is proposed to be a gain-of-function mutation, as it shows enhanced ATPase activity than its wild type counterpart (Zhang et al., 2015). In overexpression model studies performed in *Drosophila*, this mutation is observed to enhance the neurodegenerative phenotypes and is therefore also termed as a dominant active mutation (Chang et al., 2011). This mutation is in the N-terminal domain of the proteins, which is involved in interaction with its co-factors, one of which is FAF1 (Yeo and Yu, 2016; Song et al., 2005 and 2009). This mutation doesn't cause loss of interaction between VCP and its co-factors, but it is known to alter the interaction by increasing the catalytic efficiency of the co-factor (Zhang et al., 2015). The binding site of VCP with FAF1 is very close to the R155[th] position (Lee et al., 2013 and Ewens et al., 2014). Although there is no direct evidence about altered connections in case of TER94^{R152H} (or VCP^{R155H}) and Caspar (or FAF1), proofs from the literature suggests that the TER94^{R152H} mutation increases the stability of its complex with Caspar even further. Eventually, in the case of TER94^{R152H} glial overexpression, the VAP^{P58S}-Caspar-TER94^{R152H} complex with increased stability saves the system by overstimulating the protein degradation machinery (Fig. 3.16BIb). In addition to this, we have to take into account the fact that there is a presence of endogenous (wild type) TER94 in these flies, and the overexpressed TER94^{R152H} in glia competes

with binding of the endogenous TER94. Considering the flux of TER94^{R152H} versus the endogenous (wild type) TER94 is, therefore, an important facet of this result.

Figure 3.16. VAP plays an active role in controlling protein degradation in the ERAD pathway.
A.I) VAP^{P58S} forms a complex with Caspar-TER94 and enables the flux of protein degradation to shift to the right in case of glial Caspar overexpression. This eventually leads to reduced misfolded protein load and increased survival.
II) Caspar, a negative regulator of IMD pathway (NF-κB pathway), reduces the neuroinflammation when overexpressed in glia. This adds to the effect on protein degradation thus aiding increased survival.
B) VAP^{P58S} forms a complex with Caspar-TER94^{R152H}. In case of TER94^{R152H}, this complex is speculated to be more stable. This, again, causes the flux of protein degradation to shift to the right leading to increased survival of ΔVAP; $gVAP^{P58S}$ flies.

4.4. Concluding remarks

In this chapter, we characterize the genetic interactions between *VAP^{P58S}/ALS8* and *TER94^{R152H}/ALS14*. We also demonstrate the genetic interactions of *ALS8* with *caspar* (*Drosophila FAF1*). We do not see any changes in the VAP aggregation pattern or the impaired lipid levels but report the rescue in size of boutons.

Although modulation of Caspar levels does not seem to bring any change in the existing ER stress caused by VAP^{P58S} in our experiments (Section 3.2.7), the VAP^{P58S}-Caspar-TER94 interactions support the modulation of UPS (Ubiquitin proteasomal system) in ALS8. The crux of the VAP-Caspar-TER94 stable complex formation is based on the premise that VAP supports the assembly of Caspar-TER94. This stable complex regulates the downstream protein degradation associated with ERAD. Our data, therefore, suggests that VAP is not only involved in the upstream process (i.e. modulation of ER stress) but it is also contributing to the downstream of ERAD (i.e. protein degradation). Although the mechanisms which could guide this process are yet to be uncovered, this puts VAP on the map of protein degradation (Fig. 3.16). We intend to look at the protein degradation angle in our future work.

Amongst the other ALS loci, Ubiquilin2 participates in protein degradation (Chapter I, Section 2.4.2.2 and Fig. 1.2). It is a UBA-UBL family protein which binds to the polyubiquitinated proteins via its UBA domain and recruits them to the proteasome via its UBL domain. In the case of the ALS mutant form, Ubiquilin2 associates with stress granules under stress and fails to associate with the proteasome (Renaud et al., 2019). Its interaction with VCP has been confirmed to occur via Erasin, an ER stress-associated protein. The VCP-Ubiquilin2 complex via Erasin is reported to cause protein degradation in case of increased ER stress (Lim et al., 2009). Ubiquilin2 is an interactor of FAF2, an ERAD chaperone very similar to FAF1 (Xia et al., 2014). Considering

its structure and function, there is a chance that Ubiquilin2 interacts with FAF1 as well. Although Ubiquilin2's interaction with VAP hasn't been tested, it could be potentially connecting VAP and VCP or act in consort with VAP-FAF1-VCP. This interaction, if affirmative, could link ALS8, ALS15 and ALS14 (VAP^{P58S}, ubiquilin2^{mutant} and TER94^{R152H}). Testing these interactions could help us put the picture of the proteasomal pathway in ALS together (Fig. 3.17).

Our previous studies describe suppression of the mTOR signalling to be beneficial for the VAP^{P58S} flies, as it is a genetic interactor of *VAP* which causes reduction of VAP positive brain aggregates and suppression of increased bouton phenotype associated with the VAP^{P58S} neuronal overexpression (Deivasigamani et al., 2014 and Chaplot et al., 2019). mTOR signalling regulates protein homeostasis, autophagy, energy metabolism and inflammation. It is therefore also upregulated in case of increased ER stress. Also, activated NF-κB pathway positively regulates mTOR signalling (Appenzeller-Herzog and Hall, 2012). The overexpression of Caspar could be indirectly suppressing the mTOR pathway, causing the condition of Δ*VAP; gVAP^{P58S}* flies to improve. This correlates with the suppression of bouton phenotype on glial overexpression of Caspar in the Δ*VAP; gVAP^{P58S}* flies (Section 3.2.6). Furthermore, mTOR is also controlled by VCP and Ubiquilin2 levels in the system (Zhou et al., 2017 and Coffey et al., 2016), suggesting a potential interplay between mTOR and other important players in the context of our work (Fig. 3.17).
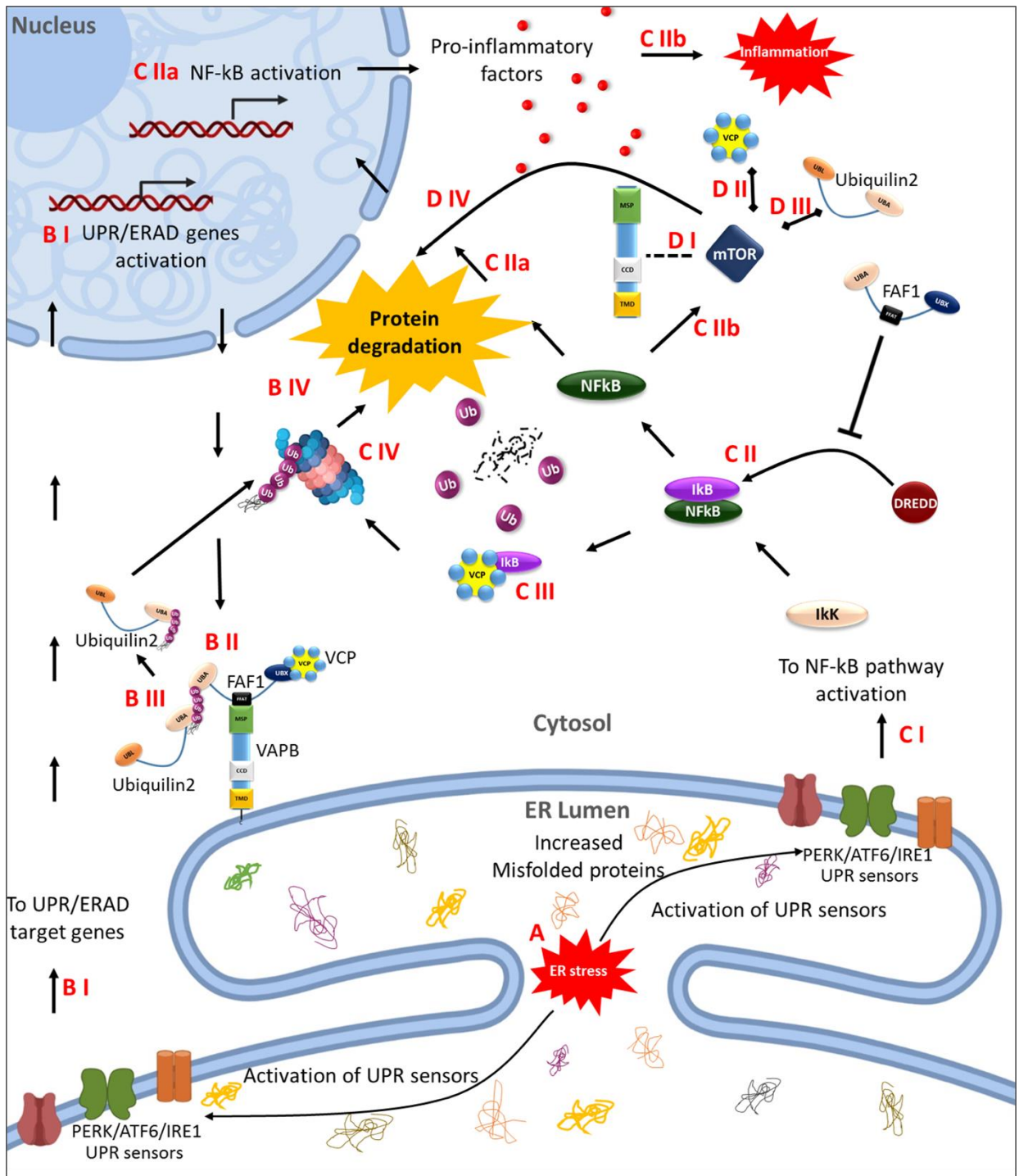
Figure 3.17. A crosstalk between VAP, VCP, FAF1, Ubiquilin2, NF-kB and mTOR potentially regulates the protein quality control in the system.

A) Increase in misfolded proteins in the ER causes ER stress, which activates ER stress sensors: ATF6, PERK and IRE1.

B) I) This causes activation of UPR genes in the nucleus, **(II)** assembles complexes like VAP-FAF1-VCP on the ER membrane, where the complex binds and pulls misfolded polyubiquitinated proteins in the cytoplasm from the ER to the cytoplasm, **(III)** Ubiquilin2 possibly interacts with this complex to transfer

the misfolded polyubiquitinated proteins to the proteasome. **(IV)** This process positively regulates ERAD and causes protein degradation.

C) I) Increased ER stress causes activation of NF-kB pathway via the ER stress sensors. IRE1 regulates IkK activity while PERK inhibits IkBα translation. **(II)** IkB is phosphorylated by IkK which causes DREDD mediated cleavage of IkB-NF-kB1 complex. FAF1 regulates this step by inhibiting the DREDD mediated cleavage. **(IIa)** The released NF-kB1 is then translocated to the nucleus for production of pro-inflammatory factors, **(IIb)** which contributes to increase in inflammation.

(III) The released IkB is bound by VCP and **(IV)** transferred for proteasomal degradation

D) I) mTOR genetically interacts with VAP. **(II)** The mTOR pathway is regulated by levels of VCP and **(III)** Ubiquilin2. **(IV)** mTOR regulates protein degradation along with many other cellular processes. References: Lee et al., 2013; Ron and Walter, 2007; Baron et al., 2014; Schmitz et al., 2018; Tam et al., 2012; Mathes et al., 2008; Jiang et al., 2003; Renaud et al., 2019; Lim et al., 2009; Xia et al., 2014; Deivasigamani et al., 2014; Chaplot et al., 2019; Appenzeller-Herzog and Hall, 2012; Zhou et al., 2017 and Coffey et al., 2016. Figure partly designed in: BioRender App.

Lastly, it is important to reiterate that, in our experiments, these interactions originate due to the gene expression in glial cells but the observations, however, are an outcome of this expression on the tripartite synapse and as a consequence, on the whole system. The tripartite is therefore a coupled system, displaying ripple effects of one cell type on others. Glial cells are great companions of the synapses when it comes to providing support for synapse maintenance. In our study, these cells surely seem to be doing their job by regulating the UPS and inflammation as an outcome of the VAP-Caspar-TER94 interactions. It would be interesting to check if muscles and motor neurons show similar phenotypes for Caspar and TER94[R152H] (Related experiments in the appendix I).

5. Materials and Methods

5.1. Reagents

This Chapter incorporates numerous techniques and assays. We have mentioned fly lines and antibodies in this Section while the rest of the reagents are mentioned along with the description of respective techniques.

Table 3.7. List of Fly lines used in the study
Description beside every fly line mentions the Bloomington number or the source from which the fly lines were obtained

Fly line	Source	Full Genotype	Other Details (if any)
UAS-VAP^{WT}	Ratnaparkhi et al., 2008	*UAS-VAP^{WT}*	
UAS- VAP^{P58S}	Ratnaparkhi et al., 2008		*Drosophila* orthologue of *VAP^{P56S}*
UAS-VAP^{RNAi}	BL 27312	*y[1] v[1]; P{y[+t7.7] v[+t1.8]=TRiP.JF02621}attP2*	
UAS-TBPH^{WT}	NCBS	*CG 10327 RB; C-terminal FLAG+HA tag*	*Drosophila* orthologue of *TDP-43*
UAS-TBPH^{RNAi}	BL 29517	*y[1] v[1]; P{y[+t7.7] v[+t1.8]=TRiP.HM05194}attP2*	
UAS-caz^{WT}	BL17010	*w[1118] P{w[+mC]=EP}caz[EP1564]*	*Drosophila* orthologue of *FUS*
UAS-caz^{RNAi}	BL34839	*y[1] sc[*] v[1] sev[21]; P{y[+t7.7] v[+t1.8]=TRiP.HMS00156}attP2*	
UAS-SOD1^{WT}	BL24754	*w[1]; P{w[+mC]=UAS-Sod1.A}B36*	
UAS-SOD1^{RNAi}	BL34616	*y[1] sc[*] v[1] sev[21]; P{y[+t7.7] v[+t1.8]=TRiP.HMS01291}attP2*	
UAS-TER94^{WT}	JP Taylor, University of Pennsylvania School of Medicine (Ritson et al., 2010)	*UAS-TER94^{WT}/ Cyo*	*Drosophila* orthologue of *VCP*
UAS-TER94^{R152H}		*UAS-TER94 ^{R152H}*	
UAS-TER94^{A229E}		*UAS-TER94^{A229E}/cyo (2Ch.)*	
UAS-TER94^{RNAi}	BL 32869	*y[1] sc[*] v[1] sev[21]; P{y[+t7.7] v[+t1.8]=TRiP.HMS00656}attP2*	
UAS-alsin^{WT}	BL 27162	*y[1] w[*]; P{w[+mC]=EP}Als2[G4607]*	
UAS-alsin^{RNAi}	BL 28533	*y[1] v[1]; P{y[+t7.7] v[+t1.8]=TRiP.HM05019}attP2*	
UAS-senataxin^{RNAi}	BL 34683	*y[1] sc[*] v[1] sev[21]; P{y[+t7.7] v[+t1.8]=TRiP.HMS01161}attP2/TM3, Sb[1]*	

MHC-Gal4	BL 38464	*w[*]; P{w[+mC]=Mhc-RFP.F3-580}2, P{w[+mC]=Mhc-GAL4.F3-580}2/SM6b*	
Repo-Gal4	Dr. Bradley Jones, University of Mississippi Lee et al., 2005		
OK6-Gal4	BL 64199	*P{w[+mW.hs]=GawB}OK6*	
ΔVAP; gVAP^{P58S}	Dr. Hiroshi Tsuda		
ΔVAP; MHC-Gal4; gVAP^{P58S}	Balanced in-house		
ΔVAP; Repo-Gal4; gVAP^{P58S}	Balanced in-house		
ΔVAP; OK6-Gal4; gVAP^{P58S}	Balanced in-house		
UAS-caspar^{WT}	NCBS	*CG 8400 RA; C-terminal FLAG+HA tag*	
UAS-caspar^{RNAi}	BL 44027	*y[1] sc[*] v[1] sev[21]; P{y[+t7.7] v[+t1.8]=TRiP.HMS02742}attP2*	
UAS-relish^{RNAi}	BL 33661	*y[1] sc[*] v[1] sev[21]; P{y[+t7.7] v[+t1.8]=TRiP.HMS00070}attP2*	
UAS-relish^{RNAi NIG1}	NIG	*CG-11992-R1*	
UAS-relish^{RNAi NIG2}	NIG	*CG-11992-R2*	
UAS-relish^{WT}	BL 9459	*w[1118]; P{w[+mC]=UAS-Rel.His6}2; l(3)*[*]/TM3, Sb[1]*	
relish^{E20}	BL 55714	*Rel[E20]*	
UAS-Imd^{RNAi}	BL 38933	*y[1] sc[*] v[1] sev[21]; P{y[+t7.7] v[+t1.8]=TRiP.HMS00253}attP2/TM3, Sb[1]*	
Canton-S (+/+)	BL 0001		Wild type control

Notes

1. Lines sourced from Bloomington Drosophila Stock Centre (BDSC) are identified with the Bloomington # and the prefix 'BL'.
2. DPiM (Drosophila protein interaction map) Collection are identified with gene name and CG number.
3. VDRC (Vienna Drosophila Research Centre) Collection are identified with the VDRC # and the prefix 'V'.
4. NIG (National Institute of Genetics) Collection are identified with gene name and CG number.

Table 3.8. List of antibodies used in the study

Antibody Used	Name of antibody/ protein	Raised in	Source	Dilution for IHC
Anti-HRP	Horse Radish Peroxidase	Rabbit	Sigma	1:500
Anti-DLG	Disc Large	Mouse	DSHB	1:250
Anti-Repo	Reverse polarity	Mouse	DSHB	1:100
Anti-ELAV	Embryonic lethal abnormal visual system	Rat	DSHB	1:100
Anti-VAP	VAMP associated protein	Rabbit	In-House	1:500
Anti-BiP	Binding immunoglobulin protein/ Hsp70	Rabbit	Cell Sig.	1:100
Anti-Caspar	Caspar	Rabbit	In-House	1:500
DAPI (dye)	4,6 diamidino-2-phenylindole		Sigma	1:1000

5.2. Larval crawling assays

Wandering third instar larvae of appropriate genotype were collected and placed on a 1% agar Petri plate of 10 cm in diameter. They were allowed to acclimatize for around 2 minutes. Followed by the acclimatization, they were placed in the centre of the dish and their distance from the centre was measured at the end of 1 min. This was repeated thrice with 3 different sets. The average was plotted using prism7 as distance crawled in cm Vs the genotypes. Statistical analysis was done using One way ANOVA followed by multiple comparison testing by Tukey test (Xia et al., 2012).

6. Contributions

Lovleen Garg repeated the motor assays post the first set of observations (Fig. 3.7). Aparna Thulasidharan contributed to dissections, staining and imaging of the adult brain (VAP positive) aggregates. The quantification for the larval and adult brain aggregates was performed by Lovleen Garg (Fig. 3.9). The Mass Spectrometry experiments for lipidomics were carried out under the supervision of Dr. Siddhesh Kamat.

7. Acknowledgements

8. References

Alami, N. *et al.* NF-κB activation in astrocytes drives a stage-specific beneficial neuroimmunological response in ALS. *EMBO J.* 37, 1–23 (2018).

Appenzeller-herzog, C. & Hall, M. N. Bidirectional crosstalk between endoplasmicreticulum stress and mTOR signaling. *Trends Cell Biol.* 22, 274–282 (2012).

Asai, T. *et al.* VCP (p97) regulates NFκB signaling pathway, which is important for metastasis of osteosarcoma cell line. *Japanese J. Cancer Res.* 93, 296–304 (2002).

Atkin, J. D. *et al.* Endoplasmic reticulum stress and induction of the unfolded protein response in human sporadic amyotrophic lateral sclerosis. *Neurobiol. Dis.* 30, 400–407 (2008).

Baron, Y. *et al.* VAPB/ALS8 interacts with FFAT-like proteins including the p97 cofactor FAF1 and the ASNA1 ATPase. *BMC Biol.* 12, 1–20 (2014).

Benedetti S, *et al*. Serum proteome in a sporadic amyotrophic lateral sclerosis geographical cluster. Proteomics Clin Appl. (2017).

Bertolotti, A *et al*. "Dynamic interaction of BiP and ER stress transducers in the unfolded-protein response." *Nature cell biology* vol. 2,6 (2000): 326-32. doi:10.1038/35014014

Blitterswijk, M. *et al.* Evidence for an oligogenic basis of amyotrophic lateral sclerosis. *Hum. Mol. Genet.* 21, 3776–3784 (2012).

Boom, J. Van Den & Meyer, H. Review VCP / p97-Mediated Unfolding as a Principle in Protein Homeostasis and Signaling. *Mol. Cell* 69, 182–194 (2017).

Bruijn, L. I. *et al.* Aggregation and motor neuron toxicity of an ALS-linked SOD1 mutant independent from wild-type SOD1. *Science (80-.).* 281, 1851–1854 (1998).

Chang, Y. C. *et al.* Pathogenic VCP/TER94 alleles are dominant actives and contribute to neurodegeneration by altering cellular ATP level in a drosophila IBMPFD model. *PLoS Genet.* 7, (2011).

Chaplot, K. *et al.* SOD1 activity threshold and TOR signalling modulate VAP(P58S) aggregation via reactive oxygen species-induced proteasomal degradation in a Drosophila model of amyotrophic lateral sclerosis. *DMM Dis. Model. Mech.* 12, (2019).

Chaves-Filho, A. B. *et al.* Alterations in lipid metabolism of spinal cord linked to amyotrophic lateral sclerosis. *Sci. Rep.* 9, 1–14 (2019).

Chen, S., *et al.* Genetics of amyotrophic lateral sclerosis: an update. *Mol Neurodegeneration* 8, 28 (2013).

Chinchore, Y., Gerber, G. F. & Dolph, P. J. Alternative pathway of cell death in Drosophila mediated by NF-κB transcription factor Relish. *Proc. Natl. Acad. Sci. U. S. A.* 109, (2012).

Cluskey, S. & Ramsden, D. B. Mechanisms of neurodegeneration in amyotrophic lateral sclerosis. *J. Clin. Pathol. - Mol. Pathol.* 54, 386–392 (2001).

Coffey, R. T., Shi, Y., Long, M. J. C., Marr, M. T. & Hedstrom, L. Ubiquilin-mediated Small Molecule Inhibition of Mammalian Target of Rapamycin Complex 1 (mTORC1) Signaling * □. 291, 5221–5233 (2016).

De Aguilar, J. L. G. Lipid biomarkers for amyotrophic lateral sclerosis. *Front. Neurol.* 10, 1–6 (2019).

Deivasigamani, S., Verma, H. K., Ueda, R. & Ratnaparkhi, A. RESEARCH ARTICLE A genetic screen identifies Tor as an interactor of VAPB in a Drosophila model of amyotrophic lateral sclerosis. 4, 1–12 (2014).

Deng, H. *et al.* FUS-Immunoreactive Inclusions Are a Common Feature in Sporadic and Non-SOD1 Familial Amyotrophic Lateral Sclerosis. (2010). doi:10.1002/ana.22051

Dorst, J *et al.* "High-caloric food supplements in the treatment of amyotrophic lateral sclerosis: a prospective interventional study." *Amyotrophic lateral sclerosis & frontotemporal degeneration* vol. 14,7-8 (2013): 533-6. doi:10.3109/21678421.2013.823999

Dresselhaus, E. C. & Meffert, M. K. Cellular Specificity of NF- κ B Function in the Nervous System. 10, (2019).

Engström Y, *et al*. kappa B-like motifs regulate the induction of immune genes in Drosophila. *J Mol Biol*. 1993;232(2):327-333. doi:10.1006/jmbi.1993.1392

Estes, P. S. *et al.* Wild-type and A315T mutant TDP-43 exert differential neurotoxicity in a Drosophila model of ALS. *Hum. Mol. Genet.* 20, 2308–2321 (2011).

Ewens, C. A. *et al.* The p97-faf1 protein complex reveals a common mode of p97 adaptor binding. *J. Biol. Chem.* 289, 12077–12084 (2014).

Frakes, A. E. *et al.* Microglia induce motor neuron death via the classical NF-κB pathway in amyotrophic lateral sclerosis. *Neuron* 81, 1009–1023 (2014).

Frakes, A. E. *et al.* Four glial cells regulate ER stress resistance and longevity via neuropeptide signaling in C. Elegans. *Science (80-.).* 367, 436–440 (2020).

Fuentes-Medel, Y. *et al.* Glia and muscle sculpt neuromuscular arbors by engulfing destabilized synaptic boutons and shed presynaptic debris. *PLoS Biol.* 7, (2009).

Gkogkas, C. *et al.* VAPB interacts with and modulates the activity of ATF6. *Hum. Mol. Genet.* 17, 1517–1526 (2008).

Hadano, S. *et al.* Loss of ALS2 / Alsin Exacerbates Motor Dysfunction in a SOD1 H46R -Expressing Mouse ALS Model by Disturbing Endolysosomal Trafficking. 5, (2010).

Haidet-phillips, A. M. *et al.* NIH Public Access. 29, 824–828 (2012).

Han, S. M. *et al.* VAPB / ALS8 MSP Ligands Regulate Striated Muscle Energy Metabolism Critical for Adult Survival in Caenorhabditis elegans. 9, (2013).

Han, S. M. *et al.* Secreted VAPB/ALS8 Major Sperm Protein Domains Modulate Mitochondrial Localization and Morphology via Growth Cone Guidance Receptors. *Dev. Cell* 22, 348–362 (2012).

Hensley, K. *et al.* Primary glia expressing the G93A-SOD1 mutation present a neuroinflammatory phenotype and provide a cellular system for studies of glial inflammation. *J. Neuroinflammation* 3, 1–9 (2006).

Hetz, Claudio, and Feroz R Papa. "The Unfolded Protein Response and Cell Fate Control." *Molecular cell* vol. 69,2 (2018): 169-181. doi:10.1016/j.molcel.2017.06.017

Huisman MH, *et al.* Effect of presymptomatic body mass index and consumption of fat and alcohol on amyotrophic lateral sclerosis. JAMA Neurol., (2015).

Huryn, D. M., Korn, D. J. P. & Wipf, P. p97 : An Emerging Target for Cancer , Neurodegenerative Diseases , and Viral Infections. (2020). doi:10.1021/acs.jmedchem.9b01318

Hussien, Y. *et al.* ER chaperone BiP/GRP78 is required for myelinating cell survival and provides protection during experimental autoimmune encephalomyelitis. *J. Neurosci.* 35, 15921–15933 (2015).

Jackson, C. L., Walch, L., Verbavatz, J. & Monod, I. J. Review Lipids and Their Trafficking : An Integral Part of Cellular Organization. *Dev. Cell* 39, 139–153 (2016).

Jiang, Hao-Yuan *et al.* "Phosphorylation of the alpha subunit of eukaryotic initiation factor 2 is required for activation of NF-kappaB in response to diverse cellular stresses." *Molecular and cellular biology* vol. 23,16 (2003): 5651-63. doi:10.1128/mcb.23.16.5651-5663.2003

Kanekura, K., Nishimoto, I., Aiso, S. & Matsuoka, M. Characterization of amyotrophic lateral sclerosis-linked P56S mutation of vesicle-associated membrane protein-associated protein B (VAPB/ALS8). *J. Biol. Chem.* 281, 30223–30233 (2006).

Kashima, R. & Hata, A. The role of TGF-β superfamily signaling in neurological disorders. *Acta Biochim. Biophys. Sin. (Shanghai).* 50, 106–120 (2018).

Kawano, M., Kumagai, K., Nishijima, M. & Hanada, K. Efficient trafficking of ceramide from the endoplasmic reticulum to the golgi apparatus requires a VAMP-associated protein-interacting FFAT motif of CERT. *J. Biol. Chem.* 281, 30279–30288 (2006).

Kerr, K. S. *et al.* Glial Wingless / Wnt Regulates Glutamate Receptor Clustering and Synaptic Physiology at the Drosophila Neuromuscular Junction. 34, 2910–2920 (2014).

Kim, M., Lee, J. H., Lee, S. Y., Kim, E. & Chung, J. Caspar, a suppressor of antibacterial immunity in Drosophila. *Proc. Natl. Acad. Sci. U. S. A.* 103, 16358–16363 (2006).

Kounatidis, I. & Chtarbanova, S. Role of glial immunity in lifespan determination: A Drosophila perspective. *Front. Immunol.* 9, 1–7 (2018).

Lanson, N. A. *et al.* A Drosophila model of FUS-related neurodegeneration reveals genetic interaction between FUS and TDP-43. *Hum. Mol. Genet.* 20, 2510–2523 (2011).

Lattante, S., Ciura, S., Rouleau, G. A. & Kabashi, E. Defining the genetic connection linking amyotrophic lateral sclerosis (ALS) with frontotemporal dementia (FTD). *Trends Genet.* 31, 263–273 (2015).

Lee, B. P. & Jones, B. W. Transcriptional regulation of the Drosophila glial gene repo. *Mech. Dev.* 122, 849–862 (2005).

Lee, J. J. *et al.* Complex of fas-associated Factor 1 (FAF1) with valosin-containing protein (VCP)-Npl4-Ufd1 and polyubiquitinated proteins promotes endoplasmic reticulum-associated degradation (ERAD)S. *J. Biol. Chem.* 288, 6998–7011 (2013).

Li, J.-M., Wu, H., Zhang, W., Blackburn, M. R. & Jin, J. The p97-UFD1L-NPL4 Protein Complex Mediates Cytokine-Induced I B Proteolysis. *Mol. Cell. Biol.* 34, 335–347 (2014).

Li, Y. X., Sibon, O. C. M. & Dijkers, P. F. Inhibition of NF-KB in astrocytes is sufficient to delay neurodegeneration induced by proteotoxicity in neurons. *J. Neuroinflammation* 15, 1–17 (2018).

Liang, C. J. *et al.* Derlin-1 Regulates Mutant VCP-Linked Pathogenesis and Endoplasmic Reticulum Stress-Induced Apoptosis. *PLoS Genet.* 10, (2014).

Liao, B., Zhao, W., Beers, D. R., Henkel, J. S. & Appel, S. H. Transformation from a neuroprotective to a neurotoxic microglial phenotype in a mouse model of ALS. *Exp. Neurol.* 237, 147–152 (2012).

Lim, P. J. *et al.* Ubiquilin and p97/VCP bind erasin, forming a complex involved in ERAD. 187, 201–217 (2009).

Lin, G., Mao, D. & Bellen, H. J. Amyotrophic Lateral Sclerosis Pathogenesis Converges on Defects in Protein Homeostasis Associated with TDP-43 Mislocalization and Proteasome-Mediated Degradation Overload. *Curr. Top. Dev. Biol.* 121, 111–171 (2017).

Loewen, C. J. R., Roy, A. & Levine, T. P. A conserved ER targeting motif in three families of lipid binding proteins and in Opi1p binds VAP. *EMBO J.* 22, 2025–2035 (2003).

Mathes E, *et al*. "NF-kappaB dictates the degradation pathway of IkappaBalpha." *The EMBO journal* vol. 27,9 (2008): 1357-67. doi:10.1038/emboj.2008.73

Mejzini, R. *et al.* ALS Genetics, Mechanisms, and Therapeutics: Where Are We Now? *Front. Neurosci.* 13, 1–27 (2019).

Meyer, H., Bug, M. & Bremer, S. Emerging functions of the VCP / p97 AAA-ATPase in the ubiquitin system. 14, 117–123 (2012).

Moustaqim-barrette, A. *et al.* The amyotrophic lateral sclerosis 8 protein, VAP, is required for ER protein quality control. *Hum. Mol. Genet.* 23, 1975–1989 (2014).

Myllymäki, H., Valanne, S. & Rämet, M. The Drosophila Imd Signaling Pathway . *J. Immunol.* 192, 3455–3462 (2014).

Nagata, Tetsuya *et al.* "Increased ER stress during motor neuron degeneration in a transgenic mouse model of amyotrophic lateral sclerosis." *Neurological research* vol. 29,8 (2007): 767-71. doi:10.1179/016164107X229803

Nagel G *et al.* Adipokines, C-reactive protein and Amyotrophic Lateral Sclerosis – results from a population- based ALS registry in Germany. Sci Rep., (2017).

Nalbandian, A. *et al.* The Multiple Faces of Valosin-Containing Protein-Associated Diseases : Inclusion Body Myopathy with Paget's Disease of Bone , Frontotemporal Dementia , and Amyotrophic Lateral Sclerosis. 522–531 (2011). doi:10.1007/s12031-011-9627-y

Nalbandian, A. *et al.* The Homozygote VCPR155H/R155H Mouse Model Exhibits Accelerated Human VCP-Associated Disease Pathology. *PLoS One* 7, 1–10 (2012).

Neurochemistry, J. O. F. Results Alteration in UBQLN2 expression adversely affects ERAD. 99–106 (2014). doi:10.1111/jnc.12606

Park, M. Y., Jang, H. D., Lee, S. Y., Lee, K. J. & Kim, E. Fas-associated Factor-1 Inhibits Nuclear Factor-κB (NF-κB) Activity by Interfering with Nuclear Translocation of the RelA (p65) Subunit of NF-κB. *J. Biol. Chem.* 279, 2544–2549 (2004).

Perry, Ryan J, and Neale D Ridgway. "Oxysterol-binding protein and vesicle-associated membrane protein-associated protein are required for sterol-dependent activation of the ceramide transport protein." *Molecular biology of the cell* vol. 17,6 (2006): 2604-16. doi:10.1091/mbc.e06-01-0060

Petersen, A. J., Katzenberger, R. J. & Wassarman, D. A. The innate immune response transcription factor relish is necessary for neurodegeneration in a Drosophila model of ataxia-telangiectasia. *Genetics* 194, 133–142 (2013).

Petersen, A. J., Rimkus, S. A. & Wassarman, D. A. ATM kinase inhibition in glial cells activates the innate immune response and causes neurodegeneration in Drosophila. *Proc. Natl. Acad. Sci. U. S. A.* 109, (2012).

Prell, T., Lautenschläger, J., Witte, O. W., Carri, M. T. & Grosskreutz, J. The unfolded protein response in models of human mutant G93A amyotrophic lateral sclerosis. *Eur. J. Neurosci.* 35, 652–660 (2012).

Prell, T. *et al.* Endoplasmic reticulum stress is accompanied by activation of NF- κ B in amyotrophic lateral sclerosis. *J. Neuroimmunol.* 270, 29–36 (2014).

Ratnaparkhi, A., Lawless, G. M., Schweizer, F. E., Golshani, P. & Jackson, G. R. A Drosophila model of ALS: Human ALS-associated mutation in VAP33A suggests a dominant negative mechanism. *PLoS One* 3, (2008).

Reichhart, J M *et al.* "Insect immunity: developmental and inducible activity of the Drosophila diptericin promoter." *The EMBO journal* vol. 11,4 (1992): 1469-77.

Renaud, L., *et al* Key role of UBQLN2 in pathogenesis of amyotrophic lateral sclerosis and frontotemporal dementia. 7, 1–11 (2019).

Ritson, G. P. The Basis of VCP-Mediated Degeneration : Insights From a Drosophila Model of Disease The Basis of VCP-Mediated Degeneration : Insights From a Drosophila. (2010).

Ron, D. & Walter, P. Signal integration in the endoplasmic reticulum unfolded protein response. *Nat. Rev. Mol. Cell Biol.* 8, 519–529 (2007).

Rosales C (April 12th 2017). Cellular and Molecular Mechanisms of Insect Immunity, Insect Physiology and Ecology, Vonnie D.C. Shields, IntechOpen, DOI: 10.5772/67107. Available from: https://www.intechopen.com/books/insect-physiology-and-ecology/cellular-and-molecular-mechanisms-of-insect-immunity

Schmitz, M. L., *et al.* The Crosstalk of Endoplasmic Reticulum (ER) Stress Pathways with NF- κ B : Complex Mechanisms Relevant for Cancer , Inflammation and Infection. 1, 1–18

Schuberth, C. & Buchberger, A. UBX domain proteins: Major regulators of the AAA ATPase Cdc48/p97. *Cell. Mol. Life Sci.* 65, 2360–2371 (2008).

Sinadinos, C., *et al.* Increased throughput assays of locomotor dysfunction in Drosophila larvae. *J. Neurosci. Methods* 203, 325–334 (2012).

Smith, J. A., Das, A., Ray, S. K. & Banik, N. L. Role of pro-inflammatory cytokines released from microglia in neurodegenerative diseases. *Brain Res. Bull.* 87, 10–20 (2012).

Song, E. J., Yim, S.-H., Kim, E., Kim, N.-S. & Lee, K.-J. Human Fas-Associated Factor 1, Interacting with Ubiquitinated Proteins and Valosin-Containing Protein, Is Involved in the Ubiquitin-Proteasome Pathway. *Mol. Cell. Biol.* 25, 2511–2524 (2005).

Song, J. S. *et al.* Structure and interaction of ubiquitin-associated domain of human Fas-associated factor 1. *Protein Sci.* 18, 2265–2276 (2009).

Stoica, R. *et al.* ALS / FTD -associated FUS activates GSK -3β to disrupt the VAPB – PTPIP 51 interaction and ER –mitochondria associations . *EMBO Rep.* 17, 1326–1342 (2016).

Stoica, R. *et al.* ER–mitochondria associations are regulated by the VAPB–PTPIP51 interaction and are disrupted by ALS/FTD-associated TDP-43. (2014). doi:10.1038/ncomms4996

Tam, Arvin B *et al.* "ER stress activates NF-κB by integrating functions of basal IKK activity, IRE1 and PERK." *PloS one* vol. 7,10 (2012): e45078. doi:10.1371/journal.pone.0045078

Tang, W. K. & Xia, D. Mutations in the human AAA+ chaperone p97 and related diseases. *Front. Mol. Biosci.* 3, 1–12 (2016).

Teuling, E. *et al.* Motor Neuron Disease-Associated Mutant Vesicle- Associated Membrane Protein-Associated Protein (VAP) B Recruits Wild-Type VAPs into Endoplasmic Reticulum- Derived Tubular Aggregates. 27, 9801–9815 (2007).

Tong, J. *et al.* Expression of ALS-linked TDP-43 mutant in astrocytes causes non-cell-autonomous motor neuron death in rats. 32, 1917–1926 (2013).

Tsuda, H. *et al.* The Amyotrophic Lateral Sclerosis 8 Protein VAPB Is Cleaved, Secreted, and Acts as a Ligand for Eph Receptors. *Cell* 133, 963–977 (2008).

Tudor, E. L. *et al.* Amyotrophic lateral sclerosis mutant vesicle-associated membrane protein-associated protein-B transgenic mice develop TAR-DNA-binding protein-43 pathology. *Neuroscience* 167, 774–785 (2010).

Wu, H., Xiong, W. C. & Mei, L. To build a synapse: Signaling pathways in neuromuscular junction assembly. *Development* 137, 1017–1033 (2010).

Wyles, J. P., McMaster, C. R. & Ridgway, N. D. Vesicle-associated membrane protein-associated protein-A (VAP-A) interacts with the oxysterol-binding protein to modify export from the endoplasmic reticulum. *J. Biol. Chem.* 277, 29908–29918 (2002).

Xia, R. *et al.* Motor neuron apoptosis and neuromuscular junction perturbation are prominent features in a Drosophila model of Fus-mediated ALS. *Mol. Neurodegener.* 7, 10 (2012).

Yamamoto, Y. & Gaynor, R. B. I k B kinases : key regulators of the NF- k B pathway. 29, (2004).

Yamanaka, K. *et al.* Mutant SOD1 in cell types other than motor neurons and oligodendrocytes accelerates onset of disease in ALS mice. 105, (2008).

Yeo, B. K. & Yu, S. W. Valosin-containing protein (VCP): structure, functions, and implications in neurodegenerative diseases. *Animal Cells Syst. (Seoul).* 20, 303–309 (2016).

Zhang, X. *et al.* Altered cofactor regulation with disease-associated p97/VCP mutations. *Proc. Natl. Acad. Sci. U. S. A.* 112, E1705–E1714 (2015).

Zhou, N., Ma, B., Stoll, S., Hays, T. T. & Qiu, H. Aging Cell. 1168–1179 (2017). doi:10.1111/acel.1265

Chapter IV

Modulation of retrograde and anterograde signaling in the ALS8 disease model

1. Summary

In this chapter, we discuss the modulation of the retrograde and anterograde pathways involved in signalling at the tripartite synapse. We express allelic variants of the components of Wnt and BMP pathways in the glial cells and score for deviation in the lifespan of the $\Delta VAP;$ $gVAP^{P58S}$ flies.

Our preliminary results suggest that the downregulation of both pathways in the glia is beneficial for the survival of the $\Delta VAP; gVAP^{P58S}$ flies as it results in suppression of the lifespan defect. In the future, we plan to validate these interactions further and look at the implications of these changes.

2. Introduction

The tripartite synapse experiences multiple signalling pathways, like the Agrin-Musk pathway, MAPK pathway, signalling associated with neurotransmitter release, Hedgehog signalling, BMP pathway and the Wnt signalling pathway. These pathways are engaged in the development, maintenance and functioning of the tripartite synapse. Some of these pathways have been studied in detail and their cell-specific components have been characterized (Wu et al., 2010). However, as glial cells are the newly introduced participants at the three-cell junction, the intricacies of signalling cascades in these cells have not been fully understood. Few studies have described crosstalk among some of these pathways at the tripartite synapse, thus enabling a finer systemic regulation. The BMP and the Wnt pathways have been reported to interact and possibly regulate the functioning of the synapse (Packard et al., 2003 and Fuentealba et al., 2007). Likewise, the MAPK pathway is reported to interact with BMP as well as the Wnt signalling pathway; potentially leading to the development and maintenance of the synapse (Aubin et al., 2004 and Xu et al., 2016). Two of the most commonly studied pathways at the tripartite synapse are the Wnt and the BMP signalling pathways.

2.1. Wingless signalling

The Wnt pathway, known as Wg (Wingless) in *Drosophila*, is involved in synaptic differentiation, presynaptic assembly during neurogenesis, regulation of neurotransmitter trafficking at the presynapse and aiding synaptic bouton formation (Kerr et al., 2014; Inestrosa and Arenas, 2010; Packard et al., 2002). It is an anterograde as well as retrograde signalling pathway at the tripartite synapse (Fig. 4.1B). It is one of the regulators of the neuroprotection and neurotoxicity linked with ALS progression (Chapter I, Section 2.9.2). So far no reports link ALS8 with the Wnt/ Wg signalling pathway.

Wg signalling is activated by the ligand Wg (Wnt in mammals) binding to its receptor Fz (Frizzled). The activated receptor then interacts with adapter protein Dsh (Dishevelled), which then inhibits the Zw3 (zeste-white 3, GSK3β in mammals) from phosphorylating Arm (Armadillo, β-Catenin in mammals). This stabilizes Arm and allows its translocation into the nucleus for target gene activation (Zeng and Verheyen, 2004) (Fig. 4.1A).
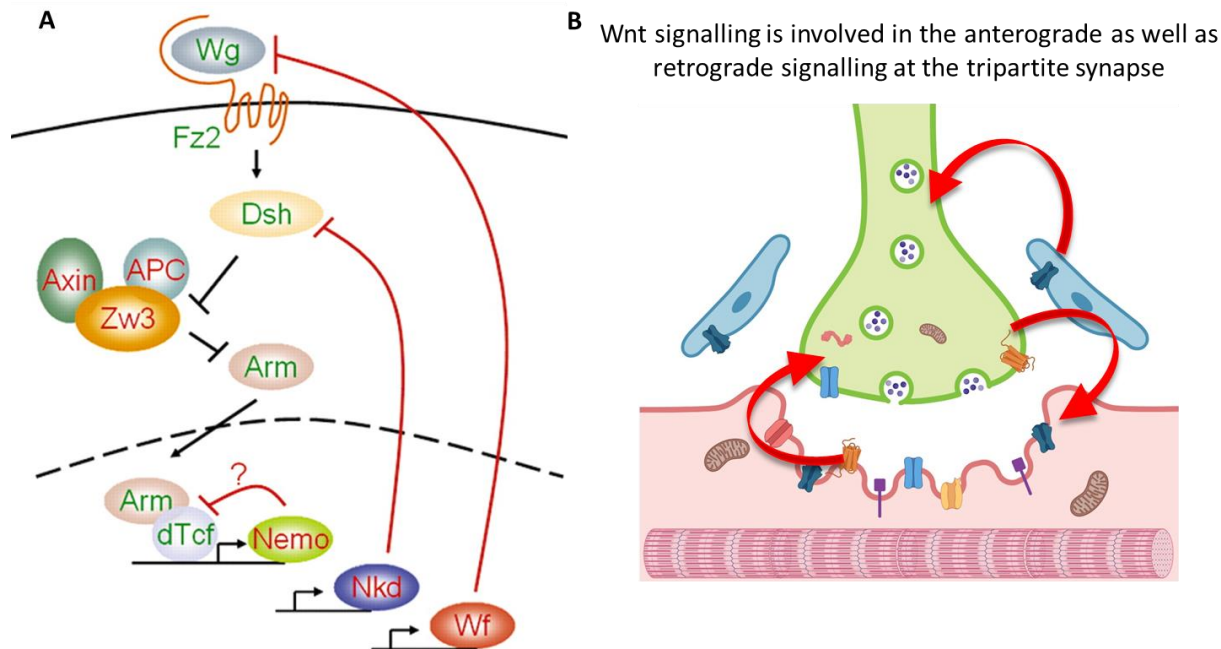
Figure 4.1. Wingless Pathway in *Drosophila*.
A) The activation on Wingless pathway in *Drosophila* takes place post binding of Wg ligand to Fz receptor which then inhibits the Axin complex activity and stabilizes Arm for target gene activation. (Zeng and Verheyen, 2004; Wu et al., 2010).
B) Wnt/Wingless signalling at the tripartite synapse has been reported to occur in the glial to neuronal cell direction (retrograde) as well as in the neuronal to muscle (anterograde) and muscle to neuronal (retrograde) cell direction (He et al., 2018; Kerr et al., 2014 and Wu et al., 2010).

2.2. Dpp signalling

The bone morphogenetic protein (BMP) pathway, known as Dpp (Decapentaplegic) in *Drosophila*, is involved in retrograde as well as anterograde signalling at the tripartite synapse (Fig. 4.2B). It is involved in the developmental neuronal modelling, synaptic growth, regulation of cell number and function of the tripartite synapse (Awasaki et al., 2011; McCabe et al., 2004; Mabie et al., 1999 and Ball et al., 2010). TGFβ, the mammalian ligand has been reported to be upregulated in certain models of ALS. This upregulation causes further aggravation of the disease phenotypes (Chapter I, Section 2.9.1). However, in the case of an overexpression study using a *Drosophila* model of ALS8, the expression of the transcription factor pMAD (a phosphorylated form of mothers against Dpp), which translocates to the nucleus on its phosphorylation is reported to be downregulated (Ratnaparkhi et al., 2008). These clues suggest that the regulation of the pathway is impaired in the case of ALS.

The Dpp/BMP signalling is a dual receptor activation pathway. It has type I and type II serine/threonine kinase receptors. On Dpp (TGFβ in mammals) ligand binding, the type II receptor activates and phosphorylates the type I receptor. To transmit the signal further, the type I receptor phosphorylates MAD (Smad in mammals) which is a downstream component of the pathway. pMAD forms a complex with Medea (Med, Smad4 in mammals). This complex then translocates to the nucleus and activates the target genes (Fig. 4.2). The type I receptors in *Drosophila* are Tkv (Thickvein)/ Sax (Saxophone)/ Babo (Baboon) and the type II receptors are Put (Punt)/Wit (Wishful thinking)/ Mav (Maverick). Some of these have been reported to be specific for a cell-type while others are ubiquitously expressed. Gbb (Glass bottom boat)/ Daw (Dawdle) are ligands of the pathway besides Dpp (https://www.sdbonline.org/sites/fly) (Fig. 4.2A).
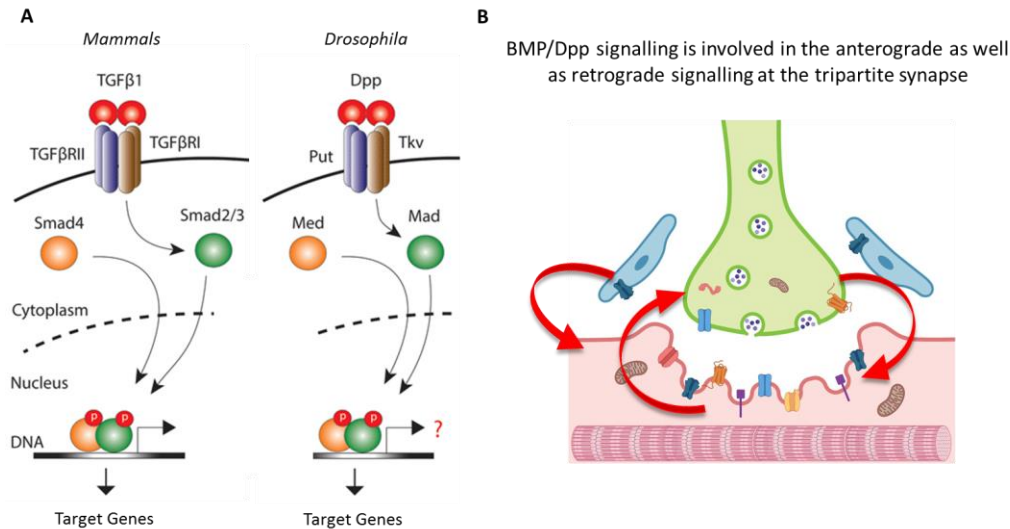
Figure 4.2. BMP signalling in mammals and *Drosophila*.
A) BMP pathway is well conserved across species. It has a heterodimeric serine/threonine kinase receptors. The activation of these receptors causes complex of cytosolic components, which further translocate to the nucleus for transcription of target genes. Image adapted and modulated from Ayyaz et al., 2017
B) BMP/Dpp signalling at the tripartite synapse has been reported to occur in the glial to muscle to neuronal cell direction (retrograde) as well as in the neuronal to muscle (anterograde) direction. (Wu et al., 2010; Bayat et al., 2011; Ball et al., 2010 and Fuentes-Medel et al., 2012).

In this chapter, we have explored the effects of glial expression of various components of the Wnt and BMP pathways in the $\Delta VAP;\ gVAP^{P58S}$ background. Our results provide preliminary evidence for these pathways contributing to the regulation of the $\Delta VAP;\ gVAP^{P58S}$ phenotypes.

3. Results

3.1. Downregulation of Wingless and BMP pathways replicates the *caspar* overexpression phenotype

The possible role of the IMD pathway in the mechanism of Caspar intrigued us to elucidate the involvement of other pathways at the tripartite synapse in regulating the lifespan defect of $\Delta VAP;\ gVAP^{P58S}$. As discussed in Chapter I, BMP and Wnt are two pathways implicated in ALS (Fuentes-Medel et al., 2012, Ratnaparkhi et al., 2008, Kerr et al., 2014). We used various *Drosophila* specific components of these pathways to investigate their roles in controlling the longevity of $\Delta VAP;\ gVAP^{P58S}$ flies via glia.

3.1.1. Change in levels of *wingless* regulates life span of Δ*VAP; gVAP^{P58S}* flies via glia

We overexpressed and downregulated *wingless* (*wg*), a ligand for the receptor Frizzled (Fz) of the Wingless/Wnt pathway in the glial cells of the Δ*VAP; gVAP ^{P58S}* flies. *wg^{RNAi}* suppresses the survival defect while its overexpression in the glia enhances it (Fig. 4.3). Though more evidence is required, our results for *caspar* (Chapter III, Section 3.2) and *wingless* together are supported by the previously studied fact that FAF1 is involved in suppression of Wnt (Wingless) pathway by degrading β- catenin (Kim et al., 2015; Zhang et al., 2011). Use of various other Wg pathway components like *Fz* (Receptor) and *Arm* (*Drosophila* orthologue of β- catenin, a transcriptional co-activator) will give us more insights about *VAP^{P58S}* and *wg* interactions. We plan to repeat this experiment with 'Gal4 controls'.

	Genotypes	ΔML	Key E= Enhancers S= Suppressors
1	Δ*VAP; Repo>+; gVAP^{P58S}/+* (Control)	0	
2	Δ*VAP; Repo>wg^{WT}; gVAP^{P58S}*	-3	
3	Δ*VAP; Repo>wg^{RNAi}; gVAP^{P58S}*	+6	
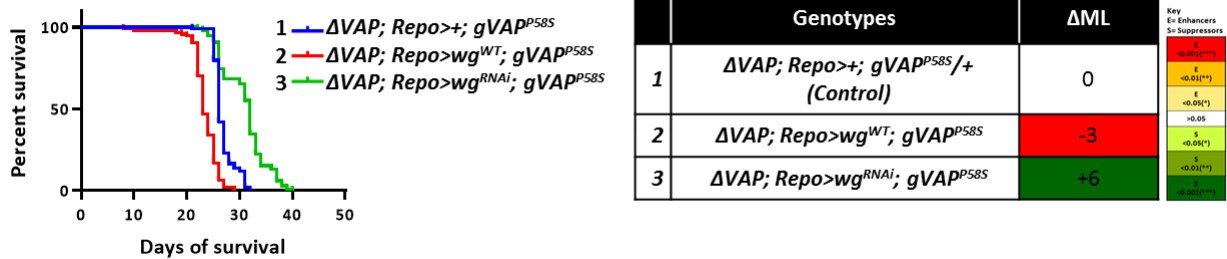
Figure 4.3. Wg levels in the glia control life span of Δ*VAP; gVAP^{P58S}* flies.
Overexpression of *Wg^{WT}* (Red curve), *Wg^{RNAi}* (Light green curve) in the Δ*VAP; Repo-Gal4; gVAP ^{P58S}* background. Δ*VAP; Repo>+; gVAP^{P58S}/+* (Curve 1 in blue color) was used as the control. The individual p-values and median are represented in the corresponding table.
The tabulated results are in the form of ΔML (Change in Median Lifespan) = Median Lifespan (Experiment) – Median Lifespan (Control). Median Lifespan for control= 26 Days.
Color/Statistical Key: The 'red-yellow tones' indicate different levels of statistical confidence (log-rank test) for the 'Enhancers (E)' while the 'green tones' represent the same for 'Suppressors (S)'.
n=80-100 for each genotype. Curve comparison was done using log-rank (Mantel-Cox test).

3.1.2. BMP pathway components seem to alter the Δ*VAP; gVAP^{P58S}* life span defect

We used various components (Table 4.1) of the Dpp signalling (BMP) pathway to elucidate its role in regulating the life span of Δ*VAP; gVAP^{P58S}*, hence attempting to establish proof for the genetic interactions between *VAP^{P58S}* and BMP pathway. RNAi based knockdown of the type I receptor, *tkv* in glia (Fig. 4.4A Curve 3 and 4) suppresses the survival defect, whereas its overexpression doesn't seem to make any substantial difference. On the other hand, *Gbb*, a ligand in the pathway shows antagonistic effects (Fig. 4.4A Curve5 and 6) to *tkv*, suggesting interplay of other receptors and ligands of the pathway given the complexity of the pathway (Ball et al., 2010;

Fuentes-Medel et al., 2012). Another ligand *Dpp* led to >90% lethality (6 out of 100 flies eclose) upon overexpression, possibly due to toxicity caused by its increased levels. The flies eclosing upon overexpression of *dpp* exhibited severe motor defects and died within five days of eclosion. Studying the interactions with *wit* (Type II receptor) and other ligands of BMP will shed more light on the interplay between *VAP^P58S* and BMP components.

Table 4.1. Dpp signalling components used to screen for lifespan deviation in Δ*VAP; gVAP^P58S* flies

BMP pathway components	Variants used	Short Form	Function
Thickvein	*RNAi, overexpression and constitutively active allele*	*tkv*	Type I Receptor
Glass bottom boat	*Overexpression, RNAi*	*gbb*	Ligand
Decapentaplagic	*Overexpression*	*dpp*	Ligand
medea	*RNAi*	*med*	Co-smad. Complexes with p-mad
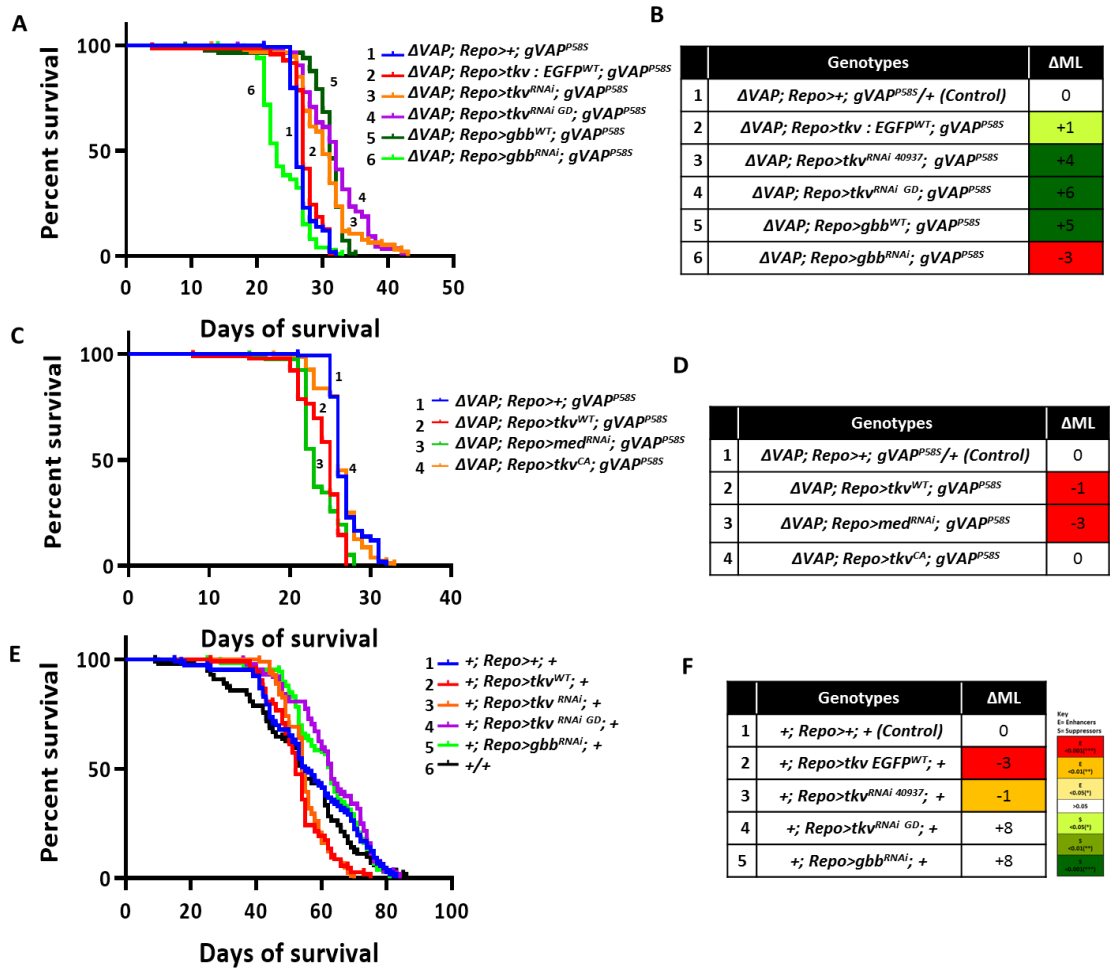
Figure 4.4. Regulating BMP signalling in the glia affect the life span of Δ*VAP; gVAP* ^{P58S} flies.

A) Overexpression of *Tkv*^{WT} (Red curve, number 2), *Tkv*^{RNAi} (Orange curve, number 3), *Tkv*$^{RNAi\ GD}$(Purple curve, number 4), *Gbb*^{WT} (Dark Green curve, number 5) and *Gbb*^{RNAi} (Light green curve, number 6) in the Δ*VAP; Repo-Gal4; gVAP*^{P58S} background. Δ*VAP; Repo>+; gVAP*^{P58S}/+ (Curve 1 in blue color) was used as the control. n=80-100 for every genotype. Curve comparison was done using log-rank (Mantel-Cox test).

B) The tabulated results are in the form of ΔML (Change in Median Lifespan) = Median Lifespan (Experiment) – Median Lifespan (Control). Median Lifespan for control= 26 Days.

Color/Statistical Key: The 'red-yellow tones' indicate different levels of statistical confidence (log-rank test) for the 'Enhancers (E)' while the 'green tones' represent the same for 'Suppressors (S)'.

C) Overexpression of *Tkv*^{WT} (Red curve, number 2), *med*^{RNAi} (Light green curve, number 3), *Tkv*^{CA} (Orange curve, number 4) in the Δ*VAP; Repo-Gal4; gVAP*^{P58S} background. Δ*VAP; Repo>+; gVAP*^{P58S}/+ (Curve 1 in blue color) was used as the control.

D) The individual p-values and median are represented in the corresponding table. Depiction of values is the same as (B).

E) 'Gal4 control' for *Tkv*^{WT} (Red curve), *Tkv*^{RNAi} (Orange curve), *Tkv*$^{RNAi\ GD}$(Purple curve) and *Gbb*^{RNAi} (Light green curve) loci expressions in Figure A.

F) The individual p-values and median are represented in the corresponding table. Depiction of values is the same as (B).

4. Discussion

In this chapter, we have studied the effects of modulation of the anterograde and retrograde pathways in the glial cells and have observed its effect on the lifespan of ALS8 flies. Suppression of both the Wingless and Dpp signalling pathways result in suppression of lifespan defect in the $\Delta VAP;\ gVAP^{P58S}$ flies.

Wg/Wnt pathway has been reported to be upregulated in a few models of ALS (Yu et al., 2013 and Chen et al., 2012). It hasn't been studied specifically in case of ALS8, but its suppression in our experiments demonstrates that its downregulation benefits the survival of the flies. This could be a result of suppressing the already upregulated signalling. More importantly, our work demonstrates this suppression via the glial cells (Section 3.1.1). Upregulation of Wnt signalling has been implicated in glial proliferation in ALS (Chen et al., 2012). Glial Wnt also participates in the release of pro and anti-inflammatory factors as the disease progresses. These factors are released as a result of the activated NF-κB pathway, which positively regulates the Wnt signalling and leads to increased glial proliferation in the early stages of neuroprotection (Alami et al., 2018). These increased glial cells release neurotoxic factors in the late stages. Therefore, blocking of the Wnt pathway or the NF-κB pathway (Chapter III, Section 3.2.8) in our case, presumably causes suppression of the phenotype. This not only alludes to the importance of glial Wnt/Wg but also signifies the correlation between Wnt signalling and NF-κB signalling in case of the $\Delta VAP;\ gVAP^{P58S}$ flies. Studies in various other diseases such as cancer have elucidated the positive as well as negative correlation of Wnt signalling with NF-κB signalling and vice versa (Ma and Hottiger, 2016). A couple of cancer-related studies, demonstrate FAF1 to be an inhibitor of Wnt activity (Kim et al., 2015; Zhang et al., 2010). It is important to look into the dynamics of Wnt/Wg signalling through the progressive stages in the ALS8 flies and correlate these with the inflammation. It would also be interesting to modulate Wg signalling in muscles and motor neurons and observe the phenotypic changes. In addition to this, Hedgehog signalling, which is antagonistic to the Wnt pathway would also be an exciting target to pursue in the context of ALS8 (Ding and Wang, 2017).

BMP/Dpp signalling, like Wnt signalling, also shows suppression of lifespan phenotype when expressed in the glia in the $\Delta VAP;\ gVAP^{P58S}$ flies, with an exception of the overexpression and downregulation of the ligand Gbb (Section 3.1.2). Further characterization using other

pathway components will define the interplay between the Dpp signalling and ALS8. This pathway is upregulated in glial as well as neuronal cells in ALS. This upregulation is reported to be acting against the neuroprotective factors, thus exacerbating neurodegeneration, while in some other cases it was observed to be downregulated (Kashima and Hata, 2018). This difference in activity seems to be linked to the stage of the disease and also the ALS locus involved. This pathway is not only reported to be interacting with the NF-κB signalling but also crosstalks with the Wnt pathway (Feng et al., 2003; Tarapore et al., 2016; Endo et al., 2015; Itasaki and Hoppler, 2010). This crosstalk, however, has not been studied in details in the context of ALS (Pinto et al., 2013).

Our work highlights the need for further investigation of the potential integration of these pathways at the tripartite synapse. Modulation of these pathways in a coordinated manner to understand how their crosstalk affects ALS8 would unravel a few more puzzles about the pathomechanism of ALS. The observations in this chapter are an outcome of the glial expression of the pathway components, however, it would be interesting to observe these effects through expression in the other cell types as well. In most studies, the activity of these pathways is considered to be context-specific i.e. the ALS causing mutation, stage of the disease and possibly the cell type observed. Answering our question about cell-specificity would clarify if the context matters in the case of ALS8 disease model as well.

5. Materials and Methods

5.1. Reagents

Table 4.2. List of Fly lines used in the study

Fly Line	Source	Full Genotype	Other Details (If any)
UAS-Tkv^{WT}	BL 51653	*w[*]; P{w[+mC]=UAS-tkv-EGFP.D}3*	
UAS-Tkv^{WT}	Michael O' Connor Lab		
UAS-Tkv^{RNAi}	BL 40937	*y[1] v[1]; P{y[+t7.7] v[+t1.8]=TRiP.HMS02185}attP40*	
UAS-Tkv^{RNAi}	GD V3059		CG14026
UAS-Tkv^{CA}	BL 36537	*w[*]; P{w[+mC]=UAS-tkv.CA}3*	
UAS-Gbb^{WT}	BL 63057	*y[1] w[*]; P{w[+mC]=UASp-gbb.GFP}3.3/CyO*	
UAS-Gbb^{RNAi}	BL 34898	*y[1] sc[*] v[1] sev[21]; P{y[+t7.7] v[+t1.8]=TRiP.HMS01243}attP2*	
UAS-Med^{WT}	BL 31928	*y[1] v[1]; P{y[+t7.7] v[+t1.8]=TRiP.JF02218}attP2*	
UAS-Dpp^{WT}	BL 53716	*w[*]; P{w[+mC]=UAS-dpp.GFP.T}3/TM3, Sb[1]*	
UAS-Wg^{WT}	Varun Chaudhary Lab		
UAS-Wg^{RNAi}	KK V104579		

6. Acknowledgements

7. References

Alami, N. *et al.* NF-κB activation in astrocytes drives a stage-specific beneficial neuroimmunological response in ALS. *EMBO J.* 37, 1–23 (2018).

Aubin, J. *et al.* In vivo convergence of BMP and MAPK signaling pathways: Impact of differential Smad1 phosphorylation on development and homeostasis. *Genes Dev.* 18, 1482–1494 (2004).

Awasaki, T., Huang, Y., O'Connor, M. B. & Lee, T. Glia instruct developmental neuronal remodeling through TGF-Î 2 signaling. *Nat. Neurosci.* 14, 821–823 (2011).

Ayyaz, A., Attisano, L. & Wrana, J. L. Recent advances in understanding contextual TGFβ signaling [version 1 ; peer review : 2 approved]. 6, 1–9 (2019).

Ball, R. W. *et al.* Retrograde BMP signaling controls synaptic growth at the nmj by regulating trio expression in motor neurons. *Neuron* 66, 536–549 (2010).

Baron, Y. *et al.* VAPB/ALS8 interacts with FFAT-like proteins including the p97 cofactor FAF1 and the ASNA1 ATPase. *BMC Biol.* 12, 1–20 (2014).

Bayat, V., Jaiswal, M. & Bellen, H. J. The BMP signaling pathway at the Drosophila neuromuscular junction and its links to neurodegenerative diseases. *Curr. Opin. Neurobiol.* 21, 182–188 (2011).

Chen, Y. *et al.* Activation of the Wnt/β-catenin signaling pathway is associated with glial proliferation in the adult spinal cord of ALS transgenic mice. *Biochem. Biophys. Res. Commun.* 420, 397–403 (2012).

Collins, C. A. & DiAntonio, A. Synaptic development: insights from Drosophila. *Curr. Opin. Neurobiol.* 17, 35–42 (2007).

Ding, M. E. I. & Wang, X. I. N. Antagonism between Hedgehog and Wnt signaling pathways regulates tumorigenicity (Review). 6327–6333 (2017). doi:10.3892/ol.2017.7030

Endo, F. *et al.* Astrocyte-Derived TGF-β1 Accelerates Disease Progression in ALS Mice by Interfering with the Neuroprotective Functions of Microglia and T Cells. *Cell Rep.* 11, 592–604 (2015).

Feng, J. Q. *et al.* NF- ☐ B Specifically Activates BMP-2 Gene Expression in Growth Plate Chondrocytes in Vivo and in a Chondrocyte Cell Line in Vitro *. 278, 29130–29135 (2003).

Fuentealba, L. C. *et al.* Integrating Patterning Signals: Wnt/GSK3 Regulates the Duration of the BMP/Smad1 Signal. *Cell* 131, 980–993 (2007).

Fuentes-Medel, Y. *et al.* Integration of a retrograde signal during synapse formation by glia-secreted TGF-β ligand. *Curr. Biol.* 22, 1831–1838 (2012).

Guan, H., Mattos, M., Yu, B., Wang, C. & Graves, D. T. HHS Public Access. 31, 52–64 (2016).

He, C., Liao, C. & Pan, C. Wnt signalling in the development of axon , dendrites and synapses. (2018).

Iłžecka, J., Stelmasiak, Z. & Dobosz, B. Transforming growth factor-beta 1 (TGF-beta 1) in patients with amyotrophic lateral sclerosis. *Cytokine* 20, 239–243 (2002).

Inestrosa, N. C. & Arenas, E. Emerging roles of Wnts in the adult nervous system. *Nat. Rev. Neurosci.* 11, 77–86 (2010).

Itasaki, N., Hoppler, S. & Wnt, T. Crosstalk Between Wnt and Bone Morphogenic Protein Signaling : A Turbulent Relationship ANTAGONISTIC EFFECTS PATHWAYS IN DIFFERENT. 16–33 (2010). doi:10.1002/dvdy.22009

Jason J et al. "TGF-beta signaling specifies axons during brain development." *Cell* vol. 142,1 (2010): 144-57. doi:10.1016/j.cell.2010.06.010

Kashima, R. & Hata, A. The role of TGF-β superfamily signaling in neurological disorders. *Acta Biochim. Biophys. Sin. (Shanghai).* 50, 106–120 (2018).

Kerr, K. S. *et al.* Glial Wingless / Wnt Regulates Glutamate Receptor Clustering and Synaptic Physiology at the Drosophila Neuromuscular Junction. 34, 2910–2920 (2014).

Kim, Hyeonwoo *et al*. "Unsaturated Fatty Acids Stimulate Tumor Growth through Stabilization of β-Catenin." *Cell reports* vol. 13,3 (2015): 495-503. doi:10.1016/j.celrep.2015.09.010

Liao, B., Zhao, W., Beers, D. R., Henkel, J. S. & Appel, S. H. Transformation from a neuroprotective to a neurotoxic microglial phenotype in a mouse model of ALS. *Exp. Neurol.* 237, 147–152 (2012).

Ma, B. & Hottiger, M. O. Crosstalk between wnt/β-catenin and NF-κB signaling pathway during inflammation. *Front. Immunol.* 7, (2016).

Mabie, P. C., Mehler, M. F. & Kessler, J. A. Mabie PC, 1999.pdf. 19, 7077–7088 (1999).

MacDonald, B. T., Tamai, K. & He, X. Wnt/β-Catenin Signaling: Components, Mechanisms, and Diseases. *Dev. Cell* 17, 9–26 (2009).

Marchetti, B. *et al.* Uncovering novel actors in astrocyte-neuron crosstalk in Parkinson's disease: The Wnt/β-catenin signaling cascade as the common final pathway for neuroprotection and self-repair. *Eur. J. Neurosci.* 37, 1550–1563 (2013).

Massague, J. TGF Signaling : Receptors , Transducers ,. 85, 947–950 (1996).

McCabe, B. D. *et al.* Highwire regulates presynaptic BMP signaling essential for synaptic growth. *Neuron* 41, 891–905 (2004).

McLoon, L. K., Harandi, V. M., Brännström, T., Andersen, P. M. & Liu, J. X. Wnt and extraocular muscle sparing in amyotrophic lateral sclerosis. *Investig. Ophthalmol. Vis. Sci.* 55, 5482–5496 (2014).

Packard, M. *et al.* The Drosophila Wnt, wingless, provides an essential signal for pre- and postsynaptic differentiation. *Cell* 111, 319–330 (2002).

Packard, M et al. "Wnts and TGF beta in synaptogenesis: old friends signalling at new places." *Nature reviews. Neuroscience* vol. 4,2 (2003): 113-20. doi:10.1038/nrn1036

Pinto, C., Cárdenas, P., Osses, N. & Henríquez, J. P. Characterization of Wnt/β-catenin and BMP/Smad signaling pathways in an in vitro model of amyotrophic lateral sclerosis. *Front. Cell. Neurosci.* 7, 1–15 (2013).

Ratnaparkhi, A., Lawless, G. M., Schweizer, F. E., Golshani, P. & Jackson, G. R. A Drosophila model of ALS: Human ALS-associated mutation in VAP33A suggests a dominant negative mechanism. *PLoS One* 3, (2008).

Speese, S. D. & Budnik, V. Wnts: up-and-coming at the synapse. *Trends Neurosci.* 30, 268–275 (2007).

Tarapore, R. S. *et al.* NF-κB Has a Direct Role in Inhibiting Bmp- and Wnt-Induced Matrix Protein Expression. *J. Bone Miner. Res.* 31, 52–64 (2016).

Wu, H., Xiong, W. C. & Mei, L. To build a synapse: Signaling pathways in neuromuscular junction assembly. *Development* 137, 1017–1033 (2010).

Xu, W. dong *et al.* Interactions between canonical Wnt signaling pathway and MAPK pathway regulate differentiation, maturation and function of dendritic cells. *Cell. Immunol.* 310, 170–177 (2016).

Yu, L., *et al.* Wnt Signaling is Altered by Spinal Cord Neuronal Dysfunction in Amyotrophic Lateral Sclerosis Transgenic Mice. *Neurochem Res* 38, 1904–1913 (2013).

Zeng, Y. A. & Verheyen, E. M. Nemo is an inducible antagonist of wingless signaling during Drosophila wing development. *Development* 131, 2911–2920 (2004).

Zhang, L. *et al.* Fas-associated factor 1 antagonizes Wnt signaling by promoting β-catenin degradation. *Mol. Biol. Cell* 22, 1617–1624 (2011).

Chapter V

Change in activity of ALS loci, at the NMJ, modulates bouton architecture

1. Summary

Expression of the fly orthologue of the ALS8 disease allele, *VAP^P58S* in the larval nervous system leads to a ~25% increase in bouton size, a feature that relates to neuronal function. Using this feature as a primary readout in this chapter, we explore roles for ALS causative genes, namely *VAP, TDP-43/TBPH, FUS/caz, SOD1* and *VCP/TER94* in the three cell types that make up the tripartite synapse. For the genes listed, we either increase or reduce mRNA transcript levels, in glia, muscle and neurons using the *UAS-Gal4* system and measure bouton architecture using HRP, DLG and BRP as markers (Fig. 5.1). This screen allows us to understand differential roles for the five ALS genes in the context of neuronal architecture at the tripartite synapse.

2. Introduction

Drosophila models of ALS8 have been generated by overexpression of the fly orthologue of *VAPB* carrying the corresponding ALS8 mutation, *VAP^P58S* (Ratnaparkhi et al., 2008; Andrea et al., 2008; Tsuda et al., 2014). As mentioned before, in the past, our laboratory has conducted two screens to elucidate *VAP*'s genetic interactors, identifying *TDP-43*, *alsin* and *SOD1* as interactors of *VAP*.

2.1. Role of VAP at the *Drosophila* NMJ

VAP is reported to control the bouton size and bouton number at the neuromuscular junction (NMJ) in *Drosophila*. Studies at the *Drosophila* NMJ have revealed that VAP is involved in the budding of the presynaptic boutons. The Bellen group in 2002 studied the role of loss-of-function allele of *VAP,* which led to increase in bouton size and decrease in bouton number (Pennetta et al., 2002). They also studied its association with microtubules and intracellular vesicles, which leads to controlling of the bouton architecture. They also observed a reduction of bouton size and increase in bouton number on *VAP* overexpression (Pennetta et al., 2002). This

effect of *VAP^WT* or *VAP^P58S* on bouton morphology appears to be a reproducible feature and a readout of VAP function (Ratnaparkhi et al., 2008).

2.2. Significance of bouton morphology in *Drosophila*

Aberrant bouton size and number is a measure of the cytoskeletal dysfunction at the synapse. There is increasing evidence of cytoskeletal abnormalities in ALS patients. The cytoskeleton slowly degenerates from the onset of the disease, which is then speculated to cause loss of synaptic connections and hence motor neurodegeneration (Baird and Bennett, 2013; Smith et al., 2014; Hensel and Claus, 2018). Thus, the bouton morphology hints at the effect of the mutations in the initial stages of the disease. The bouton morphology is also governed by the number of active zones at the synaptic ends, suggesting regulation of neurotransmitter release at the synapse. Various markers are used to observe the morphology of boutons at the NMJ. We used HRP (Horseradish peroxidase) to mark the presynapse, DLG (Disc Large) for the sub-synaptic reticulum and BRP (Bruchpilot) a presynaptic marker, in our study (Fig. 5.1).

Patient and/or animal model studies concerning ALS mutations other than *VAP*, namely *TDP-43*, *FUS, Profilin-1* and *Alsin* exhibit defects in their bouton morphology or the cytoskeleton, alluding to their role in synaptic transmission and synaptic microtubule organization. (Machamer et al., 2014; Godena et al., 2011; Henty-Ridilla., 2017; Julien et al., 2005). These studies support the strong basis for using bouton morphology as one of the readouts for analyzing early effects of ALS loci variants (wild type, knockdowns and mutants) on the tripartite synapse and explore both their neuronal as well as non-neuronal roles.
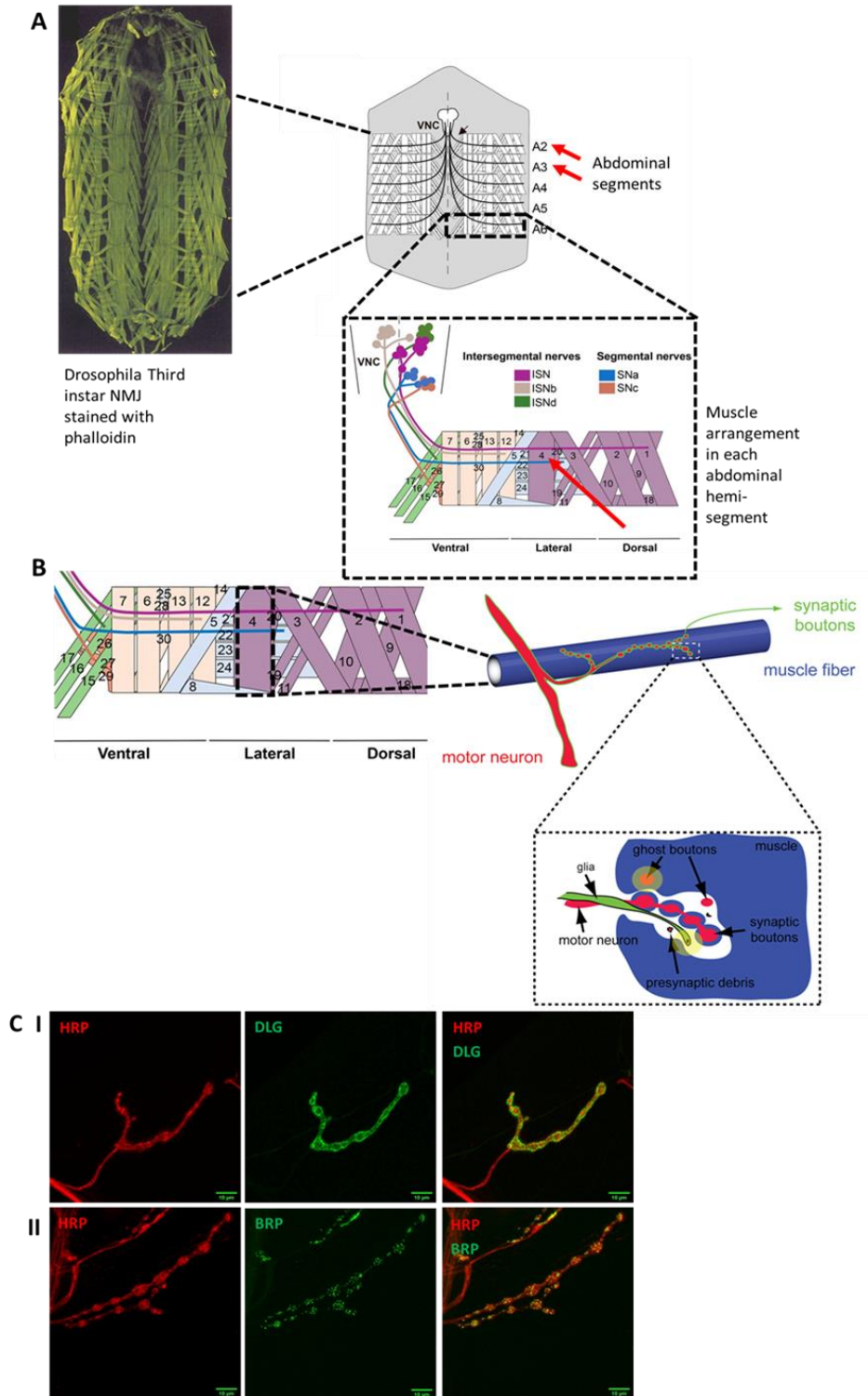
Figure 5.1. Organization of *Drosophila* NMJ.
A) This Figure is a representation of a *Drosophila* third instar larval NMJ. The first image displays a neuromuscular junction located around the body wall of a dissected third instar larva stained for phalloidin. Phalloidin stains the actin cytoskeleton and hence allows the visualization of muscles at the NMJ. The muscles are organized in a fixed pattern from the ventral to the dorsal section and this pattern repeats from

the anterior to the posterior abdominal segments (A1-A7) with a total of 60 muscles in each segment i.e. 30 in each hemi-segment. The zoomed-in image describes the arrangement of muscle segments. These muscles are innervated by the motor neurons from the ventral nerve cord (VNC) which projects axons of around 40 motor neurons. These projections occur through the 6 types of peripheral nerves, the intersegmental nerves (ISN, ISNb, ISNd) the segmental nerves (SNa and SNc) and a transverse nerve (TN). In our study, we have focused on the 4th muscle of segment A2 and A3 (red arrows).

B) Muscle 4 of the larval NMJ has a single projection and is easier to visualize. Also, because of the single innervation, spotting and quantifying defects becomes relatively less complicated. Motor neurons (presynapse of the NMJ) innervating muscles are glutamatergic in *Drosophila.* The presynaptic terminal has active zones which are rich sources of neurotransmitters. These active zones are contained by small bulb-like structures called synaptic boutons as described in the Figure, the size and number of which is dependent on the regulation of microtubule organization and neurotransmitter vesicles. We have used this flexibility in size and number of the boutons to study the homeostasis at the NMJ.

C) The boutons contain not just neurotransmitters but various other proteins involved in endocytosis, microtubule organization and pathways which function at the tripartite synapse. We made use of three such markers for our study of bouton morphology. The most important marker being HRP (horseradish peroxidase) which is a presynaptic marker which was used to measure the size of boutons. Along with HRP, we co-stained our samples either with DLG (Disc Large), a marker for the sub-synaptic reticulum at the postsynapse or BRP (bruchpilot), a presynaptic active zone marker. This image displays HRP and DLG (I), HRP and BRP (II) separately and the final merged image. All images in this chapter are represented in the merged form. (Moreno and Kane, 2019; Kohsaka et al., 2012; Pennetta., 2002; Keshishian et al. 1996; Landgraf & Thor 2006; Clarke et al., 2016; Chai et al., 2008. Figure adapted and modified from Moreno and Kane, 2019; Kazuyoshi et al., 2016; Chung and Barres, 2009).

In this chapter, we have used the *UAS-GAL4* system to explore the effect of various ALS loci on the morphology of the third instar *Drosophila* NMJ. We used the NMJ, specifically bouton architecture, as a proxy indicator of modulators at the tripartite synapse. RNAi lines, overexpression lines and mutant variants of *VAP, TDP-43/TBPH, FUS/caz, SOD1* and *TER94* were utilized in our study. We expressed the variants of these loci separately in muscle, glia and neurons, one cell type at a time, and quantified the size and number of boutons in the third instar NMJ. This was done in order to understand the differential role of each locus in each cell type. Figure 5.1 describes the *Drosophila* NMJ in detail and highlights the characteristics we have used in our work.

Our previous data suggests that the modulation of ALS loci may have cell autonomous and non-cell autonomous effects. Since this screen focuses primarily on the bouton architecture, we presumably measure the cell autonomous effects for neurons, while for glia and muscle the data corresponds to non-autonomous effects.

A

B

Locus	Loss of Function	Gain of Function		Mutant variants	
	Drosophila	*Drosophila*	*Mammalian*	*Drosophila*	*Mammalian*
VAP	*RNAi*	*VAP*	-	*P58S*	-
TDP-43/TBPH	*RNAi*	*TBPH*	*TDP-43*	-	*A315T,N345K*
FUS/caz	*RNAi*	*caz*	*FUS*	-	*R518K, R521C, R521H, ΔNES*
SOD1	*RNAi*	*SOD1*	-	-	*A4V*
VCP/TER94	*RNAi*	*TER94*	-	*R152H*	-

C

NMJ dissection of 3rd instar, fixing, staining, imaging and obtaining a maximum intensity projection image

D

Merged image → HRP only image →

Only HRP was used to quantify the size and number of boutons

Figure 5.2. Measurement of bouton size & number in NMJ of larvae expressing ALS fly orthologues in muscle, glia and neurons.
A) The screen for observing bouton morphology changes was carried out using muscle, glial and pan-neuronal drivers namely G14 and/or MHC-Gal4 for muscles, Repo-Gal4 for glia and Elav-Gal4 for neurons.

B) UAS lines of the variants of *VAP, TDP-43/TBPH, FUS/caz, SOD1* and *TER94* were mated with fly lines carrying the cell-specific drivers mentioned in 5.2A.

C) The third instar larvae of appropriate genotypes were collected from the F1 of the mated fly lines. These larvae were dissected for their NMJs, fixed, stained and imaged at 63X magnification using Zeiss confocal microscope.

D) The antibodies used for staining were HRP/DLG or HRP/BRP. HRP being the presynaptic marker was of prime importance to us, while DLG and BRP were used as co-stains. Having projected the images at their maximum intensity, the HRP channel was separated from either DLG or BRP and was further analyzed with Axiovision software for the size and number of boutons as shown in the representative image. Both bouton size and number were then counted and compared using unpaired student's t test.

3. Results

The ALS loci chosen for the study were perturbed using the *UAS-GAL4* system in muscles, glia and neuronal cells, one at a time. The effects of the perturbations were studied in the neurons, by measuring the size and number of boutons at the second and third segment of the muscle four in the third instar larval NMJ. The crosses with respective controls were set up at 25°C, unless otherwise mentioned. As mentioned before, this screen using *UAS-GAL4* system was carried out using variants of *VAP*, *TDP-43/TBPH*, *FUS/caz*, *SOD1* and *TER94/VCP*. Gal4 drivers of three cell types namely muscle (G14 and MHC), glia (Repo) and neurons (Elav) were used to drive the expression of these variants primarily at 25°C. The neuromuscular junctions of the F1 third instar larvae were dissected and stained as described in Materials and Methods, Section 5.2.1. The size and number of boutons were counted and reported as described in the Figure 5.2 and Materials and Methods, 5.2.2. Following is the scheme of the screen:

Muscle/Glial/Neuronal Gal4 X UAS- Wild type/RNAi/Mutant ALS Locus

Collect, dissect the neuromuscular junctions, fix and stain third instar larvae of the required genotype

Observe the bouton size and number by staining the NMJ using HRP and DLG as markers
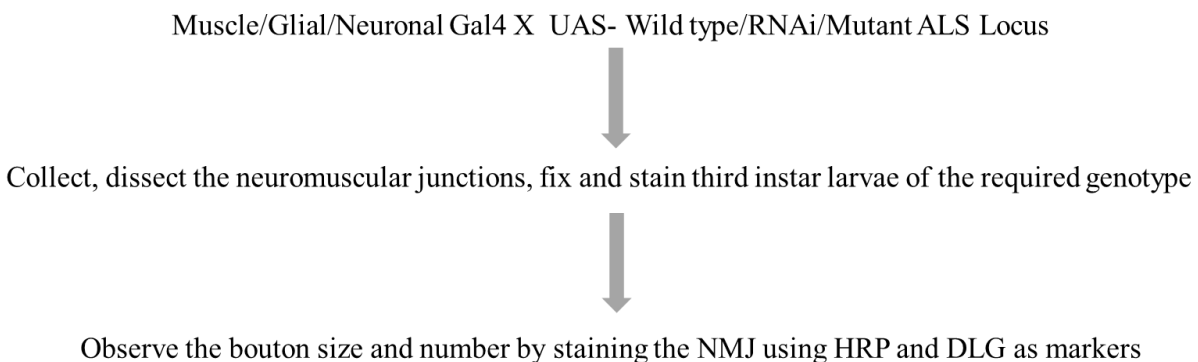
3.1. Effect of muscle expression of ALS loci on the bouton morphology

G14-Gal4 was used as the muscle driver. It is a second chromosome muscle driver expressed from the embryonic stages onwards. It is balanced over Cyo:GFP. Experimental F1 larvae chosen for the bouton analysis were GFP negative. Controls used in all cases were the Gal4 drivers crossed to Canton S (Wild Type). As *G14-Gal4* is a strong driver, F1 of a few loci variants were lethal and hence an alternative weaker driver, *MHC-Gal4* was also used. *MHC-Gal4* is a homozygous third chromosome driver, used only for the loci variants lethal on use of *G14-Gal4*.

3.1.1. Overexpression and downregulation of *VAP* in the muscle shows a change in bouton morphology, but the mutant allele shows no significant difference

Overexpression of *VAP^WT* and *VAP^RNAi* shows a significant alteration in bouton size and number, with their respective trends being opposite to each other, but *VAP^P58S* overexpression fails to show any significant change. The *G14>VAP^WT* shows drastic reduction in bouton size and an increase in bouton number. This genotype shows an increase in DLG localization as compared to the control, and the boutons are observed to be more clustered than normal. The *G14>VAP^P58S* bouton morphology was not significantly different from the control. *VAP* downregulation by using RNAi in muscles resulted in a phenotype opposite to that of its overexpression (Fig. 5.3).

B

Driver: *G14-Gal4*	Number	P value	Size in µm	P value
+	11.764±3.945		4.437±0.947	
VAP^WT	20.470±6.226	***	2.671±0.560	***
VAP^P58S	12.454±4.194	ns	3.971±0.831	ns
+	18.352±6.135		4.036±0.581	
VAP^RNAi	12.294±3.460	***	5.058±0.839	***

C

Locus/ Variant	Muscle	
	Bouton Number	Bouton size
VAP^WT	↑	↓
VAP^P58S	–	–
VAP^RNAi	↓	↑
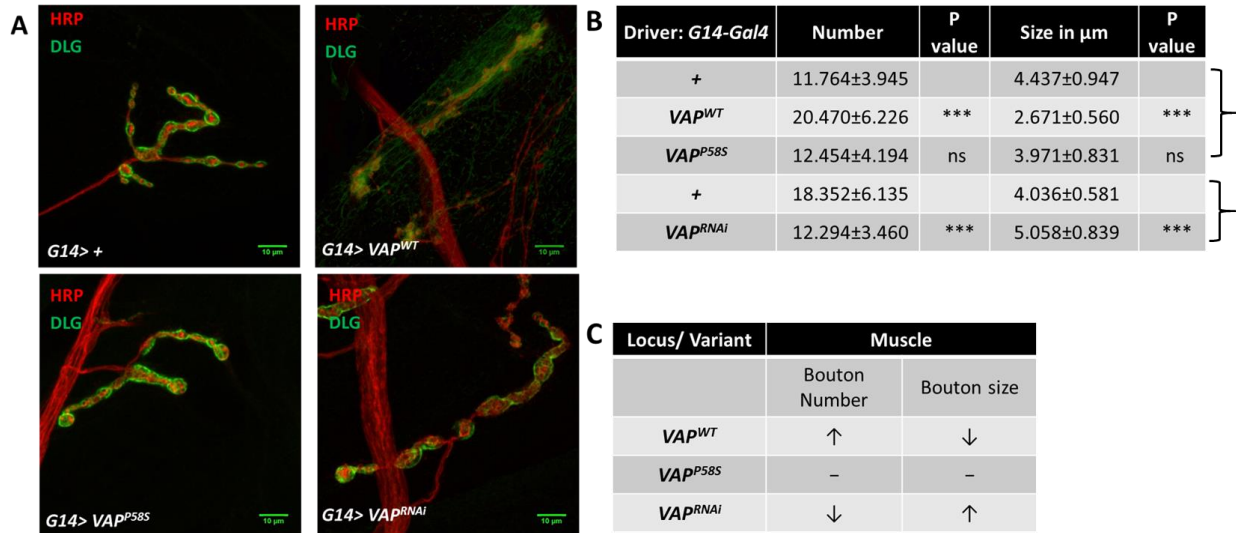
Figure 5.3. Expression of *VAP^P58S* in muscle had no effect on bouton architecture.
A) Representative confocal images of overexpression of *VAP^P58S*, *VAP^WT* and *VAP^RNAi* in the muscles using *G14-GAL4*. HRP was used to mark the neuron/boutons while DLG was used as a counterstain to mark the subsynaptic reticulum.

B) Size and number of boutons on overexpression of *VAP^P58S^, VAP^WT^ and VAP^RNAi^* were quantified in the muscle. The number of larvae used for each experiment are 4-7 and the neuromuscular junctions observed are 15-20 (all the crosses were performed at 25^0 C). *** indicates p value <0.001. Brackets on the right hand side of the table indicate sets of experiments.

C) Summary of results for effect of overexpression of variants of *VAP* in the muscles on the bouton morphology.

3.1.2. *TDP-43/TBPH* human variants are lethal when expressed using the stronger muscle-specific driver, but the *Drosophila* variants contribute to change in bouton morphology

As mentioned earlier, *TDP-43* and *TBPH* are human and *Drosophila* orthologues respectively. We discuss the detailed results of *TDP-43/TBPH* in the next two sub-sections (3.1.2.1 and 3.1.2.2). Although *TDP-43* doesn't contribute much to our knowledge of its effect on the phenotype, *TBPH* seems to be affecting the bouton size.

3.1.2.1. Expression of *TDP-43* (human mutant) variants in the muscle is lethal when driven with *G14-Gal4*

We expressed a variety of *TDP-43* fly lines (donated by Prof. Daniella Zarnescu) in the muscle using *G14-Gal4* at 25°C. The *TDP-43^N345K^* and *TDP-43^A315T^* are mutants of the glycine rich domain of TDP-43 (Romano et al., 2012). These mutants and *TDP-43 ^WT^* are human alleles cloned in *Drosophila melanogaster* and are reported to mimic the ALS phenotype in the fly (Estes et al., 2011). As indicated in table 5.1, all the variants showed lethality at 25 °C on use of *G14-Gal4* and hence did not develop till the third instar larval stage. At 18°C, where the overexpression of the genes is lowered, lethality was still observed (Table 5.1). We therefore resorted to use of a weaker muscle driver i.e. *MHC-Gal4*. This driver line allowed the development of the F1 third instar larvae at 25°C.

Table 5.1. List of *TDP-43* variants used at different temperatures using *G14-Gal4* and *MHC-Gal4*, in order to acquire third instar larvae for NMJ dissections

Use of *G14-Gal4*, a stronger driver than *MHC-Gal4* resulted in lethality at 25°C as well at 18°C. This table displays the effects of these drivers on *TDP-43* variants on use of both drivers.

Driver	Fly Line	Lethality at:
		25°C/18°C
G14-Gal4	UAS-TDP-43^{WT}	lethal
	UAS-TDP-43^{A315T}	lethal
	UAS-TDP-43^{N345K}	lethal
MHC-Gal4	UAS-TDP-43^{WT}	Non lethal
	UAS-TDP-43^{A315T}	Non lethal
	UAS-TDP-43^{N345K}	Non lethal

The bouton size and number on use of *MHC-Gal4* did not show any significant changes with any of the *TDP-43* variants (Fig. 5.4). This indicates that the use of this driver for the overexpression was either insufficient or too weak to produce any phenotypic differences.

Driver: MHC-Gal4	Number	P Value	Size in µm	P value
+	15.22±6.20		4.23±1.04	
TDP-43^{WT}	14.27±4.24	ns	4.33±0.48	ns
+	16.71±6.76		3.57±0.41	
TDP-43^{A315T}	13.33±3.24	ns	4.24±0.80	ns
TDP-43^{N345K}	16.53±6.31	ns	3.87±0.70	ns
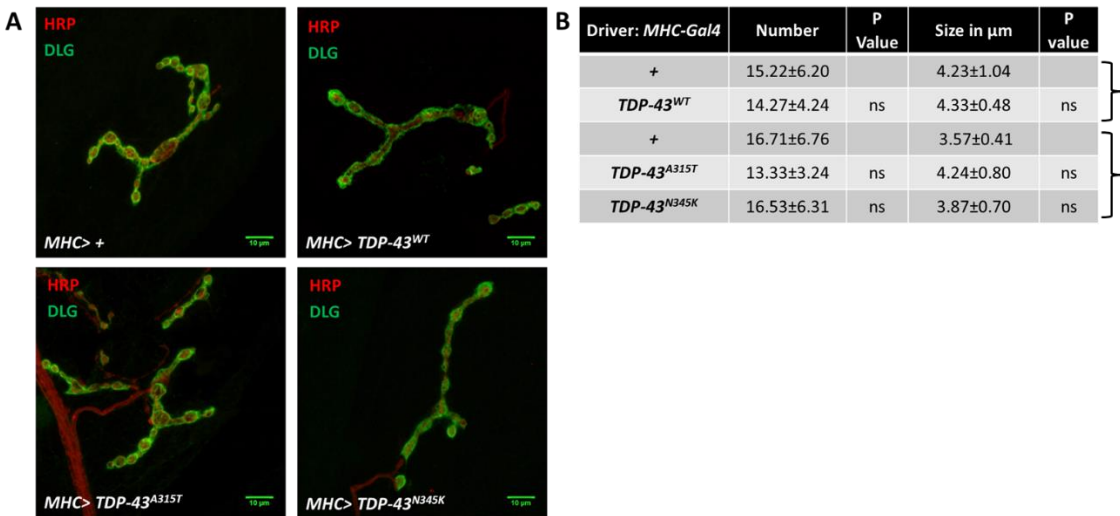
Figure 5.4. Effects of expression of *TDP-43* variants in the muscles on the bouton morphology.
A) Confocal images of overexpression of *TDP-43^{WT}, TDP-43^{A315T}* and *N345K* in the muscles using *MHC-Gal4*. The markers used were HRP and DLG.
B) Tabular representation of overexpression of TDP-43 variants using *MHC-Gal4*. *MHC>+* for *MHC>TDP-43^{WT}* has an Average bouton size= 4.23±1.04µm and
Average bouton number= 15.22±6.20) while *MHC>TDP-43^{WT}* has an Average bouton size= 4.33±0.485µm and Average bouton number= 14.27±4.24). *MHC>+* for *MHC>TDP-43^{A315T} and (N345K)* measures an Average bouton size=3.57±0.41µm and Average bouton number=16.71±6.76. Values for *MHC>TDP-*

43^{A315T} are: Average bouton size $=4.245\pm0.804\mu m$, Average bouton number= 13.33 ± 3.24) and for $MHC>TDP-43^{N345K}$ are: Average bouton size $=3.87\pm0.70\mu m$ and Average bouton number= 16.53 ± 6.31 in the muscles. The number of larvae used for each experiment are 4-7 and the neuromuscular junctions observed are 15-20 (all the crosses were performed at 25^0 C). Brackets indicate sets of experiments.

3.1.2.2. Overexpression and downregulation of *TBPH* (*Drosophila* orthologue of *TDP-43*), reduces the bouton size but doesn't affect the bouton number

After using the human isoforms of *TDP-43* mutations, we overexpressed and downregulated the *Drosophila* orthologue of *TDP-43* i.e. *TBPH* using *G14-Gal4* at 25^0 C. Both, overexpression and knockdown of *TBPH* in the muscle reduces bouton size but doesn't affect bouton number (Fig. 5.5).

A

Driver: G14-Gal4	Number	P value	Size in μm	P value
+	14.5±4.35		4.49±0.46	
TBPH^WT	14.77±4.99	ns	3.92±0.68	*
TBPH^RNAi	17.46±4.35	ns	3.78±0.50	**

Locus/ Variant	Muscle	
	Bouton Number	Bouton size
TDP-43^WT	–	–
TDP-43^A315T	–	–
TDP-43^N345K	–	–
TBPH^WT	–	↓
TBPH^RNAi	–	↓
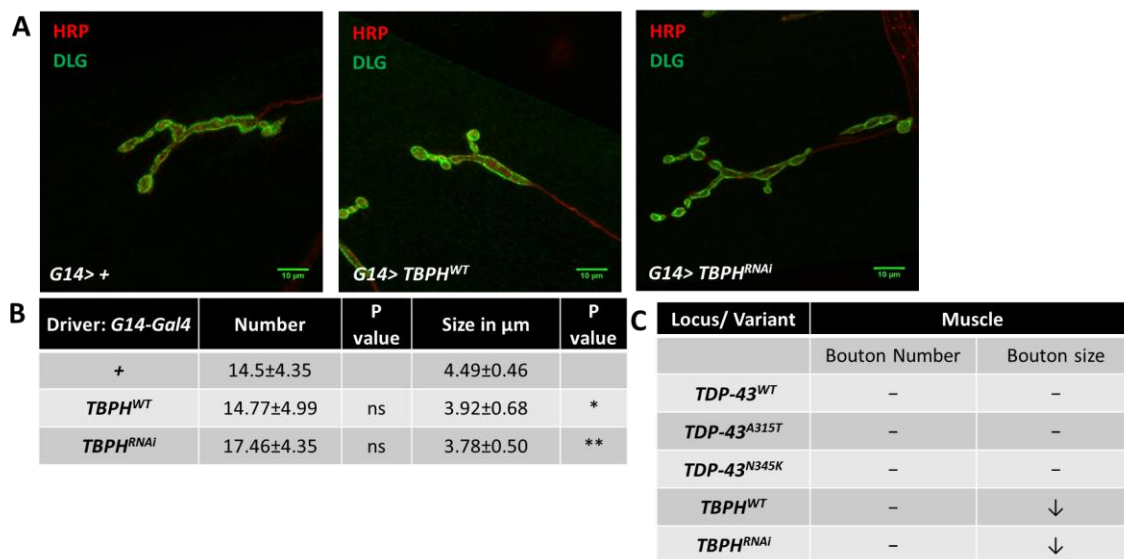
Figure 5.5. **Effects of expression of *TBPH* variants in the muscles on the bouton morphology.**
A) Confocal images of boutons at the NMJ of *G14>+, G14>TBPH^WT* and *G14>TBPH^RNAi*. The markers used were HRP and DLG.
B) Tabular representation of *G14>+* (Average bouton size= $4.49\pm0.46\mu m$. Average bouton number= 14.5 ± 4.35) in comparison with *G14>TBPH^WT* (Average bouton size= $3.92\pm0.68\mu m$. Average bouton number= 14.77 ± 4.99) and *G14>TBPH^RNAi* (Average bouton size=$3.78\pm0.50\mu m$. Average bouton number= 17.46 ± 4.35) using *G14-Gal4*. The number of larvae used for each experiment are 4-7 and the neuromuscular junctions observed are 15-20 (all the crosses were performed at 25^0 C). ** indicates p value <0.01. *indicates p value <0.05.
C) Summary of effects of *TDP-43/TBPH* variants on bouton size and number in muscle overexpression.

3.1.3. Overexpression of human as well as *Drosophila* allelic variants of *FUS/caz* in the muscles causes a change in the bouton morphology

The *FUS* mutants used in Section 3.1.3.1 and 3.1.3.2 are human alleles of the gene (orthologous to *Drosophila caz*), validated in *Drosophila* and donated by Dr. Uday Bhan Pandey's Lab (Lanson et al., 2011). The ALS mutants used in the screen are mostly *FUS* C-terminal domain mutants. The C-terminus has the nuclear localization sequence (NLS) and that's where the most prevalent ALS mutations have been detected. In addition to the C-terminus mutant variants, one other mutant used is the nuclear excision sequence mutant (ΔNES), where the NES has been deleted (Lanson and Pandey, 2012). The third sub-section (3.1.3.3) involves use of *caz* overexpression and knockdown only.

3.1.3.1. Overexpression of FUS^{R521H} and FUS^{R518K} results in altered bouton size

The FUS^{R521H} shows a significant increase in bouton size, while FUS^{R518K} shows a significant reduction in bouton size, but both the mutants fail to show any changes in bouton number when driven with *G14-Gal4*. The NES mutant shows no difference in the bouton morphology (Fig. 5.6).

Table 5.2. List of *FUS* variants used at different temperatures with *G14-Gal4* and *MHC-Gal4*, in order to acquire third instar larvae for NMJ dissections
Use of the stronger muscle driver was lethal for FUS^{WT} and FUS^{R521C} at 25 as well as 18^0 C. Use of the subtler MHC-Gal4 made it possible for us to observe change in bouton phenotype since it was non-lethal at 25^0 C.

Driver	Fly Line	Lethality at:	
		25°C	18°C
G14-Gal4	UAS-FUS^WT	Lethal	Lethal
	UAS-FUS^R521H	Non lethal	Not done
	UAS-FUS^R521C	Lethal	Lethal
	UAS-FUS^R518K	Non lethal	Not done
	UAS-FUS^ΔNES	Non lethal	Not done
	caz^WT	Non lethal	Not done
	caz^RNAi	Non lethal	Not done
MHC-Gal4	UAS-FUS^WT	Non lethal	Not done
	UAS-FUS^R521C	Non lethal	Not done

FUS^{WT} and FUS^{R521C} however, show lethality both at 25^0 C as well as 18^0 C. These two mutant fly lines were therefore tested with *MHC-Gal4* at 25^0 C (Table 5.2).
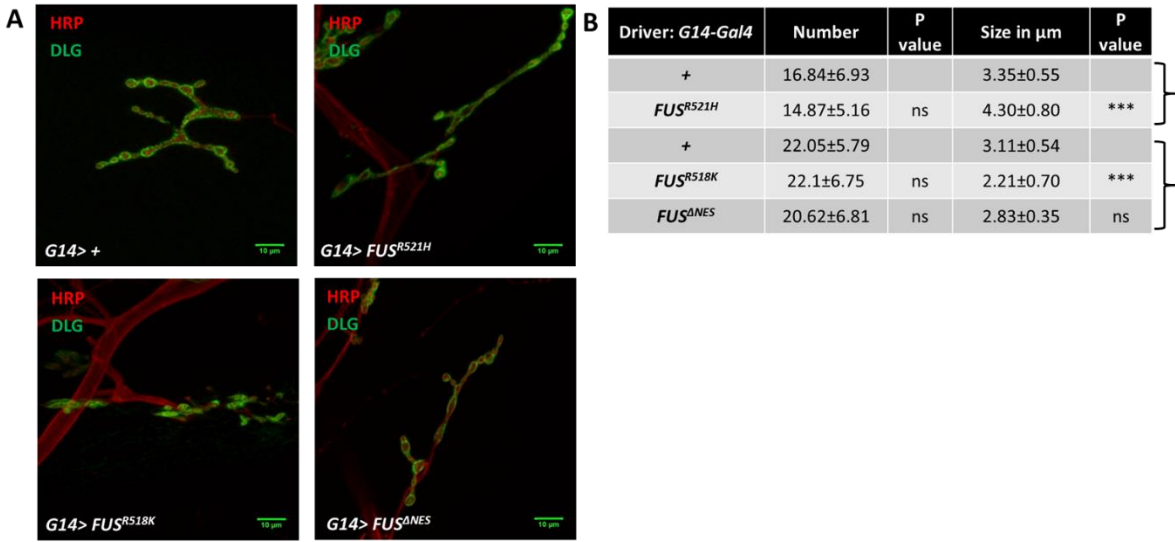
Figure 5.6. Effects of expression of *FUS* variants in the muscles, on the bouton morphology, using *G14-Gal4*.

A) Confocal images of boutons at the NMJ of *G14>+, G14>FUS^{R521H}, G14>FUS^{ΔNES}* and *G14>FUS^{R518K}*. The markers used were HRP and DLG.

B) Tabular representation of *G14>+* (Average bouton size= 3.35±0.55μm. Average bouton number= 16.84±6.93), *G14>FUS^{R521H}* (Average bouton size=4.30 ±0.80μm. Average bouton number= 14.87±5.16) and *G14>+* (Average bouton size=3.11±0.54μm. Average bouton number= 22.05±5.79), *G14>FUS^{ΔNES}* (Average bouton size= 2.83±0.35μm. Average bouton number= 20.62±6.81) and *G14>FUS^{R518K}* (Average bouton size= 2.21±0.70μm. Average bouton number= 22.1±6.75) using *G14-Gal4*. The number of larvae used for each experiment are 4-7 and the neuromuscular junctions observed are 15-20 (all the crosses were performed at 25^0 C). *** indicates p value <0.001. Brackets indicate sets of experiments.

3.1.3.2. Overexpression of *FUS^{WT}* and *FUS^{R521C}* displays clustered appearance of boutons

   FUS^{WT} overexpression by *MHC-Gal4* increases the bouton number and decreases the bouton size, hinting towards the possible toxicity caused by the extra dosage. The *FUS^{R521C}* mutant, when expressed using *MHC-Gal4* results in a very small size of boutons with clustered appearance. The DLG localization in this case seems higher than usual, while the HRP localization looks weak (Fig. 5.7).
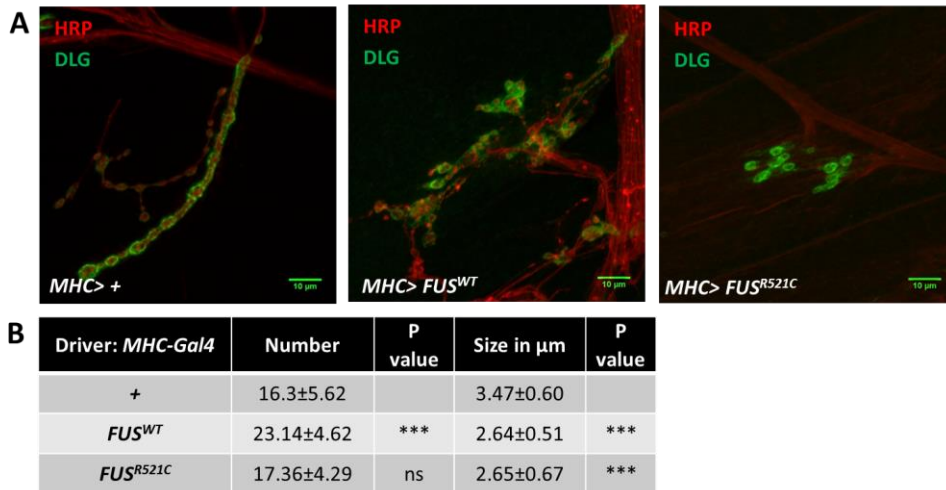
Figure 5.7. Effects of expression of *FUS* variants in the muscles on the bouton morphology using *MHC-Gal4*.
A) Confocal images of boutons at the NMJ of *MHC>+*, *MHC>FUS^WT* and *MHC>FUS^R521C*. The markers used were HRP and DLG.
B) Tabular representation of *MHC>+* (Average bouton size= 3.47±0.60μm. Average bouton number= 16.3±5.62)*, MHC>FUS^WT* (Average bouton size= 2.64±0.51μm. Average bouton number= 23.14±4.62) and *MHC>FUS^R521C* (Average bouton size= 2.65±0.67μm. Average bouton number= 17.36±4.29). The number of larvae used for each experiment are 4-7 and the neuromuscular junctions observed are 15-20 (all the crosses were performed at 25^0 C). *** indicates p value <0.001.

As the muscle expression of *FUS* variants in these experiments show drastic phenotypes, we were curious to observe their effects in the ALS8 genetic background used in Chapter II, III and IV. We therefore conducted muscle specific overexpression of *FUS^WT* and *FUS^R521C* in the Δ*VAP; gVAP^P58S* background and observed the lifespan of the resulting F1 flies (Data in appendix IV).

3.1.3.3. Downregulation of *caz*, the *Drosophila* orthologue of FUS, shows change in the bouton size via muscle expression

Cabeza (caz) downregulation using *UAS-caz^RNAi* resulted in an increase of bouton size but there was no significant difference observed in the number of boutons. Also, overexpressing the *Drosophila* orthologue in this case did not show any changes in the boutons (Fig. 5.8) unlike the overexpression of the human allele, as described in Fig. 5.7.
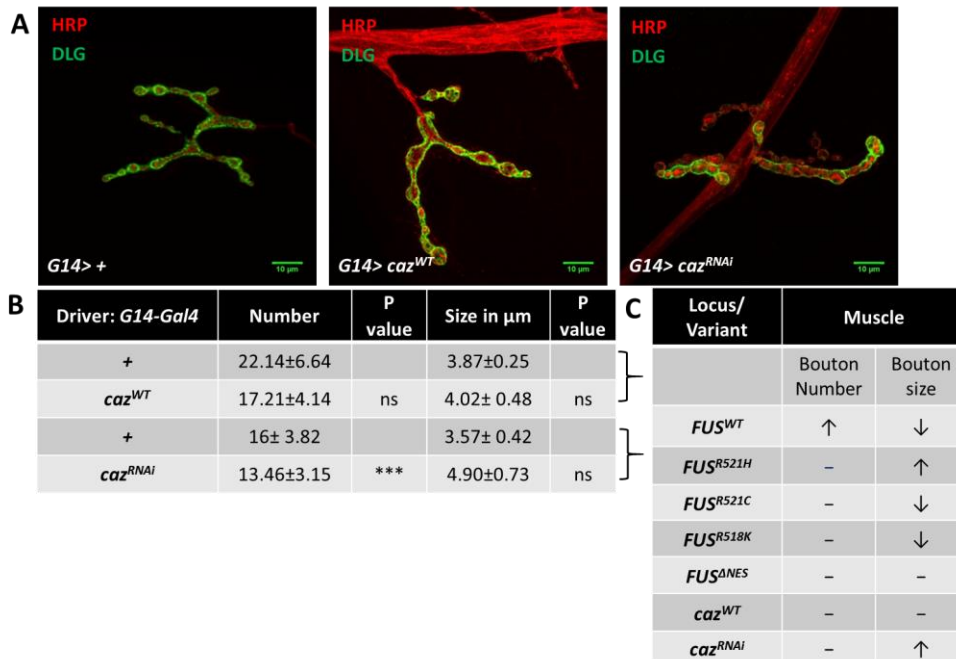
Figure 5.8. Effects of expression of *caz* variants in the muscles on the bouton morphology.
A) Confocal images of boutons at the NMJ of *G14>+, G14>caz^WT^* and *G14>caz^RNAi^*. The markers used were HRP and DLG.
B) Graphical representation of *G14>+* (Average bouton size=3.87±0.25μm. Average bouton number=22.14±6.64)*, G14>caz^WT^* (Average bouton size= 4.02± 0.48 μm. Average bouton number= 17.21±4.14) and *G14>+* (Average bouton size= 3.57± 0.42μm. Average bouton number=16± 3.82), *G14>caz^RNAi^* Average bouton size=4.90±0.73μm. Average bouton number= 13.46±3.15) in the muscles using *G14-Gal4*. The number of larvae used for each experiment are 4-7 and the neuromuscular junctions observed are 15-20 (all the crosses were performed at 25⁰ C). *** indicates p value <0.001. Brackets indicate sets of experiments.
C) Summary of effects of *FUS/caz* variants on bouton size and number in muscle overexpression.

3.1.4. Mutant *SOD1* expression in muscles leads to reduction in bouton size

$SOD1^{A4V}$ is a human *SOD1* mutant allele widely used in *Drosophila* for ALS associated studies. This is a dominant mutation and involves quick progression of ALS in patients (Saeed et al., 2009). Overexpression or knockdown of *SOD1* did not affect the bouton morphology but overexpression of $SOD1^{A4V}$ significantly reduced the bouton size without affecting the bouton number. (Fig. 5.9).
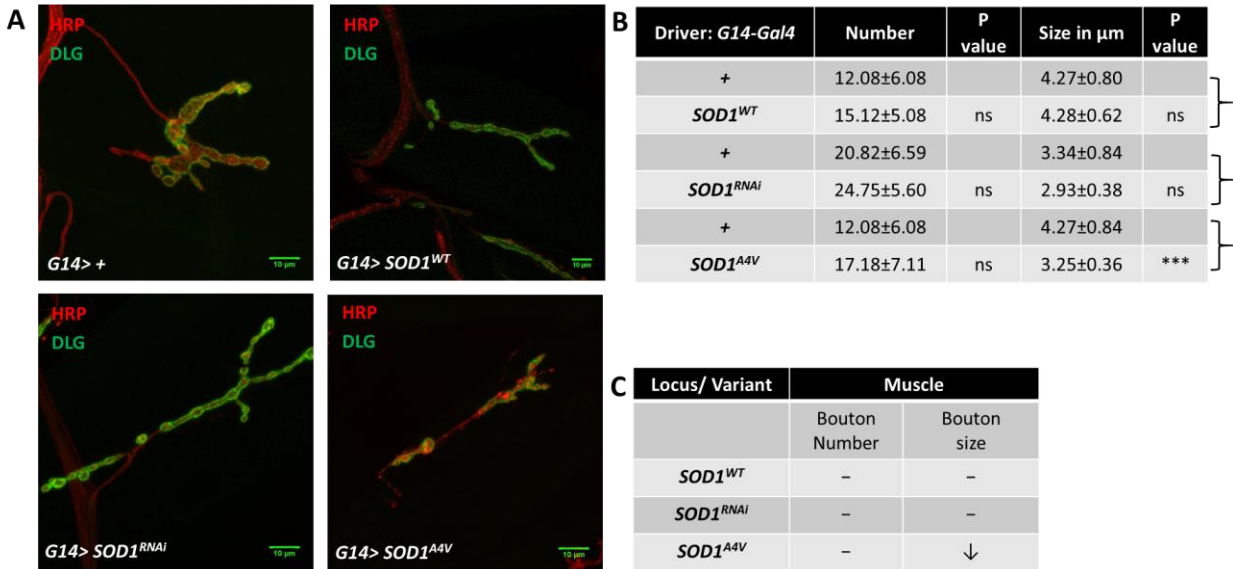
Figure 5.9. Effects of expression of *SOD1* variants in the muscles on the bouton morphology.
A) Confocal images of boutons at the NMJ of *G14>+*, *G14>SOD1^WT^*, *G14>SOD1^A4V^* and *G14>SOD1^RNAi^*. The markers used were HRP and DLG.
B) Tabular representation of *G14>+* (Average bouton size=4.27±0.80μm. Average bouton number= 12.08±6.08) versus *G14>SOD1^WT^* (Average bouton size= 4.28±0.62μm. Average bouton number= 15.12±5.08) and *G14>+* (Average bouton size=3.34±0.84μm. Average bouton number= 20.82±6.59) versus *G14>SOD1^RNAi^* (Average bouton size=2.93±0.38μm. Average bouton number= 24.75±5.60) and *G14>+* (Average bouton size=4.27±0.84μm. Average bouton number= 12.08±6.08) versus *G14>SOD1^A4V^* (Average bouton size=3.25±0.36μm. Average bouton number= 17.18±7.11). The number of larvae used for each experiment are 4-7 and neuromuscular junctions observed are 15-20 (all the crosses were performed at 25^0 C). *** indicates p value <0.001. Brackets indicate sets of experiments.
C) Summary of effects of *SOD1* variants on bouton size and number when expressed in muscles.

3.1.5. Mutant *TER94* expression in muscles leads to increase in bouton size

We obtained *Drosophila TER94* mutant fly lines, *TER94^R152H^* and *TER94^A229E^* used in Inclusion body myopathy associated with Paget's disease of bone and frontotemporal dementia (IBMPFD) studies from Prof. Paul Taylor (Ritson et al., 2010). These mutants are reported to be involved in genetic interaction with *TDP-43* and *FUS* (Ritson et al., 2010 and Azuma 2014). *TER94^A229E^* couldn't be used in this screen as it is over a *CyO* balancer. But use of *TER94^R152H^*, an N-Terminal dominant active mutant (Chang et al., 2014) resulted in an increase in bouton size without affecting the bouton number. Muscle overexpression or knockdown of *TER94* did not show any change (Fig. 5.10).

Driver: G14-Gal4	Number	P value	Size in µm	P value	
+	12.08±6.08		4.27±0.80		
TER94^{WT}	15.23±4.68	ns	3.85±0.88	ns	}
TER94^{R152H}	9.42±4.68	ns	5.51±0.47	**	
+	14.5±4.35		4.49±0.46		}
TER94^{RNAi}	16.8±5.97	ns	4.39±0.71	ns	

Locus/ Variant	Muscle	
	Bouton number	Bouton size
TER94^{WT}	–	–
TER94^{RNAi}	–	–
TER94^{R152H}	–	↑
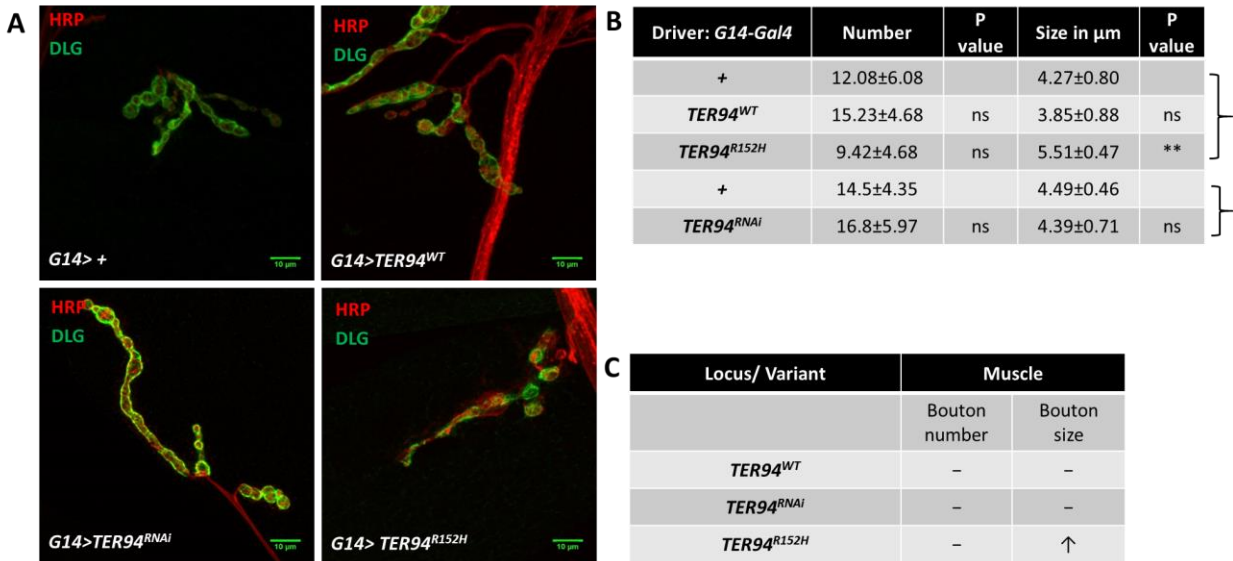
Figure 5.10. Effects of expression of *TER94* variants in the muscles on the bouton morphology.
A) Confocal images of boutons at the NMJ of *G14>+, G14>TER94^{WT}*, *G14>TER94^{R152H}* and *G14>TER94^{RNAi}*. The markers used were HRP and DLG.
B) Tabular representation of *G14>+* (Average bouton size=4.27±0.80µm. Average bouton number= 12.08±6.08)*, G14>TER94^{WT}* (Average bouton size=3.85±0.88µm. Average bouton number= 15.23±4.68), *G14>TER94^{R152H}* (Average bouton size=5.51±0.47µm. Average bouton number= 9.42±4.68) and *G14>+* (Average bouton size=4.49±0.46µm. Average bouton number= 14.5±4.35) *G14>TER94^{RNAi}* (Average bouton size=4.39±0.71µm. Average bouton number= 16.8±5.97) in the muscles using *G14-Gal4*. The number of larvae used for each experiment are 4-7 and the neuromuscular junctions observed are 15-20 (all the crosses were performed at 25^0 C). ** indicates p value <0.01. *indicates p value <0.05. Brackets indicate sets of experiments.
C) Summary of effects of *TER94* variants on bouton size and number in muscle expression.

3.1.6. Muscle summary

It is evident from our results that different loci variants show differential effects on the boutons and it is complicated to pinpoint a locus which has a prominent role in the muscles as compared to other loci. We have summarized the results (Table 5.3) and have highlighted the important observations in the form of bullet points:

1. *VAP* is important for the structural homeostasis of the presynaptic boutons, the *VAP^{P58S}*, however, doesn't seem to play a major role.

2. We speculate that the overexpression of the human *TDP-43* variants is either toxic to the *Drosophila* system, or it affects the development of the fly at very early stages leading to detrimental effects. These effects are reflected only on using a strong muscle driver.

3. The optimum dosage of *TBPH*, the *Drosophila* orthologue, seems to be more important in maintenance of the size of the boutons and not so much the number.

4. All *FUS* alleles appear to play a significant role when expressed in muscles, except the ΔNES.

5. The overexpression of *caz*, the *Drosophila* orthologue of *FUS*, doesn't affect the bouton morphology but the RNAi causes reduction in size.

6. Changes in levels of both $SOD1^{WT}$ and $TER94^{WT}$ do not seem to modify the NMJ. However, the mutant alleles for both affect the bouton size.

7. All-in-all, most alleles when expressed in the muscles appear to be having an impact on the bouton size more than the number.

Table 5.3. Effect of muscle expression of ALS loci on the bouton morphology
Expression of ALS loci (Overexpression, mutant or loss-of-function), using the *UAS-GAL4* system, in muscle. '↑' indicates a significant increase in the parameter measured, while '↓' indicates a significant decrease. '−'means that there is no significant change.
1) *'h'* indicates that a human orthologue is used for the experiment. All other constructs are *Drosophila* genes.
2) Caz is the *Drosophila* orthologue of FUS while TBPH is the *Drosophila* orthologue of TDP-43.
3) The results for the outcome from the use of *G14-Gal4* as the muscle driver are depicted in this table followed by *MHC-Gal4* which was utilized only when animals died with the use of the stronger *G14-Gal4*. Alternate loci are separated by grey shades for clearer demarcation purposes.

MUTATION	MUSCLE (G14 Gal4)		MUSCLE (MHC Gal4)	
	Bouton number	Bouton size	Bouton number	Bouton size
UAS-VAP ^{WT}	↑	↓		
UAS-VAP ^{RNAi}	↓	↑		
UAS-VAP ^{P58S}	−	−	Not done	
UAS-TDP43 ^{WT} *h*	Lethal (G14)		−	−
UAS-TDP43 ^{N345K} *h*	Lethal (G14)		−	−
UAS-TDP43 ^{A315T} *h*	Lethal (G14)		−	−
UAS-TBPH ^{WT}	−	↓		
UAS-TBPH ^{RNAi}	−	↓	Not done	
UAS-FUS ^{WT} *h*	Lethal (G14)		↑	↓
UAS-FUS ^{R521H} *h*	−	↑	Not done	
UAS-FUS ^{R521C} *h*	Lethal (G14)		−	↓
UAS-FUS ^{R518K} *h*	−	↓		
UAS-FUS ^{ΔNES} *h*	−	−		
UAS-caz ^{WT}	−	−		
UAS-caz ^{RNAi}	−	↑	Not done	
UAS-SOD1 ^{WT}	−	−		
UAS-SOD1 ^{RNAi}	−	−		
UAS-SOD1 ^{A4V} *h*	−	↓	Not done	
UAS-TER94 ^{WT}	−	−		
UAS-TER94 ^{RNAi}	−	−		
UAS-TER94 ^{R152H}	−	↑	Not done	

3.2. Effects of glial expression of ALS loci on bouton morphology

Glial based overexpression screen was carried out using *Repo-Gal4*. This is a third chromosome glial driver, expressed from the embryonic stage onwards. It is over TM3Tb balancer and has a *UAS-CD8:GFP* downstream of *Repo-Gal4* insert. F1 larvae chosen for the bouton analysis were GFP positive. Controls used in all cases were the Gal4 driver crossed to Canton S (wild type). Experiments for this part of work were done along with a BSMS student in the lab, Neena Dhiman. The markers used for observing the bouton morphology were BRP (Bruchpilot), a component of active zone at the synapse, and HRP.

3.2.1. *VAP^{WT}* and *VAP^{P58S}* overexpression in glia leads to reduction in bouton size

Glial expression of *VAP^{WT}* and *VAP^{P58S}* reduces the size of the boutons. However, it doesn't result in any change to the number of boutons. Knockdown of *VAP* using RNAi does not seem to cause any change as compared to the control (Fig. 5.11).

B)

Driver: *Repo-Gal4*	Number	P value	Size in µm	P value
+	12.81±2.1		4.26±0.14	
VAP^{WT}	13.94±2.93	ns	3.59±0.101	***
VAP^{RNAi}	13.62±3.46	ns	4.15±0.08	ns
VAP^{P58S}	13.83±4.48	ns	3.84±0.09	*

C)

Locus/ Variant	Glia	
	Bouton number	Bouton size
VAP^{WT}	–	↓
VAP^{RNAi}	–	–
VAP^{P58S}	–	↓
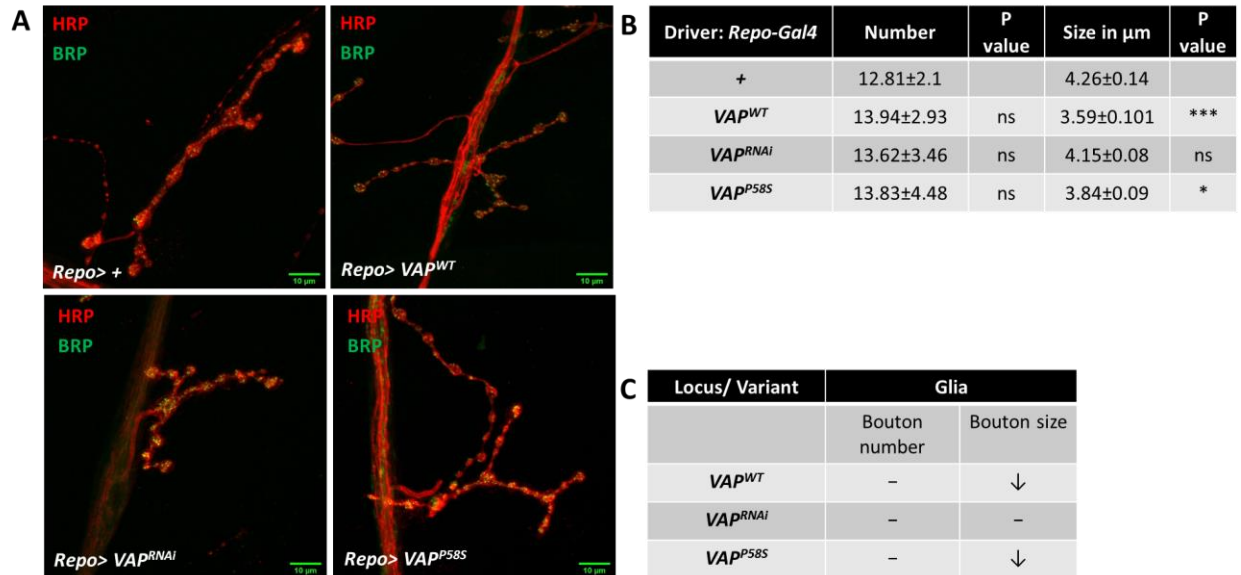
Figure 5.11. Effects of expression of *VAP* variants in the glia on the bouton morphology.
A) Confocal images of boutons at the NMJ of *Repo>+, Repo>VAP^{WT}, Repo>VAP^{RNAi}* and *Repo>VAP^{P58S}*. The markers used were HRP and BRP.
B) Tabular representation of *Repo>+* (Average bouton size=4.26±0.14µm. Average bouton number= 12.81±2.10)*, Repo>VAP^{WT}* (Average bouton size=3.59±0.10µm. Average bouton number= 13.94±2.93), *Repo>VAP^{P58S}* (Average bouton size=3.84±0.09µm. Average bouton number= 13.83±4.48) and *Repo>VAP^{RNAi}* (Average bouton size=4.15±0.08µm. Average bouton number= 13.62±3.46). The number of larvae used for each experiment are 4-7 and the neuromuscular junctions observed are 15-20 (all the crosses were performed at 25^0 C). *** indicates p value <0.001. *indicates p value <0.05.
C) Summary of results for effect of expression of variants of *VAP* in the glia on the bouton morphology.

3.2.2. Expression of *TDP-43/TBPH* in glia seems to influence the bouton size more than the bouton number

Unlike the muscle expression of *TDP-43* variants which caused lethality, their glial expression led to development of the larvae up to the third instar stages (Section 3.2.2.1). Followed by the human variants, we screened the overexpression/knockdown of the *Drosophila* orthologues (Section 3.2.2.2).

3.2.2.1. Expression of human ALS alleles of *TDP-43* in *Drosophila* glial cells leads to change in bouton morphology for most of the allelic variants

Overexpression of *TDP-43^{WT}* and *TDP-43^{A315T}* reduces the bouton size, while it has no effect on the number of boutons. *TDP-43^{N345K}*, unlike the other two variants, shows an increase in average bouton size and a decrease in bouton number (Fig. 5.12).

Driver: Repo-Gal4	Number	P value	Size in µm	P value
+	15±3.58		4.09±0.13	
TDP-43^{WT}	14±4.70	ns	3.43±0.17	***
TDP-43^{A315T}	13±3.63	ns	3.64±0.10	**
TDP-43^{N345K}	12±2.78	*	4.64±0.11	*

Figure 5.12. Effects of expression of *TDP-43* variants in the glia on the bouton morphology.
A) Confocal images of boutons at the NMJ of *Repo>+, Repo>TDP-43^{WT}, Repo>TDP-43^{A315T}* and *Repo>TDP-43^{N345K}*. The markers used were HRP and BRP.
B) Tabular representation of *Repo>+* (Average bouton size=4.09±0.13µm. Average bouton number= 15±3.58), *Repo>TDP-43^{WT}* (Average bouton size=3.43±0.17µm. Average bouton number= 14±4.70), *Repo>TDP-43^{A315T}* (Average bouton size=3.64±0.10µm. Average bouton number= 13±3.63) and *Repo>TDP-43^{N345K}* (Average bouton size=4.64±0.11µm. Average bouton number= 12±2.78). The number of larvae used for each experiment are 4-7 and the neuromuscular junctions observed are 15-20 (all the crosses were performed at 25^0 C). *** indicates p value <0.001. ** indicates p value <0.01. *indicates p value <0.05.

3.2.2.2. Glial Overexpression of *TBPH* leads to decrease in bouton number and increase in size

Having used the human isoforms of *TDP-43* mutations, we overexpressed and downregulated the *Drosophila* orthologue of *TDP-43* i.e. *TBPH* using *Repo-Gal4* at 25^0 C. Overexpression of *TBPH* in the glia reduces bouton size and increases bouton number, but the knockdown shows no effect (Fig. 5.13).
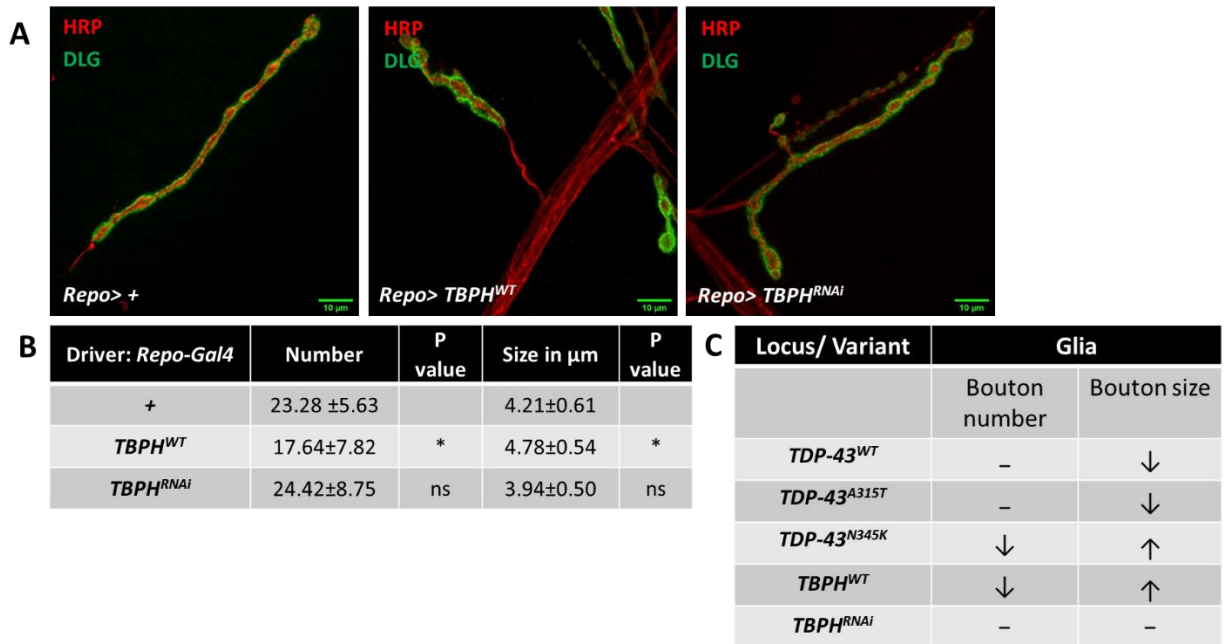
Figure 5.13. Effects of expression *TBPH* variants in the glia on the bouton morphology.
A) Confocal images of boutons at the NMJ of *Repo>+, Repo>TBPH^{WT}* and *Repo>TBPH^{RNAi}*. The markers used were HRP and DLG. .
B) Tabular representation of *Repo>+* (Average bouton size= 4.21±0.61µm. Average bouton number=23.28±5.63) in comparison with *Repo>TBPH^{WT}* (Average bouton size= 4.785±0.547µm. Average bouton number= 17.64±7.82 and *Repo>TBPH^{RNAi}* (Average bouton size= 3.94±0.50µm. Average bouton number= 24.42±8.75). The number of larvae used for each experiment are 4-7 and the neuromuscular junctions observed are 15-20 (all the crosses were performed at 25^0 C). ** indicates p value <0.01. *indicates p value <0.05.
C) Summary of results for effects of *TDP-43/TBPH* variants on bouton size and number in glial overexpression.

3.2.3. Both the human as well as *Drosophila* variants of *FUS/caz* seem to be controlling bouton architecture when expressed in glial cells

Section 3.2.3.1 describes the bouton morphology changes for human allelic variants while 3.2.3.2 describes the *Drosophila* allelic variants of *FUS/caz*

3.2.3.1. Expression of human ALS alleles of *FUS* in *Drosophila* glial cells results in lethality in a few, while change in bouton morphology for most other alleles

Expressing the human variants *FUS^{WT}* and *FUS^{R521C}* in the glia leads to lethality, which is the same as in the case of muscle expression when driven by *G14-Gal4*. Another allele which has a similar effect in glia as its expression in muscles is *FUS^{R518K}*. It shows a reduction in bouton size but no significant change in bouton number. *FUS^{ΔNES}* shows a significant reduction in bouton size

169

and an increase in bouton number unlike in case of muscle expression. FUS^{R521H} results in an opposite trend as compared to that of muscle expression, (Fig. 5.6) i.e. it shows significant reduction in size and a significant increase in number (Fig. 5.14).

Driver: Repo-Gal4	Number	P value	Size in μm	P value
+	12.81±2.10		4.26±0.14	
FUS^{R518K}	15.06±4.66	ns	3.72±0.10	**
FUS^{R521H}	15.55±4.04	*	3.71±0.07	***
$FUS^{\Delta NES}$	16.68±4.25	**	3.86±0.11	*

Figure 5.14. Effects of expression of *FUS* variants in the glia on the bouton morphology.
A) Confocal images of boutons at the NMJ of *Repo>+*, *Repo>FUS^{R518K}*, *Repo>FUS^{\Delta NES}* and *Repo>FUS^{R521H}*. The markers used were HRP and BRP.
B) Tabular representation of *Repo>+* (Average bouton size=4.26±0.14μm. Average bouton number= 12.81±2.10)*, Repo>FUS^{R518K}* (Average bouton size=3.72±0.10μm. Average bouton number= 15.06±4.66), *Repo>FUS^{\Delta NES}* (Average bouton size=3.71±0.07μm. Average bouton number= 15.55±4.04) and *Repo>FUS^{R521H}* (Average bouton size=3.86±0.11μm. Average bouton number= 16.68±4.25). The number of larvae used for each experiment are 4-7 and the neuromuscular junctions observed are 15-20 (all the crosses were performed at 25^0 C). *** indicates p value <0.001. ** indicates p value <0.01. *indicates p value <0.05.
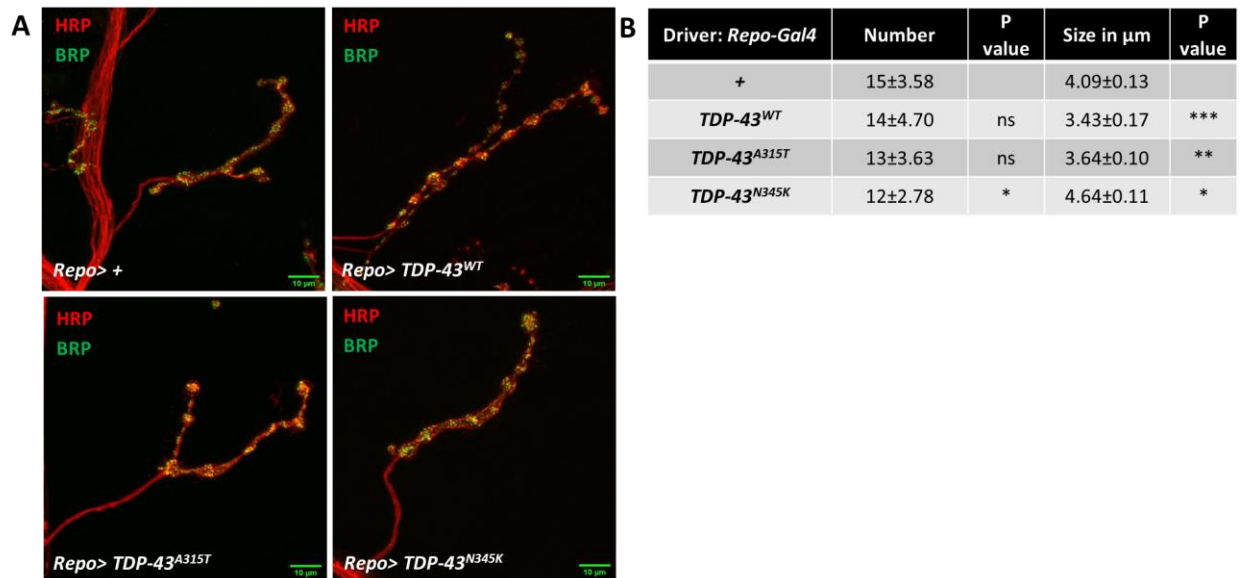
3.2.3.2. Downregulation of *caz* shows reduction in the bouton number on its glial expression

Knockdown of *caz* using *RNAi* resulted in a decrease of bouton number but there was no significant difference observed in the size of boutons. The overexpression does not show any difference (Fig. 5.15).

A

HRP DLG — *Repo> +*   HRP DLG — *Repo> caz^WT*   HRP DLG — *Repo> caz^RNAi*

B

Driver: *Repo-Gal4*	Number	P value	Size in μm	P value
+	23.28 ±5.63		4.21±0.61	
caz^WT	17.64±7.82	*	4.78±0.54	*
caz^RNAi	24.42±8.75	ns	3.94±0.50	ns

C

Locus/ Variant	Glia	
	Bouton number	Bouton size
FUS^WT	lethal	lethal
FUS^R521H	↓	↑
FUS^R521C	lethal	lethal
FUS^R518K	–	↓
FUS^ΔNES	↑	↓
caz^WT	–	–
caz^RNAi	↓	–

Figure 5.15. Effects of expression of *caz* variants in the glia on the bouton morphology.
A) Confocal images of boutons at the NMJ of *Repo>+*, *Repo>caz^WT* and *Repo>caz^RNAi*. The markers used were HRP and DLG.
B) Tabular representation of *Repo>+* (Average bouton size= 4.21±0.61μm. Average bouton number=23.28 ±5.63), *Repo>caz^WT* (Average bouton size= 4.16± 0.66μm. Average bouton number=21.85 ±3.58) and *Repo>caz^RNAi* (Average bouton size=4.44±0.45μm. Average bouton number= 19.14±4.79). The number of larvae used for each experiment are 4-7 and the neuromuscular junctions observed are 15-20 (all the crosses were performed at 25^0 C). * indicates p value <0.05.
C) Summary of results for effects of *FUS/caz* variants on bouton size and number in glial overexpression.

3.2.4. *SOD1^WT* as well as *SOD1^RNAi* increases bouton size, but does not affect bouton number

    SOD1^WT and *RNAi* based knockdown lead to an increase in bouton size on expression in the glia (Fig. 5.16). Expression of the human mutant allele *SOD1^A4V* is lethal.
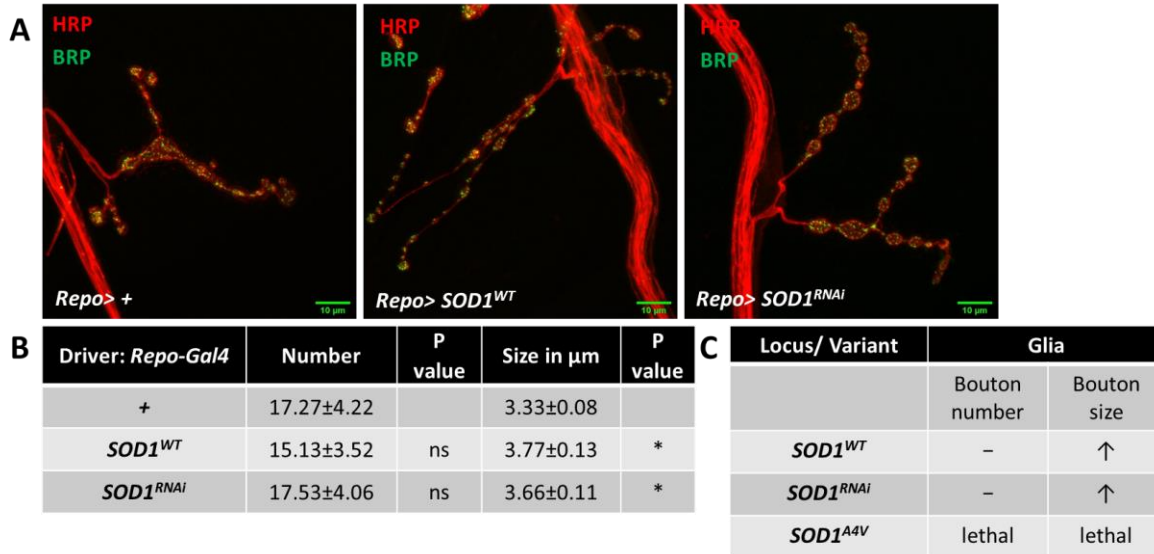
Figure 5.16. Effects of expression of *SOD1* variants in the glia on the bouton morphology.
A) Confocal images of boutons at the NMJ of *Repo>+*, *Repo>SOD1^{WT}* and *Repo>SOD1^{RNAi}*. The markers used were HRP and BRP.
B) Tabular representation of *Repo>+* (Average bouton size=3.33±0.08μm. Average bouton number= 17.27±4.22), *Repo>SOD1^{WT}* (Average bouton size=3.77±0.13μm. Average bouton number= 15.13±3.52), and *Repo>SOD1^{RNAi}* (Average bouton size=3.66±0.11μm. Average bouton number= 17.53±4.06). The number of larvae used for each experiment are 4-7 and the neuromuscular junctions observed are 15-20 (all the crosses were performed at 25^0 C). *indicates p value <0.05.
C) Summary of results for effect of expression of variants of *SOD1* in the glia on the bouton morphology.

3.2.5. Expression of *TER94* variants in glial cells leads to alteration of bouton size as well as number

Overexpression of *TER94* in the glia is lethal, whereas its knockdown reduces the bouton number but the bouton size remains unchanged. On using the *TER94^{R152H}* allele, there is a significant reduction of the bouton number and increase in the bouton size (Fig. 5.17).
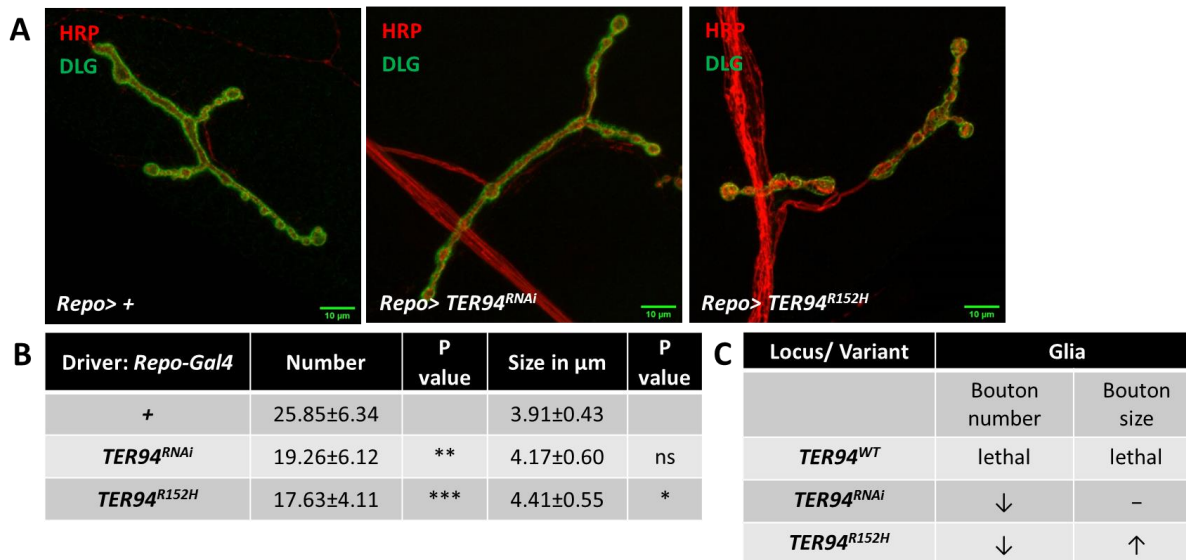
Figure 5.17. Effects of expression of *TER94* variants in the glia on the bouton morphology.
A) Confocal images of boutons at the NMJ of *Repo>+*, *Repo>TER94^{RNAi}* and *Repo>TER94^{R152H}*. The markers used were HRP and DLG. .
B) Tabular representation of *Repo>+* (Average bouton size=3.91±0.43µm. Average bouton number= 25.85±6.34), *Repo>TER94^{RNAi}* (Average bouton size=4.17±0.6µm. Average bouton number= 19.26±6.12), *Repo>TER94^{R152H}* (Average bouton size=4.41±0.55µm. Average bouton number= 17.63±4.11). The number of larvae used for each experiment are 4-7 and the neuromuscular junctions observed are 15-20 (all the crosses were performed at 25^0 C). ** indicates p value <0.01. *** indicates p value <0.001. ** indicates p value <0.01. *indicates p value <0.05.
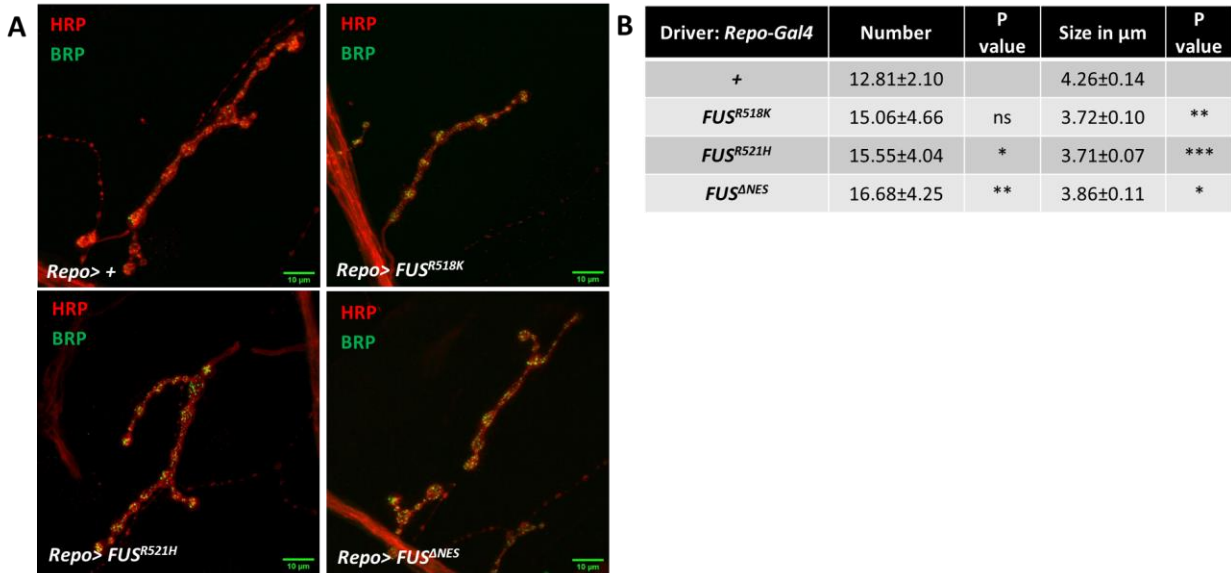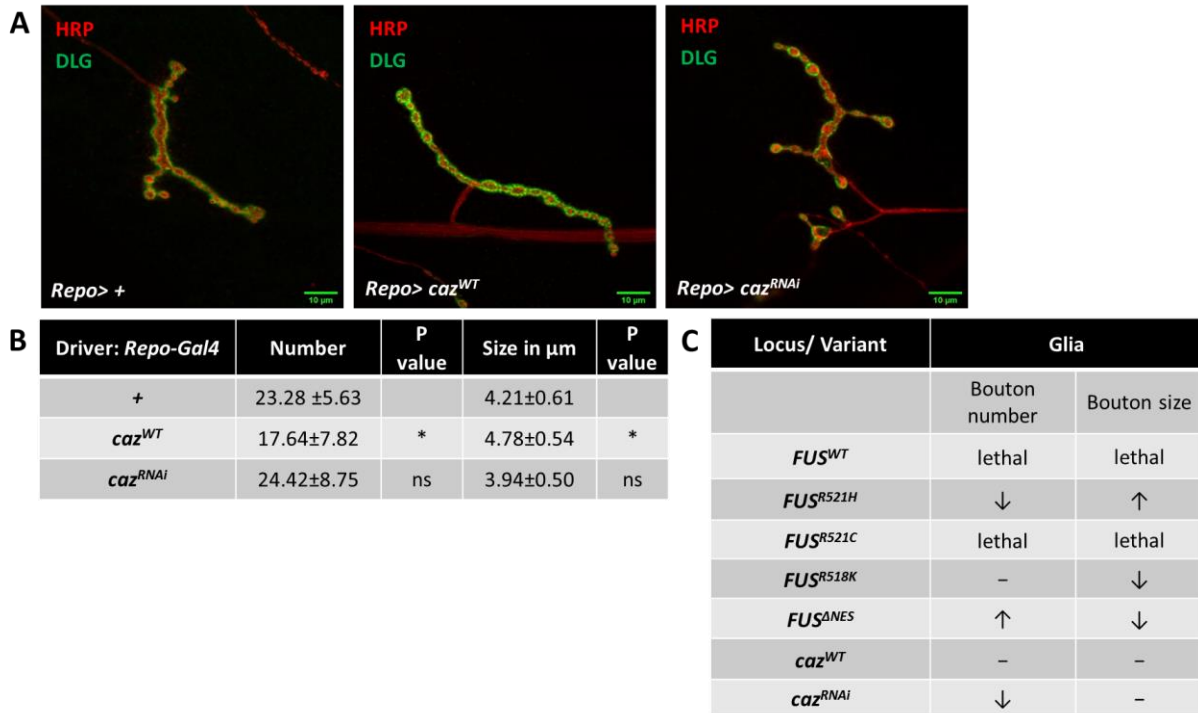**C)** Summary of results for effects of *TER94* variants on bouton size and number in glial expression.

3.2.6. Glial summary

We pinpoint the important aspects of expression of ALS allelic variants in glia in this section along with summarizing them (Table 5.4). We have also attempted to compare the glial results with the muscle results, wherever relevant:

1. Glial overexpression of *VAP^{WT}* affects the bouton size in an opposite manner as that of muscles i.e. it reduces the bouton size. In addition to the *VAP^{WT}*'s differential effect, the *VAP* mutant also causes a change in the bouton morphology, which doesn't happen on muscle expression, indicating the mutant to be playing a role via glia.

2. *TDP-43/TBPH* is an important locus in terms of its role in maintenance of the bouton architecture through glial expression.

3. Both the *NLS* as well as *NES* mutants of *FUS* play an important role in altering the bouton morphology. The *ΔNES*, which doesn't seem to act via muscles, is of particular importance when expressed in glial cells.

4. *SOD1* expression is important in terms of controlling the bouton architecture via glial-specific expression.

5. Glial expression of TER94 seems to be more important than its expression in muscles, as an increase in the levels of *TER94* leads to lethality, while lowering its expression affects the bouton number. The expression of mutant *TER94* also seems to control the bouton morphology in terms of the number as well as size.

6. Unlike the expression of ALS loci variants in muscles which affect mostly the bouton size, their expression in the glia appear to affect the number as well.

Table 5.4. Effect of glial expression of ALS loci on bouton morphology
Expression of ALS loci (Overexpression, mutant or loss-of-function), using the *UAS-GAL4* system, in muscle. '↑' indicates a significant increase in the parameter measured, while '↓' indicates a significant decrease. '−'means that there is no significant change.

1) *'h'* indicates that a human orthologue is used for the experiment. All other constructs are *Drosophila* genes.

2) *Caz* is the *Drosophila* orthologue of *FUS* while *TBPH* is the *Drosophila* orthologue of *TDP-43*.

3) The results for the outcome from the use of *Repo-Gal4* as the driver are depicted in this table. Alternate loci are separated by grey shades for clearer demarcation purposes.

MUTATION	GLIA(Repo Gal4)	
	Bouton number	Bouton size
UAS-VAP ^{WT}	–	↓
UAS-VAP ^{RNAi}	–	–
UAS-VAP ^{P58S}	–	↓
UAS-TDP43 ^{WT} h	–	↓
UAS-TDP43 ^{N345K} h	↓	↑
UAS-TDP43 ^{A315T} h	–	↓
UAS-TBPH ^{WT}	↓	↑
UAS-TBPH ^{RNAi}	–	–
UAS-FUS ^{WT} h	Lethal	
UAS-FUS ^{R521H} h	↑	↓
UAS-FUS ^{R521C} h	Lethal	
UAS-FUS ^{R518K} h	–	↓
UAS-FUS ^{ΔNES} h	↑	↓
UAS-caz ^{WT}	–	–
UAS-caz ^{RNAi}	↓	–
UAS-SOD1 ^{WT}	–	↑
UAS-SOD1 ^{RNAi}	–	↑
UAS-SOD1 ^{A4V} h	Lethal	
UAS-TER94 ^{WT}	Lethal	
UAS-TER94 ^{RNAi}	↓	–
UAS-TER94 ^{R152H}	↓	↑

3.3. Effect of neuronal expression of ALS loci on bouton morphology

Although the aim of this screen is to understand the role of ALS loci in non-neuronal cells, in order to understand their contribution, we need to also uncover their role in neurons themselves. Studies have already explored a lot in this regard, but since our readout is bouton morphology, we needed to examine the role of ALS loci with respect to this particular phenotype. We therefore carried out a screen using the same ALS loci variants as used for muscle and glia, by using *Elav-Gal4* as the neuronal driver. It is a second chromosome neuronal driver expressed from the embryonic stages onwards. It is balanced over *CyO: GFP*. F1 larvae chosen for the bouton analysis were GFP negative. Controls used in all cases were the Gal4 drivers crossed to Canton S.

3.3.1. Both *VAP* mutant and knockdown, show a significant increase in bouton size

Use of *Elav-Gal4* increased the size of boutons for the mutant and RNAi based knockdown. Neuronal expression reduced the number of boutons for VAP^{P58S}, unlike the muscle or glial expression (Fig. 5.3 and Fig. 5.11), where there was no change observed for bouton number. Also, the trend for bouton size was opposite to that of glia (Fig. 5.11) as the overexpression of VAP^{P58S} in neurons leads to increase in size (Fig. 5.18).
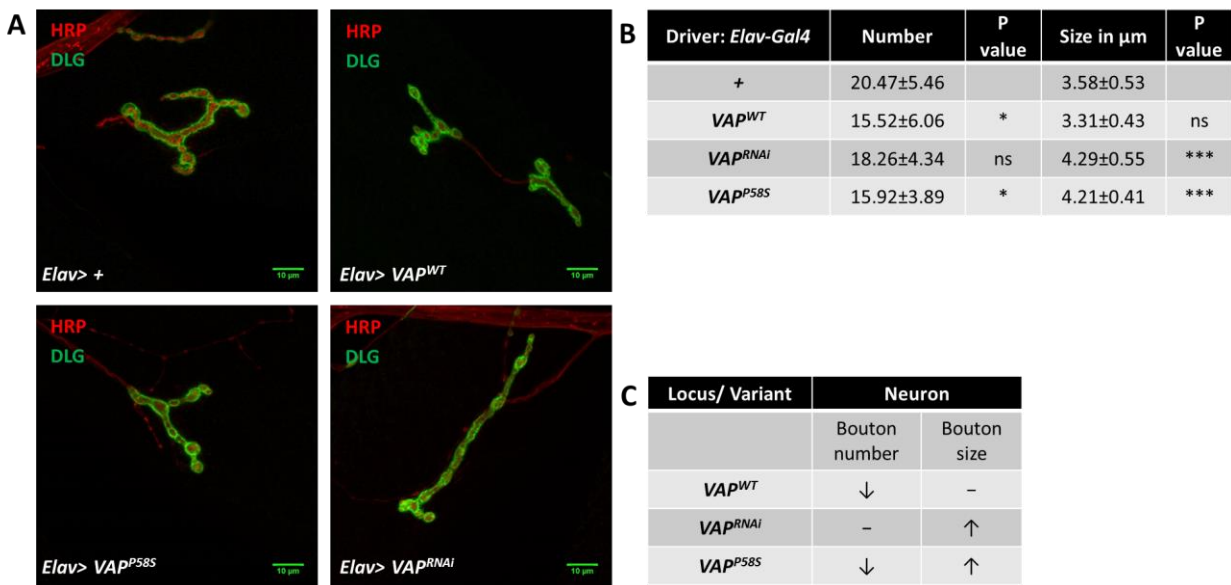
Figure 5.18. Effects of expression of *VAP* variants in the neurons on the bouton morphology.
A) Confocal images of overexpression of VAP^{P58S}, VAP^{WT} and VAP^{RNAi} in the neurons using *Elav-GAL4*. The markers used were HRP and DLG. .
B) Tabular representation of the overexpression of VAP^{P58S} (Average bouton size=4.217±0.41μm. Average bouton number= 15.92±3.89), VAP^{WT} (Average bouton size=3.31±0.43μm. Average bouton number= 15.52±6.06) and VAP^{RNAi} (Average bouton size=4.29±0.55μm. Average bouton number= 18.26±4.34). The control *Elav>+* has an average bouton size=3.58±0.53μm. Average bouton number= 20.47±5.46.The number of larvae used for each experiment are 4-7 and the neuromuscular junctions observed are 15-20 (all the crosses were performed at 25^0 C). *** indicates p value <0.001. * indicates p value <0.05.
C) Summary of results for effect of expression of variants of *VAP* in the neurons on the bouton morphology.

3.3.2. Human alleles of *TDP-43* when expressed in neurons, are lethal

Neuronal expression of $TDP-43^{WT}$, $TDP-43^{N345K}$ and $TDP-43^{A315T}$ did not develop any third instar larvae. Expression of $TDP-43^{WT}$ results in very small second instars which show severe locomotor defects as well as physical abnormalities and die before proceeding to further stages, while the other mutant alleles do not develop any larvae at all. The *Drosophila* orthologue, *TBPH*,

when overexpressed or knocked down in the neurons is not lethal and hence produces third instar larvae for NMJ dissections. Overexpression of *TBPH* in the neurons shows reduction of bouton size but there is no significant change in bouton number. Knockdown of *TBPH* does not show any changes in bouton morphology (Fig. 5.19).

B)

Driver: Elav-Gal4	Number	P value	Size in µm	P value
+	16.16±3.97		4.901±0.64	
TBPH^{WT}	16.5±5.61	ns	4.090±0.95	*
+	16.42±2.55	ns	4.334±0.26	ns
TBPH^{RNAi}	16.64±5.36	ns	3.771±0.65	ns

C)

Locus/ Variant	Neuron	
	Bouton Number	Bouton size
TDP-43^{WT}	Lethal	Lethal
TDP-43^{A315T}	Lethal	Lethal
TDP-43^{N345K}	Lethal	Lethal
TBPH^{WT}	−	↓
TBPH^{RNAi}	−	−

Figure 5.19. Effects of expression of *TDP-43/TBPH* variants in the neurons on the bouton morphology.
A) Confocal images of *Elav>+*, *Elav>TBPH^{WT}* and *Elav>TBPH^{RNAi}* in the neurons using *Elav-Gal4*. The markers used were HRP and DLG.
B) Tabular representation of *Elav>+* (Average bouton size=4.9±0.64µm. Average bouton number= 16.16±3.97), *Elav>TBPH* (Average bouton size=4.09±0.95µm. Average bouton number= 16.5±5.61) and *Elav>+* (Average bouton size=4.33±0.26µm. Average bouton number= 16.42±2.55) *Elav>TBPHi* (Average bouton size=3.77±0.65µm. Average bouton number= 16.64±5.36). The number of larvae used for each experiment are 4-7 and the neuromuscular junctions observed are 15-20 (all the crosses were performed at 25^0 C). ** indicates p value <0.01. *indicates p value <0.05. Brackets indicate sets of experiments.
C) Summary of results for effects of TDP-43/TBPH variants on bouton size and number in neuronal expression.

3.3.3. *FUS/caz* plays a vital role in regulating the bouton architecture

Section 3.3.3.1. describes the bouton morphology changes for human allelic variants while 3.3.3.2 describes the *Drosophila* allelic variants of *FUS/caz*

3.3.3.1 FUS^{R521H} expression in neurons leads to increase in bouton size and decrease in bouton number

FUS^{R518K} and FUS^{R521C} are lethal when overexpressed in neurons. FUS^{R521H} animals progress to the third instar larval stage and show significant changes in bouton morphology. Expression of FUS^{WT} shows marginal increase in bouton number. $FUS^{\Delta NES}$, however, does not cause any changes in bouton size and number (Fig. 5.20).

Driver: Elav-Gal4	Number	P value	Size in µm	P value
+	11.79±4.09		4.80±0.97	
FUS^{WT}	14.81±3.15	*	4.29±0.72	ns
FUS^{R521H}	20.53±3.95	ns	3.75±0.69	***
+	19.5±4.18		3.61±0.56	
$FUS^{\Delta NES}$	16.86±3.46	ns	3.45±0.60	ns

Figure 5.20. Effects of expression of *FUS* variants in the neurons on the bouton morphology.
A) Confocal images of *Elav>+*, *Elav>FUS^{WT}*, *Elav>FUS^{ΔNES}* and *Elav>FUS^{R521H}* in the neurons using *Elav-Gal4*. The markers used were HRP and DLG. .
B) Tabular representation of *Elav>+* (Average bouton size=4.80±0.97µm. Average bouton number= 11.79±4.09), *Elav>FUS^{WT}* (Average bouton size=4.29±0.72µm. Average bouton number= 14.81±3.15) and *Elav>FUS^{R521H}* (Average bouton size=3.75±0.69µm. Average bouton number= 20.53±3.95) and *Elav>+* (Average bouton size=3.61±0.56µm. Average bouton number= 19.5±4.18), *Elav>FUS^{ΔNES}* (Average bouton size=3.45±0.60µm. Average bouton number= 16.86±3.46). The number of larvae used for each experiment are 4-7 and the neuromuscular junctions observed are 15-20 (all the crosses were performed at 25^0 C). *** indicates p value <0.001. *indicates p value <0.05. Brackets indicate sets of experiments.

3.3.3.2. *caz* overexpressed in neurons shows presence of satellite boutons

caz overexpression leads to increase in the bouton number and shows the presence of satellite boutons. *caz* knockdown shows the opposite trend as that of the overexpression in terms of bouton number, while additionally showing an increase in bouton size (Fig. 5.21).

Figure 5.21. Effects of expression of *caz* variants in the neurons on the bouton morphology.
A) Confocal images of boutons at the NMJ of *Elav>+, Elav>caz^WT* and *Elav>caz^RNAi*. The markers used were HRP and DLG.
B) Tabular representation of *Elav>+* (Average bouton size=3.55±0.44μm. Average bouton number=23.15±2.98), *Elav>caz^WT* (Average bouton size= 3.29±0.38μm. Average bouton number=27.71±5.46) and *Elav>+* (Average bouton size=3.48±0.24μm. Average bouton number=22.62±5.26), *Elav>caz^RNAi* Average bouton size=4.73±0.73μm. Average bouton number=15.77±4.36) .The number of larvae used for each experiment are 4-7 and the neuromuscular junctions observed are 15-20 (all the crosses were performed at 25^0 C). **indicates p value <0.01. ***indicates p value <0.001. Brackets indicate sets of experiments.
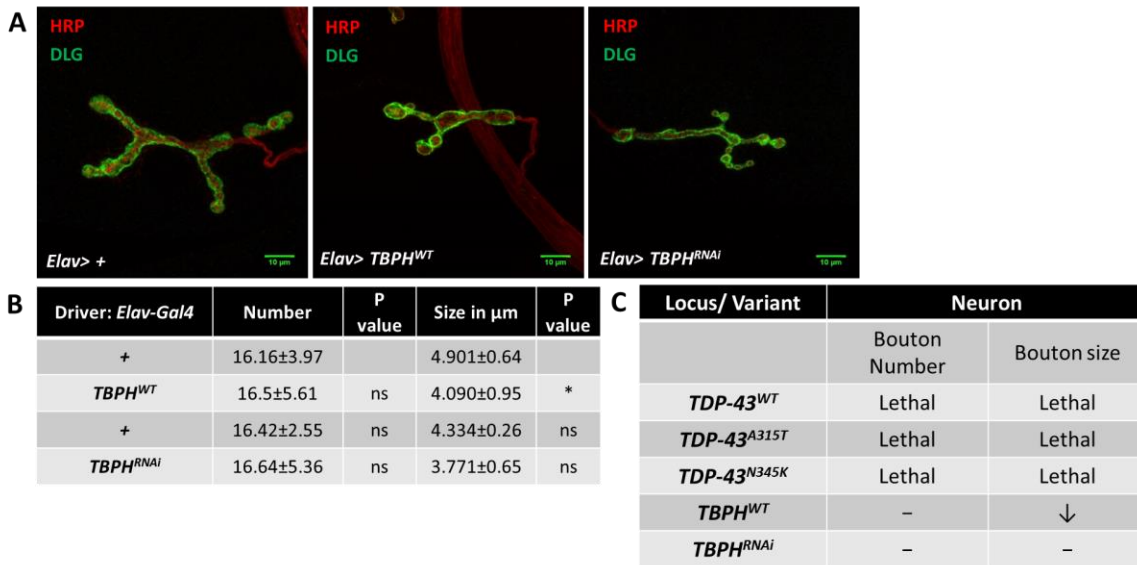**C)** Summary of results for effects of *FUS/caz* variants on bouton size and number in neuronal overexpression.

3.3.4. Knockdown of *SOD1* using RNAi, leads to reduction in bouton size

Neuronal overexpression of *SOD1* and its mutant *SOD1^A4V* does not show any significant changes in the boutons unlike their expression in glia. Nevertheless, downregulation of *SOD1* leads to a slight reduction in bouton size (Fig. 5.22).

Driver: Elav-Gal4	Number	P value	Size in µm	P value
+	16.42±2.55		3.47±0.26	
$SOD1^{WT}$	15.87±2.59	ns	3.73±0.49	ns
SOD^{A4V}	15.38±5.32	ns	3.64±0.47	ns
+	16.16±3.97		4.90±0.64	
$SOD1^{RNAi}$	17±5.25	ns	4.25±0.69	*

Locus/ Variant	Neuron	
	Bouton number	Bouton size
$SOD1^{WT}$	–	–
$SOD1^{RNAi}$	–	↓
$SOD1^{A4V}$	–	–
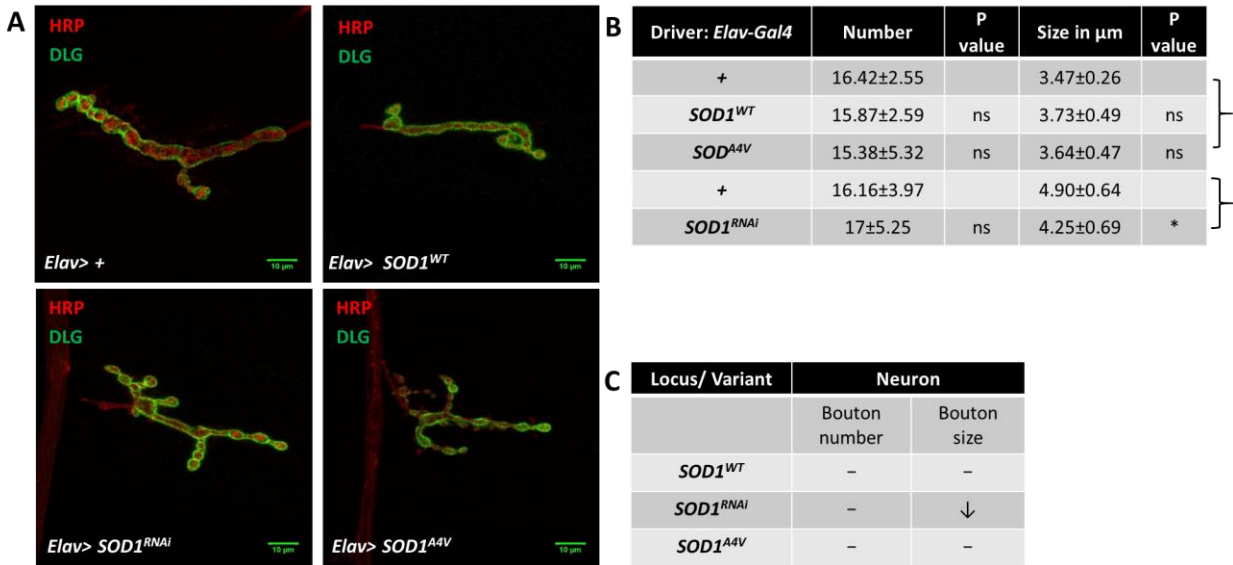
Figure 5.22. Effects of expression of *SOD1* variants in the neurons on the bouton morphology.
A) Confocal images of *Elav>+*, *Elav>SOD1^{WT}*, *Elav>SOD1^{A4V}* and *Elav>SOD1^{RNAi}* in the neurons using *Elav-Gal4*. The markers used were HRP and DLG.
B) Tabular representation of *Elav>+* (Average bouton size=3.47±0.26µm. Average bouton number= 16.42±2.55)*, Elav>SOD1^{WT}* (Average bouton size=3.73±0.49m. Average bouton number= 15.87±2.59), *Elav>SOD1^{A4V}* (Average bouton size=3.64±0.47µm. Average bouton number= 15.38±5.32) and *Elav>+* (Average bouton size=4.90±0.64µm. Average bouton number= 16.16±3.97)*, Elav>SOD1 ^{RNAi}* (Average bouton size=4.25±0.69µm. Average bouton number= 17±5.25). The number of larvae used for each experiment are 4-7 and the neuromuscular junctions observed are 15-20 (all the crosses were performed at 25^0 C). *indicates p value <0.05. Brackets indicate sets of experiments.
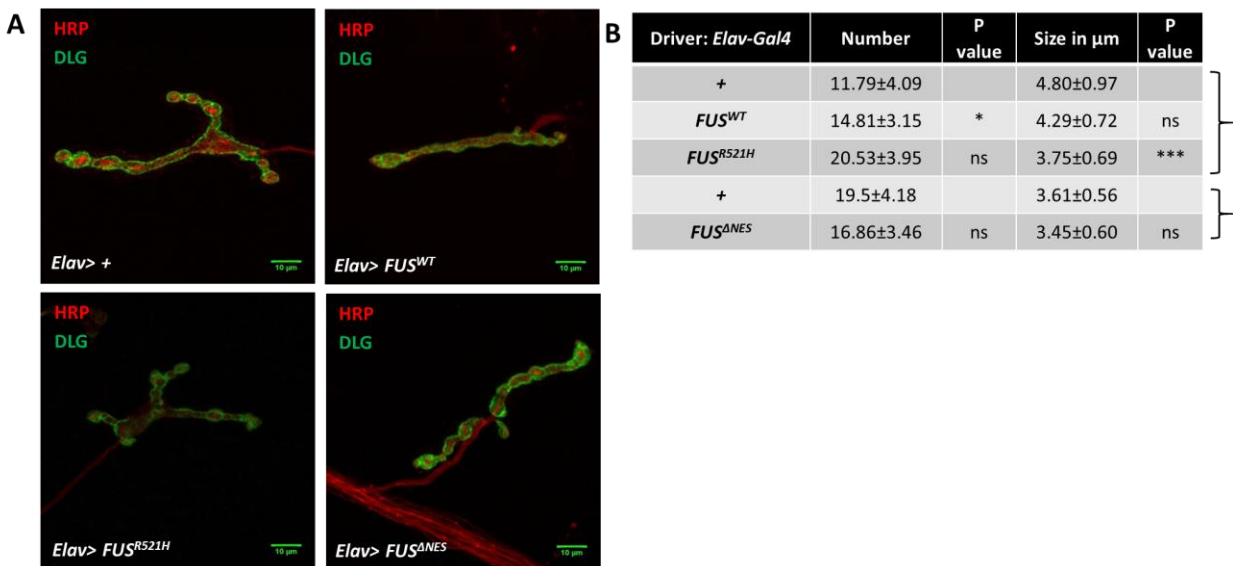**C)** Summary of results for effects of *SOD1* variants on bouton size and number in neuronal expression.

3.3.5. Effect of neuronal expression of *TER94* variants on the bouton morphology differ from their muscle or glial expression

TER94^{WT} and the mutant *TER94^{R152H}* expression lead to reduction in bouton size, whereas knockdown of *TER94* leads to reduction in bouton number (Fig. 5.23).
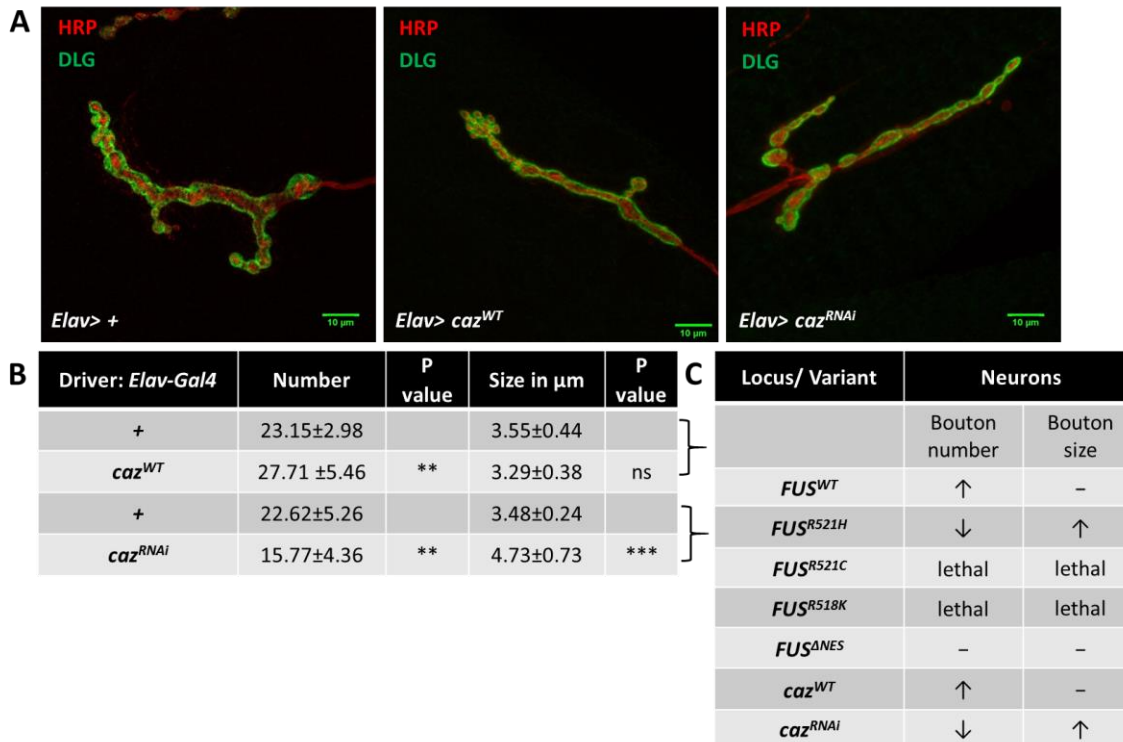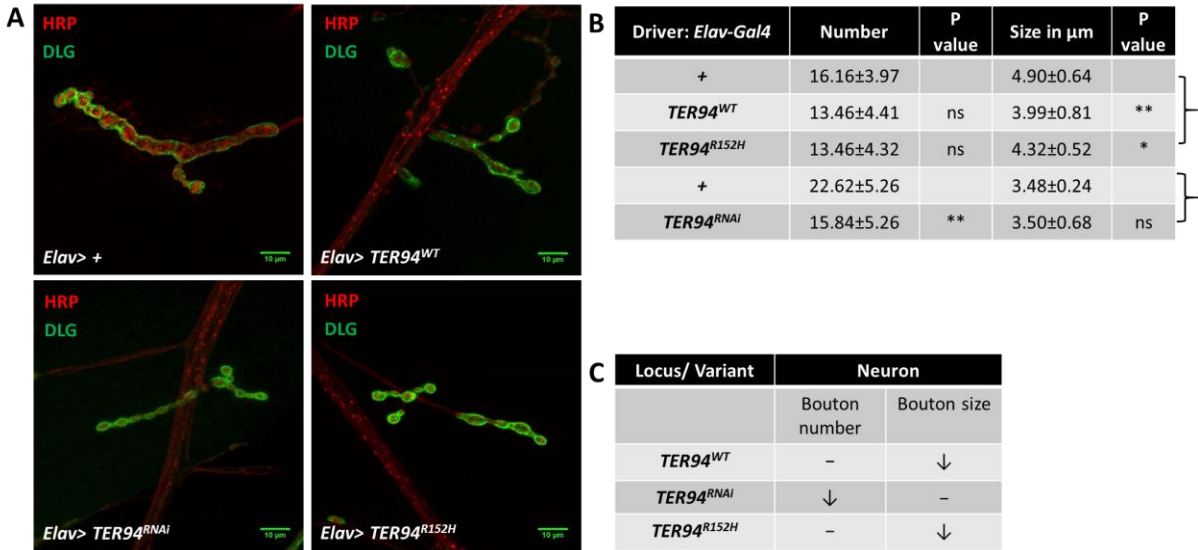
Figure 5.23. Effects of expression of *TER94* variants in the neurons on the bouton morphology.
A) Confocal images of *Elav>+, Elav>TER94^{WT}* and *Elav>TER94^{R152H}, Elav>TER94^{RNAi}* in the neurons using *Elav-Gal4*. The markers used were HRP and DLG.
B) Tabular representation of *Elav>+* (Average bouton size=4.90±0.64µm. Average bouton number= 16.16±3.97)*, Elav>TER94^{WT}* (Average bouton size=3.99±0.81µm. Average bouton number= 13.46±4.41), *Elav>TER94^{R152H}* (Average bouton size=4.32±0.52µm. Average bouton number= 13.46±4.32) and of *Elav>+* (Average bouton size=3.48±0.24µm. Average bouton number= 22.62±5.26)*, Elav>TER94^{RNAi}* (Average bouton size=3.50±0.68µm. Average bouton number= 15.84±5.26). The number of larvae used for each experiment are 4-7 and the neuromuscular junctions observed are 15-20 (all the crosses were performed at 25^0 C). ** indicates p value <0.01. *indicates p value <0.05. Brackets indicate sets of experiments.
C) Summary of results for effects of *TER94* variants on bouton size and number in neuronal expression.

3.3.6. Neuron summary

The results from neuronal perturbations of ALS loci render us with the information of cell autonomous effects as we observed the bouton architecture which is an asset of the presynapse. In this section as well as the discussion of this chapter (Section 4) we have compared these results with the non-cell autonomous/non-neuronal cell-specific results to realize the differential roles of each of these variants (Table 5.5 and 5.6). Following are a few striking observations from the neuronal results:

1. *VAP* in its mutant as well as wild type form is important in the neurons as it governs the bouton architecture in terms of both size and number.

2. *TDP-43*, like muscles, is lethal when expressed via the neurons making it hard for us to decide if this effect is because of its toxic levels or if it affects the development of the animal in any other way.

3. *TBPH* overexpression, the *Drosophila* orthologue of *TDP-43*, again acts similar to that of muscles by lowering the bouton size.

4. The involvement of *FUS* alleles appears to be equally important in its neuronal expression as compared to that of muscle and glia. The *ΔNES* however doesn't affect the neurons as that of muscles making it specifically important in the glia.

5. A unique observation with respect to *caz* overexpression in the neurons is the presence of satellite boutons.

6. *SOD1* doesn't display its importance when it comes to its role in regulating the structural homeostasis of the boutons on neuronal expression.

7. The overexpression, knockdown as well as expression of the mutant of *TER94,* causes a change in either size or number of boutons at the NMJ, suggesting its neuronal expression to be important. This characteristic is similar to its importance in the glia but not the muscles.

Table 5.5. Effect of neuronal expression of ALS loci on bouton morphology
Expression of ALS loci (Overexpression, mutant or loss-of-function), using the *UAS-GAL4* system, in muscle. '↑' indicates a significant increase in the parameter measured, while '↓' indicates a significant decrease. '−'means that there is no significant change.

1) *'h'* indicates that a human orthologue is used for the experiment. All other constructs are *Drosophila* genes.

2) *Caz* is the *Drosophila* orthologue of *FUS* while *TBPH* is the *Drosophila* orthologue of *TDP-43*.

3) The results for the outcome from the use of *Elav-Gal4* as the driver are depicted in this table. Alternate loci are separated by grey shades for clearer demarcation purposes.

MUTATION	NEURON(Elav Gal4)	
	Bouton number	Bouton size
UAS-VAP^{WT}	↓	−
UAS-VAP^{RNAi}	−	↑
UAS-VAP^{P58S}	↓	↑
UAS-TDP43^{WT} h	Lethal	
UAS-TDP43^{N345K} h	Lethal	
UAS-TDP43^{A315T} h	Lethal	
UAS-TBPH^{WT}	−	↓
UAS-TBPH^{RNAi}	−	−
UAS-FUS^{WT} h	↑	−
UAS-FUS^{R521H} h	↑	↓
UAS-FUS^{R521C} h	Lethal	
UAS-FUS^{R518K} h	Lethal	
UAS-FUS$^{\Delta NES}$ h	−	−
UAS-caz^{WT}	↑	−
UAS-caz^{RNAi}	↓	↑
UAS-SOD1^{WT}	−	−
UAS-SOD1^{RNAi}	−	↓
UAS-SOD1^{A4V} h	−	−
UAS-TER94^{WT}	−	↓
UAS-TER94^{RNAi}	↓	−
UAS-TER94^{R152H}	−	↓

4. Discussion

The experiments address differences in the behavior of muscles, glia and neurons after modulation of activity of different ALS variants (mammalian and fly). Although most of the human mutants have been used and have been tested for phenotypes in *Drosophila* in independent studies, there has been no comparative study between the different cell types. Therefore, in the above screen, we used this approach to compare the involvement of different ALS loci via cell types and further understand the disease mechanism. Table 5.6 presents a consolidated account of how each locus affects the NMJ morphology through each cell type.

Table 5.6. Elucidating roles for ALS loci at the tripartite synapse

Expression of ALS loci (Overexpression, mutant or loss-of-function), using the *UAS-GAL4* system, independently in muscle, glia or neurons. '↑' indicates a significant increase in the parameter measured, while '↓' indicates a significant decrease. '−'means that there is no significant change.

1) *'h'* indicates that a human orthologue is used for the experiment. All other constructs are *Drosophila* genes.

2) *Caz* is the *Drosophila* homologue of *FUS* while *TBPH* is the *Drosophila* homologue of *TDP-43*.

3) The results for the outcome from the use of *G14-Gal4* as the muscle driver are depicted in this table. As *MHC-Gal4* was utilized only when animals die on the use of the stronger *G14-Gal4*, the results for *MHC-Gal4* are not mentioned in the table to avoid complications. *Repo-Gal4* is the glial driver and *Elav-Gal4* was used for neurons. Alternate loci are separated by grey shades for clearer demarcation purposes.

MUTATION	MUSCLE (G14 Gal4)		GLIA(Repo Gal4)		NEURON(Elav Gal4)	
	Bouton number	Bouton size	Bouton number	Bouton size	Bouton number	Bouton size
UAS-VAP ^{WT}	↑	↓	−	↓	↓	−
UAS-VAP ^{RNAi}	↓	↑	−	−	−	↑
UAS-VAP ^{P58S}	−	−	−	↓	↓	↑
UAS-TDP43 ^{WT} *h*	Lethal (G14)		−	↓	Lethal	
UAS-TDP43 ^{N345K} *h*	Lethal (G14)		↓	↑	Lethal	
UAS-TDP43 ^{A315T} *h*	Lethal (G14)		−	↓	Lethal	
UAS-TBPH ^{WT}	−	↓	↓	↑	−	↓
UAS-TBPH ^{RNAi}	−	↓	−	−	−	−
UAS-FUS ^{WT} *h*	Lethal (G14)		Lethal		↑	−
UAS-FUS ^{R521H} *h*	−	↑	↑	↓	↑	↓
UAS-FUS ^{R521C} *h*	Lethal (G14)		Lethal		Lethal	
UAS-FUS ^{R518K} *h*	−	↓	−	↓	Lethal	
UAS-FUS ^{ΔNES} *h*	−	−	↑	↓	−	−
UAS-caz ^{WT}	−	−	−	−	↑	−
UAS-caz ^{RNAi}	−	↑	↓	−	↓	↑
UAS-SOD1 ^{WT}	−	−	−	↑	−	−
UAS-SOD1 ^{RNAi}	−	−	−	↑	−	↓
UAS-SOD1 ^{A4V} *h*	−	↓	Lethal		−	−
UAS-TER94 ^{WT}	−	−	Lethal		−	↓
UAS-TER94 ^{RNAi}	−	−	↓	−	↓	−
UAS-TER94 ^{R152H}	−	↑	↓	↑	−	↓

Table 5.6 hints towards the activity of each locus acting differently via muscle or glia or neuron. A few loci affect the system more strongly by imparting lethality or resulting in evident changes in bouton morphology. A few other loci are involved via one or two cell types, but it has to be noted that there is not a single locus which is not participating in contributing to changes at the tripartite at all. Also, it is essential to note that the trend of change for some loci with respect to the bouton size or number is in the same direction for all cell types while it's the opposite for some loci.

VAP^{P58S} demonstrates changes in bouton architecture strongly via the neurons. It also acts very subtly (p< .05) via glia in terms of changing only the bouton size but not the number. As VAP is involved not only in the anterograde (Tsuda et al., 2008, Han et al., 2012) but also the retrograde signalling at the NMJ (Ratnaparkhi et al., 2008), it is surprising to note that the mutant is not acting via the muscles which are postsynaptic to the NMJ. The overexpression of the wild type form seems to be acting via all cell types, this could perhaps be a side effect of the toxicity of the overexpressed protein in the system. The bouton size increase and reduction in number for VAP^{P58S} when expressed in neurons, is consistent with the literature, which highlights the involvement of VAP in bouton budding (Pennetta et al., 2002). Although, it is interesting to note that expression of the mutant exhibits the opposite phenotype i.e. reduction of size on glial expression (Table 5.6).

According to our observations (Table 5.6), *TDP-43/TBPH* seems to be acting through all cell types. The lethality caused by the use of human variants in muscles and neurons, however, isn't helpful in studying its effects on the bouton morphology. Nevertheless, an interesting observation to be noted about the overexpression of the *Drosophila* variant, *TBPH*, is its similar trend in changing the bouton morphology i.e. reduction of bouton size on expression in muscles and neurons. This change in size is however in the opposite direction (increase) in case of glial expression, possibly because of a different pattern of functioning in the glia as against the muscles and neurons. Various studies discuss the contribution of glia as well as muscles in *TDP-43* mediated pathogenesis in ALS, most of them are related to aggregate and motor defects in various model organisms and patient samples (Neumann et al., 2006, Diaper et al., 2013; Godena et al., 2011). A study in *Drosophila* sheds light on toxic gain-of-function as well as loss-of-function of *TBPH* (*TDP-43*), inferring both to be associated with the abnormal development of flies and also leading to partial lethality in adults (Diaper et al., 2013). Even though we haven't followed up on the adult lethality, *TBPH* seems to have an effect on its overexpression and downregulation in all three cell types in the larvae as mentioned earlier. The toxicity of *TDP-43* variants used by us, however, is quite evident as all variants exhibit lethality on muscle and neuronal expression. Other studies in *Drosophila* using the same human variants of *TDP-43* as ours, witness bouton morphology changes when expressed in glial cells, imparting confidence to our observations which show changes in bouton size and number on glial expression (Estes et al., 2011 and 2013).

The human variants of *FUS* display a diverse pattern. The overexpression of human wild type *FUS* is lethal when expressed in muscles using *G14-Gal4* and in glia as well, but surprisingly

is not lethal when expressed in neurons and neither does it show any changes in the boutons, suggesting its dosage could be more sensitive in glia and muscles. However, use of *MHC-Gal4* instead of *G14-Gal4*(for muscles) allowed us to lower the levels of *FUS*, overcome the lethality and hence observe the phenotype which displayed not just changes in bouton size and number but also clustering of boutons, which is similar to the of *VAP^{WT}* overexpression in muscles (Fig. 5.6, 5.7, 5.8). Amongst the other variants used, a nuclear localization sequence (NLS) mutant, *FUS^{R521C}* looks like the most potent of them all, as its expression in all cell types causes lethality. Again, on use of milder overexpression in muscles using *MHC-Gal4*, it was observed that the bouton morphology looked similar to that of *FUS^{WT}* (on use of *MHC-Gal4*) i.e. small in size and clustered (Fig. 5.6, 5.7, 5.8). *FUS^{R518K}* and *R521H* are other *NLS* mutant variants used in our study, all of which show perturbation of bouton morphology affirming the importance of the *NLS* of *FUS*. These results are consistent with the idea of the *FUS* variants being gain-of-function/gain-of toxicity mutants leading to detrimental effects, be it aggregation of the protein in the cytoplasm or ubiquitination or lethality or motor defects or neuronal degeneration (Lanson and Pandey, 2012; Lanson et al., 2011). Another human variant used in our study was *FUS$^{\Delta NES}$*, which shows no change when overexpressed in muscles or neurons suggesting that blocking of the nuclear export may not be an essential activity for the structural homeostasis at the NMJ via muscles and neurons. Nevertheless, the *FUS$^{\Delta NES}$* shows significant changes when expressed in glia alluding to the idea of its importance in the glia. This indirectly hints towards the involvement of *FUS* in the glial-neuronal signalling. Lastly, the overexpression or knockdown of *caz* (*Drosophila* orthologue of *FUS*) seems to be acting via all three cell types. The effects via the neurons themselves seem to be the strongest, witnessing the presence of satellite boutons (Fig. 5.21) which are small ectopic boutons arising from the main nerve and are thought to be involved in endocytic mutants (O'Connor-Giles 2008). Further studies will provide clarity on the possible endocytic dysfunction related to *caz* on its expression in the neurons.

SOD1 seems to be a locus participating more via the glial cells than the muscles or neurons, when it comes to bouton morphology changes (Table 5.6). Although the mutant shows a difference via the muscle expression, it imparts lethality via glial cells. The overexpression and knockdown, both have no effect via muscles, but it does increase the bouton size via glial cells.

The final locus explored in our screen was *TER94*, which seems to be affecting majorly via neurons and glia. Moreover, the glial effect of the locus is overwhelming as compared to neurons

as the wild type overexpression leads to lethality, the N-terminal *R152H* dominant active mutant (Chang et al., 2011) leads to changes in both size and number and knockdown causes an increase in numbers. The mutant also seems to cause change in muscle expression (Table 5.6).

Apart from the individual summaries discussed after each cell-specific section (3.1.6, 3.2.6 and 3.3.6) and the above inferences, we draw the following conclusions from our study of the effect of various ALS loci on the morphology of boutons at the NMJ:

1. All variants, Human and *Drosophila*, play an instrumental role in controlling the bouton morphology.

2. It is interesting to observe that in most cases the bouton number is compensated by an inverse change in the bouton size, thus possibly keeping the presynaptic surface area near to constant and maintaining the homeostasis at the tripartite synapse.

3. Muscle expression of most alleles seems to be affecting the bouton size and rarely alters the number, which is not the case for glial and neuronal expression.

4. All the *Drosophila* loci studied control the NMJ phenotype via at least one or all the cell types. However, each locus holds a degree of importance in each cell type. This degree of importance is a measure of a locus' cumulative impact on change in the bouton morphology (Table 5.7)

Table 5.7. Degrees of the importance of each *Drosophila* locus at the tripartite synapse
This table discusses the broad importance of each *Drosophila* locus in each cell type. The asterisk indicate the degree of their importance based on their overall impact in the three cell types.

Loci (*Drosophila* Orthologues)	Muscle	Glia	Neurons
VAP	**	*	***
TBPH	**	**	*
Caz	*	*	***
VCP	*	***	**
SOD1	*	***	*

5. Lastly, to bring to notice some starkly outstanding phenotypes: Loci like *VAP* (wild type overexpression, Fig. 5.3) and *FUS* (mutant overexpression, Fig. 5.6 and 5.7) appear to have distinguishingly smaller and clustered bouton abnormalities when expressed via muscles, which is not the case in glia or neurons. Also, *caz* overexpression in neurons exhibits the satellite bouton phenotype (Fig. 5.21).

Although we are aware of the varying strengths of the muscle, the glial and the neuronal drivers in comparison to each other and that drawing a direct correlation would require more investigation, we can use this screen as a platform of mere comparison between the contributions of each cell type. This being an overexpression screen, the burden of toxicity of overexpression in presence of an endogenous protein on the system cannot be neglected and we therefore advocate the use of genomic systems for accurate understanding of cell-specific behaviors of different loci. Also one has to note that the absence of change in our readout doesn't necessarily mean that a particular variant doesn't act through a cell type, it is only a means of elimination of the locus which is simply not perturbing the phenotype and is therefore not followed up. There are studies based on increase or decrease in bouton size and number, which talk about the functional relevance of our readout. We will however have to look into various markers at the synapse to comment on the details of the functional contributions of the loci we have studied (Diaper et al., 2013; Lanson et al., 2011; Forrest et al., 2013; Chai et al., 2008). A thorough study on the receptors at the NMJ and cytoskeletal proteins would shed further light on the cell-specific investigation.

5. Materials and Methods

5.1. Reagents

This chapter consists of fly work and IF experiments. The following tables mention details of all the fly lines and antibodies used for our work.

Table 5.8. List of Fly lines used in this study
Table lists the name, source and full genotype of the line. RNAi lines target mRNA transcripts of the native fly. Please note that *TDP-43* and *TBPH* are human and *Drosophila* orthologues respectively; FUS and caz are human and *Drosophila* orthologues respectively.

Fly line	Source	Full Genotype	Other Details (if any)
UAS-VAP^{WT}	Ratnaparkhi et al., 2008		
UAS-VAP^{P58S}	Ratnaparkhi et al., 2008		*Drosophila* Orthologue
UAS-VAP^{RNAi}	BL 27312	*y[1] v[1]; P{y[+t7.7] v[+t1.8]=TRiP.JF02621}attP2*	
UAS-TDP-43^{WT}	Daniella Zarnescu, University of Arizona (Estes et al., 2013).	*UAS-TDP-43^{WT} (2Ch.)*	Human orthologue
UAS-TDP-43^{N345K}		*UAS-TDP-43^{N345K} (3Ch)*	Human orthologue
UAS-TDP-43^{D169G}		*UAS-TDP-43^{D169G}(X)*	Human orthologue
UAS- TDP-43^{A315T}		*UAS-TDP-43^{A315T} (3Ch.)*	Human orthologue
UAS-TBPH^{WT}	CG 10327 RB		*Drosophila* orthologue of *TDP-43*
UAS-TBPH^{RNAi}	BL 29517	*y[1] v[1]; P{y[+t7.7] v[+t1.8]=TRiP.HM05194}attP2*	
UAS-FUS^{WT}	Udai Bhan Pandey, Louisiana State University Health Sciences Center (Lanson et al., 2011).	*UAS-FUS^{WT}(3Ch) #5*	Human orthologue
UAS-FUS^{R521H}		*UAS-FUS^{R521H} (2Ch.) #9*	
UAS-FUS^{R521H}		*UAS-FUS^{R521H}(2Ch.) #13*	
UAS-FUS^{R521C}		*UAS-FUS^{R521C} (3Ch.) #18*	
UAS-FUS^{R521C}		*UAS-FUS^{R521C}(2Ch.) #20*	
UAS-FUS^{R518K}		*UAS-FUS^{R518K} (X) #30*	
UAS-FUS^{ΔNES}		*UAS-FUS^{ΔNES} (X) #159*	

UAS-caz^{WT}	BL17010 EP	*P{EP}caz[EP1564]*	
UAS-caz^{RNAi}	BL34839	*P{TRiP.HMS00156}attP2*	*Drosophila* Orthologue of *FUS*
UAS-SOD1^{A4V}	BL33607	*w[1118]; P{w[+mC]=UAS-hSOD1.A4V}9.1/TM6B, Tb[1]*	Human orthologue
UAS-SOD1^{WT}	BL24754	*w[1]; P{w[+mC]=UAS-Sod1.A}B36*	
UAS-SOD1^{RNAi}	BL34616		
UAS-TER94^{WT}	JP Taylor, University of Pennsylvania School of Medicine (Ritson et al., 2010)	*UAS-TER94^{WT}/ Cyo*	
UAS-TER94^{R152H}		*UAS-TER94^{R152H} (2Ch.)*	*Drosophila* Orthologue
UAS-TER94^{A229E}		*UAS-TER94^{A229E}/cyo (2Ch.)*	*Drosophila* Orthologue
UAS-TER94^{RNAi}	BL 32869	*P{TRiP.HMS00656}attP2*	*Drosophila* Orthologue
G14-Gal4	Ratnaparkhi et al., 2008	*G14-Gal4/Cyo::nuc GFP*	
MHC-Gal4	BL 55133	*P{Mhc-GAL4.K}2*	
Repo-Gal4	BL 7415	*Repo-GAL4;UAS-MCD8-GFP/TM6B TB*	
Elav-Gal4	Ratnaparkhi et al., 2008	*Elav-Gal4/Cyo*	

Table 5.9. List of antibodies used in the study

Antibody Used	Name of antibody	Raised in	Source	Dilution for IHC
Anti-HRP	Horseradish Peroxidase	Rabbit	Sigma	1:500
Anti-DLG	Disc Large	Mouse	DSHB	1:250
Anti- BRP	Bruchpilot	Mouse	DSHB	1:250

5.2. Immunostaining and image analysis

5.2.1. Neuromuscular Junction dissections and immunostaining

To observe the boutons, NMJ dissections of the *Drosophila* third instar larvae were carried out. The dissections were performed in 1X PBS and fixed with Bouin's fixative (combination of formaldehyde and picric acid from Sigma) for 10 to 15 minutes. The fixation was followed by 3 washes with Phosphate buffered saline (PBS). The tissues were then blocked with PBS containing 0.3% TritonX-100 and 2% BSA and incubated with primary antibody at 4 ℃ overnight. Samples were then washed and incubated with the appropriate secondary antibodies overnight at 4 ℃. Samples were then washed with 1XPBS and mounted using 70% glycerol with n-propyl gallate.

5.2.2. Bouton imaging and analysis

The primary antibodies used for the bouton imaging were HRP and DLG/BRP followed by Alexa fluor 488 and 568 secondary conjugate antibodies. The images were taken on Zeiss confocal microscope at 63X oil magnification and 1.5 zoom in order to observe the bouton size and number of the 2nd and 3rd segment of the fourth muscle at the NMJ. For the analysis, a minimum of 4 larvae i.e. 16 NMJs were observed for each set of crosses performed. The images, projected at maximum intensity, were analyzed using Axiovision software. The measurement was done by separating the HRP channel from the DLG or BRP. Both bouton size and number were analyzed using unpaired student's t-test. Please refer to Figure 5.2D for further details of the imaging and quantification.

6. Contributions

Neena Dhiman, a BSMS student contributed to the HRP/BRP specific glial expression screen along with its image analysis and quantification for the human mutant variants.

7. Acknowledgements

8. References

Acosta, J. R. *et al.* Mutant Human FUS Is Ubiquitously Mislocalized and Generates Persistent Stress Granules in Primary Cultured Transgenic Zebrafish Cells. 9, (2014).

Azuma, Y. *et al.* Identification of ter94, drosophila VCP, as a strong modulator of motor neuron degeneration induced by knockdown of Caz, Drosophila FUS. *Hum. Mol. Genet.* 23, 3467–3480 (2014).

Baird, Fiona J, and Craig L Bennett. "Microtubule defects & Neurodegeneration." *Journal of genetic syndromes & gene therapy* vol. 4 (2013): 203. doi:10.4172/2157-7412.1000203

Broadie, K. & Bate, M. The Drosophila NMJ: a genetic model system for synapse formation and function. *Semin. Dev. Biol.* 6, 221–231 (1995).

Brunner, A. & O'Kane, C. J. The fascination of the Drosophila NMJ. *Trends Genet.* 13, 85–87 (1997).

Chai, A. *et al.* hVAPB, the causative gene of a heterogeneous group of motor neuron diseases in humans, is functionally interchangeable with its Drosophila homologue DVAP-33A at the neuromuscular junction. *Hum. Mol. Genet.* 17, 266–280 (2008).

Chang, Y. C. *et al.* Pathogenic VCP/TER94 alleles are dominant actives and contribute to neurodegeneration by altering cellular ATP level in a drosophila IBMPFD model. *PLoS Genet.* 7, (2011).

Chung, W. S. & Barres, B. A. Selective remodeling: Refining neural connectivity at the neuromuscular junction. *PLoS Biol.* 7, 8–11 (2009).

Clark, J. A., Yeaman, E. J., Blizzard, C. A., Chuckowree, J. A. & Dickson, T. C. A case for microtubule vulnerability in amyotrophic lateral sclerosis: Altered dynamics during disease. *Front. Cell. Neurosci.* 10, 1–16 (2016).

Collins, C. A. & DiAntonio, A. Synaptic development: insights from Drosophila. *Curr. Opin. Neurobiol.* 17, 35–42 (2007).

Daigle, G. G. *et al.* Rna-binding ability of FUS regulates neurodegeneration, cytoplasmic mislocalization and incorporation into stress granules associated with FUS carrying ALS-linked mutations. *Hum. Mol. Genet.* 22, 1193–1205 (2013).

Diaper, D. C. *et al.* Loss and gain of Drosophila TDP-43 impair synaptic efficacy and motor control leading to age-related neurodegeneration by loss-of-function phenotypes. *Hum. Mol. Genet.* 22, 1539–1557 (2013).

Diaper, D. C. *et al.* Drosophila TDP-43 dysfunction in glia and muscle cells cause cytological and behavioural phenotypes that characterize ALS and FTLD. 1–11 (2013). doi:10.1093/hmg/ddt243

Estes, P. S. *et al.* Wild-type and A315T mutant TDP-43 exert differential neurotoxicity in a Drosophila model of ALS. *Hum. Mol. Genet.* 20, 2308–2321 (2011).

Estes, P. S. *et al.* Motor neurons and glia exhibit specific individualized responses to TDP-43 expression in a Drosophila model of amyotrophic lateral sclerosis. *DMM Dis. Model. Mech.* 6, 721–733 (2013).

Forrest, S. *et al.* Increased levels of phosphoinositides cause neurodegeneration in a Drosophila model of amyotrophic lateral sclerosis. 1–16 (2013). doi:10.1093/hmg/ddt118

Godena, V. K. *et al.* TDP-43 regulates drosophila neuromuscular junctions growth by modulating futsch/MAP1B levels and synaptic microtubules organization. *PLoS One* 6, (2011).

Han, S. M. *et al.* Secreted VAPB/ALS8 Major Sperm Protein Domains Modulate Mitochondrial Localization and Morphology via Growth Cone Guidance Receptors. *Dev. Cell* 22, 348–362 (2012).

Hensel, N. & Claus, P. The Actin Cytoskeleton in SMA and ALS: How Does It Contribute to Motoneuron Degeneration? *Neuroscientist* 24, 54–72 (2018).

Henty-Ridilla, J. L., Juanes, M. A. & Goode, B. L. Profilin Directly Promotes Microtubule Growth through Residues Mutated in Amyotrophic Lateral Sclerosis. *Curr. Biol.* 27, 3535-3543.e4 (2017).

Hosler, B. A., Cortelli, P., Jong, P. J. De, Yoshinaga, Y. & Haines, J. L. Mutations in the FUS/TLS Gene on Chromosome 16 Cause Familial Amyotrophic Lateral Sclerosis. 547, 1205–1209 (2009).

Julien, Jean-Pierre *et al*. "Cytoskeletal defects in amyotrophic lateral sclerosis (motor neuron disease)." *Novartis Foundation symposium* vol. 264 (2005): 183-92; discussion 192-6, 227-30

Kazuyoshi I *et al*., GlycoPOD https://jcggdb.jp/GlycoPOD. Web.1,7,2020. (2016).

Kohsaka, H., Okusawa, S., Itakura, Y., Fushiki, A. & Nose, A. Development of larval motor circuits in Drosophila. *Dev. Growth Differ.* 54, 408–419 (2012).

Keshishian H *et al*., Annual Review of Neuroscience 1996 19:1, 545-575

Landgraf, Matthias, and Stefan Thor. "Development of Drosophila motoneurons: specification and morphology." *Seminars in cell & developmental biology* vol. 17,1 (2006): 3-11. doi:10.1016/j.semcdb.2005.11.007

Lanson, N. A. *et al.* A Drosophila model of FUS-related neurodegeneration reveals genetic interaction between FUS and TDP-43. *Hum. Mol. Genet.* 20, 2510–2523 (2011).

Lanson, Jr, N. A. & Pandey, U. B. FUS-related proteinopathies : Lessons from animal models. *Brain Res.* 1462, 44–60 (2012).

Machamer, J. B., Collins, S. E. & Lloyd, T. E. The ALS gene FUS regulates synaptic transmission at the Drosophila neuromuscular junction. 23, 3810–3822 (2014).

Mcmurray, C. T. Neurodegeneration : diseases of the cytoskeleton ? 861–865 (2000).

Menon, K. P., Carrillo, R. A. & Zinn, K. Development and plasticity of the Drosophila larval neuromuscular junction. *Wiley Interdiscip. Rev. Dev. Biol.* 2, 647–670 (2013).

Milton, V. J. *et al.* Oxidative stress induces overgrowth of the Drosophila neuromuscular junction. *Proc. Natl. Acad. Sci.* 108, 17521–17526 (2011).

Moustaqim-barrette, A. *et al.* The amyotrophic lateral sclerosis 8 protein, VAP, is required for ER protein quality control. *Hum. Mol. Genet.* 23, 1975–1989 (2014).

Neumann, M. *et al.* Ubiquitinated TDP-43 in Frontotemporal Lobar Degeneration and Amyotrophic Lateral Sclerosis.

O'Connor-Giles, K. M. & Ganetzky, B. Satellite signaling at synapses. *Fly (Austin).* 2, 259–261 (2008).

Pennetta, G., Hiesinger, P. R., Fabian-Fine, R., Meinertzhagen, I. A. & Bellen, H. J. Drosophila VAP-33A directs bouton formation at neuromuscular junctions in a dosage-dependent manner. *Neuron* 35, 291–306 (2002).

Pérez-Moreno, J. J. & O'Kane, C. J. GAL4 drivers specific for type Ib and type is motor neurons in drosophila. *G3 Genes, Genomes, Genet.* 9, 453–462 (2019).

Ratnaparkhi, A., Lawless, G. M., Schweizer, F. E., Golshani, P. & Jackson, G. R. A Drosophila model of ALS: Human ALS-associated mutation in VAP33A suggests a dominant negative mechanism. *PLoS One* 3, (2008).

Romano, M., Feiguin, F. & Buratti, E. Drosophila Answers to TDP-43 Proteinopathies. 2012, (2012).

Saeed, M. *et al.* Age and founder effect of S0D1 A4V mutation causing ALS. *Neurology* 72, 1634–1639 (2009).

Smith, M A *et al.* "LIM proteins in actin cytoskeleton mechanoresponse." *Trends in cell biology* vol. 24,10 (2014): 575-83. doi:10.1016/j.tcb.2014.04.009

Wang, J., Brent, J. R., Tomlinson, A., Shneider, N. A. & Mccabe, B. D. The ALS-associated proteins FUS and TDP-43 function together to affect Drosophila locomotion and life span. 121, (2011).

Xia, R. *et al.* Motor neuron apoptosis and neuromuscular junction perturbation are prominent features in a Drosophila model of Fus-mediated ALS. *Mol. Neurodegener.* 7, 10 (2012).

Appendix I

Modulation of *caspar* and *TER94^{R152H}* levels in the muscles, as well as motor neurons, in the ALS8 flies

1. Introduction

We have characterized the genetic interactions of *VAP^{P58S}-TER94-caspar* in Chapter III. These interactions were mediated via the glial expression of *caspar* and *TER94* variants. We were unaware if *VAP^{P58S}-TER94-caspar* follow the same interaction patterns via the muscles as well as the motor neurons. We have characterized muscle and motor neuronal interactions of *VAP^{P58S}-TER94-caspar* in this section.

2. Results and Discussion

2.1. Overexpression of *caspar* in the muscles, as well as motor neurons, suppresses the Δ*VAP; gVAP^{P58S}* lifespan defects

caspar overexpression in muscles as well the motor neurons in the Δ*VAP; gVAP^{P58S}* background, using Δ*VAP; MHC-Gal4; gVAP^{P58S}* and Δ*VAP; OK6-Gal4; gVAP^{P58S}* respectively shows suppression of lifespan defect (Fig. I.1A and C , red curve, number 2), which is similar to its glial overexpression. The RNAi based knockdown of *caspar* causes a reduction in lifespan when expressed in muscles (Fig. I.1.A, B), but shows no change when expressed in motor neurons (Fig. I.1C and D). The overexpression of the *TER94^{R152H}* in muscles and motor neurons, however, doesn't show a suppression (Fig. I. 1A and C, purple curve, number 4) as is seen in the case of its glial overexpression (Chapter III, Fig. 3.6).
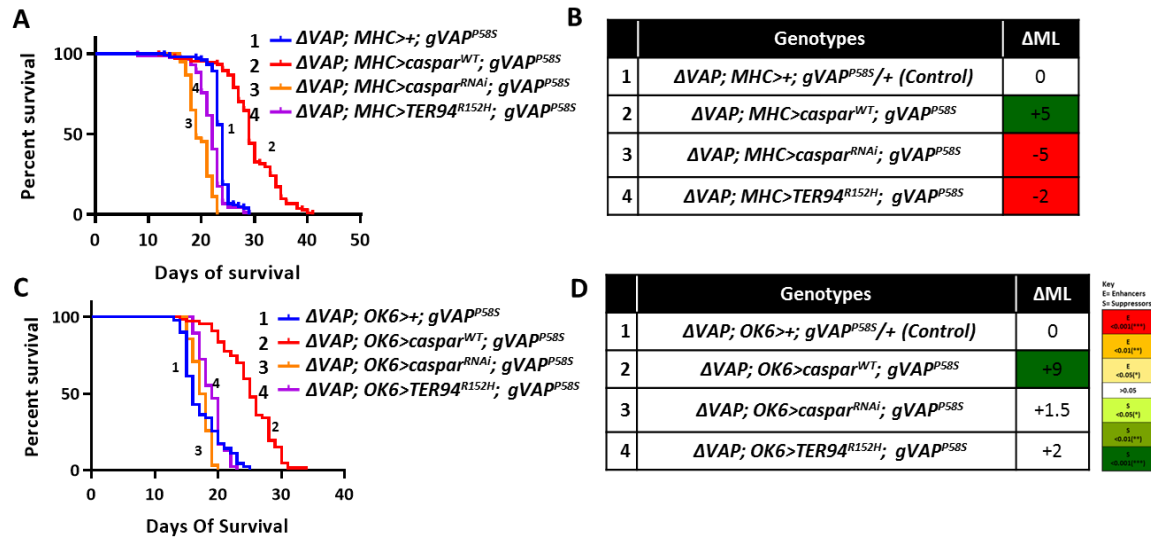
Figure I.1. *caspar* **overexpression in muscles as well as motor neurons in Δ*VAP; gVAP^{P58S}* background leads to an increase in survival as compared to Δ*VAP; MHC>+; gVAP^{P58S}/+* and Δ*VAP; OK6>+; gVAP^{P58S}/+.*

A) Overexpression of *caspar^{WT}* (Red curve, number 2), *caspar^{RNAi}* (Orange curve, number 3), *TER94^{R152H}* (Purple curve, number 4) in the Δ*VAP; MHC-Gal4; gVAP^{P58S}* background. Δ*VAP; MHC>+; gVAP^{P58S}/+* (Curve 1 in blue color, media lifespan= 24 Days) was used as the control. n=80-100 flies for each genotype. Curve comparison was done using log-rank (Mantel-Cox test). The combined p-value for the whole set is <0.001.

B) The results are in the form of ΔML (Change in Median Lifespan) = Median Lifespan (Experiment) – Median Lifespan (Control).
Color/Statistical Key: The 'red-yellow tones' indicate different levels of statistical confidence (log-rank test) for the 'Enhancers (E)' while the 'green tones' represent the same for 'Suppressors (S)'.

C) Overexpression of *caspar^{WT}* (Red curve, number 2), *caspar^{RNAi}* (Orange curve, number 3), *TER94^{R152H}* (Purple curve, number 4) in the Δ*VAP; OK6-Gal4; gVAP^{P58S}* background. Δ*VAP; OK6>+; gVAP^{P58S}/+* (Curve 1 in blue color, media lifespan= 16 Days) was used as the control. n=80-100 flies for each genotype. Curve comparison was done using log-rank (Mantel-Cox test). The combined p-value for the whole set is <0.001.

D) The results are in the form of ΔML (Change in Median Lifespan) = Median Lifespan (Experiment) – Median Lifespan (Control).
Color/Statistical Key: The 'red-yellow tones' indicate different levels of statistical confidence (log-rank test) for the 'Enhancers (E)' while the 'green tones' represent the same for 'Suppressors (S)'.

The non-cell autonomous effect of *caspar* on the lifespan of *VAP^{P58S}* is quite evident as its overexpression and knockdown in muscles, as well as glia, causes a change in the lifespan (Fig. I.1, and chapter III, Fig. 3.6 and 3.7). Furthermore, results also highlight the fact that *caspar* interacts with *VAP^{P58S}* non-cell autonomously, as its overexpression in the non-neuronal cells suppresses the life span defect whereas its knockdown enhances it. Motor neuronal overexpression

of *caspar* but not its knockdown shows a change in the life span of $\Delta VAP; gVAP^{P58S}$ flies, alluding to the cell autonomous effect of *caspar*, which seems to be more sensitive with respect to increase in its levels in the motor neurons and not so much with its reduction.

The *TER94* mutant (R152H) acts as a suppressor on its glial expression, fails to show any change in case of its motor neuronal expression (Fig. I.1. C and D), while it enhances the $\Delta VAP; gVAP^{P58S}$ lifespan marginally in muscles. $TER94^{R152H}$ thus seems to be interacting with VAP^{P58S} via glia and possibly also via muscles. These interactions are consistent with the effects of overexpression and knockdown of *TER94* in muscles, glia and motor neurons, which show potential interactions with VAP^{P58S} via glia and muscles but not via motor neurons (Chapter III, Table 3.5).

Appendix II

Overexpression of VAP^{P58S} in muscles, glia and motor neurons enhances the ΔVAP; $gVAP^{P58S}$ lifespan defects

Section 3.1.4 of Chapter III consolidates the outcome of the enhancer-suppressor screen performed in the three cell types of the tripartite synapse in the VAP^{P58S} background. Reiterating the outcome of perturbation of VAP levels in the three cell types, it was observed that the levels of VAP hold different degrees of importance among muscles, glia and motor neurons. We suspect that this difference of importance could be because of the differential importance of VAP or differential regulation of flux of VAP in the three cell types.

Observations from Chapter II (Chapter II, section 3.1 and 4) hint towards the possible role of the flux of VAP in the control of ΔVAP; $gVAP^{P58S}$ survival. The fact that flies with a single copy of $gVAP^{P58S}$ in the ΔVAP background survive for a few more days than the double copy, suggests enhanced toxicity caused by the second copy of $gVAP^{P58S.}$ Also, the fact that one copy of $gVAP^{WT}$ in combination with a single copy of $gVAP^{P58S}$ is sufficient to rescue the survival completely is another piece of evidence that fits into the idea of the importance of flux of VAP. However, this effect is not observed in the case of overexpression of VAP^{WT} in muscles or glia or motor neurons in the ΔVAP; $gVAP^{P58S}$ flies. In fact, the overexpression worsens the survival defect when overexpressed in muscles and glia (Chapter III, table 3.5), suggesting that regulated expression of VAP by its genomic promotor (like in case of $gVAP^{WT}$) probably manages the expression levels in such a manner that it is enough for the survival of the animal. This regulated expression also ensures no detrimental effects of VAP on the system.

Considering the data we have, overexpression of VAP^{P58S} in the $gVAP^{P58S}$ background might affect the flux of VAP in the system. This change of flux could be detrimental to the survival of the fly, given that it is a cell-specific expression of a mutant form of VAP. We overexpressed $UAS\text{-}VAP^{P58S}$ in muscles, glia and motor neurons in the ΔVAP; $gVAP^{P58S}$ flies and observed the lifespan of the F1 males. As predicted, excess VAP^{P58S} indeed causes a further reduction of life span in all three cases underpinning the toxic effects of its expression in all cells.
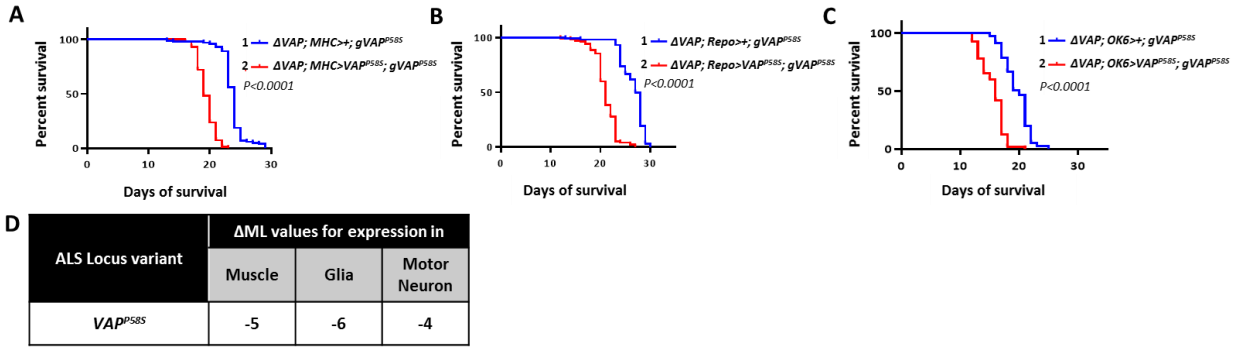
Figure II.1. Survival assay results for overexpression of VAP^{P58S} in muscles, glia and motor neurons in $gVAP^{P58S}$ background.
The blue curve represents **(A)** $\Delta VAP;\ MHC>+;\ gVAP^{P58S}$ (median=24), **(B)** $\Delta VAP;\ Repo>+;\ gVAP^{P58S}$ (median=27) **(C)** $\Delta VAP;\ OK6>+;\ gVAP^{P58S}$ (median=20) which are the controls for muscle, glial and motor neuronal expression respectively. The red curve represents the VAP^{P58S} overexpressed in muscles, glia and motor neurons respective types. The p-value from the log-rank test mentioned in each graph is the comparison of the red curve with the blue curve in each graph. n= around 60 flies. **(D)** Tabulated values of ΔML (Change in Median Lifespan) which is Median Lifespan (Experiment) – Median Lifespan (Control) for muscle, glial and motor neuronal overexpression of VAP^{P58S} respectively.

This result not only highlights the importance of regulated levels of *VAP* or VAP^{P58S} but also pinpoints that the overexpression of VAP^{P58S} in a cell autonomous, as well as the non-cell autonomous manner, is detrimental for the survival of the flies. Further investigation of the pattern of aggregates and progression of motor defects in these genotypic combinations will enable us to understand the dynamics of the extra dosage of VAP^{P58S} to the $\Delta VAP;\ gVAP^{P58S}$ flies.

Appendix III

Modulation of *VAP, TER94* and *SOD1* levels in the muscles in the ALS8 disease model

1. Introduction

As a follow up on the cell specific screen, we further validated few genetic interactions from the muscle specific screen from Chapter III. Here, we repeated the survival assays for muscle specific expression of *VAP, TER94, SOD1* and *alsin* using the $\Delta VAP; MHC$-$Gal4; gVAP^{P58S}$ fly line and have confirmed our results from Chapter III, Section 3.1.1. Unlike the initial screen (chapter III, Section 3.1.1), we have also used 'Gal4 controls' with these experiments. We have also performed motor assays for these genotypes and observe a trend of deterioration as an outcome of most allelic variants.

2. Results and Discussion

2.1. Muscle overexpression and knockdown of *VAP* leads to enhancement of lifespan defect and deterioration of motor abilities

VAP overexpression as well as knockdown in the muscle specific survival screen acts as an enhancer of $\Delta VAP; gVAP^{P58S}$ lifespan defect (Fig. III.1A and Chapter III, Section 3.1.1). The *VAP* knockdown in the wild type background, i.e. the Gal4 control, exhibits comparable lifespan to the master control (Fig. III.1A, Curve 3 Vs 1). Overexpression of *VAP* in the wild type background, however, seems to exert toxicity in the system by showing deterioration in lifespan (Fig. III.1A, Curve 2). This toxicity is consistent with the bouton morphology change of VAP overexpression in the muscles (Chapter V, Section 3.1.1).

The climbing assays for *VAP* modulated flies also demonstrate the same trend as that of its survival. The $\Delta VAP; MHC>VAP^{WT}; gVAP^{P58S}$ is worse than $\Delta VAP; MHC>VAP^{RNAi}; gVAP^{P58S}$, which is worse than the control (Fig. III.1B. Graph III, V and I) at a given time interval. The deterioration of climbing abilities for each genotype is evidently worse than their respective 'Gal4 controls' (Fig. III.1B, III Vs IV and V Vs VI). The 'Gal4 controls' show gradual deterioration in climbing, but except VAP^{WT} overexpression, the other genotypes display decent climbing abilities

(Fig. III.1B). Again, as we suspect, the worsening of the motor abilities in case of VAP^{WT} overexpression in muscles in the wild type background as compared to other genotypes is an effect of its toxicity in the system.
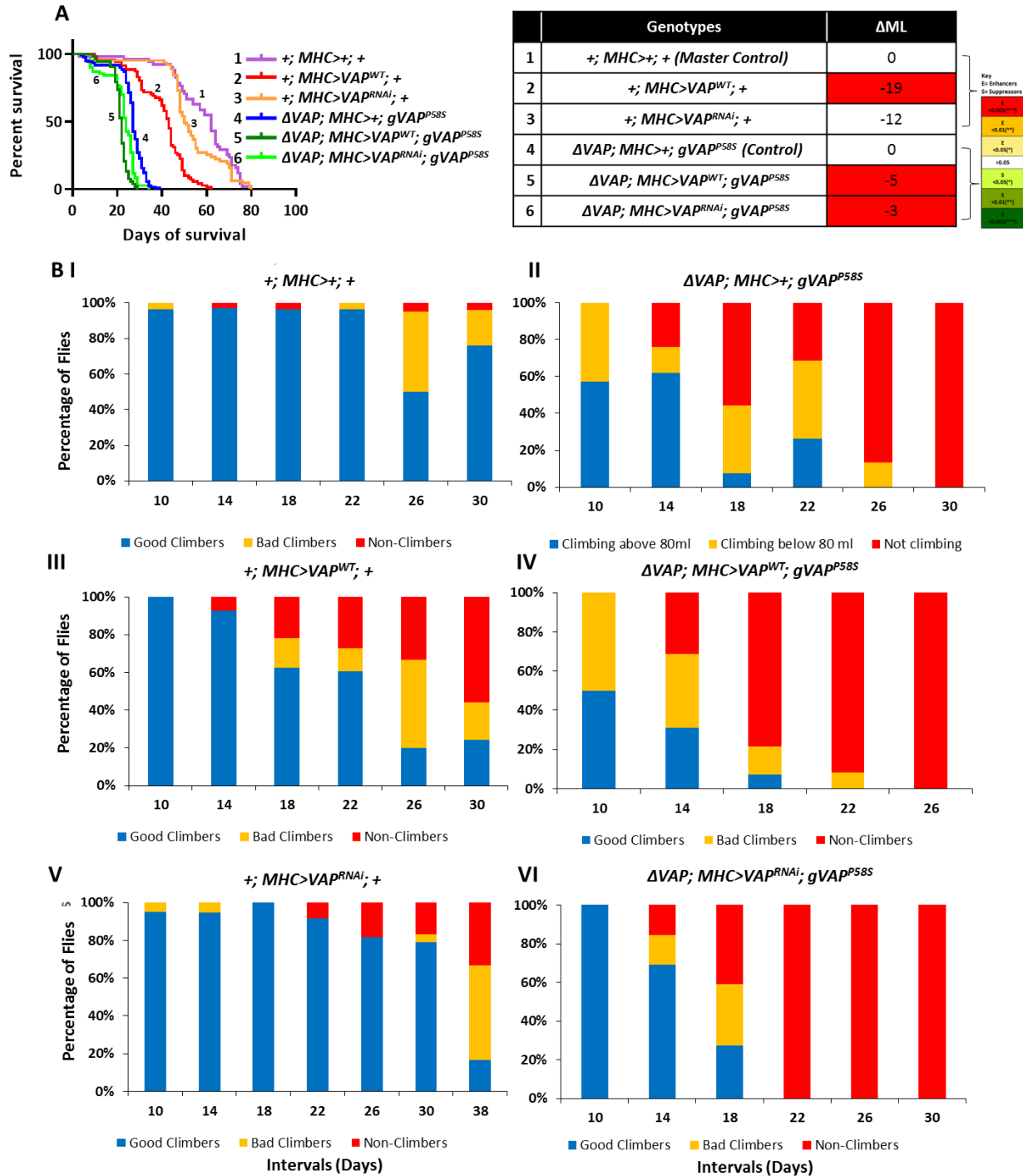
Figure III.1. Muscle expression of VAP^{WT} and VAP^{RNAi} in the ΔVAP; $gVAP^{P58S}$ background, leads to reduction of lifespan and deterioration of motor defects.

A) Overexpression of *VAP^WT^* (Red curve, number 2) and *VAP^RNAi^* (Orange curve, number 3), in the wildtype background; Overexpression of *VAP^WT^* (Dark green curve, number 5) and *VAP^RNAi^* (Light green curve, number 6), in the Δ*VAP; MHC-Gal4; gVAP^P58S^* background. Δ*VAP; MHC>+; gVAP^P58S^/+* (Curve 4 in blue color) was used as the control for curve 5 and 6, while *+; MHC>+;+* (Purple curve, number 1)was used as master control. Curve comparison was done using log-rank (Mantel-Cox test). Combined p-value for the whole set is <0.001.

The corresponding tabular results are in the form of ΔML (Change in Median Lifespan) = Median Lifespan (Experiment) – Median Lifespan (Control). Median Lifespan for control= 27 Days and for master control is 62 days.

Color/Statistical Key: The 'red-yellow tones' indicate different levels of statistical confidence (log-rank test) for the 'Enhancers (E)' while the 'green tones' represent the same for 'Suppressors (S)'. The brackets denote sets used for comparison.

B) Graphical representation of percentage of good climbers, bad climbers and non-climbers with time for *+; MHC>+;+*(I) , *+; MHC>VAP^WT^;+*(III), *+; MHC>VAP^RNAi^;+* (V), Δ*VAP; MHC>+; gVAP^P58S^/+* (II) , Δ*VAP; MHC>VAP^WT^; gVAP^P58S^/+* (IV), and Δ*VAP; MHC>VAP^RNAi^; gVAP^P58S^/+* (VI).

2.2. *TER94* overexpression and knockdown in Δ*VAP; gVAP^P58S^* background follows the same trend as that of *VAP* in the Δ*VAP; gVAP^P58S^* and wild type background

TER94 overexpression as well as knockdown shows an enhancement in lifespan defect as compared to the controls in Δ*VAP; gVAP^P58S^* background. It is also worth noting that *TER94* when overexpressed in muscles using *MHC-Gal4* in a wild type background, shows a reduction in lifespan as compared to the master control (Fig. III.2A, Curve 2). This outcome is similar to that of *VAP^WT^* overexpression in the wild type background (Fig. III.1). This suggests that TER94 affects the muscles independent of its interactions with *VAP^P58S^*, thus controlling the lifespan in flies. It also suggests that like in the case of VAP, even *TER94* has possible toxic effects on the system, although this effect is not reflected in the bouton architecture screen (Chapter V, Section 3.1.5).

TER94 variants also show progressive motor defects. The overexpression exhibits worsening of climbing ability in the Δ*VAP; gVAP^P58S^* as well as the wild type background (Fig. III.2B).

A)

	Genotypes	ΔML
1	*+; MHC>+; +* (Master Control)	0 62
2	*+; MHC>TER94^{WT}; +*	-26.5
3	*+; MHC>TER94^{RNAi}; +*	+2
4	*ΔVAP; MHC>+; gVAP^{P58S}* (Control)	0
5	*ΔVAP; MHC>TER94^{WT}; gVAP^{P58S}*	-3
6	*ΔVAP; MHC>TER94^{RNAi}; gVAP^{P58S}*	-5

Figure III.2. *TER94* overexpression as well as knockdown in Δ*VAP; gVAP^{P58S}* background, shows a deterioration in lifespan as well as motor defects as compared to Δ*VAP; MHC>+; gVAP^{P58S}* flies.
A) Overexpression of *TER94^{WT}* (Red curve, number 2) and *TER94^{RNAi}* (Orange curve, number 3), in the wildtype background; Overexpression of *TER94^{WT}* (Dark green curve, number 5) and *TER94^{RNAi}* (Light green curve, number 6), in the Δ*VAP; MHC-Gal4; gVAP^{P58S}* background. Δ*VAP; MHC>+; gVAP^{P58S}*/+ (Curve 4 in blue color) was used as the control for curve 5 and 6, while *+; MHC>+;+* (Purple curve,

203

number 1) was used as master control. Curve comparison was done using log-rank (Mantel-Cox test). Combined p-value for the whole set is <0.001.

The corresponding tabular results are in the form of ΔML (Change in Median Lifespan) = Median Lifespan (Experiment) – Median Lifespan (Control). Median Lifespan for control= 27 Days and for master control is 62 days.
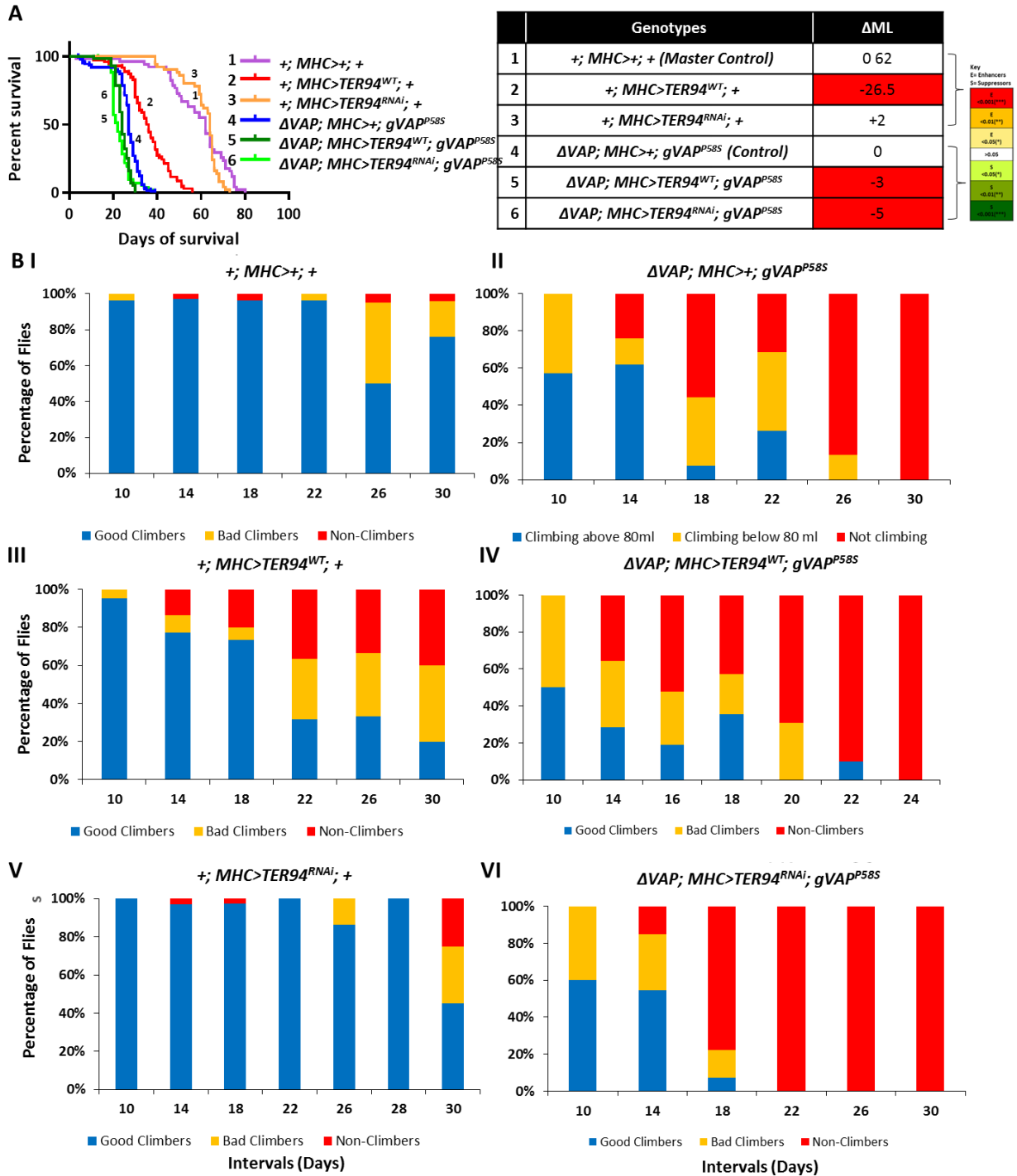
Color/Statistical Key: The 'red-yellow tones' indicate different levels of statistical confidence (log-rank test) for the 'Enhancers (E)' while the 'green tones' represent the same for 'Suppressors (S)'. The brackets denote sets used for comparison.

B) Graphical representation of percentage of good climbers, bad climbers and non-climbers with time for *+; MHC>+;+*(I) , *+; MHC>TER94^{WT};+*(III)*, +; MHC>TER94^{RNAi};+* (V)*, ΔVAP; MHC>+; gVAP^{P58S}/+* (II) *, ΔVAP; MHC>TER94^{WT}; gVAP^{P58S}/+* (IV)*,* and *ΔVAP; MHC>TER94^{RNAi}; gVAP^{P58S}/+* (VI).

2.3. Muscle overexpression and knockdown of *SOD1* in *ΔVAP; gVAP^{P58S}* background shows further reduction in lifespan and deterioration of climbing abilities

As observed in the Chapter III, Section 3.1.1, *SOD1^{WT}* as well as RNAi based knockdown were showing a significant enhancement in lifespan defects as compared to the control (Chapter III, Table 3.2). We repeated the experiment along with 'Gal4 controls' (Fig. III.3A). It is worth noting that, unlike overexpression of *VAP^{WT}* and *TER94^{WT}*, muscle overexpression of *SOD1^{WT}* in the wild type background doesn't result in reduction of lifespan as compared to *ΔVAP; MHC>SOD1^{WT}; gVAP^{P58S}* (Fig. III.3, Curve II and V). This result gives us confidence that *SOD1* in *ΔVAP; gVAP^{P58S}* background is in fact interacting with *VAP^{P58S}* via muscles and hence is contributing to the enhancement of the lifespan defect and it doesn't seem to affect the lifespan in the wildtype background. It could, however, also allude to the fact that increased SOD1 in the system is safer than increased VAP or TER94. Alternatively, SOD1 levels might be tightly regulated in the system than the VAP and TER94 levels.

The climbing assay for SOD1 muscle overexpression and knockdown, brings out the clear picture of SOD1 being involved in the deterioration of motor abilities of *ΔVAP; gVAP^{P58S}* via muscles (Fig. III.3B). As observed in the survival curve, the motor assays also depict that the phenotype of *SOD1* is majorly appearing in the *ΔVAP; gVAP^{P58S}* background and not in the wild type background. This steer clears of the possible artifacts of SOD1 muscle overexpression and knockdown.

Figure III.3. *SOD1* muscle overexpression as well as knockdown in *ΔVAP; gVAP^{P58S}* background, shows enhancement of lifespan and motor defects as compared to *ΔVAP; MHC>+; gVAP^{P58S}* flies.
A) Overexpression of *SOD1^{WT}* (Red curve, number 2) and *SOD1^{RNAi}* (Orange curve, number 3), in the wildtype background; Overexpression of *SOD1^{WT}* (Dark green curve, number 5) and *SOD1^{RNAi}* (Light green curve, number 6), in the *ΔVAP; MHC-Gal4; gVAP^{P58S}* background. *ΔVAP; MHC>+; gVAP^{P58S}/+* (Curve 4 in blue color) was used as the control for curve 5 and 6, while *+; MHC>+;+* (Purple curve, number 1) was used as master control. Curve comparison was done using log-rank (Mantel-Cox test). Combined p-value for the whole set is <0.001.

The corresponding tabular results are in the form of ΔML (Change in Median Lifespan) = Median Lifespan (Experiment) – Median Lifespan (Control). Median Lifespan for control= 27 Days and for master control is 62 days.

Color/Statistical Key: The 'red-yellow tones' indicate different levels of statistical confidence (log-rank test) for the 'Enhancers (E)' while the 'green tones' represent the same for 'Suppressors (S)'. The brackets denote sets used for comparison.

B) Graphical representation of percentage of good climbers, bad climbers and non-climbers with time for +; MHC>+;+(I) , +; MHC>SOD1^{WT};+(III), +; MHC>SOD1^{RNAi};+ (V), ΔVAP; MHC>+; gVAP^{P58S}/+ (II) , ΔVAP; MHC>SOD1^{WT}; gVAP^{P58S}/+ (IV), and ΔVAP; MHC>SOD1^{RNAi}; gVAP^{P58S}/+ (VI).

Appendix IV

Muscle expression of human allelic variants of *FUS* (mammalian *caz)* enhances the survival defect of Δ*VAP; gVAP^P58S^*

1. Introduction

In the enhancer-suppressor screen performed in Chapter III, section 4.1, we did not make use of the mutant variants of any ALS loci. However, these variants were used in the bouton morphology screen performed in Chapter IV. Out of these variants, muscle expression of FUS^{R521C} and FUS^{WT} using *MHC-Gal4* caused drastic NMJ defects along with significant changes to bouton size and bouton number (Chapter V, Figure 5.7). These two variants are human orthologues expressed in *drosophila* and are lethal when overexpressed in glia and motor neurons (Chapter V, Table 5.6). They also cause lethality on use of the stronger muscle driver, *G14-Gal4* (Chapter V, Section 3.1.3). Since the use of *MHC-Gal4* for these variants of *FUS* shows bouton morphology change, we were curious to observe the outcome of the muscle expression of these variants on the lifespan of the Δ*VAP; gVAP^P58S^* flies using *MHC-Gal4.*

2. Results and Discussion

The mating scheme followed for these experiments was same as Chapter III, Fig. 4.2. On performing survival assay by crossing $UAS\text{-}FUS^{R521C}$ and $UAS\text{-}FUS^{WT}$ to Δ*VAP; MHC-Gal4; gVAP^P58S^*, we observed that both result in significant enhancement of lifespan defect. Further investigation using appropriate Gal4 controls will shed more light on the possible interaction of FUS^{R521C} and FUS^{WT} with $VAP^{P58S.}$
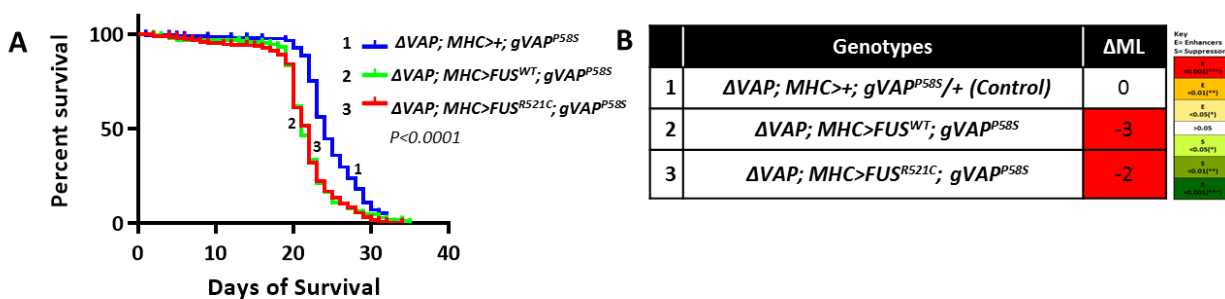
Figure IV.1. Survival analysis of Δ*VAP; MHC>FUS^WT^; gVAP^P58S^* **and** Δ*VAP; MHC>FUS^R521C^; gVAP^P58S^* **versus** Δ*VAP; MHC>+; gVAP^P58S^* .

A) The blue curve (#1) represents the $\Delta VAP; MHC>+; gVAP^{P58S}$ (median=24) which is the control. The red curve (#2) represents $\Delta VAP; MHC>FUS^{WT}; gVAP^{P58}$ (median=21) and the light green curve (#3) represents $\Delta VAP; MHC>FUS^{R521C}; gVAP^{P58S}$ (median=22). The overall p-value as well as individual p-value (on comparison with blue curve) is <0.0001. n= about 100 flies for each genotype.

B) Tabulated results are in the form of ΔML (Change in Median Lifespan) = Median Lifespan (Experiment) – Median Lifespan (Control).

Color/Statistical Key: The 'red-yellow tones' indicate different levels of statistical confidence (log-rank test) for the 'Enhancers (E)' while the 'green tones' represent the same for 'Suppressors (S)'.

Despite of the possible genetic interactions, it is important to note that the expression of human variants in *Drosophila* causes an exogenous gene to be overexpressed in the system, which could impart toxicity and possible artefactual effects. Therefore resorting to use of *Drosophila* orthologues of these variants for further studies is recommended.

Appendix V

Development of a *LexA-LexAop* system for *VAP^WT* or *VAP^P58S* overexpression

1. Introduction

LexA-LexAop system, similar to the *UAS-Gal4* system, is a binary overexpression system adapted from yeast. The *LexA* is the transcriptional activator and *LexAop* is the effector (Rodriguez et al., 2011; Lai and Lee, 2006; Yagi et al., 2010, Gohl et al., 2011). It can be used in combination with the *UAS-Gal4* system to regulate the expression of two genes temporally and/or spatially in *Drosophila*. We aimed to build *VAP^WT-LexAop* and *VAP^P58S-LexAop* fly lines to use in combination with the *UAS-Gal4* system, to gain more insight into the non-cell autonomous role of *VAP* for our future work.

2. Methodology

2.1. Molecular Cloning

To generate the *LexAop* fly lines, the *VAP^WT* or *VAP^P58S* genes with Not1 and Xba1 flanked on the two sides were PCR amplified using 5'TTCAGGCGGCCGC-ATGGACTACAAAGACGATGACAAGATGGCAAATCACTCTTCCG3' as the forward primer and 5'ATCCTCTAGATCAGAGAAAGAATTTGCCCAGCA 3' as the reverse primer. The forward primer has a Not1 site followed by a FLAG tag while the reverse primer has an Xba1 site. The amplified gene was cloned using restriction digestion method in pJRFC19-13XLexAop2-IVS-myr:: GFP (addgene26224, 9011bp) vector by replacing the myr-mCD8::GFP with *VAP^WT* and *VAP^P58S* in two separate constructs. The insertions were confirmed using restriction digestion and PCR for both constructs.
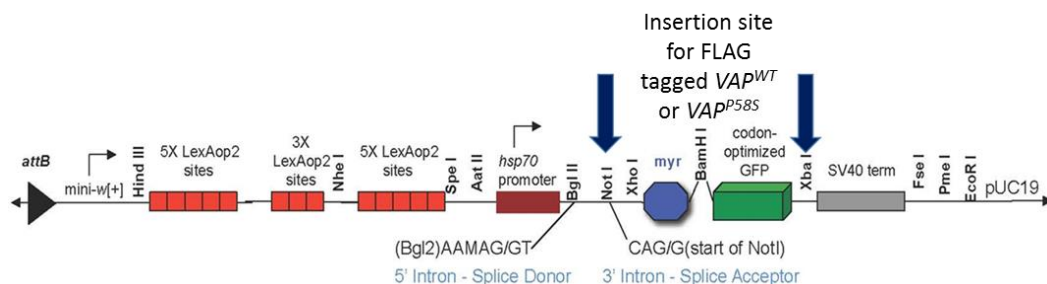
Figure V.1. Cloning strategy for the *LexAop* constructs.

The parent vector in a linearized form, displays the *myr:: GFP* site in between Not1 and Xba1. The *VAP^{WT}* and *VAP ^{P58S}* genes replaced the myr:: GFP. The cloning strategy used was ligation based cloning. Not1 and Xba1 are the restriction sites of interest. On excision of the *myr:: GFP*, the FLAG tagged *VAP^{WT}* and *VAP^{P58S}* were ligated in two separate constructs.

2.2. Fly strains for the binary system experiments

Site specific insertion of the *VAP^{WT}-LexAop* and *VAP^{P58S}-LexAop* constructs was done in the C-CAMP facility, Bangalore. The insertions are in the second chromosome's AttP40 site.

3. Results and Discussion

Two fly lines each, were made for the *LexAop-VAP^{WT}* and *LexAop-VAP^{P58S}* constructs. These are balanced with *CyO* as well as *Cyo:: GFP* separately. As described earlier, the overexpression of *VAP^{P58S}* pan-neuronally using the *UAS-Gal4* system, leads to aggregation of VAP in the third instar larval brains, unlike in the case of *VAP^{WT}* overexpression (Chaplot et al., 2019). These results were observed on use of an anti-VAP antibody.

In order to confirm if the *LexAop-VAP^{WT}* and *LexAop-VAP^{P58S}* fly lines replicate the aggregation phenotype, we used *Elav-LexA* (BL 52676), a pan-neuronal LexA driver, to drive the expression of *VAP^{WT}* and *VAP^{P58S}*. The third instar larval brains of the F1 of these crosses were stained for VAP in order to observe the presence of aggregates. The *LexAop-VAP^{P58S}* shows presence of aggregates, while the *LexAop-VAP^{WT}* shows absence of aggregates.
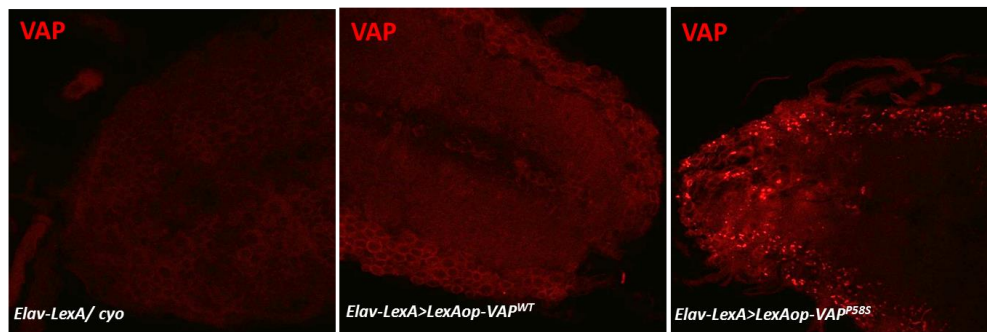
Figure V.2. Neuronal overexpression of VAP^{P58S} using the *LexA-LexAop* system causes punctate localization of VAP.
The ventral nerve cord of third instar larval brains for *Elav-LexA* and *Elav-LexA>LexAop-VAP^{WT}* show VAP staining around the membranes and an absence of VAP aggregates. The ventral nerve cord of the third instar larval brains for *Elav-LexA>LexAop-VAP^{P58S}* shows presence of VAP aggregates, similar to *Elav-Gal4>UAS- VAP^{P58S}* (not shown).

The *LexA-LexAop* system thus replicates the aggregation phenotypes of *UAS-VAP*[P58S.] Further characterization of bouton morphology, motor defects and life span will tell us more about this system. Nevertheless, it is a good tool to be used along with the *UAS-Gal4* (Ting et al., 2011) and the *VAP* genomic expression system, to perturb different genes simultaneously, in order to delve deeper into the gene regulatory networks of *VAP* and other ALS loci.

4. References

Gohl, D. M. *et al.* A versatile in vivo system for directed dissection of gene expression patterns. *Nat. Methods* 8, 231–237 (2011).

Lai, S., Lee, T. Genetic mosaic with dual binary transcriptional systems in *Drosophila*. *Nat Neurosci* 9, 703–709 (2006).

Rodríguez, Alberto *et al.* "Power tools for gene expression and clonal analysis in Drosophila." *Nature methods* vol. 9,1 47-55. 28 Dec. 2011, doi:10.1038/nmeth.1800

Ting, Chun-Yuan *et al*. "Focusing transgene expression in Drosophila by coupling Gal4 with a novel split-LexA expression system." *Genetics* vol. 188,1 (2011): 229-33. doi:10.1534/genetics.110.126193

Yagi, R., *et al*. Refined LexA transactivators and their use in combination with the Drosophila Gal4 system. *Proc. Natl. Acad. Sci. U. S. A.* 107, 16166–16171 (2010).

Appendix VI

Monensin sensitive 1 regulates dendritic arborization in *Drosophila* by modulating endocytic flux

Rohit H Krishnan[A,1,#], Shweta Tendulkar[1,#], Senthilkumar Deivasigamani[B,1,*], Anuradha Ratnaparkhi[2,*], Girish S Ratnaparkhi[1,*]

[1]Indian Institute of Science Education & Research (IISER), Pune, INDIA

[2]Agharkar Research Institute, Pune, INDIA

*Corresponding authors

#Equal contribution

Abbreviations

Monensin sensitive 1 (Mon1), Ramification Index (R.I), Dendritic area (D.A), Dendrite length (D.L) and Dendritic branch points (D.BP)

1. Summary

Monensin Sensitive 1 (Mon1) is a component of the Mon1:Ccz1 complex that mediates Rab5 to Rab7 conversion in eukaryotic cells by serving as a guanine nucleotide exchange factor for Rab7 during vesicular trafficking.

We find that Mon1 activity modulates the complexity of Class IV dendritic arborization (da) neurons during larval development. Loss of Mon1 function leads to an increase in arborization and complexity, while increased expression, leads to reduced arborization. The ability of Mon1 to influence dendritic development is possibly a function of its interactions with Rab family GTPases that are central players in vesicular trafficking. Earlier, these GTPases, specifically Rab1, Rab5, Rab10 and Rab11 have been shown to regulate dendritic arborization. We have conducted genetic epistasis experiments, by modulating the activity of Rab5, Rab7 and Rab11 in da neurons, in *Mon1* mutants, and demonstrate that the ability of Mon1 to regulate arborization is possibly due to its effect on the recycling pathway.

Dendritic branching is critical for proper connectivity and physiological function of the neuron. An understanding of regulatory elements, such as Mon1, as demonstrated in our study, is essential to understand neuronal function.

2. Introduction

Dendritic arbors are complex neuronal structures with distinct morphological features (Cajal, 1999;Garcia-Lopez et al., 2010;Berry and Nedivi, 2017). During neuronal development, morphogenetic processes that are not yet completely understood, lead to formation of arbors with defined size, geometry, innervation and tiling patterns. The dendritic tree structure is unique to a given neuronal cell type and plays a fundamental role in establishing specific neuronal connectivity. An intrinsic genetic program patterns the arbors using molecular processes that are distinct from those that make axons. These are found to be dependent on both, internal as well as external cues (Parrish et al., 2007;Jan and Jan, 2010). The growth and development of dendritic arbors are also concurrent in time and space with synapse formation with proteins of the postsynaptic density playing an integral role in morphogenesis (Cantallops et al., 2000;Cline, 2001;Peng et al., 2009).

The embryonic and larval peripheral nervous system (PNS) in *Drosophila melanogaster* has served as an excellent model system for studying mechanisms that govern dendritic arbor complexity and tiling. The PNS consists of 45 sensory neurons per hemisegment which are classified into type I and type II neurons (Grueber et al., 2003;Orgogozo and Grueber, 2005). The type II neurons are multidendritic whose dendrites innervate the epidermis. Dendritic arborization (da) neurons are a type of multidendritic neurons which are further classified into class I to IV on the basis of their dendrite field complexity with class IV da neurons having the most complexity in terms of the number of dendrites and their branching (Grueber et al., 2002). The arbor complexity in da neurons is determined through a combinatorial expression of transcription factors indicating the process is hard-wired and intrinsic to the neuronal class (Jinushi-Nakao et al., 2007).

As in other organisms (Dong et al., 2015;Prigge and Kay, 2018) the process of morphogenesis is regulated by signaling mediated by external cues such as Slit and Semaphorins (Jan and Jan, 2010;Meltzer et al., 2016), kinases such as Tricornered (Emoto et al., 2004) and a range of cellular processes that include intracellular trafficking, translational control and cytoskeletal dynamics (Ye et al., 2004;Satoh et al., 2008;Delandre et al., 2016).

Rab proteins are key regulators of intracellular trafficking. Both endocytic and exocytic pathways are believed to contribute to dendrite growth and branching (Jan and Jan, 2010;Dong et al., 2015;Valnegri et al., 2015). Constituents implicated include Rab5 (Satoh et al., 2008;Mochizuki et al., 2011;Copf, 2014;Zhang et al., 2014;Kanamori et al., 2015;Wang et al., 2017), Rab10 (Zou et al., 2016), Shrub (Sweeney et al., 2006) and Rop (Peng et al., 2015).

In this study we demonstrate that *Drosophila* Monensin Sensitivity 1 (DMon1; (Yousefian et al., 2013;Deivasigamani et al., 2015;Dhiman et al., 2018), a core component of the Mon1:CCZ1 complex (Wang et al., 2002;Nordmann et al., 2010;Poteryaev et al., 2010), and central to conversion of early endosomes to late endosomes, regulates morphogenesis of Class IV da (CIVda) neurons. We uncover a role for Mon1 by demonstrating that CIVda patterning can be regulated by increasing or decreasing Mon1 function during embryonic/larval development: loss of Mon1 leads to increased branching while overexpression suppresses it. Consistent with its position in the endocytic pathway, we find that Mon1 functions genetically downstream of Rab5. Surprisingly however, the regulation by Mon1 does not seem to be dependent on the late endosomal-lysosomal pathway. Rather, the modulation appears to be via the Rab11 mediated recycling pathway. We

propose that in the context of the da neurons, Mon1 serves to balance the endocytic flux flowing through the endo-lysosmal and recycling pathways to regulate dendrite morphogenesis.

3. Results

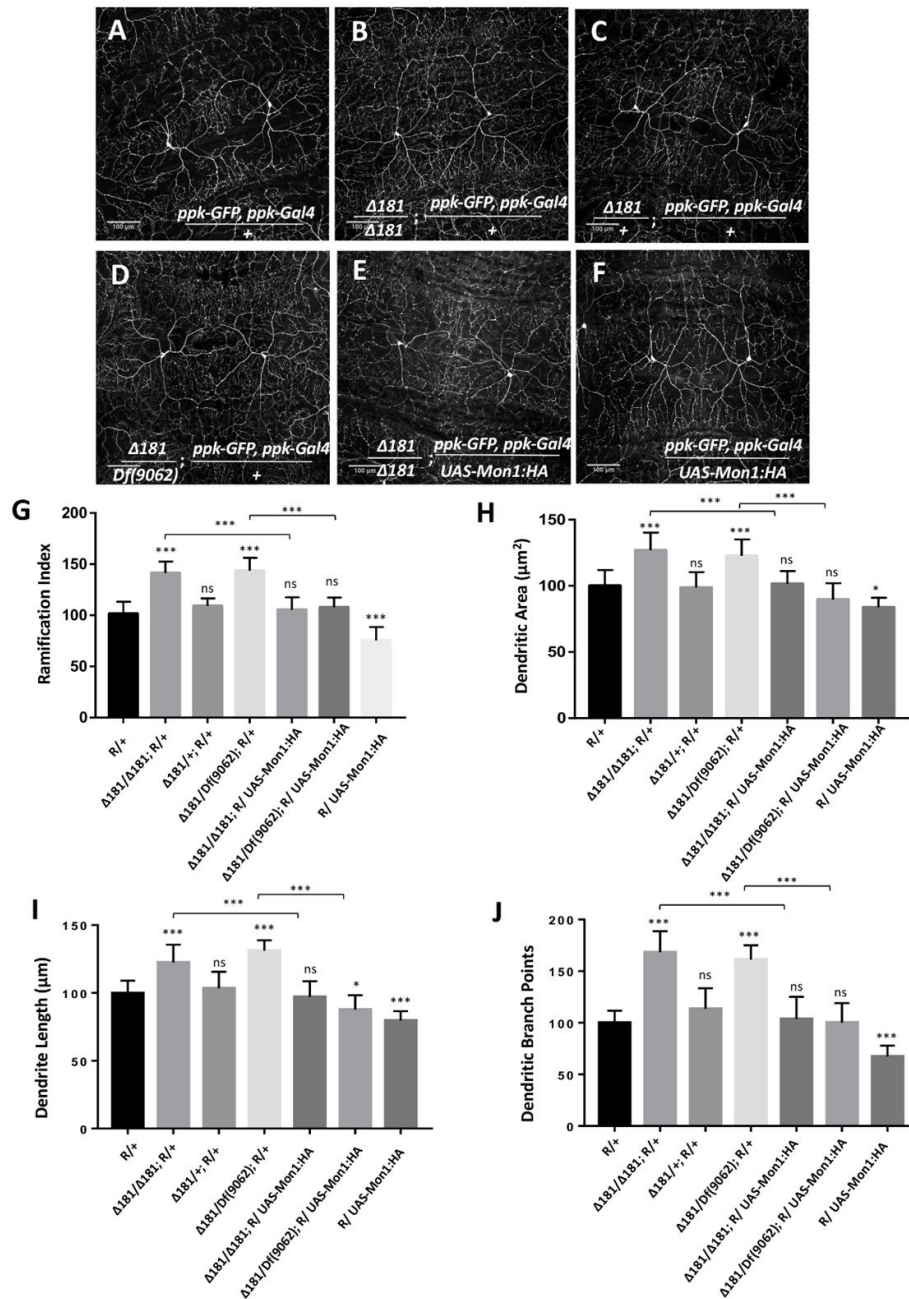### 3.1. Mon 1 modulates dendritic branching in Class IV da neurons

CIVda neurons express *pickpocket* (*ppk*), a gene involved in nociception in *Drosophila* (Adams et al., 1998;Crozatier and Vincent, 2008). We recombined *ppk-Gal4* (BL32079; (Grueber et al., 2007;Kanamori et al., 2013)) with a membrane localized GFP expressed under a *ppk* regulatory element (*ppk-GFP* (BL35843)(Kanamori et al., 2013), and generated a reporter line ('R', See Materials & Methods, Appendix VI) that allows visualization of CIVda neuron morphology in response to genetic manipulation either through gene knock-down and overexpression in the third instar larva of *Drosophila* (Fig. VI.1A). This reporter ('R') line was used to observe the arborization of CIVda in the *Dmon1^{Δ181}* (Δ181) line, a loss of function allele of *Mon1* (Deivasigamani et al., 2015). When compared to a wild-type control, CIVda in *Dmon1* mutant showed enhanced dendritic branching with a ramification index (R.I), of approximately 80 as compared to 60 in wild type larvae. On normalization, with the reporter line set to 100, *Dmon1* mutant shows 45% increase in R.I. (Fig. VI.1B, 1G). This increase in R.I was however not observed in a heterozygous condition (Fig. VI.1C, 1G), suggesting that a single copy of *Dmon1* is sufficient to regulate dendritic arborization in the CIVda neurons. In order to confirm the result, we quantified R.I in *Dmon1^{Δ181}/Df(9062)*, an allelic combination, where Df(9062) is a deficiency that uncovers the *Mon1* locus (Deivasigamani et al., 2015). An increase in RI by 47% (Fig. VI.1G) similar to that in *Dmon1^{Δ181}* homozygote confirmed that it is the loss of *Dmon1* that leads increased R.I of CIVda neurons. Other parameters (see Materials & Methods, Appendix VI), such as dendritic area (D.A; μM^2), dendritic length (D.L; μM) and number of dendritic branch points (D.BP) were also measured for the same set of images. Loss of *Dmon1* also led to an increase in average values, as compared to controls for D.A (51843 vs 65787 μM^2), D.L (14549 vs 17811 μM) and D.BP (492 vs 829). Normalized values, with the control R/+ set to 100 are displayed in the figures (Fig. VI.1H-J).

Further confirmation for the role for Mon1 in regulating CIVda branching was demonstrated by rescue of the dendritic phenotypes in homozygous *Dmon1^{Δ181}* (Fig. VI.1E) and *Dmon1^{Δ181}/* Df(9062) animals through expression of DMon1 in the *ppk* domain (Fig. VI.1G). In

both examples, the R.I, D.A, D.L and D.BP were restored to wild type or near wild type levels (Fig. VI.1).

In addition, overexpression of Mon1 in wildtype animals using *ppk*-GAL4 led to reduction of all four parameters measured (Fig. VI.1). R.I, D.L and D.BP were reduced significantly, while the reduction of D.A had lower statistical significance ('*';Fig. VI.1H). Together, these results demonstrate that arborization of the CIVda neurons during development is sensitive to the dose of Mon1 with decrease in Mon1 function leading to increased branching, dendritic length and area while enhancement of Mon1 function leads to a decrease in the measured parameters.

Figure VI.1. *Dmon1* **modulates dendritic arborization in Class IV da -neurons.**

A) A reporter (*ppk-Gal4; ppk-GFP*, diminutive 'R') line is used to visualize arborization in CIVda neurons at the third instar larval stage in *Drosophila melanogaster*. Sholl analysis (Image J) is used to calculate Ramification Index (R.I), which is then normalized, setting the 'R/+' at 100. The IMARIS software is used for neuron tracing and calculation of Dendritic area (D.A), Dendrite length (D.L) and Dendritic branch points (D.BP), with each parameter for the R/+ set at 100. n=15 (neurons), N=4 animals. Representative images are shown for this and other panels (B-F).

B) *Dmon1$^{\Delta181}$/Dmon1$^{\Delta181}$* larvae show enhanced arborization for Class IV arbors. n= 15, N=4.

C) A Single copy of *Dmon1* (*Dmon1$^{\Delta181}$/+*) does not show any significant increase in arborization. n= 14 neurons, N=4,

D) *Dmon1$^{\Delta 181}$/Df(9062)* increases arborization to the same extent as *Dmon1$^{\Delta 181}$/Dmon1$^{\Delta 181}$*. n= 15, N=4.

E) *UAS-Mon1:HA* driven by *ppk-Gal4* in *Dmon1* $^{\Delta 181}$ larvae, rescues the arborization defect in *Dmon1$^{\Delta 181}$/Dmon1$^{\Delta 181}$* and *Dmon1$^{\Delta 181}$/Df(9062)* (Image not displayed) to near normal levels. n=18, N=5 and n=9, N=4 respectively.

F) Overexpression of *Dmon1* in a wild type background, reduces the branching (D.BP), R.I and D.L significantly. The reduction in D.A is less significant. n=35, N=8.

G-J) Quantitation of the extent of arborization in CIVDa using four parameters, R.I, D.A, D.L and D.BP. Statistical analysis using Dunnet's multiple comparison test using GraphPad Prism 7 with exact p values listed in Suppl. Table VI.1. ns: not significant. ***p<0.001, *p<0.05 Error bars represent standard error.

3.2. Rabs modulate dendritic arborization

Mon1/SAND1 regulates Rab conversion in yeast, *C. elegans* and mammalian cells (Nordmann et al., 2010;Poteryaev et al., 2010;Yousefian et al., 2013). Mon1 in complex with Ccz1 functions as a guanine nucleotide exchange factor for Ypt7, the yeast orthologue of Rab7 (Nordmann et al., 2010). As in other model systems, in *Drosophila*, the recruitment of Rab7 on late endosomes is mediated by the Mon1-Ccz1 complex (Yousefian et al., 2013). In the study by Yousefian et. al., Mon1 loss of function leads to enlargement/enrichment of Rab5 positive early endosomes and concomitant loss of association of mature endosomes with Rab7, a feature that is replicated in CIVda neurons (Fig. VI.2). Rab4 and Rab5 co-localized on early endosomes while Rab11 distributions between mutant and wild-type cells were indistinguishable (Yousefian et al., 2013), a feature seen here in CIVda neurons (Fig. VI.2).
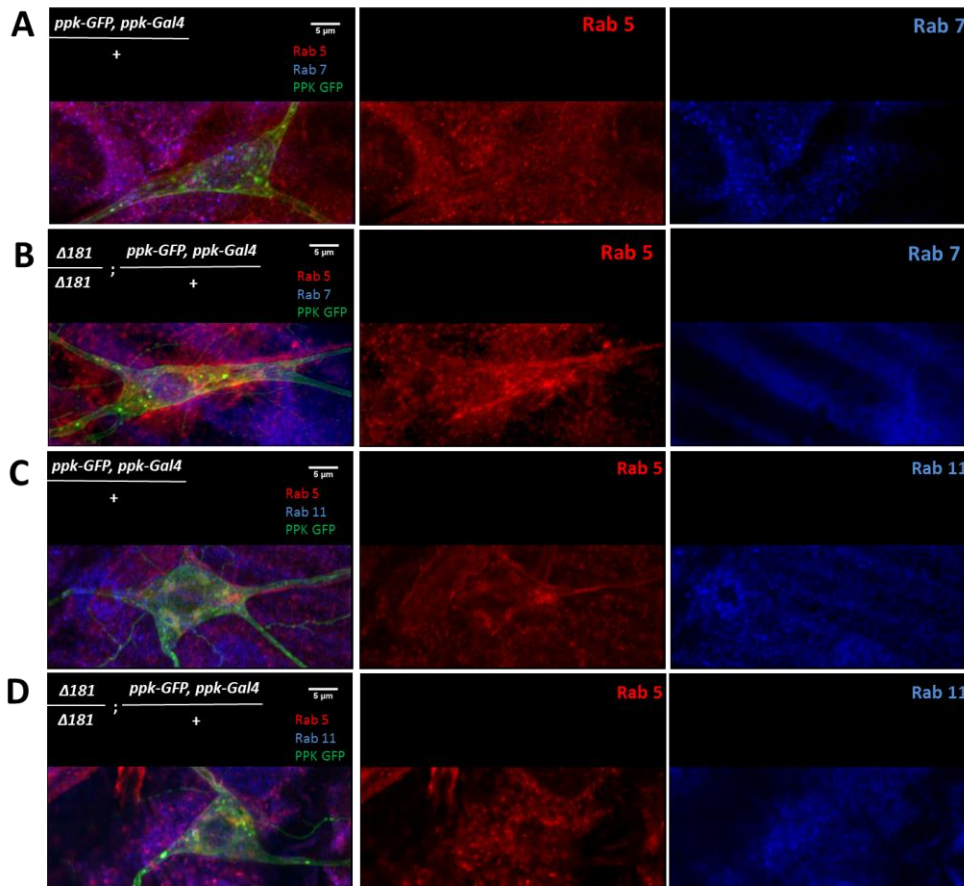
Figure VI.2. Antibody staining of cell body of CIVDa neurons with antibodies against GFP, Rab5, Rab7 and Rab11.
A) Control larvae with the reporter (R: *ppk-GFP, ppk-Gal4*) show localization of Rab5 and Rab7 as distinct punctate.
B) *Dmon1^{Δ181}/Dmon1^{Δ181}* displays enhanced accumulation of Rab5 as compared to the control, while the Rab7 does not show localization in endosomes.
C) Control larvae with the reporter (R: *ppk-GFP, ppk-Gal4*) show localization of Rab5 and Rab 11 as distinct punctate.
D) *Dmon1^{Δ181}/Dmon1^{Δ181}* mutant shows enhanced accumulation of Rab5, as compared to control, with increase in punctae. Rab11 punctae do not appear to change significantly.

Given the role of Mon1 in endocytic trafficking, we sought to explore the role of Rab proteins in Mon1 mediated CIVda morphogenesis (Fig. VI.3; Fig. VI.5A, B). An earlier study in *Drosophila* has implicated Rab5 and the distribution of Rab5 endosomes in the patterning of da neurons (Satoh et al., 2008), while Rab11 mediated recycling has been shown to be important in dendritic branching in rat hippocampal neurons (Satoh et al., 2008;Lazo et al., 2013). In *Drosophila*, the roles of Rab11 mediated recycling pathway or the Rab7 mediated degradative pathway in dendrite morphology has not been tested. We therefore sought to test this in the context

of Mon1 mutants through genetic epistasis, by using loss-of-function and gain-of-function transgenic lines against *Drosophila* Rab5, Rab7 and Rab11 genes. In agreement with earlier studies (Satoh et al., 2008), expression of Rab5 dominant negative (Rab5DN; Rab5 in a GDP-bound form) or knockdown using RNA interference, using *ppk-Gal4*, show a drastic reduction in the extent of arborization and branching (Fig. VI. 3B, D, J-K, Fig. VI.5A-B), with hypomorphic RNAi alleles demonstrating weaker effects. Our analysis indicated a 60-70% decrease in R.I., D.A, D.L and D.BP for the Rab5DN allele. In contrast, the constitutively active form of Rab5 (RAB5CA, GTP-bound form) did not show any significant differences in R.I, D.A and D.L (Fig. VI.3C, J, K; Fig. VI.5B), while the D.BP were decreased by 20% (Fig. VI.5A) in CIVda as compared to the control (Fig. VI.3A, J, K, Fig. VI.5A, B).

Cargo present in Rab5 positive early endosome cycle can be channeled down the degradation pathway involving Rab7 or the recycling pathway, marked by Rab11. We tested the involvement of these pathways by modulating the activity of Rab7 and Rab11. We found that increasing Rab7 activity through expression of a constitutively active (CA) form, or decreasing Rab7 function by using a dominant negative (DN) form of Rab7 or through expression of Rab7 RNAi the *ppk* domain (Fig. VI.3E, F, G, J, K; Fig. VI.5A, B) does not affect the arborization, branching, length or area of CIVda neurons. In contrast, expression of both, Rab11CA and Rab11DN altered arborization patterns in an opposing manner: increase in Rab11 activity increased R.I, D.A, D.L and D.BP, while a decrease in Rab11 activity reduced these parameters (Fig. VI.3H-K; Fig. VI.5A, B). Interestingly, the increase in parameters (15-40%) seen upon expression of Rab11CA (Fig. VI.3H-K) were correlated to and comparable with increase seen in Mon1 mutants, with the exception of D.BP, where Rab11CA has a weaker effect, suggesting that the Rab11 mediated recycling pathway plays a central role in CIVda patterning.
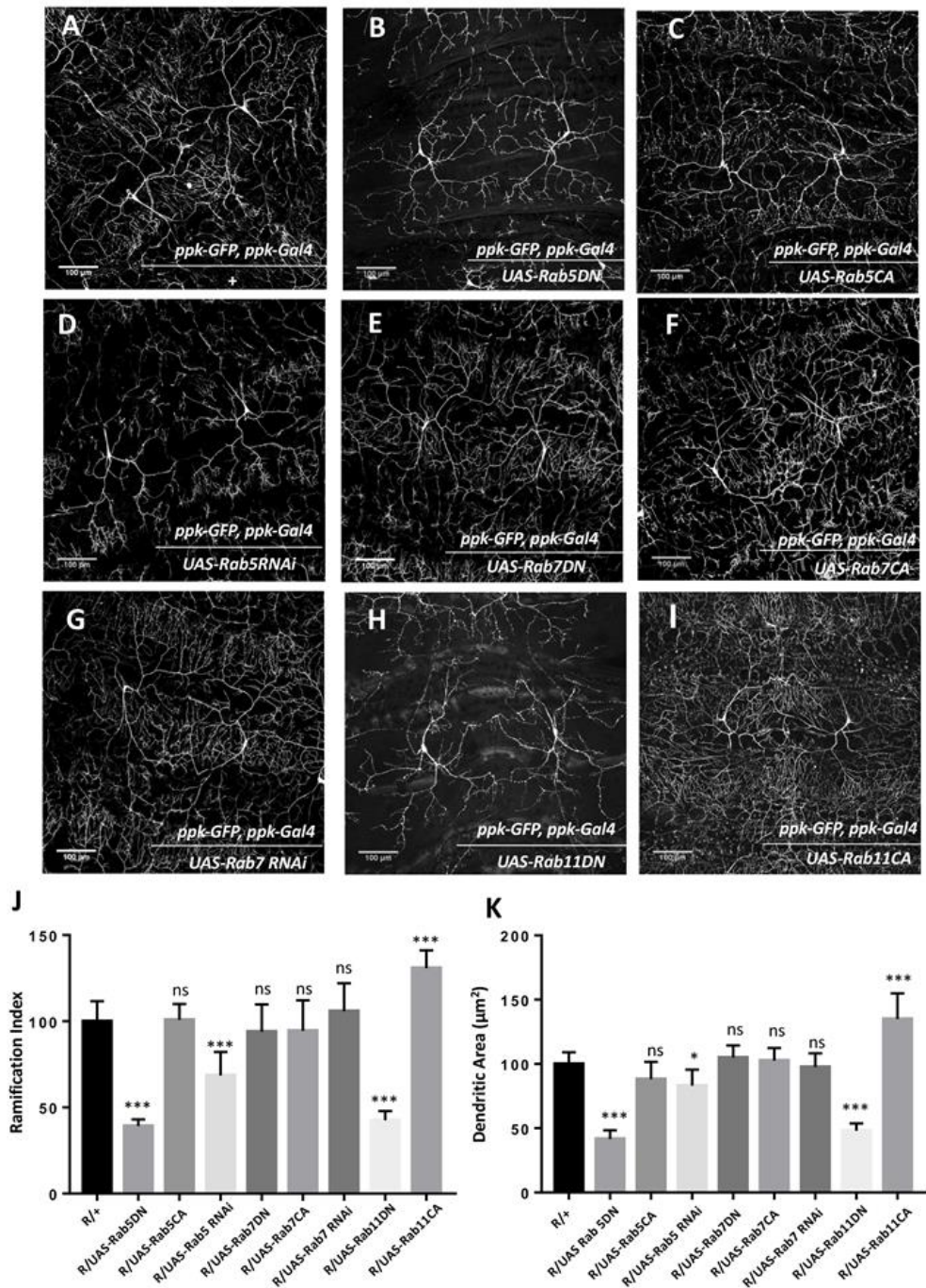
Figure VI.3. Rabs modulate dendritic arborization.

A) CIVda larvae imaged with the 'wild type' reporter line (R/+: *ppk-GFP, ppk-Gal4*). Representative images are shown (panel B-I) for all experiments.

B-D) Rab5DN mutant expression or Rab5 knockdown using RNAi, reduces arborization (for Rab5 DN: n=23, N=4; for Rab5 RNAi: n=40, N=7) in Class IV neurons but Rab5CA mutant expression does not show any change (n=18, N=4), when compared to control R/+ (n=55, N=5).

E-G) Rab7DN mutant expression, Rab7 knockdown using RNAi and Rab7CA mutant expression using

ppk-Gal4, do not show any difference in arborization as compared to wild type control (for Rab7DN: n=35, N=6; for Rab7 RNAi: n=43, N=7; for Rab7CA: n= 16, N=4).

H-I) Rab11DN reduces arborization (n=18, N=4) when expressed in Class IV da neurons whereas Rab11CA mutant expression increases dendritic arbor complexity (n=8, N=3).

J-K) Quantitation of the extent of arborization in CIVDa using R.I and D.A. Values for D.L and D.BP are displayed in Fig. VI.5.

ns: not significant, *$p<0.05$, ***$p<0.001$. Error bars represent standard error. Statistical analysis using Dunnet's multiple comparison test using GraphPad Prism 7 with exact p values listed in Suppl. Table VI.1.

3.3. Mon1 interacts with Rabs to modulate da

Since the activity of Rab5 and Rab11 strongly modulates arborization of CIVda neurons, we explored the nature of the interaction between these Rabs 5, 7 & 11 and Mon1 to uncover features of vesicular recycling that are important for CIVda morphogenesis (Fig. VI.4; Fig. VI.5C-H). We tested this by modulating activity of Rab5, Rab7 and Rab11 in the *Dmon1* loss-of-function line (*Dmon1$^{\Delta181}$* or Δ181), in combination with the reporter line (R) generated earlier (Fig. VI.1A, Materials & Methods, Appendix VI). Expression of Rab5CA in the *Dmon1$^{\Delta181}$* larvae showed a partial rescue (Fig. VI.4C, G, J; Fig. VI.5.C, F) of the increase in R.I, D.A, D.L and D.BP, seen in the mutants, while expression of Rab5DN in the *Dmon1$^{\Delta181}$* larvae led to a quantitative parameters (D.A., D.L and D.BP) that were comparable to that of Rab5DN alone (Fig. VI.4D, G, J; Supp. Fig. 2C, F).

Although Rab7 on its own does not seem to participate in the regulation of da (Fig. VI.3F, G, J, K), we found that expression of Rab7CA leads to a significant reduction of R.I, D.A., D.L and D.BP, as compared to control *Dmon1$^{\Delta181}$* larvae (Fig. VI.4H-K; Fig. VI.5D, G; Images not displayed) suggesting that activation of the downstream endo-lysosomal pathway can suppress excess arborization in the mutant. This may be an outcome of a flux change due to modulation of the lysosomal branch. Interestingly, Rab7 RNAi also suppresses Mon1 loss of function phenotype (Fig. VI.4H, K; Fig. VI.5D, G; Images not displayed), again suggesting change in flux of recycling vesicular trafficking in response to modulation of the lysosomal pathway. Expression of Rab11CA in *Dmon1$^{\Delta181}$* larvae (weakly) rescues all measured parameters (R.I, D.A, D.L) except D.BP. Expression of Rab11DN, with or without *Dmon1$^{\Delta181}$* in the background leads to lower values (decrease of 60-70%) of R.I, D.A., D.L and D.BP. This lends support to the view that the Rab11 mediated re-cycling pathway functions downstream of Mon1 and may play an important role in manifestation of the arborization defect in Dmon1$^{\Delta181}$ mutants.
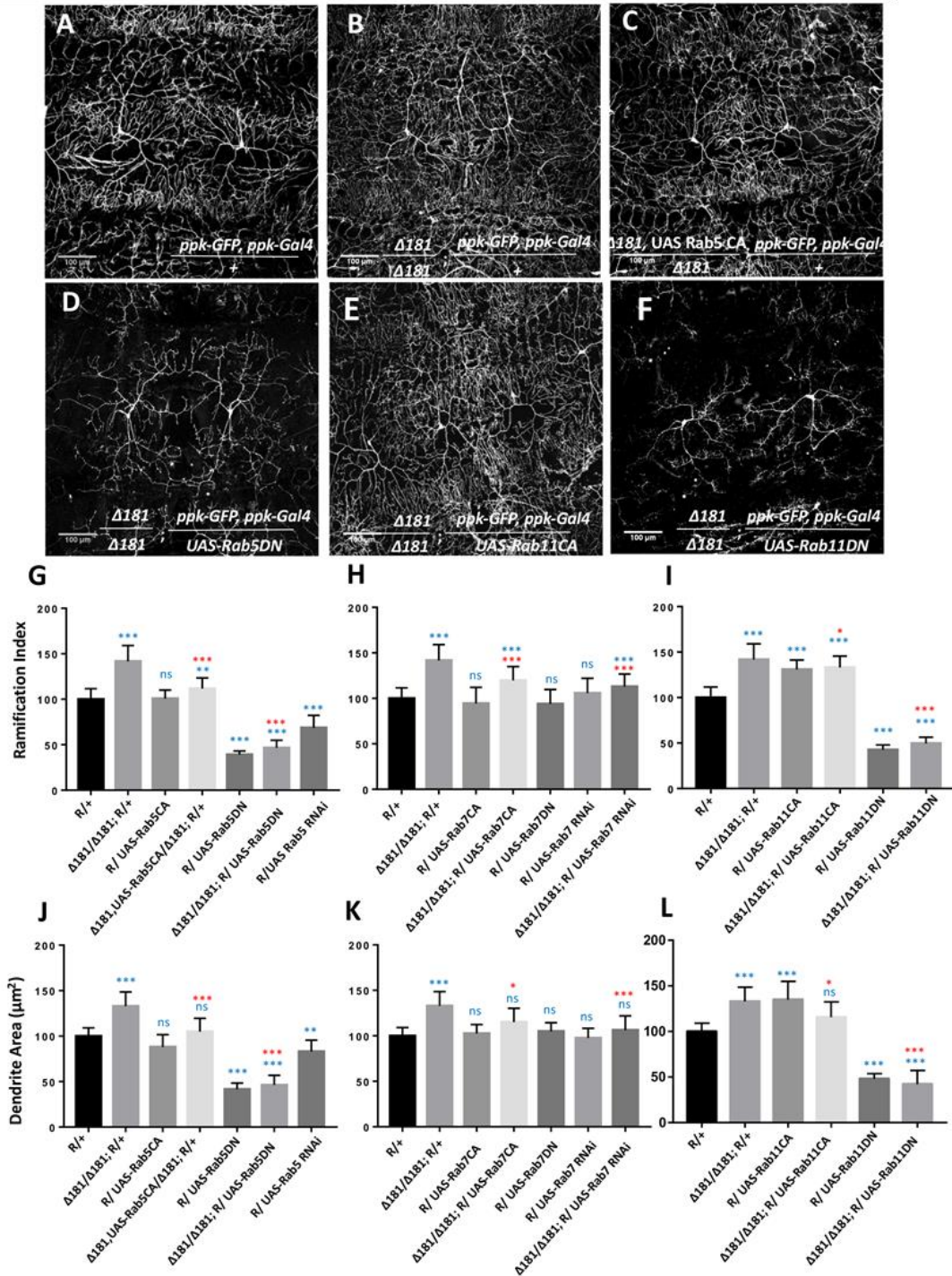
Figure VI.4. Mon1 interacts with Rabs to modulate dendritic arborization.
A-B) CIVda larvae imaged with the reporter line R/+ (n=55, N=7) and the *Dmon1$^{\Delta181}$/Dmon1$^{\Delta181}$; R/+*((n= 38, N=7). Representative images are shown (panel B-F) for all experiments. For panels G-L, blue asterix/n.s represents statistical comparison with wild type (R/+) while red asterix/n.s is a comparison with *Dmon1$^{\Delta181}$*. C-D) Rab5CA expression in *Dmon1$^{\Delta181}$* larvae shows significant reduction in parameters measured (R.I, D.A, D.L, D.BP) as compared to *Dmon1$^{\Delta181}$* (n=30, N=7). Rab5DN in *Dmon1$^{\Delta181}$* larvae shows reduction

in arborization as compared to both *Dmon1*^{*Δ181*} (n=26, N=5) and wild type larvae (n=26, N=5). Rab7CA expression in *Dmon1*^{*Δ181*} larvae shows reduction in arborization as compared to *Dmon1*^{*Δ181*} (n=20, N=4) and increase with respect to the wild-type (n=20 N=4). Rab7 RNAi in *Dmon1*^{*Δ181*} larave shows reduction in arborization as compared to *Dmon1*^{*Δ181*} (n=43, N=7) and increase with respect to the wild type (n=43, N=7). Images for these experiments are not shown but data is quantified in panels H &K.

E-F) Rab11CA in *Dmon1*^{*Δ181*} background shows reduction in arborization as compared to *Dmon1*^{*Δ181*} larvae (n=36, N=6) and increase with respect to the wild type larvae (n=36, N=6). Rab11 DN in *Dmon1*^{*Δ181*} larvae shows reduction in arborization as compared to *Dmon1*^{*Δ181*} (n=19, N=4) and decrease with respect to the control larvae (n=19, N=4).

G-L) Quantitation of the extent of arborization in CIVDa using R.I and D.A. Values for D.L and D.BP are displayed in Fig. VI.5.

ns: not significant, *$p<0.05$, **$p<0.01$, ***$p<0.001$. Error bars represent standard error. Statistical analysis using Dunnet's multiple comparison test using GraphPad Prism 7 with exact p values listed in Suppl. Table VI.1.
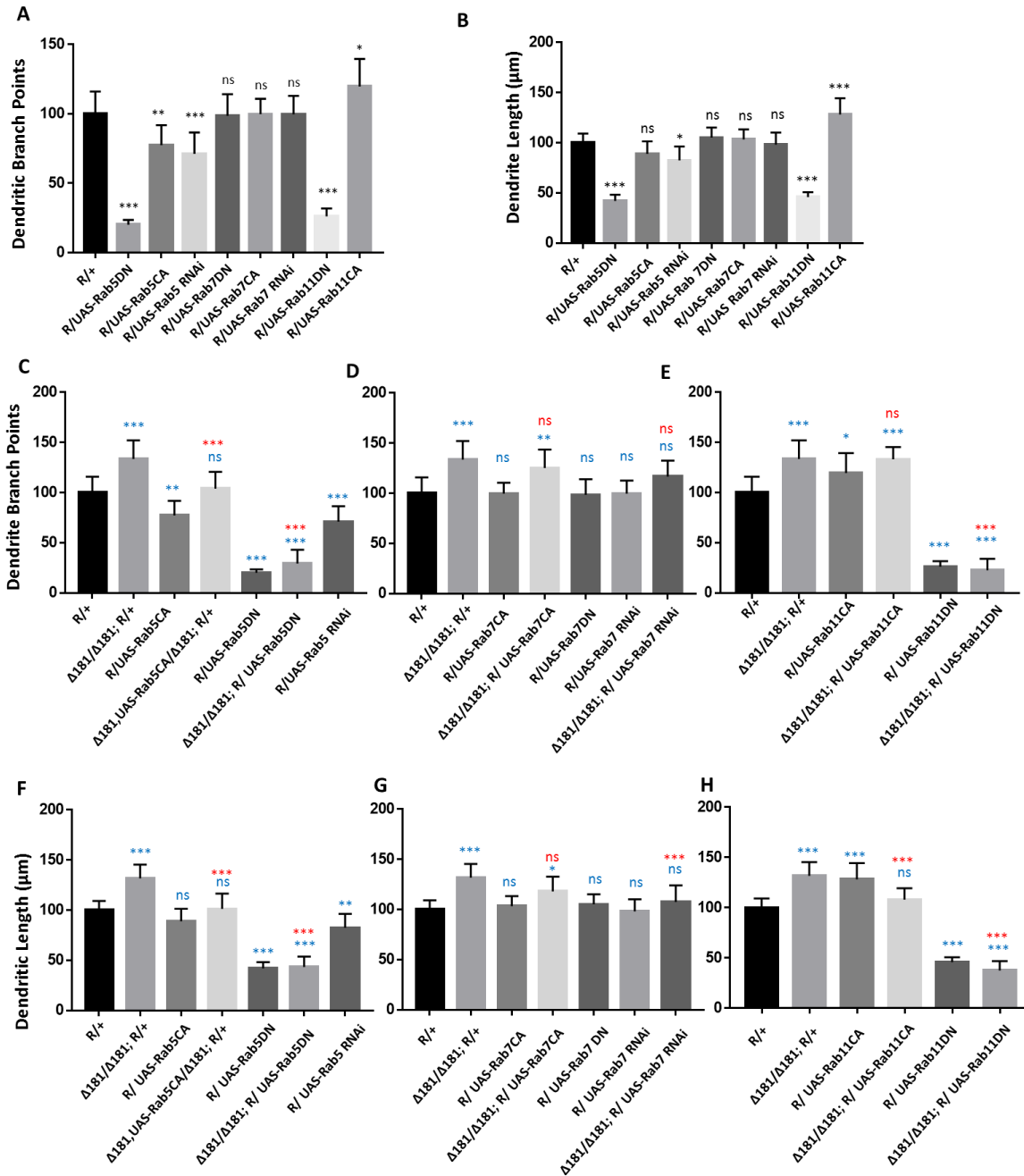
Figure VI.5. Quantitative parameters (D.BP, D.L, and D.A) for experiments displayed in Figures (VI.1, 3 and 4).

For all panels, blue asterix/ns represents statistical comparison with wild type (R/+) while red asterix/ns is a comparison with Dmon1$^{\Delta181}$.

A) Graph represents normalized values that appear to follow similar trend as that of the R.I.(Fig. VI.3). Statistical values for the genotypes when expressed in the *ppk-Gal4* domain in wild type animals: Rab5CA expression (N= 4, p=0.0073), Rab5DNexpression (N= 4, p=0.0001), Rab5 knockdown using RNAi (N= 4, p=0.0002), Rab7C expression (N= 4, p=0.9999), Rab7DN expression (N= 4, p=0.9997), Rab7 knockdown

226

using RNAi (N= 4, p=0.9999), Rab11CA expression (N= 4, p=0.0329), Rab11DN expression (N= 4, p=0.0001). n(number of neurons) analysed for each genotype is 10.

B) Quantitation of (total) dendritic length (D.L). Statistical Values for the genotypes when expressed using *ppk-Gal4* in wild type background are as follows: Rab5CA expression (N= 4, p=0.3142), Rab5DN expression (N= 4, p=0.0001), Rab5 knockdown using RNAi (N= 4, p=0.0164), Rab7CA expression (N= 4, p=0.9991), Rab7DNexpression (N= 4, p=0.9754), Rab7 knockdown using RNAi (N= 4, p=0.9996), Rab11expression (N= 4, p=0.0329), Rab11DN expression (N= 4, p=0.0001).

C-E) Quantification of number of Dendrite Branch points (D.BP) for the interaction of *Mon1* with different *Rabs*. Statistical values (blue *'s or ns), for the genotypes when expressed using *ppk-Gal4* in *Dmon1$^{\Delta 181}$* background as compared to control alone are as follows: Rab5CA expression(N= 4, p=0.9990), Rab5DN expression (N= 4, p=0.0001), Rab7CA expression (N= 4, p=0.0019), Rab7 knockdown using RNAi (N= 4, p=0.0992), Rab11CA expression (N= 4, p=0.0001), Rab11 DN expression (N= 4, p=0.0001).

Statistical values (red *'s or ns) for the genotypes when expressed with *ppk-Gal4* in *Dmon1$^{\Delta 181}$* background as compared to *Dmon1$^{\Delta 181}$* are as follows: Rab5CA expression(N= 4, p=0.0002), Rab5DN expression (N= 4, p=0.0001), Rab7CA expression (N= 4, p=0.8603), Rab7 knockdown using RNAi (N= 4, p=0.1021), Rab11CA expression (N= 4, p=0.9999), Rab11DN expression (N= 4, p=0.0001).

F-H) Quantification of Dendrite Length (D.L) for the interaction of *Mon1* with different *Rabs*. The graph represents normalized values which follow similar trend as that of the R.I.(Fig. VI.4). Statistical values (blue *'s or ns) for each of the genotypes when expressed in the *ppk-Gal4* domain in *Dmon1$^{\Delta 181}$* background as compared to control alone are as follows: Rab5CA expression(N= 4, p=0.9997), Rab5DN expression (N= 4, p=0.0001), Rab7CA expression (N= 4, p=0.0125), Rab7 knockdown using RNAi (N= 4, p=0.7656), Rab11CA expression (N= 4, p=0.7089), Rab11DN expression (N= 4, p=0.0001).

Statistical values (red *'s or ns) for the genotypes when expressed using *ppk-Gal4* in *Dmon1$^{\Delta 181}$* background as compared to *Dmon1$^{\Delta 181}$* are as follows: Rab5CA mutant overexpression(N= 4, p=0.0001), Rab5DN expression (N= 4, p=0.0001), Rab7CA expression (N= 4, p=0.1130), Rab7 knockdown using RNAi (N= 4, p=0.0002), Rab11CA expression (N= 4, p=0.0003), Rab11DN expression (N= 4, p=0.0001).

Note: Number of neurons analysed for all genotypes= 10, ns: not significant,. ***$p<0.001$, **$p<0.01$, *$p<0.05$ Error bars represent standard error. p values generated using Dunnet's multiple comparison test using Graphpad Prism 7.

Table VI.I. Consolidated values of statistical significance for Figure VI.1-VI.5

Fig VI. 1 (p-values)				
Genotype	R.I	D.A.	D.L.	D.N.P
R/+				
Δ181/Δ181; R/+	0.0001	0.0001	0.0001	0.0001
Δ181/+; R/+	0.354	0.9996	0.9459	0.3069
Δ181/Df 9062; R/+	0.0001	0.0002	0.0001	0.0001
Δ181/Δ181; R/ UAS-Mon1:HA	0.8759	0.9995	0.9726	0.9932
Δ181/Df 9062; R/ UAS-Mon1:HA	0.6435	0.1896	0.0475	0.9999
R/ UAS-Mon:HA	0.0001	0.0113	0.0003	0.0004

| FIG VI.3 (p-values)				
Genotype	R.I	D.A.	D.L.	D.N.P
			Suppl	Suppl
R/ UAS-Rab5DN	0.0001	0.0001	0.0001	0.0001
R/ UAS-Rab5CA	0.9997	0.3225	0.3142	0.0073
R/ UAS-Rab5 RNAi	0.0001	0.0482	0.0164	0.0002
R/ UAS-Rab7DN	0.1705	0.9904	0.9754	0.9997
R/ UAS-Rab7CA	0.5413	0.9994	0.9991	0.9999
R/ UAS-Rab7 RNAi	0.1571	0.9994	0.9996	0.9999
R/ UAS-Rab11DN	0.0001	0.0001	0.0001	0.0329
R/ UAS-Rab11CA	0.0001	0.0001	0.0329	0.0001
FIG VI.4 (p-values)	As compared to R/+			
Genotype	R.I	D.A.	D.L.	D.N.P
			VI.5	VI.5
Δ181/Δ181; R/+	0.0001	0.0001	0.0001	0.0001
R/ UAS-Rab 5CA	0.9997	0.3225	0.3142	0.0073
Δ181,UAS-Rab5CA/Δ181; R/+	0.0013	0.9908	0.9997	0.999
R/ UAS-Rab5DN	0.0001	0.0001	0.0001	0.0001
Δ181/Δ181; R/ UAS-Rab5DN	0.0001	0.0001	0.0001	0.0001
R/ UAS-Rab5 RNAi	0.0001	0.0482	0.0164	0.0002
R/ UAS-Rab7CA	0.5413	0.9994	0.9991	0.9999
Δ181/Δ181; R/ UAS-Rab7CA	0.0001	0.106	0.0125	0.0019
R/ UAS-Rab7DN	0.1705	0.9904	0.9754	0.9997
R/ UAS-Rab7 RNAi	0.1571	0.9994	0.9996	0.9999
Δ181/Δ181; R/ UAS-Rab7 RNAi	0.0001	0.9591	0.7656	0.0992
R/ UAS-Rab11CA	0.0001	0.0001	0.0329	0.0001
Δ181/Δ181; R/ UAS-Rab11CA	0.0446	0.085	0.7089	0.0001
R/ UAS-Rab11DN	0.0001	0.0001	0.0001	0.0329
Δ181/Δ181; R/ UAS-Rab11DN	0.0001	0.0001	0.0001	0.0001
FIG VI.4	As compared to Δ181/Δ181; R/+			
Genotype	R.I	D.A.	D.L.	D.N.P
			VI.5	VI.5
Δ181/Δ181; R/+				
R/ UAS-Rab 5CA				
Δ181,UAS-Rab5CA/Δ181; R/+	0.0001	0.0001	0.0001	0.0002
R/ UAS-Rab5DN				
Δ181/Δ181; R/ UAS-Rab5DN	0.0001	0.0001	0.0001	0.0001
R/ UAS-Rab5 RNAi				
R/ UAS-Rab7CA				
Δ181/Δ181; R/ UAS-Rab7CA	0.0001	0.0331	0.113	0.8603
R/ UAS-Rab7DN				
R/ UAS-Rab7 RNAi				
Δ181/Δ181; R/ UAS-Rab7 RNAi	0.0001	0.0002	0.0002	0.1021
R/ UAS-Rab11CA				
Δ181/Δ181; R/ UAS-Rab11CA	0.0001	0.0427	0.0003	0.9999
R/ UAS-Rab11DN				
Δ181/Δ181; R/ UAS-Rab11DN	0.0001	0.0001	0.0001	0.0001

4. Discussion

Mon1 is a conserved eukaryotic protein with a 'longin' domain. The domain has an alpha-beta-alpha sandwich architecture and is a feature of endocytic trafficking proteins (De Franceschi et al., 2014). Protein containing 'longin' domains include SANDs, SNAREs, targetins, adaptins and sedlins (De Franceschi et al., 2014). The dimeric Mon1:CCZ complex is involved in Rab conversion and is a GEF for Rab7 (Fig. VI.6A). Additionally, there is evidence that Mon1 can be secreted by neurons, either in membrane bound or unbound form (Deivasigamani et al., 2015). Mon1 may thus regulate anterograde signaling in synapses, both neuron:neuron or neuron:muscle. Recent research from our laboratory (Dhiman et al., 2018) also suggests that Mon1 in Octopaminergic neurons regulates systemic insulin signaling by regulating insulin producing cells.

CIVda neurons are sensitive to the dose of DMon1 in the cell. Decrease in *Dmon1* leads to increased complexity of arborization, which includes increase in branching, length and area covered by the axons. Increase in *Dmon1* decreases complexity of arborization and reduces the values of the parameters measured. Since Mon1 is primarily known for its role as a Rab converter in eukaryotic cells, we explored functions of Rab proteins Rab5, Rab 7 and Rab11 in regulating da by themselves and also in the context of *Dmon1* loss of function. Amongst the Rabs tested, Rab7 activity did not appear to affect dendritic morphology, suggesting that perturbation of late endosomal trafficking does not affect morphogenesis of CIVda neurons in larvae. This premise however can be strengthened by using Mosaic analysis with a repressible cell marker, studies. In contrast, Rab11 activity altered arbor complexity with decrease in Rab11activity leading to a dramatic decrease in arborization and expression of Rab11CA having an opposite effect (Fig. VI.4). This suggests that recycling endosomes play critical roles in determining arbor complexity which is in agreement with the role of Rab11 in dendrite morphogenesis in vertebrate systems (Villarroel-Campos et al., 2014;Peng et al., 2015;Gu et al., 2016). Since reduction of Rab5 activity also decreases arbor complexity, and Rab5 'sorting' endosomes are upstream (Fig. VI.6A) of both recycling endosomes (RE) and late endosomes (LE), we propose that vesicular flux through the RE but not the LE is a central determinant of CIVda morphogenesis (Fig. VI.6C). Loss of Rab5 leads to a decrease in the rate of RE formation, while loss of DMon1 changes the endocytic flux, shunting excess early endosomes (EE's) towards the RE pathway. In our model (Fig. VI.6C),

increase in activity of Mon1 enhances Rab5 to Rab7 conversion, reducing RE traffic leading to decreased arborization.

How does increase in RE flux lead to increase in dendritic complexity? Since endosomes marked with Rab11 can be exocytosed, we suggest that enhanced vesicular flux in the RE pathway leads to enhanced exocytosis, which in turn is correlated to increase dendritic arborization. This is in agreement with earlier studies where trafficking of cargo in Rab11 vesicles regulated dendritic complexity. For example, Lazo et. al. (Lazo et al., 2013) demonstrate that Rab11 regulates trafficking of brain derived neurotrophic factor along with its receptor TrkB while Peng et. al. (2015) have shown that the Rop-exocyst complex is important for dendritic branching in CIVda neurons. In contrast, data from the Klein lab (Yousefian et al., 2013), with experiments performed in the wing imaginal disc, suggest that Rab11 is not affected in the $Dmon1^{mut4}$ lines, and instead find changes in the Rab4 associated fast recycling pathway. In addition to protein and RNA based cargo, exocytosis also provides neuronal membrane that is critical for growth of the arbor, underscoring the importance of RE flux and exocytosis.

The balance of endocytosis and exocytosis is crucial for the growth and maintenance of CIVda arbors. Mon1 activity in the early 'sorting' endosomes may be important for modulating the flux through either the LE or RE pathways which in turn could lead to modulation of neuronal architecture. Our results thus underscore the role of endocytic flux in dendrite morphogenesis. The genetic interactions described here suggest a cell-autonomous role for Mon1. Given the ability of Mon1 to be secreted, it would be interesting, in future studies, to test for possible non-autonomous roles in dendrite development.
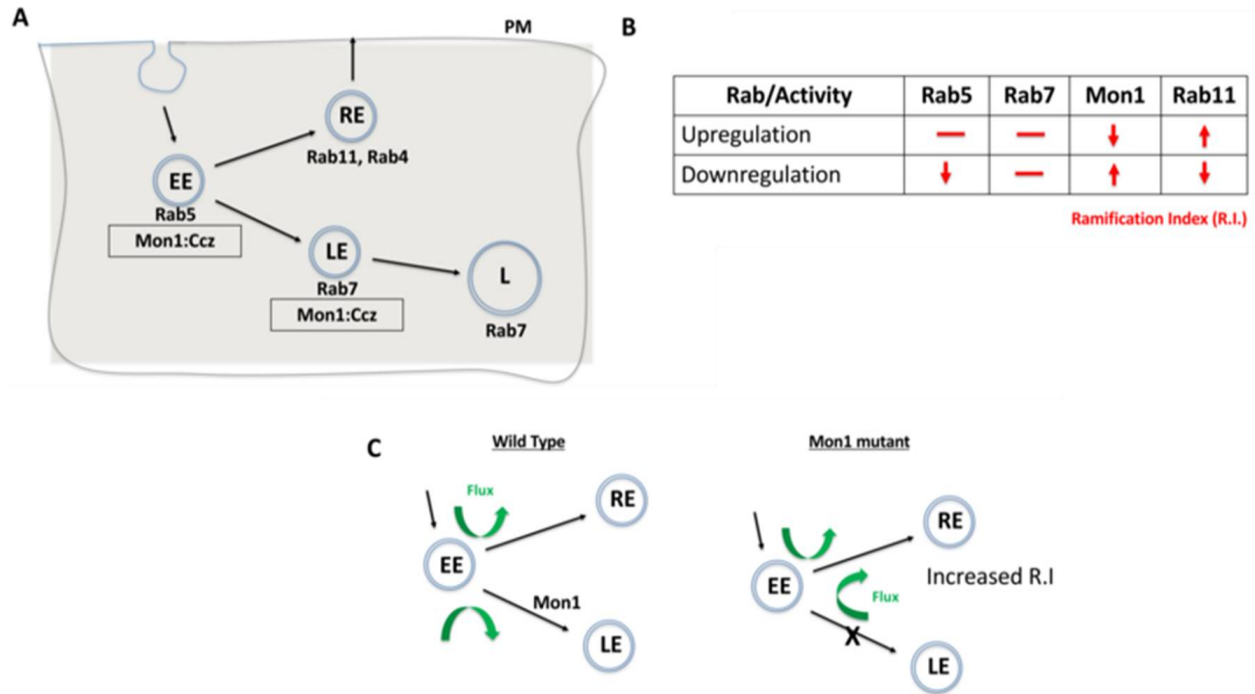
Figure VI.6. Mon1 levels may regulate vesicular flux through the recycling pathway.
A. Schematic shows the endocytic pathway branching at the early endosome, with vesicles entering either the degradative or recycling pathways. Rab5 marks early endosomes (EE), Rab7 marks late endosomes (LE) while Rab11 marks the recycling endosome (RE). The Mon1:Ccz complex acts as a GEF for conversion of EE to LE.
B. Effect of upregulation or downregulation of Rab or Mon1 activity on complexity of dendritic arborisation, as measured by change in R.I. (red lines/arrows). R.I decreases with decrease in Rab5 and Rab11 activity as also with increase of Mon1 function. In contrast, R.I increases with decrease in Mon1 function and increase in Rab11 activity. Similar trends are seen in D.A, D.L and D.BP.
C. A hypothetical model, that agrees with our data, is the requirement of endocytic recycling for increase in dendritic arborization. Thus, increase in RE endosomal flux may influence branching. This can be done directly by increasing RE by overexpressing Rab11, or indirectly by increasing the endocytic flux to the RE pathway, either by decreasing Mon1 function or by decreasing Rab5 activity. The proposed model relies on a minimal role for Rab7 in regulating R.I. Green arrows depict the increase in flux of vesicular trafficking in the RE pathway when Mon1 function is reduced.

5. Materials and Methods

5.1. Transgenic Lines

$Dmon1^{A181}$ was generated earlier through excision of *pUAST-Rab21:: YFP* insertion (Deivasigamani et al., 2015). Lines procured through the Bloomington *Drosophila* Stock Centre include Df(2L)9062, 35843 (*ppk-GFP*), 32079 (*ppk-Gal4*), 9772 (*UAS-Rab5-DN*), 9773 (*Rab5CA*), 34832 (*Rab5 RNAi*), 9779 (*UAS-YFP:Rab7CA*), 9778 (*UAS-Rab7DN*), 27051 (*UAS-Rab7 RNAi*), 9792 (*UAS-Rab11DN*), 9791 (*UAS-Rab11CA*) . *UAS-Mon1:HA/TM6Tb* is a kind gift from Prof. Thomas Klein.

5.2. Immunohistochemistry & Imaging

Wandering third instar larvae were collected, filleted in 1X PBS, dissected and fixed in Bouins solution (HT10132, Sigma) for 7 minutes. The tissues were then blocked in 1X PBS +0.3%Triton (194854, MP Biomedicals) and 2% BSA stained overnight in anti-GFP (Chk, A10262, Invitrogen, 1:500 and Rb, A6455, 1:1000) incubated in 4 ºC overnight. This was followed by washes with 1X PBS +0.3%Triton and 2% Triton-X and incubated in secondary antibody at room temperature for 1.5 hours. The final step involved washes and mounting of tissues in 70% glycerol with n-propyl gallate. Confocal imaging was carried out using a Zeiss LSM 710 microscope at 20X magnification. For Rab staining, dilutions used were as follows. Anti Rab5 (1:500), Rab7(1:500), Rab11(1:500)(Tanaka and Nakamura, 2008). Fixative used for staining with Rab antibodies was 4% PFA. Secondaries used were, Rab5 (1:1000 Guinea Pig Alexa fluor 568, Invitrogen A11075), Rab7 and Rab11 (1:1000 Rabbit Alexa Fluor 647, Invitrogen A21244), Chicken Alexa Fluor 488 from Invitrogen (A11039) and Rabbit Alexa Fluor 488 from Invitrogen (A11034). Rab antibodies were a kind gift by Prof. Akira Nakamura (RIKEN Center for Developmental Biology, Kobe, Hyogo 650-0047, Japan). For Rabs, confocal imaging was carried out using a Zeiss LSM 710 microscope at 63X magnification.

5.3. Sholl Analysis

Sholl analysis, to measure the ramification index (R.I), was performed using the NIH ImageJ Sholl Analysis Plugin (v1.0) downloaded from the Ghosh lab website (http://wwwbiology.ucsd.edu/labs/ghosh/software/). Briefly, the maximum intensity projection for z stacks of each neuron was converted to a segmented grayscale image using ImageJ.

Background dendrites extending into the image view from neighbouring neurons were manually deleted. Sholl analysis was performed by drawing a straight line from the cell body to the distal tip of the neuron. The area for the analysis was hence defined by this straight line which is considered as the radii for each image. The origin of the concentric radii was set at the midpoint of the longest axis of the soma. Analysis was performed in automated way using the following parameters: starting radius, 1 μm; radius step size, 2 μm; span, 1 μm; span type, median. The number of dendrite intersections for each circle is measured and the highest value is divided by the number of primary dendrites (intersections at the starting radius) to obtain the Schoen ramification index (R.I.). This parameter is dependent on maximum number of intersections and the number of primary dendrites. Statistics were performed using the Prism statistical package (GraphPad, San Diego, CA).

5.4. Neuromorphometric analysis of da neurons

The Filament dendrite tracer plug-in of the IMARIS 7 software was used to trace the dendrites in 3D and generate quantitative data for each genotype. The analysis was performed on dendritic arbor's arising from a single neuron and the branches from neighbouring neurons were deleted manually. The cell body was defined as the origin by adjusting the threshold for the largest diameter. The 'Dendritic Area (D.A)' measured in μm^2 refers to the total area occupied by the traced filament. The 'Dendritic length (D.L)', measured in μm refers to the sum of all filaments traced within an arbor. The total number of 'Dendritic Branch points (D.BP)' in each arbor have also been measured for each genotype. The numbers for D.BP are the sum of all branch points in the image (primary, secondary and tertiary).

6. Author Contributions

SD, RK, AR, GR conceived the project and designed the experiments. RK, ST and SD performed all the experiments. RK, SD, AR, ST, GR analysed the data and wrote the manuscript. The authors declare no conflict of interest.

7. Acknowledgements

8. References

Adams, C.M., Anderson, M.G., Motto, D.G., Price, M.P., Johnson, W.A., and Welsh, M.J. (1998). Ripped pocket and pickpocket, novel Drosophila DEG/ENaC subunits expressed in early development and in mechanosensory neurons. *Journal of Cell Biology* 140**,** 143-152.

Berry, K.P., and Nedivi, E. (2017). Spine Dynamics: Are They All the Same? *Neuron* 96**,** 43-55.

Cajal, S.R. (1999). *Texture of the Nervous System of Man and the Vertebrates.* Springer.

Cantallops, I., Haas, K., and Cline, H.T. (2000). Postsynaptic CPG15 promotes synaptic maturation and presynaptic axon arbor elaboration in vivo. *Nature Neuroscience* 3**,** 1004-1011.

Cline, H.T. (2001). Dendrite arbor development and synaptogenesis. *Current Opinion in Neurobiology* 11**,** 118-126.

Copf, T. (2014). Developmental shaping of dendritic arbors in Drosophila relies on tightly regulated intra-neuronal activity of protein kinase A (PKA). *Developmental Biology* 393**,** 282-297.

Crozatier, M., and Vincent, A. (2008). Control of multidendritic neuron differentiation in Drosophila: The role of Collier. *Developmental Biology* 315**,** 232-242.

De Franceschi, N., Wild, K., Schlacht, A., Dacks, J.B., Sinning, I., and Filippini, F. (2014). Longin and GAF Domains: Structural Evolution and Adaptation to the Subcellular Trafficking Machinery. *Traffic* 15**,** 104-121.

Deivasigamani, S., Basargekar, A., Shweta, K., Sonavane, P., Ratnaparkhi, G.S., and Ratnaparkhi, A. (2015). A Presynaptic Regulatory System Acts Transsynaptically via Mon1 to Regulate Glutamate Receptor Levels in Drosophila. *Genetics* 201**,** 651-+.

Delandre, C., Amikura, R., and Moore, A.W. (2016). Microtubule nucleation and organization in dendrites. *Cell Cycle* 15**,** 1685-1692.

Dhiman, N., Deshpande, G., Ratnaparkhi, G.S., and Ratnaparkhi, A. (2018). Rab converter DMon1 constitutes a novel node in the brain-gonad axis essential for female germline maturation. *BioRxiv***,** 508598.

Dong, X.T., Shen, K., and Bulow, H.E. (2015). Intrinsic and Extrinsic Mechanisms of Dendritic Morphogenesis. *Annual Review of Physiology, Vol 77* 77**,** 271-300.

Emoto, K., He, Y., Ye, B., Grueber, W.B., Adler, P.N., Jan, L.Y., and Jan, Y.N. (2004). Control of dendritic branching and tiling by the tricornered-kinase/furry signaling pathway in Drosophila sensory neurons. *Cell* 119**,** 245-256.

Garcia-Lopez, P., Garcia-Marin, V., Martinez-Murillo, R., and Freire, M. (2010). Cajal's achievements in the field of the development of dendritic arbors. *International Journal of Developmental Biology* 54**,** 1405-1417.

Grueber, W.B., Jan, L.Y., and Jan, Y.N. (2002). Tiling of the Drosophila epidermis by multidendritic sensory neurons. *Development* 129**,** 2867-2878.

Grueber, W.B., Ye, B., Moore, A.W., Jan, L.Y., and Jan, Y.N. (2003). Dendrites of distinct classes of Drosophila sensory neurons show different capacities for homotypic repulsion. *Current Biology* 13**,** 618-626.

Grueber, W.B., Ye, B., Yang, C.H., Younger, S., Borden, K., Jan, L.Y., and Jan, Y.N. (2007). Projections of Drosophila multidendritic neurons in the central nervous system: links with peripheral dendrite morphology. *Development* 134**,** 55-64.

Gu, Y., Chiu, S.L., Liu, B., Wu, P.H., Delannoy, M., Lin, D.T., Wirtz, D., and Huganir, R.L. (2016). Differential vesicular sorting of AMPA and GABA(A) receptors. *Proceedings of the National Academy of Sciences of the United States of America* 113**,** E922-E931.

Jan, Y.N., and Jan, L.Y. (2010). Branching out: mechanisms of dendritic arborization. *Nature Reviews Neuroscience* 11**,** 316-328.

Jinushi-Nakao, S., Arvind, R., Amikura, R., Kinameri, E., Liu, A.W., and Moore, A.W. (2007). Knot/Collier and cut control different aspects of dendrite cytoskeleton and synergize to define final arbor shape. *Neuron* 56**,** 963-978.

Kanamori, T., Kanai, M.I., Dairyo, Y., Yasunaga, K., Morikawa, R.K., and Emoto, K. (2013). Compartmentalized Calcium Transients Trigger Dendrite Pruning in Drosophila Sensory Neurons. *Science* 340**,** 1475-1478.

Kanamori, T., Yoshino, J., Yasunaga, K., Dairyo, Y., and Emoto, K. (2015). Local endocytosis triggers dendritic thinning and pruning in Drosophila sensory neurons. *Nature Communications* 6.

Lazo, O.M., Gonzalez, A., Ascano, M., Kuruvilla, R., Couve, A., and Bronfman, F.C. (2013). BDNF Regulates Rab11-Mediated Recycling Endosome Dynamics to Induce Dendritic Branching. *Journal of Neuroscience* 33**,** 6112-+.

Meltzer, S., Yadav, S., Lee, J., Soba, P., Younger, S.H., Jin, P., Zhang, W., Parrish, J., Jan, L.Y., and Jan, Y.N. (2016). Epidermis-Derived Semaphorin Promotes Dendrite Self-Avoidance by Regulating Dendrite-Substrate Adhesion in Drosophila Sensory Neurons. *Neuron* 89**,** 741-755.

Mochizuki, H., Toda, H., Ando, M., Kurusu, M., Tomoda, T., and Furukubo-Tokunaga, K. (2011). Unc-51/ATG1 Controls Axonal and Dendritic Development via Kinesin-Mediated Vesicle Transport in the Drosophila Brain. *Plos One* 6.

Nordmann, M., Cabrera, M., Perz, A., Brocker, C., Ostrowicz, C., Engelbrecht-Vandre, S., and Ungermann, C. (2010). The Mon1-Ccz1 Complex Is the GEF of the Late Endosomal Rab7 Homolog Ypt7. *Current Biology* 20**,** 1654-1659.

Orgogozo, V., and Grueber, W.B. (2005). FlyPNS, a database of the Drosophila embryonic and larval peripheral nervous system. *Bmc Developmental Biology* 5.

Parrish, J.Z., Emoto, K., Kim, M.D., and Jan, Y.N. (2007). Mechanisms that regulate establishment, maintenance, and remodeling of dendritic fields. *Annual Review of Neuroscience* 30**,** 399-423.

Peng, Y., Lee, J., Rowland, K., Wen, Y.H., Hua, H., Carlson, N., Lavania, S., Parrish, J.Z., and Kim, M.D. (2015). Regulation of dendrite growth and maintenance by exocytosis. *Journal of Cell Science* 128**,** 4279-4292.

Peng, Y.R., He, S., Marie, H., Zeng, S.Y., Ma, J., Tan, Z.J., Lee, S.Y., Malenka, R.C., and Yu, X. (2009). Coordinated Changes in Dendritic Arborization and Synaptic Strength during Neural Circuit Development. *Neuron* 61**,** 71-84.

Poteryaev, D., Datta, S., Ackema, K., Zerial, M., and Spang, A. (2010). Identification of the Switch in Early-to-Late Endosome Transition. *Cell* 141**,** 497-508.

Prigge, C.L., and Kay, J.N. (2018). Dendrite morphogenesis from birth to adulthood. *Current Opinion in Neurobiology* 53**,** 139-145.

Satoh, D., Sato, D., Tsuyama, T., Saito, M., Ohkura, H., Rolls, M.M., Ishikawa, F., and Uemura, T. (2008). Spatial control of branching within dendritic arbors by dynein-dependent transport of Rab5-endosomes. *Nature Cell Biology* 10**,** 1164-1171.

Sweeney, N.T., Brenman, J.E., Jan, Y.N., and Gao, F.B. (2006). The coiled-coil protein shrub controls neuronal morphogenesis in Drosophila. *Current Biology* 16**,** 1006-1011.

Tanaka, T., and Nakamura, A. (2008). The endocytic pathway acts downstream of Oskar in Drosophila germ plasm assembly. *Development* 135**,** 1107-1117.

Valnegri, P., Puram, S.V., and Bonni, A. (2015). Regulation of dendrite morphogenesis by extrinsic cues. *Trends in Neurosciences* 38**,** 439-447.

Villarroel-Campos, D., Gastaldi, L., Conde, C., Caceres, A., and Gonzalez-Billault, C. (2014). Rab-mediated trafficking role in neurite formation. *Journal of Neurochemistry* 129**,** 240-248.

Wang, C.W., Stromhaug, P.E., Shima, J., and Klionsky, D.J. (2002). The Ccz1-Mon1 protein complex is required for the late step of multiple vacuole delivery pathways. *Journal of Biological Chemistry* 277**,** 47917-47927.

Wang, Y., Zhang, H., Shi, M., Liou, Y.C., Lu, L., and Yu, F.W. (2017). Sec71 functions as a GEF for the small GTPase Arf1 to govern dendrite pruning of Drosophila sensory neurons. *Development* 144**,** 1851-1862.

Ye, B., Petritsch, C., Clark, I.E., Gavis, E.R., Jan, L.Y., and Jan, Y.N. (2004). nanos and pumilio are essential for dendrite morphogenesis in Drosophila peripheral neurons. *Current Biology* 14**,** 314-321.

Yousefian, J., Troost, T., Grawe, F., Sasamura, T., Fortini, M., and Klein, T. (2013). Dmon1 controls recruitment of Rab7 to maturing endosomes in Drosophila. *Journal of Cell Science* 126**,** 1583-1594.

Zhang, H., Wang, Y., Wong, J.J.L., Lim, K.L., Liou, Y.C., Wang, H.Y., and Yu, F.W. (2014). Endocytic Pathways Downregulate the L1-type Cell Adhesion Molecule Neuroglian to Promote Dendrite Pruning in Drosophila. *Developmental Cell* 30**,** 463-478.

Zou, W., Shen, A., Dong, X.T., Tugizova, M., Xiang, Y.K., and Shen, K. (2016). A multi-protein receptor-ligand complex underlies combinatorial dendrite guidance choices in C. elegans. *Elife* 5.